A Model of the Velocity Structure of the Ivrea-Verbano Lower Crustal Section, Northern Italy

by

Jalal Khazanehdari

A thesis submitted to the University of Manchester
for thedegree of Doctor of Philosophy
in the Faculty of Science

Department of Earth Sciences

Contents

Chapter 6

Chapter 7

List of Figures

List of Tables

Abstract

A large number of laboratory velocity measurements (both compressional & shear velocities) of representative rock samples from an exposed lower crustal section (Ivrea-Verbano zone, N.Italy) have been carried out in order to help clarify the interpretation of contemporary deep seismic reflection and refraction data. The Ivrea-Verbano zone and adjacent Serie dei Laghi are believed to represent a section through middle and lower Post-Hercynian continental crust which were emplaced to present vertical attitude during the Alpine orogeny.

During two field seasons the most representative geological units from the Ivrea-Verbano zone and the Serie dei Laghi were sampled systematically and extensively. A total of 558 oriented and mostly fresh cores were collected from 40 locations. The samples were prepared for both mineralogical studies and laboratory seismic measurements. The mineralogy and modal composition of all the samples used for velocity experiments were studied.

Two high pressure apparatuses were modified and the necessary parts were designed and made so they could be used for high pressure and temperature velocity measurements. One of the apparatuses was used for measuring compressional and shear velocities of the samples at room temperature and elevated pressure up to maximum of 550 MPa. The second apparatus was designed for both elevated temperature (0 to 700 °C) and elevated pressure (0 to 500 MPa) compressional velocity measurements.

The experimentally determined velocities indicate that ultramafic and mafic rocks have higher compressional velocity (ranging from 6.89 km/s to 8.2 km/s) and shear velocity (ranging from 3.7 km/s to 4.63 km/s) than metasedimentary rocks (Vp ranging from 5.54 km/s to 6.98 km/s & Vs ranging from 3.14 km/s to 4.07 km/s). Seismic anisotropy seems to be high (around 8 to 16 %) in most metasedimentary rocks and low in igneous rocks (e.g. granite, less than 1 %). It was inferred from fabric study that seismic anisotropy is due to crystallographic preferred orientation and mineral alignment at high pressure (< 250 MPa) when all the microcracks and pores are closed.

The pressure and temperature coefficients of compressional velocity and density of 23 rock types were used in conjunction with a reconstructed geological cross sections of the Ivrea-Verbano zone and Serie dei Laghi to create a series of velocity, density and reflection coefficient models.

The results of modelling indicate a number of important points: i) in general the Serie dei Laghi is less reflective than the Ivrea -Verbano Zone. ii) The Ivrea-Verbano zone seems to be extremely reflective in the central part of the section. This is associated with presence of series of horizontal and sub-horizontal layers of different lithology with alternating low and high velocity and density. iii) Effect of pressure and temperature in terms of producing acoustic impedance contrast seems to be of second order and less important than original compositional variation.

Generally, four factors are suggested to explain the reflectivity of the Ivrea-Verbano zone and similar lower crustal sections. These are, in order of importance, i) compositional layering ii) mafic intrusions iii) lenses of ultramafic mantle-derived rocks and finally iv) shear zones and associated deformation.

Declaration

No portion of the work refereed to in this thesis has been submitted in support of an application for another degree or qualification of this or any other University or other institution of learning.

Copyright

Acknowledgements

I would like to thank and express my gratitude to my supervisor Prof. E.H Rutter, without his advice and his experimental expertise this investigation would have not been so fruitful.

I would also like to thank Mr. Rob. Holloway for his continuous and crucial help in design, maintenance and operation of two seismic apparatuses. Special thank to Rob for his help during two field seasons. Special thank to Dr. Kate. Brodie for her help with mineral and microstructural studies and her reading of the relevant chapters.

I am also grateful to Mr. R. Mason for his important role during the development of seismic velocity systems. I would like to thank Mr. T. James for his help on seismic modelling and his critical reading of a number of chapters. Special thanks to Tony for providing the sample location map.

I would like also to thank Prof. D. Mainprice (University Montpellier, France), for use of his seismic velocity programs and his valuable discussions and advice, Dr. M. Casey (ETH, ZÜrich) for providing texture goniometery data of a number of samples, Drs. L. Burlini & A. Zappone (Milan Uni, Italy) for their help during my field work and advice on seismic velocity measurements.

I would like to take this opportunity to thank some of the past, present and hopefully not permanent student members (Paul, Steve, Iona, Bob, Peter, Dan, Tony and Rob) of Rock Def Lab for their friendship.

I owe a particular debt of gratitude to my parents and my two brothers for their continual love, concern, support and encouragement. Without it I would not have started and completed this research. Finally, thanks to my wife Azadeh for her love and support.

Chapter 1
Introduction

1.1 Earth Structure

Much of the information about the internal structure of the Earth is derived from the study of seismic waves. Seismic waves are subjected to reflection and refraction at the surface of a discontinuity. On the basis of major velocity changes which correspond to major physical and/or chemical changes, the Earth's interior is divided into three principal layers. The Crust; from the surface down to the first major discontinuity known as the Mohorovicic discontinuity, the Mantle; from the base of the crust to the Wiechert-Gutenburg discontinuity and finally the Core, from the Wiechert-Gutenburg discontinuity to the centre of the earth.

Recent advances in geophysical exploration techniques and especially seismic methods (reflection and wide angle reflection) have resulted in better subsurface imaging of the crust and upper mantle. Geophysical information from seismic profiling, especially from the lower continental crust, have revealed a much more complex structure than was initially expected (Matthews, 1986).

1.2 Structure of the Continental Lower Crust (C.L.C)

Most of the information regarding the nature and structure of the contemporary Continental Lower Crust comes from indirect methods such as seismic and electrical conductivity studies (see chapter 2). Unfortunately, due to the complexity of the CLC that has been observed on many seismic reflection and wide angle reflection profiles, and difficulties of objective interpretation, little is still known about this part of the crust (Cao et al., 1990). Analysis of seismic reflection data reveals a highly complex structure for the CLC in many areas (e.g. the continental shelf around British Isles & the Basin and Range province of the western USA). In these areas the CLC frequently appears highly reflective and anisotropic, whereas the middle crust seems transparent to seismic waves (fig 1.1). On these seismic sections the entire lower crust and Moho is often laminated

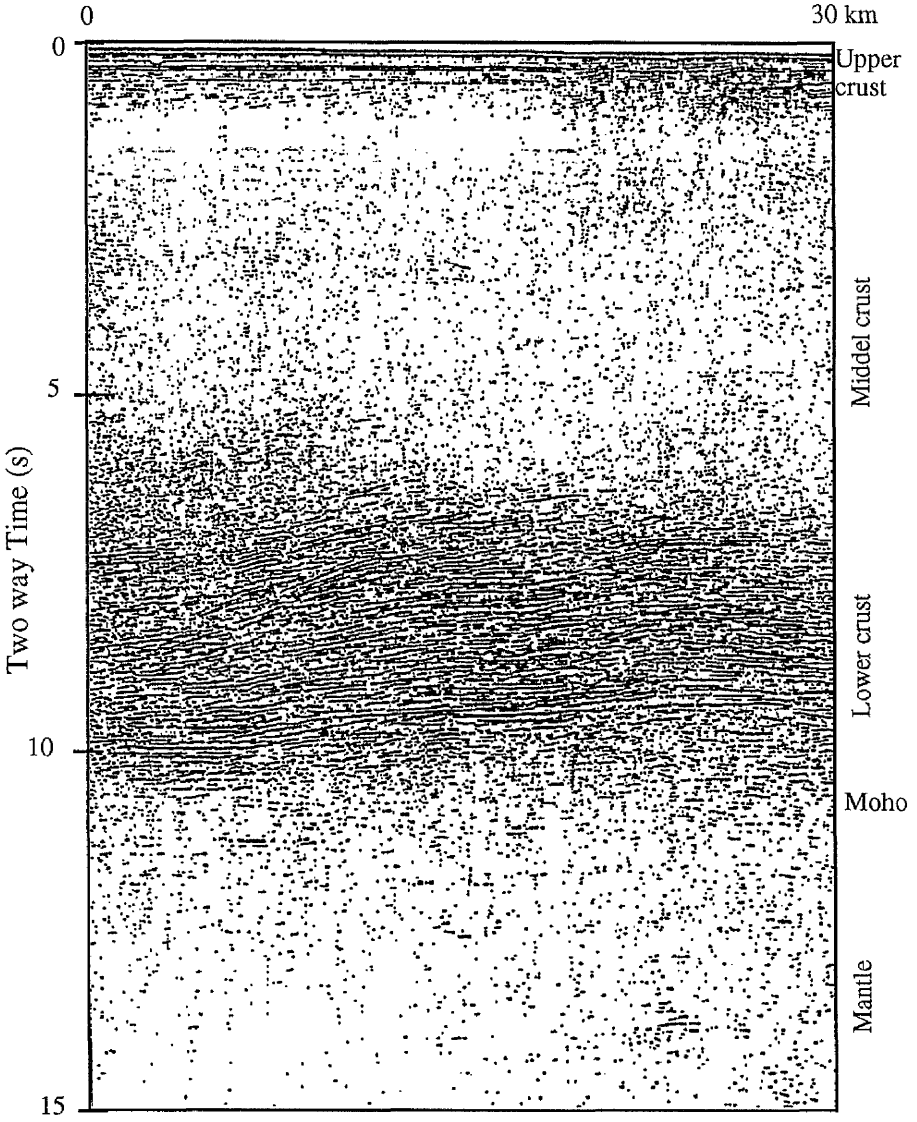

Figure 1.1 : Stacked seismic reflection section over an area of continental crust south west of Britain. This fascinating seismic section shows strong lower crustal reflections with horizontal to sub-horizontal reflectors. The upper crust is reflective with number of horizontal and continuous reflectors. The middle crust appears to be transparent to the seismic waves. The Moho is defined where the intensity of the reflecters reduces dramatically (Warner 1990 a).

with thin, alternating high and low velocity layers. Despite a huge collection of contemporary deep seismic, and other geophysical data across the world, answers to the key questions regarding the nature and structure of the CLC remain ambiguous and maybe in some cases impossible. Some of these questions are:

i) What causes high reflectivity and laminated pattern, observed on many deep seismic reflection profiles of continental lower crust?

ii) What is the nature of the Moho and why it does not always appear as a strong and continuous reflector on the seismic sections?

iii) What are the seismic properties of low angle shear zones which appears to makes them reflective?

So far a number of theories have been proposed to explain the complexity of the lower crust and to find answers to some of the above questions. Among the most favoured theories (fig 1.2) are compositional layering (e.g. Christensen, 1989), extensive networks of shear zones (e.g. Meissner & Sadowiak, 1990), zones of high pore fluid pressure (e.g. Fyfe et al., 1978) and finally sheets of igneous intrusions (e.g. McCarthy & Thompson, 1988; Warner, 1990).

None of these theories on its own is capable of providing all the answers to these questions regarding the CLC. There seems to be a lack of understanding of the seismic and physical properties of rocks at high pressure (about 700 MPa and above) and at high temperatures (400-800 °C) associated with the CLC. This can lead to poor processing and interpretation of remote sensing data, especially seismic reflection data, which requires good quality velocity information coupled with a realistic geological framework.

Laboratory measurements have been used to provide information on the velocity of rocks at high pressure and temperature (e.g. Birch, 1960; Christensen, 1965; Kern & Richter, 1981). Seismic modelling has also been used with the aim to reproduce the velocity patterns of the lower crust (e.g. Hall & Thompson, 1982; Kern & Schenk, 1988). Technical problems associated with high pressure and especially high temperature laboratory velocity measurements and lack of fresh and representative lower crustal samples has limited the number of available data. Moreover, the geological structures used for seismic modelling have been either unrealistic and hypothetical or

poorly geologically defined. These problems have resulted in relatively ill-constrained or unsuccessful seismic velocity modelling of the lower continental crust (e.g. Wenzel et al., 1987; Reston, 1987).

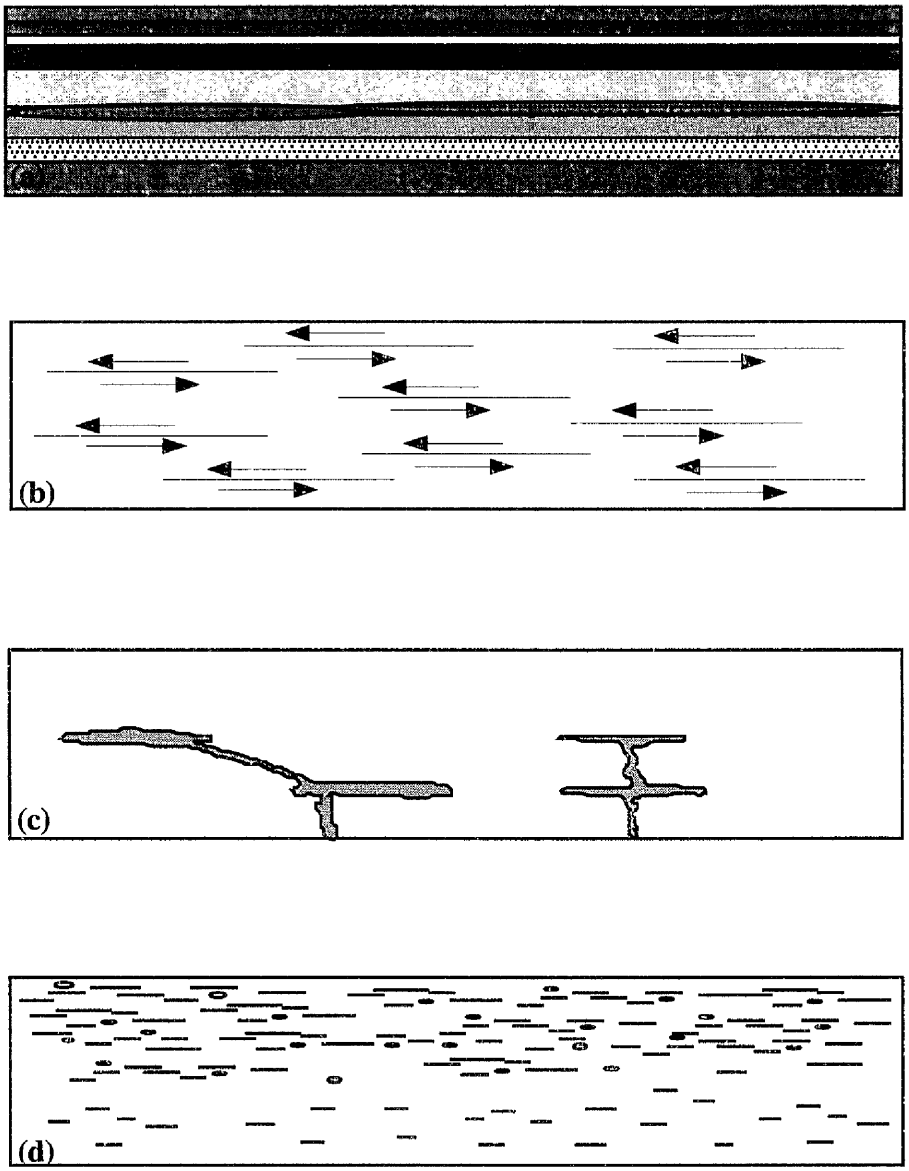

Figure 1.2: Schematic cross sections of the continental lower crust showing four models for its reflectivity. (a) Layers of different velocity and/or density (b) Low angle shear zones juxtaposing rocks of different properties (c) Sheets of igneous intrusions, sandwiched between different rock types and (d) Presence of fluid in a relatively porous lower crustal rocks (the diagram shows the lower crust such that its top half has relatively higher porosity than its lower half).

1.3 Aims of this work

The principal aims of this study are:

i) To tackle the technical problems associated with combined high pressure and temperature laboratory velocity measurements by setting up a new apparatus to make such measurements.

ii) To carry out laboratory velocity measurements (e.g. compressional & shear wave velocities and seismic anisotropy) at high pressure and temperature on various lower crustal rocks collected from an exposed Permo Triassic lower crustal section in northern Italy (the Ivrea-Verbano and Serie dei Laghi complexes, see chapter 2).

iii) To seek relationships between seismic velocity, mineralogy and microstructure of rocks by careful study of sample mineralogies, microstructures and by measuring velocities in three orthogonal orientations. This should help the inference of lithology from seismic velocity.

iv) Finally, the major goal of this research is to combine seismic, petrologic and structural data from the Ivrea-Verbano zone and Serie dei Laghi to produce number of 2 dimensional velocity, density and reflection coefficient sections. Such models are a first step towards making a 2 dimensional synthetic seismic reflection profile which would be a useful tool in helping the interpretation of contemporary deep seismic reflection profiles.

1.4 Outline of Methodology

Sample collection was undertaken during two field seasons in order to collect a selection of most representative lower crustal rocks from the Ivrea-Verbano zone and Serie dei Laghi in northern Italy. The samples were cored either *in-situ* or from blocks in the laboratory in three orthogonal directions. Seismic compressional and shear velocities of the cores were measured using two newly constructed apparatuses. The velocity measurements were carried out at both elevated pressure up to 500 MPa and at temperatures up to 700 °C using the ultrasonic Pulse Transmission Method.

Oriented thin sections were prepared from all samples used for velocity measurements, to study the mineralogy and microstructure. Furthermore, attempts were

made to establish some empirical relationships between seismic velocity and (a) mineralogy (b) microstructures and (c) density of the samples.

The pressure and temperature coefficients of compressional velocity were used in conjunction with a reconstructed geological cross section of the Ivrea-Verbano zone and the adjacent Serie dei Laghi to make a series of velocity, density and reflection coefficient sections.

Computer software, either purpose-written or commercial software, were used for data processing and modelling as appropriate.

1.5 Thesis Structure

Chapter 2 provides a brief description of the geological and geophysical methods which are used to study the physical state of the continental lower crust.

Chapter 3 begins with a brief summary of the lithology and structure of the Ivrea-Verbano zone and Serie dei Laghi. It is followed by a short review of the geology of the region and its major rock types. This chapter ends by describing the methods and the techniques used for sample collection.

Chapter 4 reports the mineralogy and microstructures of the main rock types for which seismic velocities were measured.

Chapter 5 opens with a brief description of common methods of generating and measuring elastic waves in the laboratory. Then a detailed description is given of the two newly established apparatuses for high pressure and high temperature velocity measurements. The chapter ends by discussing the errors associated with laboratory velocity measurements.

Chapter 6 reports the results of the high pressure and room temperature compressional and shear wave velocities measurements made on about 35 rock types. The velocity data are used to find the pressure coefficient of velocity for the samples and also to calculate some other relevant elastic properties.

Chapter 7 describes the results of combined high pressure and high temperature compressional velocity on 14 rock types. The results were used to find the temperature coefficients of velocity of these samples.

Chapter 8 describes how the pressure coefficient of velocity (results from chapter 6) and temperature coefficient of velocity (results from chapter 7) were used in conjunction with reconstructed geological cross section of the Ivrea-Verbano zone to produce a series of velocity, density and reflection coefficient distribution sections.

Chapter 9 provides a general discussion on the results of seismic velocity data and the velocity maps of the Ivrea-Verbano zone and their implications for the nature and structure of contemporary lower crustal sections. The chapter ends by summarising the major achievements during the course of this study and suggestions for future work.

Chapter 2

Background to the Study of the Continental Lower Crust

2.1 Introduction

During the past few decades, an enormous amount of information concerning the nature and structure of the continental crust has been obtained. Yet there persist uncertainties regarding the composition and genesis of the middle and especially the lower parts of the continental crust (Percival, et al., 1992). Most of the uncertainties come from the difficulty of directly sampling a major portion of the crust in one place. The deepest borehole yet made is the *Kola Borehole*, about 13 km deep (Kozlovsky, 1984) but this is nothing compared to the thickness of the continental crust (in the range 20 - 60 km, averaging 39 km).

Samples of continental lower crust can be obtained from tectonically uplifted lower crustal regions (e.g. Kapuskasing uplift, Ontario, Canada; Ivrea-Verbano zone, southern Alps, Italy ; Kohistan arc, Kohistan, Pakistan & the Arunta block, central Australia) or from xenoliths (e.g. granulite xenoliths of Chinese Peaks, California; Eifel, Germany & Massif Central, France). Such samples are either rare to obtain or they have suffered substantial changes and the depths from which they come from and such effects may not be known accurately. All the above reasons are why more and more remote sensing methods are used for indirect study of lower crustal rocks. Geophysical methods offer the best indirect approaches to the study of the lower crust at any given location (Holbrook et al., 1992).

Seismic reflection profiling and refraction (wide angle reflection) reveals geometry and internal velocity (from which rock compositions may be inferred) far better than any other geophysical technique. However different rocks may display identical velocities due to various factors, for instance particular combinations of pressure and temperature (see chapter 6 & 7).

Unlike seismic methods, which differentiate rocks on the basis of their seismic properties, gravity and magnetic methods sense variations in density and magnetic properties of rocks respectively. Aeromagnetic surveys have been used to study the

magnetic properties of deep rocks (Krutikhovskaya et al., 1977 & 1979). The deep source magnetic anomalies are distinguishable from shallow anomalies by their long wavelength and low amplitude. But such differentiation is problematic due to the common occurrence of long-wavelength noise sources. This is why laboratory studies have been made of the magnetic susceptibility of deep origin rocks. The laboratory information then has been used to find a source or sources for observed long-wavelength magnetic anomalies. Shive et al., (1992) explain that some long-wavelength magnetic anomalies may be produced by rock bodies that contain 5% or even more magnetite by volume. He concludes that, considering the ambient conditions of the lower continental crust (high pressure and high temperature), only mafic and ultramafic rocks can produce such magnetic anomalies. At the same time, high density minerals such as olivine, pyroxene (3.22 & 3.2 g/cm^3) constituting these anomalous bodies can lead to high Bouguer gravity anomalies.

Electrical methods, such as electromagnetic sounding, have been used to assess the electrical properties of lower crustal rocks. To the surprise of many geoscientists the electrical resistivity of the lower crust observed in many places (e.g. Canadian, Baltic & Siberian shields) was far lower (10 to 500 Ωm; Jones & Hutton, 1979; Ritz, 1983) than what once was expected for deep and dry crystalline rocks (10^3 to 10^5 Ωm). These results led to many speculations regarding the nature of lower crustal rocks, and many possibilities have been suggested to explain their high electrical conductivities. The most favoured ones include the presence of; saline fluids (Hyndman & Hyndman 1968; Brace, 1971 & Jones, 1987), grain-boundary carbon films (Duba et al., 1988 & Frost et al., 1989), conducting minerals such as sulphides and graphite (Jones & Craven, 1990; Olhoeft, 1981; Glover & Vine, 1994). It was also suggested that the presence of free water could account for the layered lower crust (Hall, 1986) observed on many deep seismic reflection profiles. On the other hand there are petrological objections to the presence of substantial free water in the CLC. The strongest objections are the existence of small scale heterogeneities in oxygen isotopes ratio (Valley, 1986) which would be rapidly homogenised in presence of water and the common preservation of granulite

facies minerals assemblages in exposed lower crustal terrains, that would become hydrated if free water were not removed prior to uplifting.

The following sections present an overview of the recent geological and geophysical studies regarding the nature and structure of the continental lower crust. It is not within the scope of this work to review all geophysical data and techniques which are used for studying the physical state of the lower continental crust. However, as seismic data (near vertical reflection and wide angle reflection) are closely related to the nature of the present work a broader review of their methods and their acquisition/interpretations will be presented.

2.2 Geological information

Geological information concerning deep crustal rocks comes from two main sources, field data and experimental/analytical data. Information such as tectonic and structural data are obtained from direct study of uplifted and exposed deep crustal sections. Most petrological, mineralogical, geochemical and rheological data are obtained by studying rock samples of lower crustal origin collected either from exposed lower crustal terrains or xenoliths.

2.2.1 Exposed crustal cross sections

Our understanding of the nature and structure of the CLC is under continual refinement as more geological and geophysical data become available. Much of our information comes through the study of exposed crustal sections. There are three major mechanisms which, have been suggested for uplifting the lower crust (Percival et al, 1992).

i) Compressional uplift

ii) Extensional uplifts

iii) Impactogenic uplifts

The first two are by far the most common mechanisms for the uplift of the crust (Fountain & Salisbury, 1981). Uplift along a great fault (*thrust faulting*) occurs either at plate margins or in an intracratonic setting. In some cases older, deeper crust is thrust

over younger rocks (e.g. Ivrea-Verbano Zone, Italy or Cab ortegal Complex, NW Spain). In most cases of exposed CLC an increase in metamorphic grade up to granulite facies has been observed (Percival, 1992 & Zingg, 1983). The age of the uplift varies with respect to the crust formation. Chamberlain et al., (1989) believe that the Kohistan arc (Pakistan) was abducted while it was going through its metamorphic peak whereas the Kapuskasing (Canada) uplift was exposed long after crust formation (Percival et al., 1988).

It is crucial not to mistake high-grade metamorphic terrains with lower crustal exposures. They may have similar characteristics, most notably the pressure and temperature of formation [4-12 kbar; 700-900°C (Newton & Perkins, 1982)], but comparable pressure and temperature conditions can occur in several different environments (Percival, 1989). Fountain & Salisbury (1981) and Percival (1992) suggest employing other types of information such as gravity and seismic to make a distinction. Exposed lower crustal sections are mostly still attached to the present lower crust, and such attachment can be traced using geophysical methods (e.g. Ivrea-Verbano Zone, see chapter 3).

The most detailed geological information (e.g. petrological, structural) about lower crustal rocks comes from systematic mapping and sampling of the exposed lower crustal sections. The advantages of these types of studies are that the relative volumes and thickness of rock units and the relationships between them can be extracted directly. Moreover, samples from the exposed crustal section can be used for petrophysical studies (e.g. seismic velocity, magnetic susceptibility). The petrophysical data then can help to improve the interpretation of contemporary deep seismic, aeromagnetic or electrical conductivity data.

Despite all the above advantages for studying the exposed lower crustal sections there are number of disadvantages. These cross sections often do not represent complete lower crustal sections. Also retrograde metamorphism may have destroyed the highest grade mineral assemblages that constituted the rocks when the sections were originally deep in the crust. In addition, subsolidious exsolution, weathering and later deformation

may change the mineralogy and fabric of the rocks or distort the geometry of the sections.

2.2.2 Deep-origin Xenoliths

Fragments of the crust and even of the upper mantle can be carried rapidly to the surface during volcanic eruptions. The lower crustal xenoliths are defined as rocks which came from the lower half the crust. Normally, lower crustal xenoliths have mineral assemblages characteristic of the granulite facies and have equilibration pressures in the range from 0.8 to 1.4 GPa (Wood, 1987). Most granulite xenoliths are mafic and their common minerals are pyroxenes, plagioclase and garnet. Olivine, spinel, amphibole, biotite and quartz are also reported. The physical properties of these rocks depends upon bulk composition and pressure and temperature history. Knowing some of these rocks originated from the CLC their physical properties, such as seismic velocity, heat production and resistivity can be measured. There are a number of lines of evidence that can be used to judge whether a xenolith is from the lower crust or not. The most distinctive ones are mineralogy, pressure and temperature estimation and the primitive composition of the host magma.

Lower crustal xenoliths provide us with valuable information regarding the composition of the CLC and they are quite abundant, but there are outstanding questions and important points which need more consideration. Some xenoliths do not contain garnet, therefore their pressure and temperature conditions cannot be estimated and they could easily come from a shallower depth. As mentioned earlier, their composition has been changed during ascent to the surface. Finally the small sizes of these xenoliths means that they cannot represent the overall composition of the CLC, which from seismic data seems highly heterogeneous.

2.2.3 Composition of the CLC

The bulk composition of the CLC can be estimated by a number of methods and sources such as;

i) exposed lower crustal sections, granulite terrains and xenoliths (e.g. Weaver & Tarney, 1984)

ii) relating the observed deep seismic velocity to rock types and therefore estimating rock composition (e.g. Rudnick & Fountain, 1995)

iii) mixing mafic and silicic rocks types in appropriate proportions to satisfy observed heat flow (e.g. Taylor & McLennan, 1985)

iv) estimating composition from isotope data (e.g. Farmer, 1992).

Although there are considerable data regarding the composition of the crust, there is no definite answer to the fundamental question which is whether the lower crust is dominantly felsic or mafic in composition. This is mainly due to the wide variation in mineral composition of the lower crustal rocks. For example the relative abundance of mafic granulite varies considerably from nearly nothing in some regions to about sixty percent in others (Shaw et al., 1986). Fig 2.1 shows three estimates of lower crustal compositions using some of the above mentioned methods.

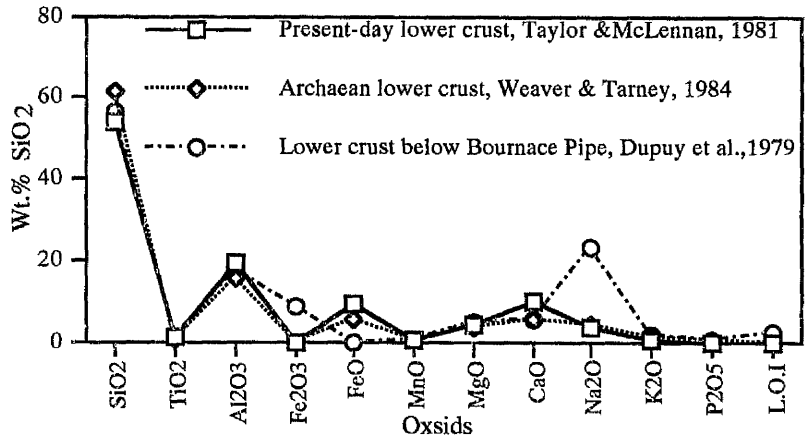

Figure 2.1 Estimates of lower crustal compositions for three lower crust regions with different age. The SiO_2 values are between 54% to 62 % (after Anderson, 1989).

By no means these are representative of the bulk composition of the CLC. This demonstrates the uncertainties and variation in compositional estimations. A recent review on the composition of the continental crust by Rudnick (1996) shows that there is a variation of more than a factor of 2 in the estimation of abundance of some elements, such as K, Fe. Apart from such uncertainty most of the data are indicative of an intermediate composition (57-64% SiO_2) for the continental lower crust. However, the

results of Taylor and McLennan's (1985) model, the analysis of Eastern Australian xenoliths (Griffin & O'Reilly, 1986) and samples from the Ivrea-Verbano Zone (Sinigoi et al., 1995) would seem to indicate a more mafic composition for the CLC.

2.2.4 Rheology of the CLC

The rheology of the CLC is most likely to be controlled by a combination of the following parameters:

i) Mineral composition

ii) Heat flow

iii) Stress conditions and overall thickness of the crust

iv) Occurrence of syntectonic metamorphic reactions.

The most abundant mineral constituents of the rocks of the lower continental crusts are quartz, feldspar, amphiboles, pyroxenes, olivine and garnet. Also some phyllosilicate minerals such as biotite and aluminium silicates (e.g. sillimanite) can be volumetrically important. It is believed that 'wet' quartz controls ductile deformation in upper and middle crust. Lower crustal rheology is more likely to be controlled by the plastic deformation of plagioclase and to lesser extent amphibole and pyroxene. Unfortunately, the mechanical properties of important minerals such as plagioclase are not as well established as for quartz, pyroxene or olivine. Figure 2.2 shows a plot of strain rate verses temperature for some important minerals controlling the deformation of the middle and lower crust. The depth of the critical temperature required to generate significant geological strain rates (e.g. 10^{-13} or 10^{-15} s^{-1}) depends on the geothermal gradient. For example in the case of quartz subjected to 50 MPa differential stress only 300°C would be needed to achieve a geologically significant strain rate whereas for dry olivine a temperature of 800°C and for wet olivine 600°C is required.

Rutter & Brodie (1992) presents the results of series of experiments on calcite and quartz. These data indicate that at higher differential stress the required temperature to make a significant strain is less but there is a temperature at any given strain rate below which the resistance to plastic flow increases very rapidly (fig 2.3).

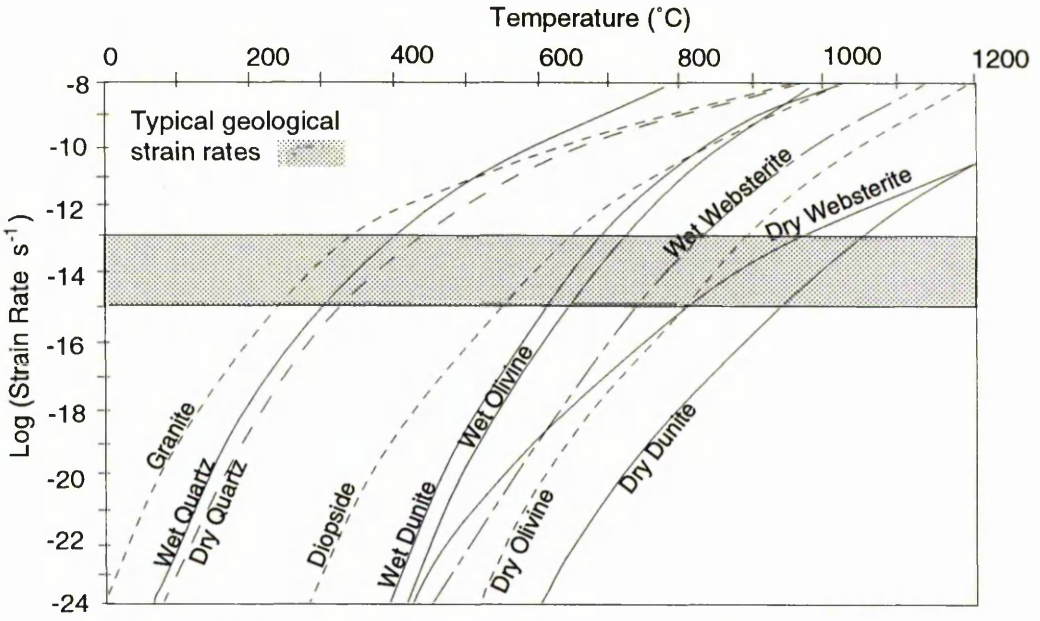

Figure 2.2: Variation in log strain rate with temperature for some important lower crustal minerals. The curves are derived from experimental data extrapolated 50 MPa differential stress and various temperatures (after Kusznir, & Park 1986).

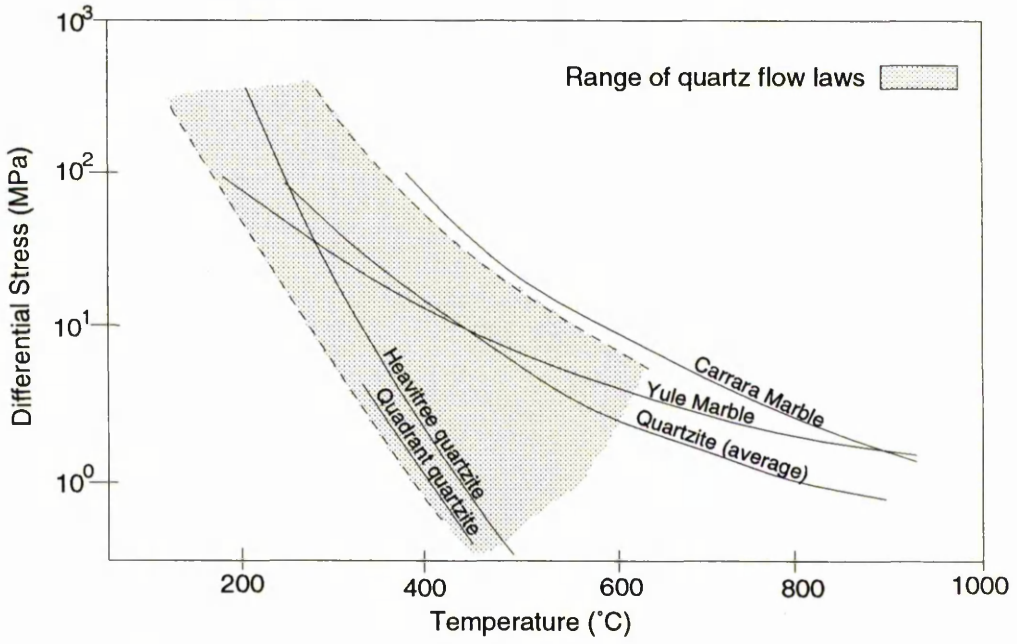

Figure 2.3: Assembly of experimentally obtained constitutive flow low data for quartz and two marble samples, extrapolated to a geologically representative strain-rate of 3 x10 $^{-4}$ s $^{-1}$(after Rutter& Brodie, 1992).

These experimental results highlight the importance of all above factors and their interaction in determining the rheology of the CLC. There are 3 principal rock deformation mechanisms. These are (a) cataclastic deformation, (b) intracrystalline plasticity and (c) diffusive mass transfer flow. Depending on the thermal gradient, state of the stress field, pore fluid pressure and deformability of the minerals, lower crustal rocks can deform differently, resulting in various microstructures.

Cataclastic deformation mainly acts in the upper to middle crust, but also at greater depths if pore pressure is high. It involves brittle fracturing plus frictional sliding of fragments. Intracrystalline plasticity acts mainly in the region of the middle and lower crust because flow strengths are strongly temperature dependent. If temperature and stress are appropriate and the crystals have sufficient slip systems then a rock can deform at constant volume without pressure-sensitivity. Intracrystalline deformation results in grain size reduction by dynamic recrystallization and the production of a crystallographic fabric. This fabric can affect some physical properties of the rock such as seismic or thermal conductivity anisotropy. The diffusive mass transfer mechanism proceeds by stress-induced diffusion of matter. Like intercrystalline plasticity, this process is generally temperature sensitive and pressure insensitive but unlike intercrystalline plasticity is strongly favoured at small grain sizes. Unlike intracrystalline plasticity, which results in crystallographic preferred orientation, diffusive mass transfer can at most form a strong grain-shape fabric which may change the seismic anisotropy.

2.3 The Continental Lower Crust as Perceived from the Results of Seismic Studies

One of the physical properties which can be measured geophysically is seismic velocity. The seismic velocity of the CLC can be estimated in two ways; either through seismic experiments (wide angle and near vertical reflections) which provide us with *in-situ* seismic velocity, or by measuring the seismic velocity of rock samples believed to come from the CLC in the laboratory.

2.3.1 Seismic Refraction (wide angle reflection)

Refraction experiments are the main source of *in-situ* seismic velocity information. They are recorded with a long shot-to-receiver offset (of the order of 200 to 300 km), a receiver spacing of 1-5 km and finally shot spacings of the order of 10-100 km. For a relatively simple subsurface with no lateral variation in the velocity, a one dimensional method is used. However for relatively complex geological problems such as the continental lower crust a two dimensional method is preferable. The two dimensional method takes account of laterally variable structures such as dipping layers, faults and igneous intrusions as well as crystallographic preferred orientation of constituent minerals.

2.3.2 Seismic Reflection (near vertical reflection)

It was not until the 1950's that the first observations of near-vertical reflections from the lower continental crust were reported. In 1964, crustal reflectors were observed by both near-vertical and wide-angle incidence at Augsburg, Germany (Meissner, 1986) and also at the same time in Australia (Moss, 1962). Additional results from Canada (Kanasewich & Cummings, 1965; Clowes et al., 1968) led to conclusive evidence for the reflectivity of lower crust and Moho.

These promising results, plus advances in computing (greater processing power) and instrumentation technology (greater numbers of recording channels) led to the establishment of many research groups world wide. In the USA, (COCORP), Canada (LITHOPROBE), Britain (BIRPS), Australia (ACORP), Germany (DEKORP), France (ECORS) and elsewhere. The main aim of these research groups has been to discover more about the nature and structure of the crust and the Moho by using seismic methods, especially the near vertical reflection method. The imaging of lower crust and upper mantle were so fascinating that some of above groups did not attempt to measure lower crustal seismic velocities. However, recently more effort has gone into determination of seismic velocities and anisotropy in order to infer more about the composition and physical state of the lower crust and upper mantle (e.g. Mooney & Brocher, 1987; Wenzel et al., 1987; Valasek et al., 1989; Goodwin & McCarthy, 1990).

2.3.2.1 Acquisition, Resolution & Uncertainties

Seismic reflection data are typically acquired with shot spacing in the order of 50-500m and a receiver spacing in the order of 25-100m and much smaller offset than seismic refraction method (2-10 km). Resolution of seismic reflections mainly depends on the frequency of the seismic waves and it is of two types; Vertical and Horizontal.

The vertical resolution is generally comparable to one fourth of the wavelength of the seismic signal. Assuming an average crustal velocity of 6.0 km/s and seismic frequency ranging between 20 to 60 Hz (typical seismic frequency for deep reflection profiling), the seismic wavelength will be 100 m to 300 m. Therefore the seismic vertical resolutions of seismic reflection signals will be between 25 m to 75 m. Layers thinner than the vertical resolution of seismic waves cannot be resolved. It is clear that using a higher frequency signal would led to better vertical resolution but the signal amplitude falls rapidly because of attenuation as frequency increases.

The horizontal resolution of seismic reflections is described by the Fresnel zone (Telford, 1990). The radius of the Fresnel zone, which is also the minimum length of a well-resolved reflecting horizon, is dependent on the distance from the source to the reflector and on the frequency of the seismic signal. For a seismic signal of 25 Hz the first Fresnel zone radius for a crustal velocity of 6 km/s and at depth of 20 km is about 1.5 km and at 30 km depth is about 1.9 km. This means any feature smaller than this may not be detected by this method, and features discontinuous on this scale may appear more continuous than they actually are.

So it is important to note that not only does the amplitude of seismic waves fall with depth due to geometrical spreading and inelasticity but also both the vertical and horizontal resolution decrease resulting in overall decrease in the quality of seismic data.

2.3.2.2 Examples of deep seismic reflection data from the lower continental crust

Thousands of kilometres of deep reflection data have been collected from various geological environments world-wide during the past two decades. Lower continental crust has been classified on the basis of its reflection response into four groups (a) non-reflective lower crust, (b) horizontal to sub horizontal reflectors, (c) broadly arched

reflectors, (d) intersecting dipping events. Smithson (1986) believes that such a classification is extremely limited due to incomplete understanding of reflection results as well as possible reflection artefacts associated with recording and processing of data. On the basis of geological environments, the seismic reflection data can be grouped into four categories as suggested by Holbrook et al., (1992). These are (a) Precambrian crusts, (b) ancient orogenic belts (Proterozoic to Mesozoic), (c) Mesozoic crust and (d) recently extended crusts.

a) Precambrian crusts (Archean crust)

Deep seismic reflection profiles over Precambrian crust have been recorded in the United States (e.g. Behrendt et al., 1990; Cannon et al., 1991), Australia (e.g. Finlayson et al., 1989; Goleby et al., 1990) Kapuskasing and elsewhere. All these profiles show strong lower crustal reflectivity and the Moho appears continuous and reflective (fig 2.4).

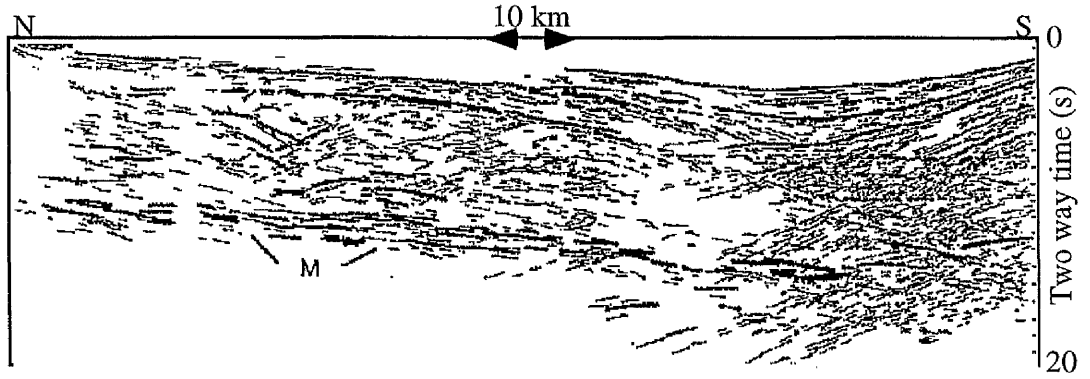

Figure 2.4: Line drawing of an un-migrated seismic reflection profile over a part of the Keweenawan Rift system in central Michigan. A zone of reflections extending over two seconds (10 to 12 s) is interpreted as evidences of magmatic underplating. The strong reflections are shown with heavy lines possibly indicating the crust mantle transition zone. ('M' stands for Moho, after Behrendt et al., 1990).

Figure 2.5 shows an enlargement of a part of the above seismic section containing the bands of strong lower-crustal reflections. The discontinuous and highly reflective reflectors with an interfingering pattern are believed to represent a complex of felsic granulites, originally emplaced as crustal melts (e.g. Behrendt et al., 1990; Furlong & Fountain, 1986).

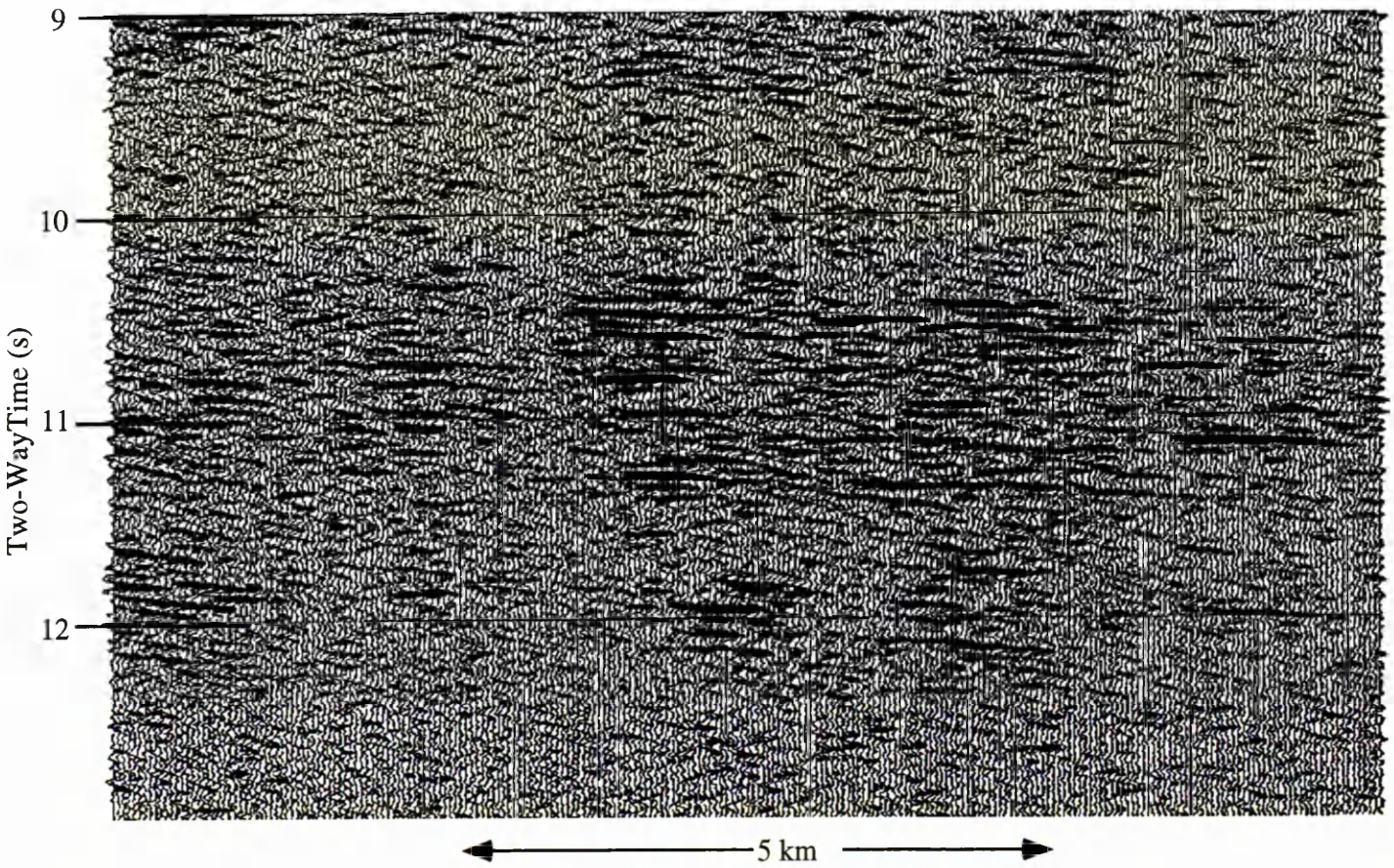

Figure 2.5: Enlarged part of true-amplitude seismic reflection section from figure 2.4. It shows strong bands of reflections, with estimated acoustic impedance of 0.05, 0.1 (after Behrendt et al. 1990).

b) Proterozoic through Palaeozoic crusts

In many Proterozoic belts the lower crust appears to be highly reflective. In places such as the Arunta Block in central Australia the crustal root is, to some extent, visible, indicating that crustal creep or delamination has not eliminated this root (fig 2.6).

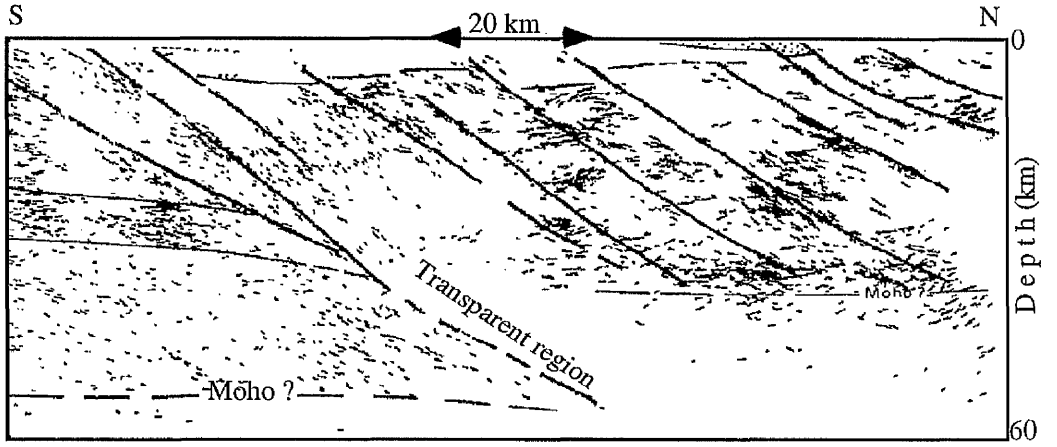

Figure 2.6: A depth migrated, line drawing and interpretation of the Proterozoic Arunta Block in central Australia. There is a marked offset on the crust-mantle boundary (about 15 km) with mantle material up thrust with part of the Central Arunta Province (after Goleby et al., 1990)

However, in Europe the Caledonian and Variscan orogenic belts show no sign of their crustal root, possibly due to late stage extension which overprints the previous compressional features by tectonic delamination of the root (fig 2.7).

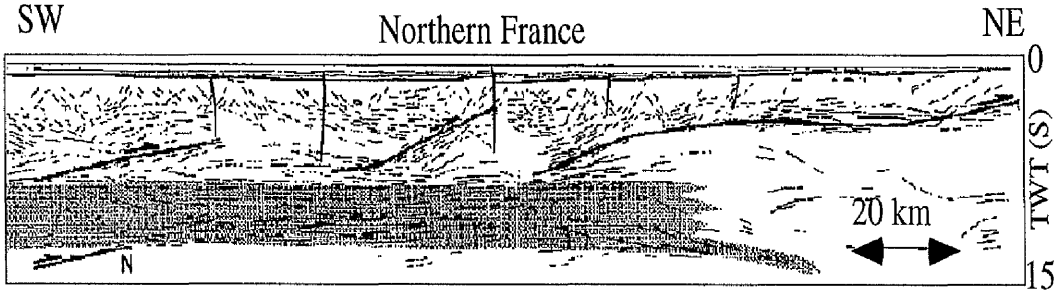

Figure 2.7: Line drawing of un-migrated, seismic section across the Variscan belt in western France. On this section the lower crust appears highly reflective with no obvious crustal root (after Pinet & Colletta, 1990).

c) Mesozoic orogens and younger

Some good examples of seismic structure of younger orogenies are provided by the Swiss Eastern Alpine and Pyrenees profiles. These profiles, like most other young orogenic belts, shows crustal roots that are approximately in isostatic equilibrium with

their high topography. In the Alps, the lower crust dips towards the centre of the root from both sides and shows strong seismic laminations which terminate at about the refraction Moho (fig 2.8). England and Houseman (1989) suggested that extensive crustal shortening and deformation along the shear zones in the Alps might have delaminated the lower crustal material beneath the deepest part of the root, causing strong reflective patterns. The seismic profile across Pyrenees (fig 2.9) indicates two important points, crustal shortening accompanied by crustal thickening and Moho offset.

d) Recently extended crust

Regions such as Western Europe and the Basin and Range (USA), where the last tectonic event was extensional, produce excellent reflection data (Matthews, 1986; Le Gall, 1990; Warner, 1990a &1990b). In these areas the upper crust is transparent to seismic waves whereas the lower crust is highly reflective. The Moho appears flat, highly reflective and continuous (fig 2.10).

2.3.3 Reflectivity of the CLC

The lower crust is commonly characterised as a highly reflective zone in which numerous short, horizontal to sub-horizontal, reflections occur. These seismic reflection, can only occur if there are interfaces between two media with contrasting acoustic impedance (the acoustic impedance is the product of density and seismic velocity). Warner (1990c) has shown that bright reflections in the lower crust have normal incidence reflections coefficients of around 0.1. This requires an acoustic impedance contrast of about 20%.

As indicated earlier, many explanations for reflectivity of the CLC and its laminated pattern have been proposed. There are lines of geological and geophysical evidences which supporting each of the various hypotheses. At the same time there are some geological and geophysical objections. Recently Warner (1990c) & Jones (1992) have discussed some of the proposed explanations in detail, therefore no discussion of individual models has been presented here. However in chapter 9 some of the proposed models will be challenged.

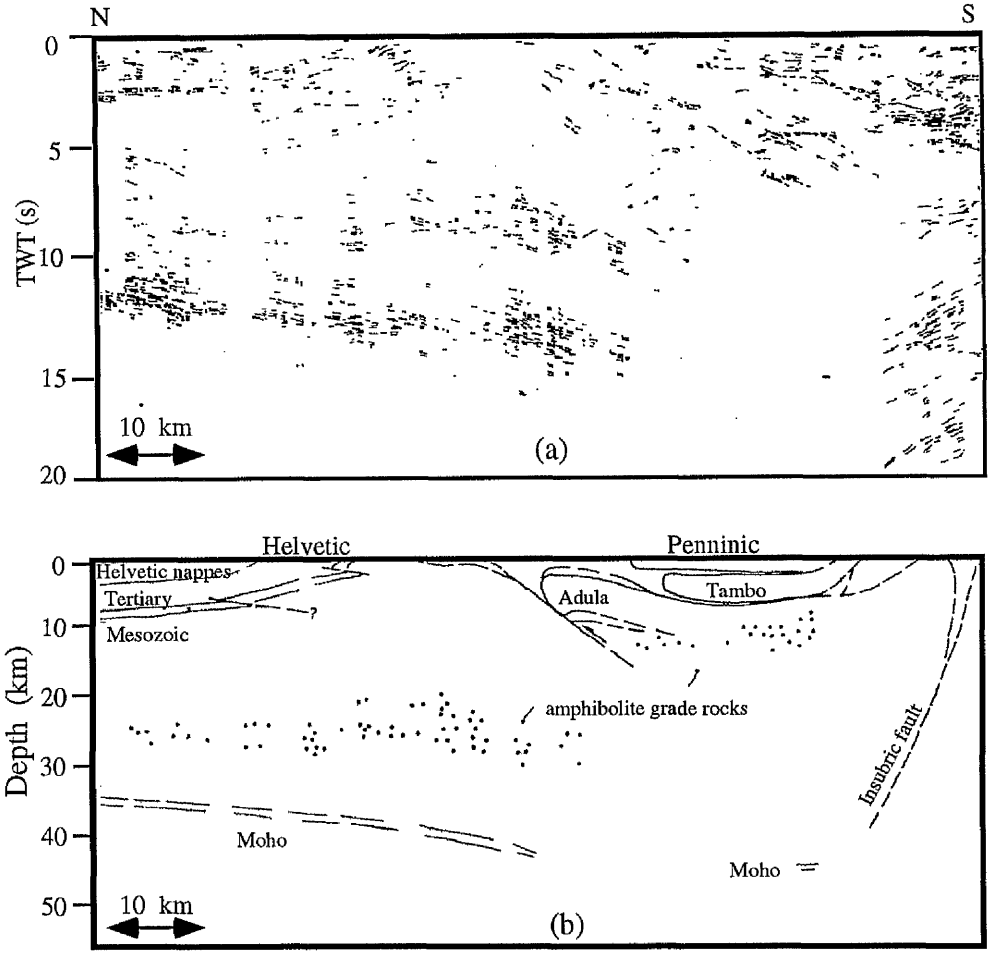

Figure 2.8: (a) Composite line drawing derived from individual shot gathers of a reflection profile (NFP 20-EAST) along a north-south transect across the Alps of eastern Switzerland. Horizontal reflections can be tracd over several shots. (b) preliminary geologic interpretation. (after Pfiffner et al., 1988).

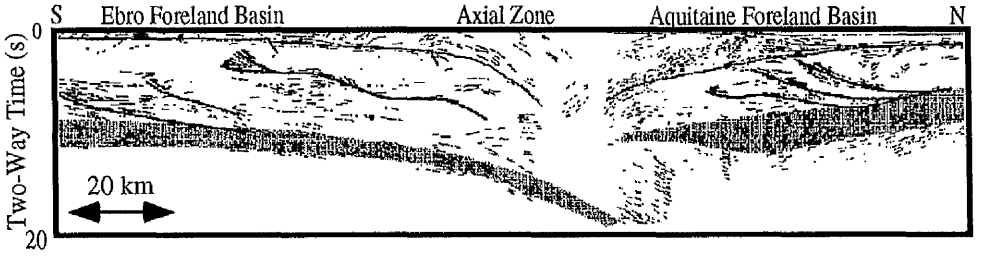

Figure 2.9: Line drawing of seismic reflection within the Aquitaine foreland along the ECORS Pyrenees Line. The section shows northward lithospheric convergence (after Choukroune et al., 1990).

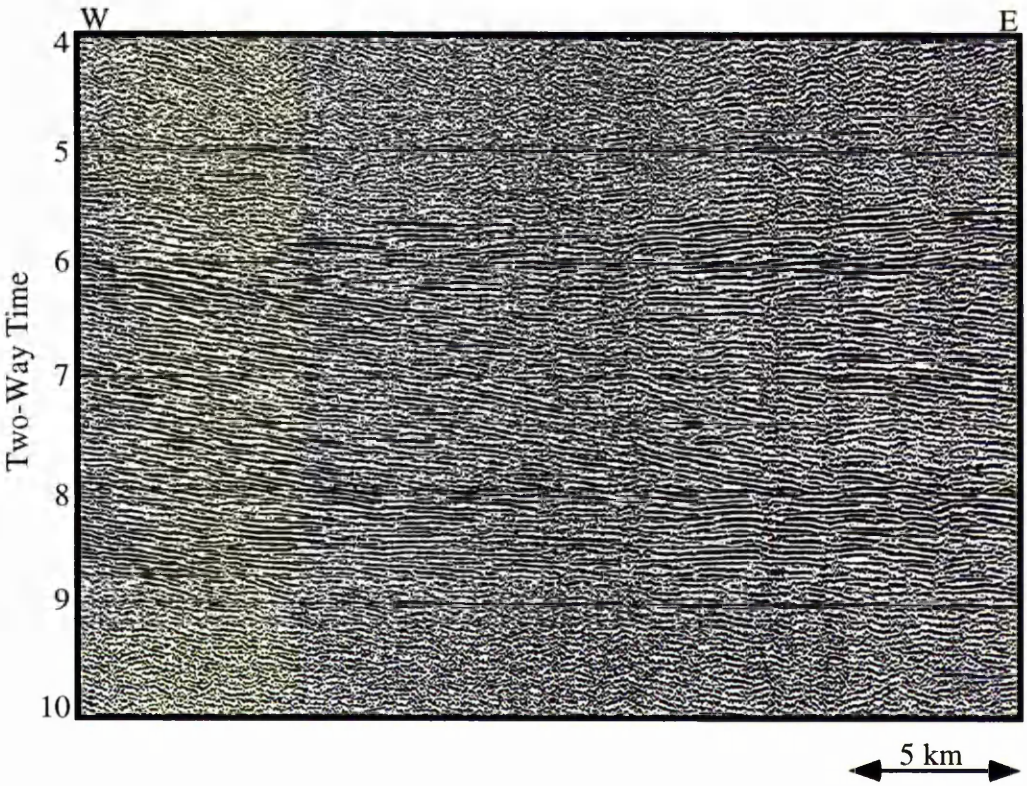

Figure 2.10 : Deep seismic reflection profile recorded in the Black Forest, SW Germany. Crustal reflectivity increases sharply at about 5.5 s two-way time and terminates at about 9 s. Extensive lower crustal lamella and high amplitude of the reflections require alternating layers with large velocity and/or density contrast (after Lueschen et al., 1987).

2.3.4 Laboratory Measurements

The physical properties of rocks that originated from the lower crust and upper mantle can be measured in the laboratory. The result of such experiments can be used to help evaluate some of the explanations proposed for high reflectivity of some lower crustal sections and seismic patterns (e.g. possible shear zones, wedges) associated with them. Seismic compressional and shear wave velocities of rock samples are measured using ultrasonic velocity methods. The seismic velocity of crustal rocks primarily depends on the following environmental factors and intrinsic characteristics:

i) Hydrostatic pressure

ii) Temperature

iii) Pore fluid pressure

iv) Mineralogy and mineral chemistry

v) Mineral preferred orientations

vi) Density.

Any accurate laboratory measurements of seismic velocity of deep crustal rocks should be conducted with attention to all the six factors above. Estimation of pressure and temperature of the crust is moderately well constrained but little is known about the anisotropy and fluid content. Therefore it is important to combine the laboratory measurements with geological and mineralogical data wherever is available.

The effects of pressure and to a lesser extent, temperature on seismic velocity have been studied for a number of years (e.g. Birch, 1960; Christensen, 1965; Kern & Richter, 1981). These results indicate a linear velocity-pressure relationship for dry and crack free or closed rocks. Temperature dependence of seismic velocity has not been studied as thoroughly as the pressure effect. This is mainly due to the technical problems associated with such measurements (see chapter 5). Generally, as temperature increases, velocities decreases, with typical temperature coefficient of velocity about 2.0-6.0×10^{-6} km/s/°C (e.g. Kern, 1982).

The effect of pore pressure on the velocity of compressional and shear waves is considered to be very important in low-porosity rocks. Todd & Simmons, (1972) confirmed the theoretical results of Brandet (1955) and Biot (1956), suggesting that

effective pressure is the determining factor in the behaviour of seismic waves not the pore pressure. The work Christensen (1984) concludes that pore pressure plays an important role in influencing the velocity and elastic moduli of rocks. Their findings show that at constant confining pressure, both shear and compressional velocities are lowered by increasing pore pressure. When both confining pressure and pore pressure are varied, velocity increases with increasing effective pressure at constant pore pressure. The effect of pore pressure can be important for the study of the physical properties of lower continental crust and upper mantle rocks where the water is released as the dehydration of hydrous minerals takes place. In this situation the pore pressure may rise to a substantial fraction of the total mean pressure.

Recent results of deep seismic reflection profiling and teleseismic data indicate a strong seismic anisotropy of lower crustal and upper mantle rocks (e.g. Mainprice & Silver, 1992 and Barruol & Mainprice, 1993). These results, plus some laboratory measurements, show the importance of seismic anisotropy in deep crustal rocks. Due to high pressure at lower crustal depth (800 -1000 MPa) and high temperature (≥ 350 °C) no cracks or pores can be open therefore the presence of oriented cracks is not the source of seismic anisotropy (unlike in upper crustal rocks). Lattice preferred orientation of constituent minerals of a crystalline aggregate can account for seismic anisotropy. To evaluate seismic anisotropy in the laboratory it is common to measure the seismic velocity of each rock in three orthogonal directions (see chapter 6).

Once the effect of pressure, temperature, pore fluid pressure and seismic anisotropy are accounted for, it is justifiable to consider the seismic velocity of deep rocks to depend mainly on mineralogical composition. Therefore seismic velocity can be used to infer composition. Thus by comparing the velocities determined in the field experiments with laboratory data we might make inferences about the composition of lower crustal rocks.

2.4 Summary

In this chapter the different methods and techniques which are used to obtain geological and geophysical information about the CLC have been described. Their

advantages and their limitations have been briefly described.

It has been explained that lower crustal sections are brought to the surface by various mechanisms. These sections are a source of important information regarding the structure and nature of the CLC. The dominant rocks are ultramafic, metabasic and metasedimentary and there is a transition from granulite facies rocks to amphibolite facies rocks. The average composition of the CLC is seems to be intermediate (dioritic).

There are lower crustal regions (e.g. Baltic shield) which show anomalous electrical conductivity. The electrical conductivity of these regions some areas is some order of magnitude higher than the conductivity of dry crystalline rocks. Many theories have been suggested to explain this high electrical conductivity. The most favoured one is the presence of saline water. Although it is proven that even a low percentage of water can increase the electrical conductivity dramatically (but if pore pressures are high) there are strong lines of petrological evidence which make this explanation seen unlikely.

Deep seismic reflection profiling have been used for studying the structure of the continental crust. Most of deep seismic profiles show the CLC, as a zone of high reflectivity. This zone is variable in its reflectivity, the size and length of reflectors. Generally the reflectors are horizontal to sub horizontal. The reflectors are very strong and dense within the crust which has gone under extension recently. The reflectivity of the CLC seems to be due to combination of factors such as mineral composition, pressure, temperature and deformation. Deep seismic reflection profiling has a number of limitations. Mostly it cannot resolve a reflector thinner than about 25 m and shorter than about 1.5 km. Moreover, lack of borehole control makes the interpretation of the data fraught with uncertainty.

Laboratory velocity measurements carried out at room pressure and temperature show very similar velocities for most lower crustal rocks. However, combination of the effects of temperature, pressure and pore fluid pressure plus strong anisotropic minerals may produce sufficient velocity and density contrasts, which can account for the observed high reflection coefficients in the lower crust.

Chapter 3

Ivrea-Verbano zone and Serie dei Laghi: General Geology & Sample Collection

3.1 Introduction

In the previous chapter it was explained that important knowledge regarding the continental lower crust comes from the study of exposed lower crustal profiles and that the Ivrea-Verbano (IV) zone plus the adjacent Seri dei Laghi (S.d.L) is one of these. The IV zone has number of advantages compared to the other exposed lower crustal sections. These are the extensive exposures, rock freshness and a complete section from middle continental crust of SdL to lower crust close to the Moho in the adjacent IV zone. These advantages have attracted many geoscientists to study the area. Extensive geological information has been collected during past few decades from the IV zone (e.g. Schmid, 1967; Zingg, 1990; Boriani et al, 1990; Brodie et al., 1992; Rutter et al., 1993 & Quick et al., 1994).

It is not within the scope of this study to explain all the geological aspects of the IV zone/SdL. This chapter is intended to provide a brief summary of lithology and structure of the IV zone/SdL. It starts with a short review of the geology and the major rock types of the region. The method of collecting samples for the petrophysical and mineralogical studies carried out during this research are also described.

3.2 Geographical and Geological Setting

3.2.1 Geology of the Ivrea-Verbano Zone

The Ivrea-Verbano zone is located in the north-west Italy. It is bounded to the south-east by the Serie dei Laghi, a 'relatively' low grade terrain of schist, granites and ortho-gneisses and to the north-west by a greenschist facies belt of mylonites known as Insubric line which separates it from the main Alpine metamorphic rocks (fig 3.1). It is about 100 km along strike and 20 km across strike (at the widest points). The zone consists of a steeply dipping series of pelitic and mafic rocks with lenses of calcareous and ultramafic rocks (figs 3.2 & 3.3).

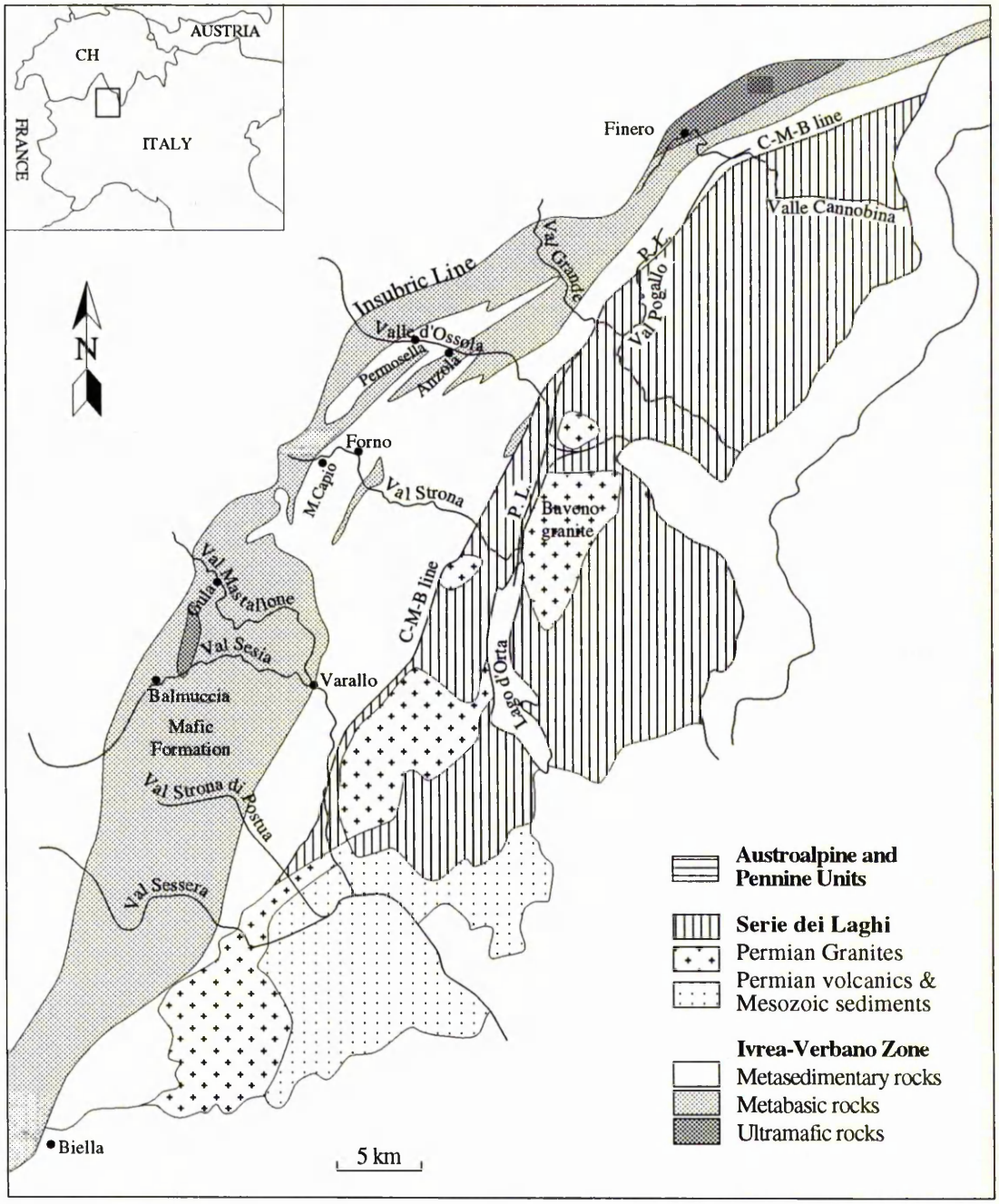

Figure 3.1: Simplified geological map of the Ivrea-Verbano zone, the adjacent Serie dei Laghi and surrounding areas. (P.L. = Pogallo Line/fault, C-M-B = Cossato-Mergozzo-Brissago after Zingg, 1980).

(a)

(b)

Figure 3.2: General views of Ivrea-Verbano zone. (a) View north side of Val d'Ossola taken from near Anzola. The approximate height from valley floor to the ridge is about 2 km. (b) View looking east of the upper part of Val Mastallone.

(a) (b)

Figure 3.3: (a) View north along Val Grande, illustrating typical access difficulties. (b) View of the north side of Valle d'Ossola showing the Massone antiform.

Metamorphic grade increases from mid-amphibolite facies in the south-east to granulite facies in the north-west. Metamorphism took place during the Caledonian, Hercynian and Alpine orogenies. It is generally agreed that the IV zone represents a section through the late/post Hercynian lower continental crust which has been uplifted and tilted to its present position during Alpine orogeny (Zingg et al., 1990).

The central and southern parts of the IV zone are dominated by a major basic complex which is intrusive into the surrounding gneisses. A wide zone of migmatization of country rocks is seen in the contact with the dioritic roof of the mafic complex (Brodie et al., 1992). Several high temperature shear zones cutting the regional banding at low angle have been observed in many parts of IV zone (e.g. Schmid, 1967; Boriani et al., 1977; Brodie, 1980; Brodie & Rutter, 1987; Rutter & Brodie, 1992; Evans, 1995). Brodie and Rutter (1987) interpreted these high temperature shear zones as low-angle extensional faults which accommodated the thinning and extension of the sequence under sub-solidus lower crustal conditions.

Results of geophysical investigations (Wagner et al., 1984) suggest that the upper mantle rises from about 30 km depth to close to the surface (about 3 km) under the IV zone. Recent gravimetric and vertical seismic reflection profiles support this interpretation (fig 3.4; Wagner & Mueller, 1984). These geophysical data support the geological interpretation that the Ivrea-Verbano zone represents a very deep crustal slab. Geothermometric and geobarometric investigations of Schmid & Wood (1976) suggest temperatures of 700 - 820°C and pressures of 9-11 kbar for the high grade part of the IV zone. Recent work by Smith (1995) indicates a temperature range of 640 - 1000°C and a pressure range of 6.7 to 12.9 kbar for the northern part of the IV zone (Val Strona to Val d'Ossola).

3.2.2 Geology of the Serie dei Laghi

The Serie dei Laghi is situated to the SE of the IV zone, separated from it by the Pogallo fault and Cossato-Mergozzo-Brissago (CMB) line (fig 3.5 & see fig 3.1). It consists mainly of a series of, paragneisses, orthogneisses and schists which have been studied by Boriani et al., (1990). Rocks within this zone are of amphibolite facies and

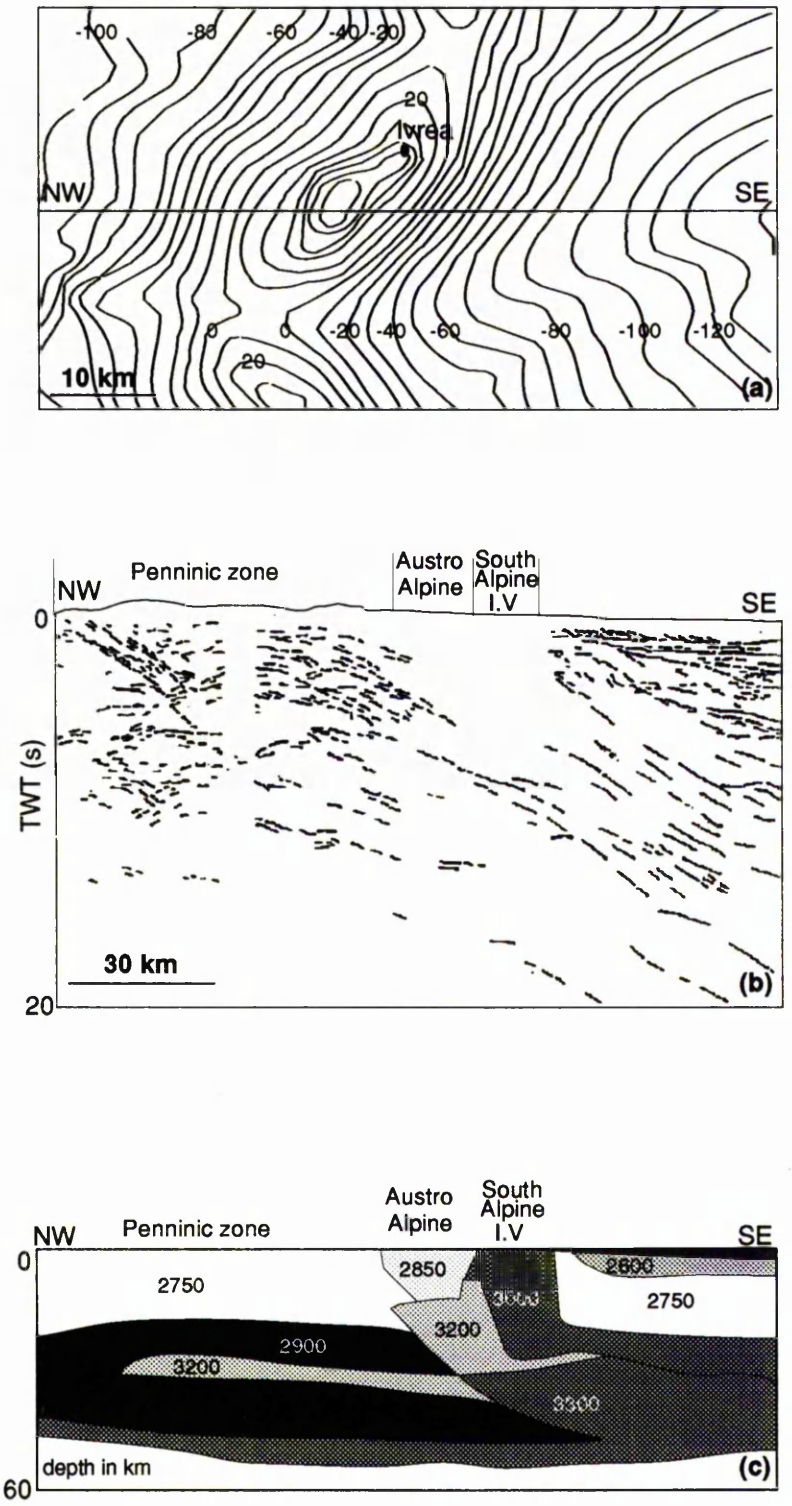

Figure 3.4: Geophysical data from southern border of the Western Alps. (a) Bouguer gravity anomaly map (mgal) of the Western Alps. The positive highs correspond to the geophysical Ivrea-Verbano anomaly. (b) Line drawing of seismic reflection a long the Western Alps. (c) A density (g/cm^3) model of the Western Alps showing the up lifted Lower crust.

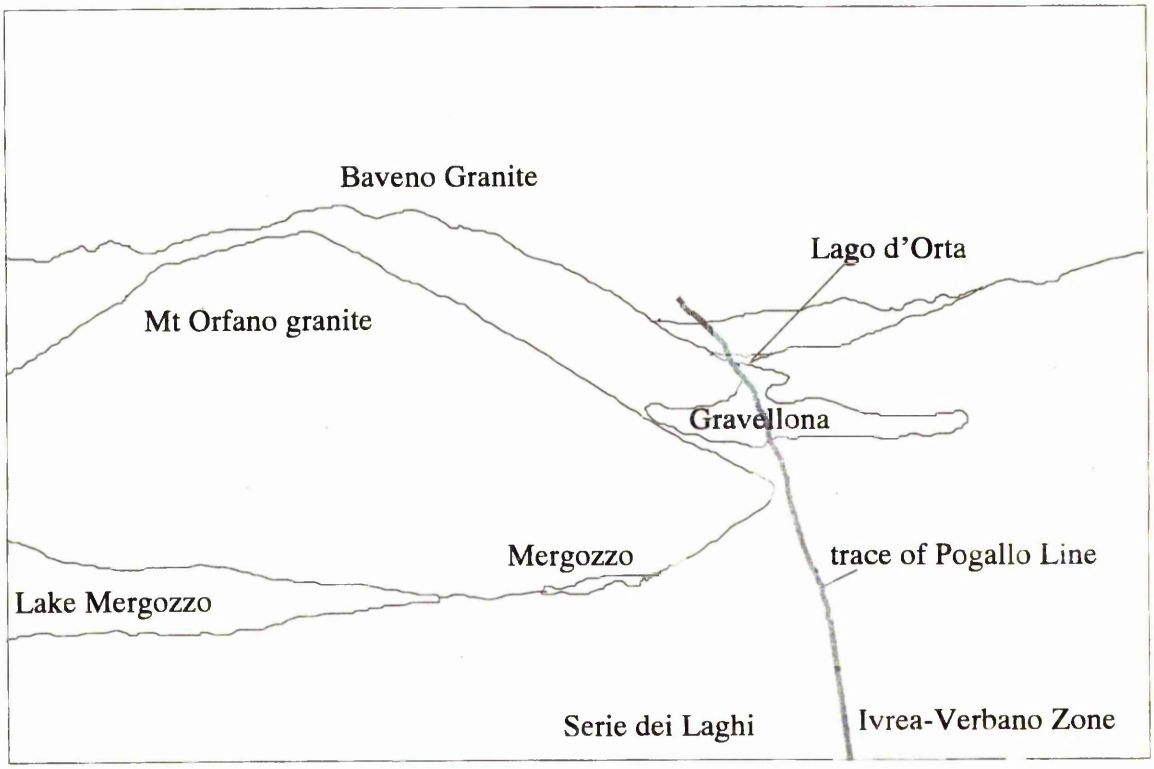

Figure 3.5: View south towards Lago d'Orta, along the trace of the Pogallo Line.

sometimes show poikiloblastic textures. A number of calc-alkaline granitic and granodioritic bodies are seen emplaced in the SdL. These show no sign of deformation therefore are considered as post-metamorphic intrusions. Only a few samples from the SdL were collected for seismic study as the zone represents middle crustal rocks which were not the main focus of the present work. Moreover, a comprehensive velocity evaluation of the rocks has already been carried out by Fountain (1976) and Burlini (1990, 1991).

3.3 Lithologies in the Ivrea-Verbano Zone

Metasedimentary, metabasic, basic and ultrabasic are the major rock types in the IV zone. Metasedimentary and metabasic rocks dominate, and occur mainly as continuous and parallel layers whereas ultrabasic rocks occur as scattered lenses. The metasedimentary rocks consist of metapelites, metasemi-pelites, metaquartzites and calc-silicate marbles. The metabasic rocks are partly interlayered with the metasediments. The southern part of the IV zone (south of Val Strona) is dominated by a large basic-ultrabasic body, known as the Mafic Formation. Some clearly igneous textured mafic rocks such as gabbro and diorite are present within the Mafic Formation, which is intrusive into the surrounding gneisses. Other large, metabasic bodies such as the Anzola gabbro are also considered to be intrusive. The ultrabasic rocks include scattered dunite, peridotite and pyroxenite lenses, more frequently orienting towards the north-west.

3.3.1 Metasedimentary rocks

Metasedimentary rocks are the most abundant rocks in the NE part of the IV zone. They range in composition from metapelites to metaquartzite and calc-silicate marble. As metamorphic grade increases from amphibolite facies in the south-east to granulite facies in the north-west, the mineralogy of the metasediments also changes (Bertolani, 1968; Hunziker & Zingg, 1980). Generally the most mica-rich metasediments occur in amphibolite facies region and are locally referred to as kinzigites (fig 3.6). The most garnet rich metasediments occur in the granulite facies and are

known as stronalites. The metasedimentary rocks, with the exception of marble, are therefore classified into two groups (kinzigite and stronalite, Zingg 1980). Biotite is normally well oriented within the kinzigite. Stronalite has less biotite and a coarser grain size than kinzigite. It shows strong compositional banding (on a centimetric to decimetric scale; fig 3.7). Segregation of mafic (garnet & sillimanite) and felsic (quartz & feldspar) phases into different horizons define these bands, which are probably the products of migmatization.

It is not always easy to distinguish between kinzigite and stronalite as they pass from one to the other as the distinction is based on the garnet to biotite ratio. This ratio depends on original chemical composition as well as metamorphic grade. For this reason the two units are commonly not distinguished on geological maps although their seismic velocity characteristics are quite different (see chapter 6).

The marbles and calc-silicates are relatively abundant within the metasediments. These carbonates mainly occur as lenses or bands. They can be as long as 700 m and 200 m wide, as reported by Evans (1995). They contain a large variety of mineral assemblages (Zingg, 1980). Marbles in the IV zone appear to have been extremely ductile under the peak metamorphic condition (fig 3.8). This is also demonstrated by a strong crystallographic preferred orientation of calcite grains (see chapter 6).

3.3.2 Metabasic rocks

The basic rocks in the IV zone can be divided into two groups, (a) the basic rocks which are interlayered with the metasediments, and (b) large bodies of basic rocks which are intrusive into the sequence, some of which presence igneous textures.

(a) Basic rocks interlayered with the metasediments

These rocks have a similar metamorphic history as the metasediments. Amphibolite facies metabasic rocks dominate the south-east part of the IV zone, and granulite facies rock are volumetrically prominent in the north-west. The boundary between these two facies is defined by the appearance of orthopyroxene in metabasic

Figure 3.6: Photograph of a Kinzigite within which there are bands of biotite-rich melanosome and quartz-feldspathic leucosomes from Val Sesia.

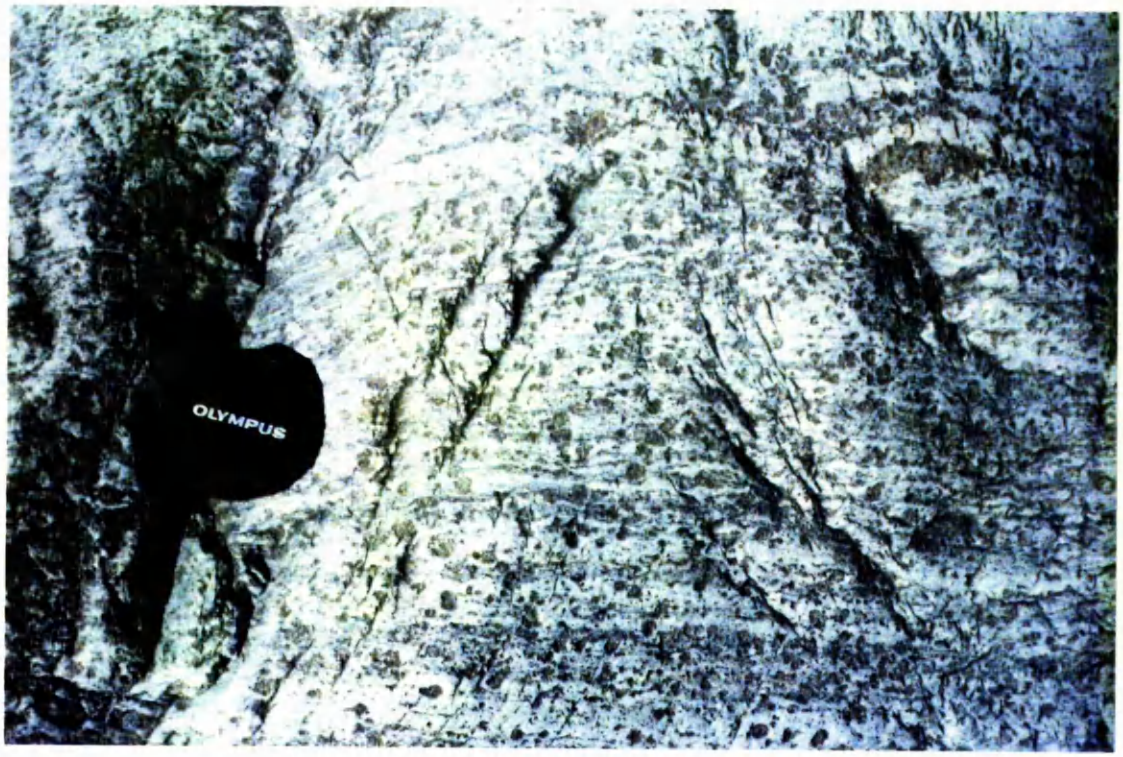

Figure 3.7: Photograph of Stronalite, showing strong compositional banding, from Anzola village .

(a)

(b)

Figure 3.8: Photographs of heavily deformed marble. (a) folds of metapelitic bands in mylonitic marble. (b) Metapelitic lithoclasts within mylonitic marble.

rocks, and in many places (e.g. Val Strona, Vall d'Ossola) this boundary lies parallel to the compositional banding.

The amphibolites occur in the form of layers or lenses ranging in thickness from a few centimetres to about 500 m. These rocks often show strong compositional banding defined by mafic and felsic horizons (fig 3.9). Some small bodies are also well foliated due to aligned elongated hornblende. Granulite facies metabasic rocks in places such as Val Strona and Val d'Ossola are represented as massive metabasic bodies (two pyroxene-plagioclase-garnet). They show compositional banding on the scale of a few centimetres with a granoblastic polygonal texture and interpreted as basic lavas (Sill & Tarney, 1984; fig 3.10).

(b) Intrusive, igneous textured Basic rocks

In the south of the IV zone, in Val Sesia, there is a large mafic body, known as Mafic Formation which contains rocks ranging in composition from mafic to ultramafic (Rivalenti, 1981). The top part of the mafic formation mainly consists of gabbro (fig 3.11) which gradually changes to diorite upwards (fig 3.12). The diorite forms the roof of the mafic formation from Val Mastallone to Val Sesia and even further south to Val Sessera. It is generally agreed that the mafic formation was formed from a magmatic body, either during episodes of magma underplating or by intrusion deep into the crust and involving in the melting of some crustal rocks (Quick et al., 1994; Quick et al., 1995). Crustal melt mixed with mafic magma led to production of amphibole bearing gabbros, norites and charnockites. Whatever was left over from the melt formed migmatite (fig 3.13) and migmatitic kinzigite (fig 3.14) of the country rock assemblage.

3.3.3 Ultrabasic rocks

The ultrabasic bodies in the IV zone are composed of peridotites, pyroxenites and dunites. Most ultramafic bodies crop out within the granulite facies part of the IV zone, close to the Insubric fault zone. They range in length along strike from a few meters to a few kilometres. The largest and best studied bodies are the Balmuccia and Finero peridotites. These ultrabasic bodies are believed to have various origins. Shervais

Figure 3.9: Photograph of banded amphibolite, showing strong compositional banding defined by hornblende and plagioclase rich horizons.

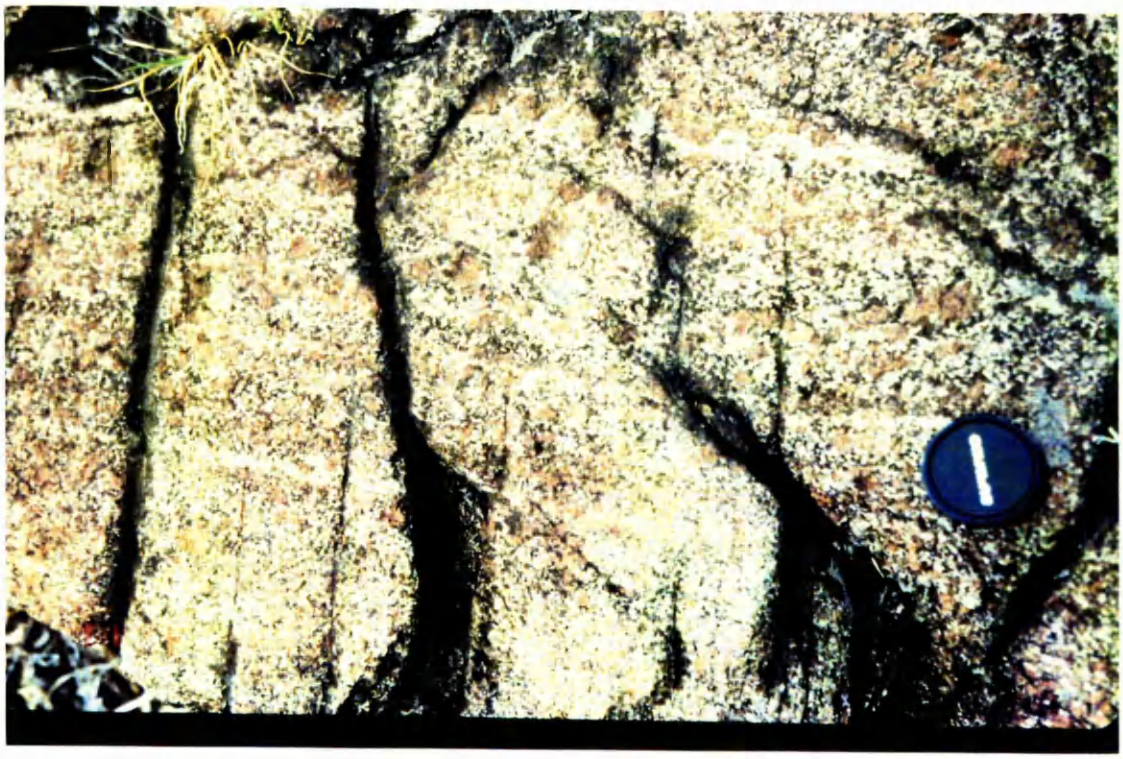

Figure 3.10: Photograph of garnet-plagioclase-pyroxene granulite. Strong compositional banding associated with these rocks are defined by felsic horizon rich in plagioclase and mafic horizons rich in garnet or/and pyroxenes.

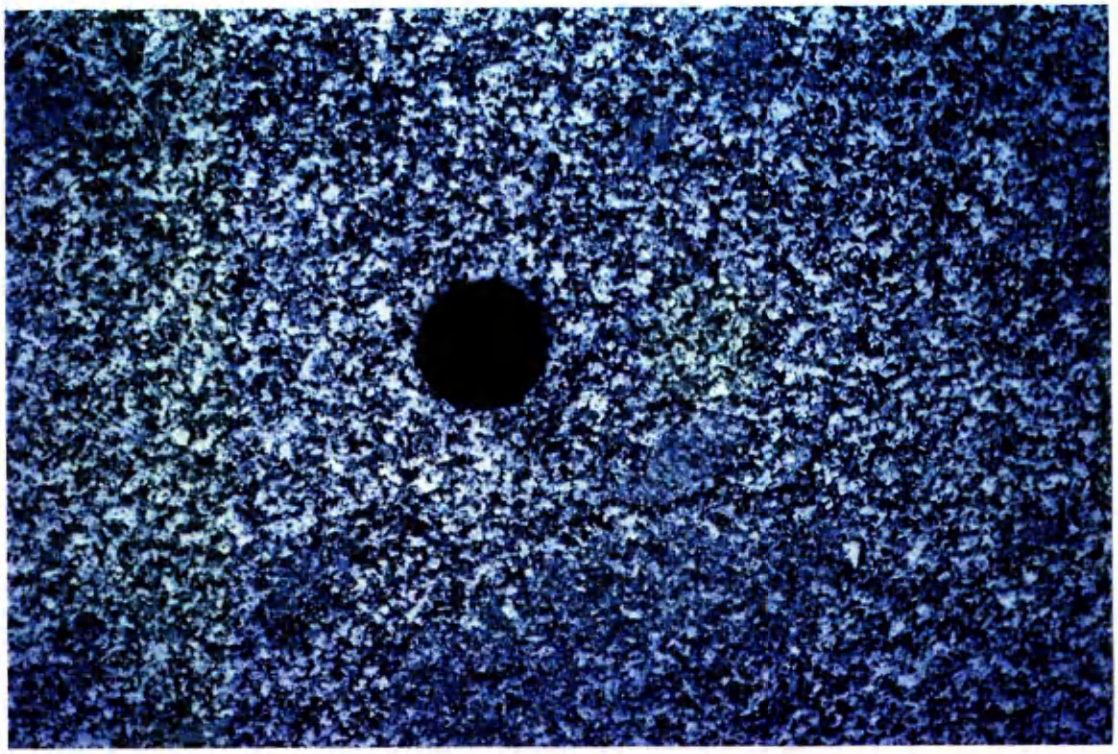

Figure 3.11: Photograph of Diorite (from Val Sesia) that forms the roof of Mafic Formation.

Figure 3.12: Photograph of Gabbro (from Val Sesia) which shows a pre metamorphic peak folding (possibly a magmatic slump fold).

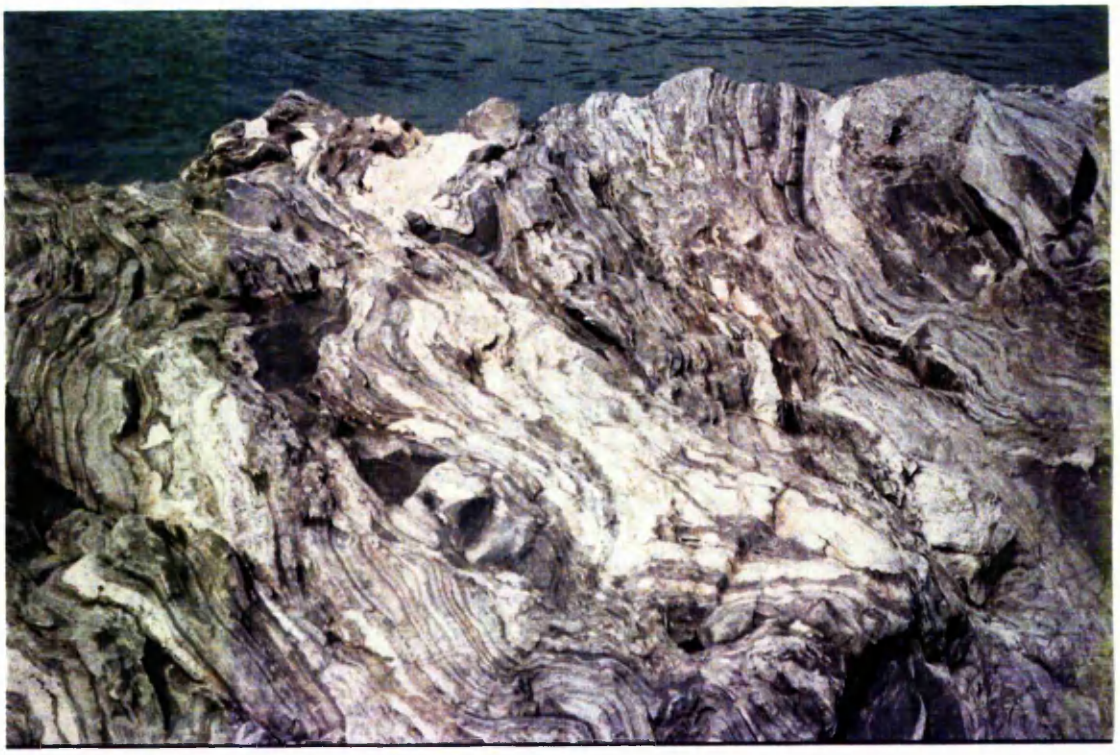

Figure 3.13: Photograph of migmatite from Val Sesia, showing mafic boudinage bands within less competent felsic layers.

Figure 3.14: Photograph of migmatitic kinzigite from Val Sessera.

(1979) believed that some of these peridotite bodies (e.g. Balmuccia) were emplaced at the bottom of the crust during magmatic underplating. This suggests that the petrological Moho can be observed in the IV zone. The validity of this argument has been challenged with new field geological information (Quick et al., 1995) indicating that the Balmuccia peridotite is surrounded by metasedimentary and metabasic rocks.

The Balmuccia peridotite body is a large (3 km × 1 km) spinel-peridotite and lherzolite which forms part of the Mafic Formation in Val Sesia (fig 3.15). It is regarded as being formed by differentiation from the mantle (Ernst, 1978; Rivalenti et al., 1981). Within the Mafic Formation a number of other ultrabasic bodies (dunites, harzburgites and pyroxenite) can be found interlayered with gabbros. These ultrabasic bodies are considered to have originated by lower crustal magmatic differentiation (Rivalenti, 1978 &1979; Rivalenti et al., 1981).

The largest ultrabasic body in the IV zone is the Finero peridotite situated in Valle Cannabino (fig 3.16). It consists of two units, a core of phlogopite peridotite and an outer zone of hornblende peridotite. These two units are separated by a metagabbroic layer which has undergone granulite facies metamorphism (Ernst 1978). The origin of the Finero peridotites is not well understood. Lensch & Rost (1972) suggested that it is a fragment of solid mantle body which was tectonically up lifted and emplaced into the lower crust. However, Cowthorn (1973) believed that it was injected into the lower crust as a hydrous mafic-ultramafic melt, which subsequently differentiated through crystal fractionation.

3.4 Sample Collection

In order to construct a velocity structure of the IV zone as realistically and accurately as possible, the most representative geological units were sampled systematically as well as extensively. During two field seasons about 558 oriented cores and 16 rock blocks from at least 40 lithological units were collected (appendix 1). Optical and electron microscopy was used for petrological and mineralogical characterisation of the samples (see chapter 4). Microstructure and fabric of some of the highly deformed samples were studied in order to investigate the effects of CPO on

Figure 3.15: Photograph of Balmuccia peridotites in Isola (looking north) separated by a fault from a more oranged colour dunite body.

Figure 3.16: Photograph of Phlogopite-rich Finero peridotite which shows discontinuous bands defined by clots of phlogopite (Centimetric scale bar).

seismic properties. The best cores from each lithology were used for seismic velocity measurements.

3.4.1 Representative Nature and Freshness of Samples

Collecting samples of highly deformed rocks that have been exposed at the surface for a long time raises the question of how representative are these rocks of fresh and intact lower crustal rocks. Direct collection of lower crustal rocks is impossible for the present. Therefore, with exception of lower crustal xenoliths (which may be highly altered), rock samples from lower crustal exposures such as the IV zone are the best that one can expect. Rocks that appear fresh in hand specimen may contain narrow zones of alteration or grain boundary alteration, on a microscopic scale. Retrogressive metamorphism may destroy the original mineral assemblages of the rocks. In the IV zone retrogressive effects are largely limited to late greenschist facies faults. However, effects of weathering and fracturing are widely present. Fracturing is a particular problem in the fine grained mylonites. These disadvantages can be limited by systematic sample collection, and avoidance of altered and weathered areas.

Apart from freshness of the samples, the following points were observed during sampling:

i) Samples should be ideally of small grain size (less than 1 mm) for ultrasonic velocity measurements due to the small wavelength used (a few millimetres) and for a representative number of grain within the sample.

ii) All structural information (e.g. lineation, foliation, degree of plastic and brittle deformation) must be measured and noted at each exposure.

iii) If the rocks showed compositional banding, the aim was to collect cores from area where these bands were thin allowing several bands to be sampled in one core.

iv) Extra numbers of cores were collected from highly heterogeneous units (e.g. stronalites, charnockites, migmatite) in order evaluate the effects of this heterogeneity.

3.4.2 Coring Equipment

It was clear from the start that it would be difficult to sample more than 30 geological units as blocks by means of hammer and chisel. Therefore it was decided to core the rocks in situ. The advantages for coring are:

i) Coring is not limited by the size or place of exposures

ii) The total weight of collected samples can be greatly reduced

iii) The cores can be examined in the field for freshness and presence of cracks by using a hand lens

A hand held drilling rig was used for coring. It comprises a portable petrol-driven drill, a pressurised water tank and diamond-crowned coring bits (fig 3.17). The drill uses a two-stroke light petrol engine. The water tank has a capacity of about 20 litres and a hand pump can produce a maximum pressure of about 3 bars inside the tank. The water tank is connected via a high pressure pipe to a water swivel which is, in turn, connected to the 3-jaw drill chuck. The diamond crowned bit is screwed to the end of the water swivel.

3.4.3 Coring Procedure

Once the coring equipment is assembled the coring operation may proceed (fig 3.18). First the water container has to be pumped several times to pressurise adequately the water. By turning the tap on the water swivel, water flows through the water hose, through the end of drilling tool. Pressurised water is necessary for two reasons. Firstly it cools the tool so it improves its performance and increase its life. Secondly, it forces rock fragments out of the hole and prevents the drill becoming jammed.

After selecting a place for coring, the rock was marked at the point of coring so the original orientation of the core would be noted. The rate of drill penetration depends on many factors such as the toughness of the rock, water pressure, condition of drilling tools and most importantly the operator. It was essential to hold the drill firmly and straight otherwise the vibration would either break the tool or the core or result in a bent or tapered core. It was found that by starting the drill slowly at the beginning, not only would the drill not vibrate excessively, but also the core would be much straighter. Once

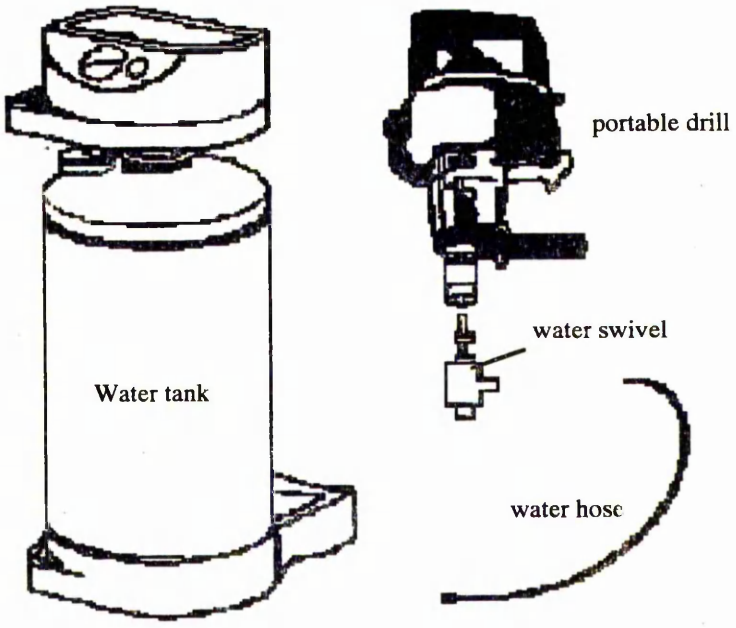

(a)

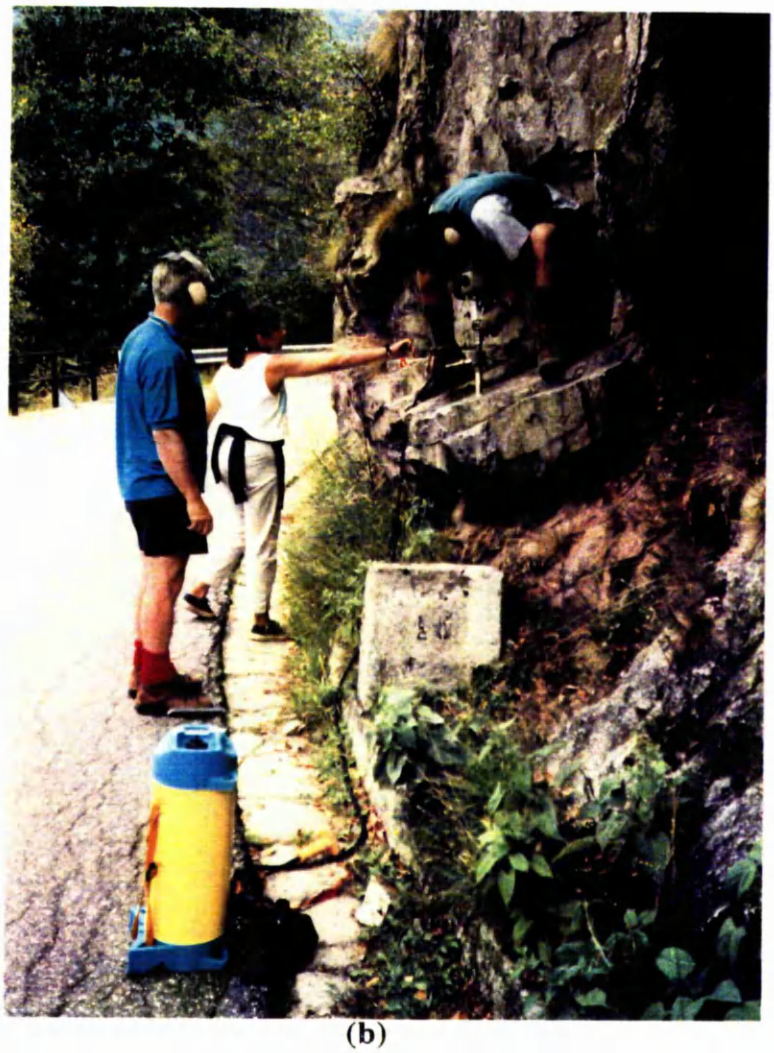

(b)

Figure 3.17: (a) A schematic drawing of the drilling rig. (b) Photograph showing the hand held drilling rig in operation with its various parts.

Figure 3.18: Photographs showing drilling at various exposures. Drilling generally required the help of at least one other person.

the tool is a few centimetres in the rock then the speed of the drill can be increased. A uniform pressure on the drill is essential to avoid uneven core diameters or stepped cores.

Where the rocks were hard to drill (as was commonly the case) the force of more than one person was needed to push the drill in, especially for non-vertical holes (fig 3.19). Extra care had to be taken to keep the drill and the tool straight otherwise the core or even the tool would break. Once the core is broken, it is difficult to take it out of the tool. Ideally, the core would be still attached at its base to the rock. Before breaking it and taking the core out it was marked so its orientation could be measured.

3.4.4 Core Orientation

Cores were collected in at least three orthogonal directions defined by planar and linear structures in the rock (Fig 3.20). Therefore the orientation of the cores had to be measured with respect to these structures so that later the measured seismic velocities could be related to the field structures. Where no foliation or lineation was evident, three orthogonal direction was chosen to correspond with the usually known regional banding and lineation attitudes. Although all efforts were made to core the rocks exactly along the above structural directions, due to the vibration of the drill and an imperfect positioning of the tool the core directions can differ from the derived orientation by as much as ±10 degrees.

To orient the samples, the dip and dip direction of the holes were measured using a specially corresponded compass/clinometer (fig 3.21). This allowed the measurements of the orientation of the holes within ±2 degrees on plunge and azimuth. Measurements were made in three steps; first, by inserting the tube attached to the measuring tool into the hole, secondly by levelling the two spirit levels on the compass platform. This was done by rotating the tool along the hole axis coupled with tilting the compass platform, backwards or forwards. Finally the compass can be adjusted so the red needle is directly above the red arrow of the compass. The reading for each core orientation would consist of a pair of numbers of three digits and two digits respectively indicating the azimuth and the plunge of each core. The direction of the plunge was marked as an arrow on the top

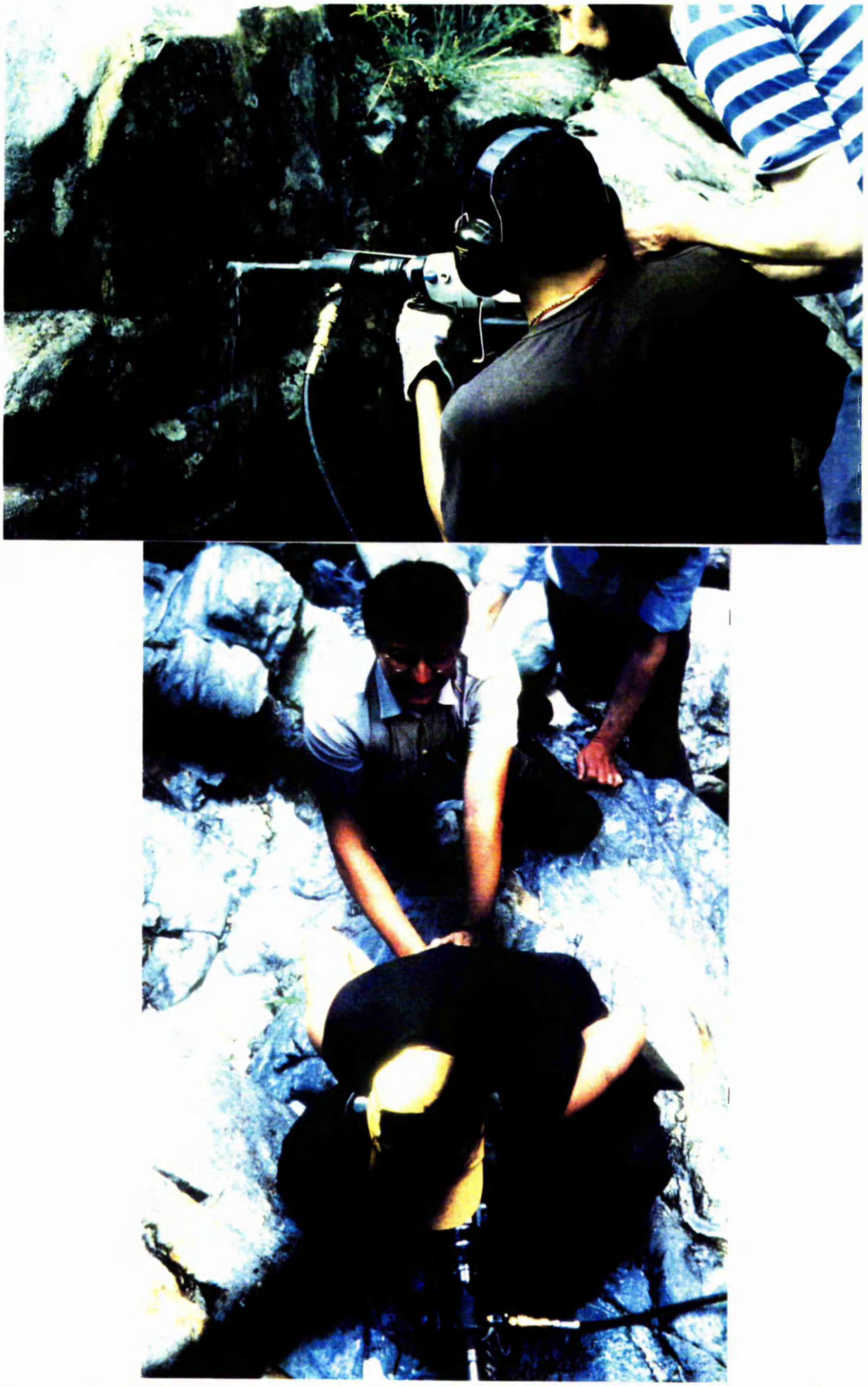

Figure 3.19: Photographs showing drilling at various exposures. Drilling sometimes was facilitated by help from a number of people.

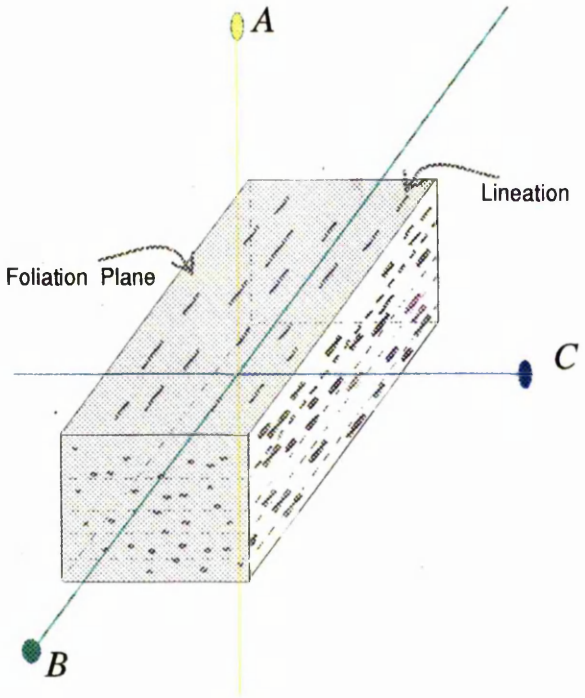

Figure 3.20: Schematic diagram showing the three orthogonal directions defined by planar and linear structures in the rock which were used for labelling the cores cores. '**A**' defines the direction normal to the foliation plane, '**B**' is for the direction parallel to the foliation the lineation, and '**C**' defines the direction parallel to the foliation and normal to the lineation.

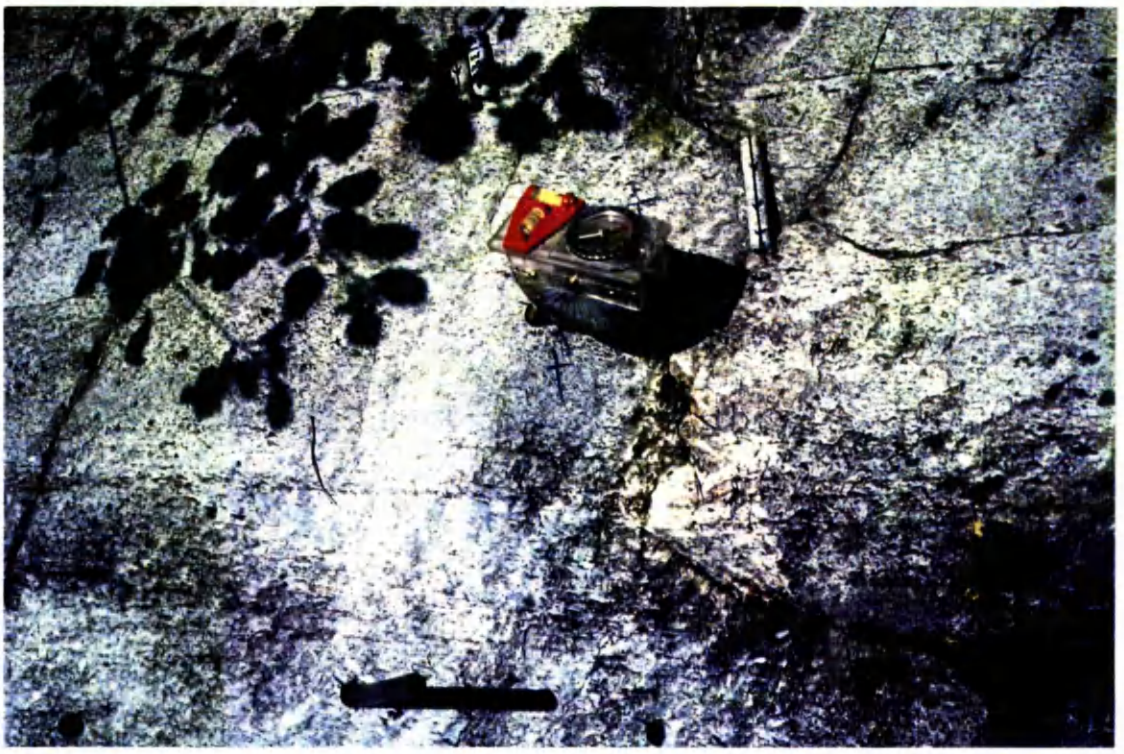

Figure 3.21: Photograph showing the specially made compass-clinometer tool used for orienting the core holes. A steel tube was used extract cores from the holes. A core with its orientation mark is also shown in the photograph.

of each core, pointing down plunge. At the location of each sample collection, the local foliation and lineation were measured so that the core orientation could be related to the field structures.

3.4.5 Environmental Aspects

Clusters of core holes can be very unsightly on rock exposures (Coring of geologically spectacular and photogenic locations was avoided). Coring was therefore generally carried out at easily accessible or road side exposures. Exposures in stream beds were favoured, both for freshness and for water supply. Where possible core holes were disguised by hammering pebbles or fallen tree branches into them.

3.4.6 Concluding Points

Extensive variation in mineral assemblage, modal proportion, mineral chemistry and degree of deformation of most rocks in the IV zone, makes it impossible to collect samples from every geological unit. Samples collected for this study are probably the only oriented ones covering a large part of the IV zone. Oriented samples were collected systematically taking account of field structure, compositional and variability in deformation. The collected samples may be useful for future mineralogical, petrological and petrophysical studies which need oriented and representative sample of the IV zone.

Chapter 4

Mineralogy and Microstructures

4.1 Introduction

This chapter describes the general mineralogy and microstructures of the main rock types from the IV zone. A more comprehensive study of the mineralogy, microstructures and mineral chemistry of the majority of the rock types can be found in Zingg (1980, 1983), Evans (1995) and Smith (1995) as well as detailed of deformed rocks in Brodie et al., (1992) and Rutter et al., (1993).

All thin sections for microscopic work were cut perpendicular to the foliation plane or compositional banding (where no foliation was present) and parallel to the lineation. In samples without visible foliation and/or compositional banding and lineation, the regional foliation orientation was used. The mineral chemistry of selected samples was studied, using EDS analysis on a scanning electron microscope. The microstructures were examined using both optical and scanning electron microscopy. The modal portions of the phases in polycrystalline samples were also estimated by using image analysis on back scattered electron SEM images.

4.2 Microstructures

The structures of the IV rocks may be divided into two groups, (a) pre-metamorphic-peak structures and (b) post-metamorphic-peak structures (after Rutter et al., 1993). The pre-metamorphic-peak structures are those which were formed before the thermal peak of metamorphism. They show annealed microstructures and equilibrium granoblastic texture. The thermal peak of metamorphism caused grain growth to occur and for almost all the optical strain features to be removed. Post-metamorphic-peak structures are those where the annealed metamorphic-peak mineral assemblages have undergone subsequent plastic and/or brittle deformation. The dominant form of post-metamorphic-peak structures are zones of high strain and folds. Microstructurally grains of minerals such as plagioclase, quartz and olivine show plastic flattening, optical strain features such as wavy extention, subgrains and various stages of

dynamic recrystallization, normally leading to tectonic grain refinement (grain size reduction). Plastic flattening of grains can usually be distinguished in the field from the characteristic granular, equant texture of the thermally annealed rocks.

4.2.1 Pre-metamorphic-peak Microstructures

The dominant measurable pre-metamorphic-peak microstructures are the compositional banding and lineation. Tectonic foliations are mainly parallel with the compositional banding, both in the amphibolite and the granulite facies rocks. In the kinzigites this foliation is defined by oriented and elongated grains such as biotite and muscovite, whereas in the stronalites, amphibolites and other metabasic rocks, it is defined by mineral segregations and compositional banding. The lineations are defined by the alignment of inequant metamorphic minerals. A lineation is generally well developed within the amphibolite facies rocks. Stretching lineations are also observed in the form of elongated quartz, sillimanite and feldspar on the foliation planes (e.g. S19 & S72). The microstructural features of the main rock types are described individually and summarised in table 4.1.

4.2.1.1 Kinzigites

Kinzigite is a highly abundant amphibolite facies aluminous metasedimentary schist characterised by the abundance of biotite in contrast to garnet. Samples of this rock were collected from two different locations. The rock is always highly foliated. The foliation is mainly defined by alignment of grains of biotite and muscovite (S133) producing a schistosity (fig 4.1). Two generation of muscovite have been observed in kinzigite samples from the IV zone (Handy, 1986). The first muscovites are parallel to the foliation and, like biotite, are interpreted to be syn-kinematic with the foliation. A second generation occurs as large plates which grow across the foliation. Both types of muscovite are present in some samples (e.g. S133). Quartz occurs as coarse to medium grains (>0.5 mm) which is strongly elongated and shows evidence of plastic deformation and dynamic recrystallization. The elongated grains lie within the foliation, which is segregated into quartz- and mica-rich bands. Plagioclase (An 30-50) is the

Sample No	Lithology	Ol	Cpx	Opx	Spl	Hbl	Pl	Gr	Bi	Sil	Qz	Op	Av Grain Size (mm)	Comments
S01A	Peridotite	*	*	*	*	*						*	1.7	Coarse grained granoblastic, no sign of grain size reduction
S32A	Peridotite	*	*	*	*	*						*	2.5	Highly strained with subgrains of olivine (0.5mm)
S60A	Peridotite	*	*	*	*	*					*	*	2.2	Elongated Phlogopite defines the foliation/ recrystallized Ol
S89A	Peridotite	*	*	*	*	*						*	1.5	Flattened hornblende defines a shape foliation
S24A	Pyroxenite	*	*	*		*	*					*	1.4	Coarse granoblastic texture
S63A	Granulite			*			*	*				*	0.7	
S69A	Px Granulite	*	*	*			*	*		*		*	1.5	Granoblastic with good equlibrium texture
S87A	Granulite					*	*	*					2.1	Symplectite of garnet
S88A	Px Granulite			*		*	*	*					2	Symplectite of garnet, alteration of pyroxenes along the fractures
S26A	Metagabbro			*			*		*				0.6	Granoblastic texture
S28A	Garnet Granulite		*				*	*	*				0.9	Plagioclase is highly deformed
S71A	Granulite		*	*			*	*				*	0.9	Granoblastic with equlibrium texture
B06	Metagabbro			*		*	*					*	0.7	Granoblastic polygonal and close to equliberium
B01	S- Metagabbro			*		*	*					*	0.1	Porphyroclastic/ grain size reduction/ weak compositional banding
S35A	Amphibolite		*	*		*	*				*		0.7	Granoblastic/ alteration along grain boundaries (epidote,titanite)
S50A	Amphibolite				*	*	*		*		*	*	0.9	Granoblastic/ equlibirum grain boundary/Strong shape fabric
S75A	Diorite					*	*					*	1.2	Equigranular with Poikilitic texture in hornblende
S41A	Diorite					*	*		*			*	0.8	Bioite-rich
S42A	Diorite					*	*		*			*	0.7	Biotite-rich

Table 4.1: Summary of the mineralogy, average grain size and microstructures of the selected samples used for seismic velocity measurements. The rock names were those assigned in the field.

Sample No	Lithology	Cpx	Opx	Hbl	Pl	Kf	Bi	Mus	Qz	Gr	Sil	Cal	Dol	Op	Av Grain Size (mm)	Comments
S126A	Charnockite	*	*		*	*									1.1	
S129C	Charnockite				*	*			*	*					0.6	Granoblastic texture
S133A	Migmatite					*	*		*	*				*	0.8	
S135A	Migmatite	*	*	*	*		*								0.6	
S04	Px Stronalite	*	*	*	*	*	*			*				*	0.6	Coarse grained granoblastic
S19A	Stronalite				*	*	*		*	*	*			*	0.5	Highly deformed/ shape fabric & Gr porphyroclasts
S72A	Stronalite				*	*	*		*	*	*			*	0.45	Evidence of crystallization/ biotite shape fabric
S73A	Stronalite				*	*	*		*	*	*				0.37	Same as S72
S74A	Metasediment				*	*	*		*	*	*				1.2	Qtz show ductile deformation & grain size refinement
S43A	Kinzigite						*		*		*				0.7	
S52A	Marble				*			*	*			*	*		1.1	Highly twinned, with porphyroclasts of Qz and Pl
LCFA	Sheared Marble				*				*			*	*	*	0.05	Grain size reduction & recrystallized calcite
S59	Ceneri Gneiss				*	*	*	*	*						0.3	Secondary Mus/ Cordierite/Andalusite
S11A	Gniess Minoti				*	*	*	*	*						0.2	Foliation is defined by oriented Bi & Mus grains
S123A	Orthogneiss				*	*	*	*	*						0.3	
S99A	Schist d Lughi				*	*	*	*	*						0.24	Plastic Strain in Qtz
B11A	Schist d Lughi				*	*	*	*	*						0.26	
S92A	White Granite				*	*	*	*	*					*	1.1	Coarse grained equigranular
S94A	Pink Granit				*	*	*	*	*					*	1.2	Coarse grained equigranular
B17A	Gr amphibolite			*	*		*	*		*					0.85	

Table 4.1: Contd.

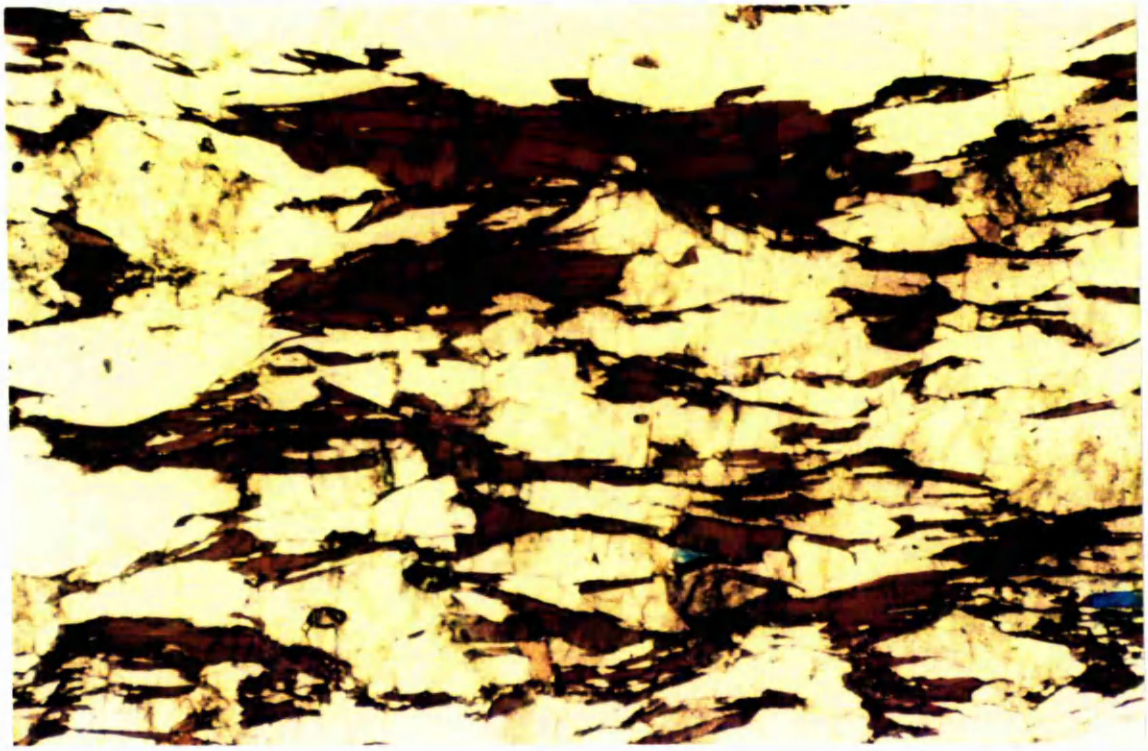

(a)

1 mm

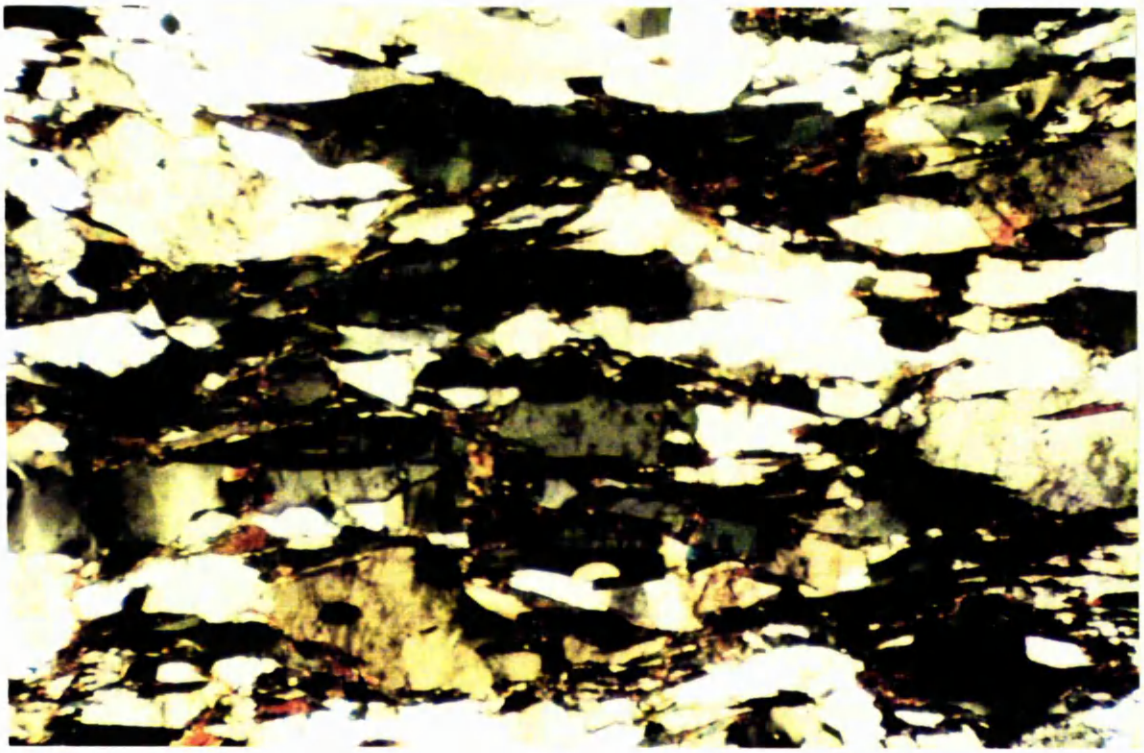

(b)

Figure 4.1: Photomicrographs of a kinzigite consisting mainly of biotite, plagioclase and quartz (sample S43). The foliation is defined by aligned biotite and elongated quartz (a = plane polarised light, b = cross polarised light).

dominant feldspar and is elongated parallel to the foliation plane. Sillimanite is present in the kinzigite in both prismatic and fibrolitic habits elongated parallel to foliation. Almandin garnet (pyrope 10) generally occurs as round to subhedral porphyroblasts.

4.2.1.2 Stronalites

Stronalites, which are granulite facies metasedimentary gneisses, were collected from three localities within the IV zone. The main minerals are plagioclase, garnet, quartz, pyroxene and sillimanite. Compositional banding, defined by alternating mafic and felsic-rich horizons, is the dominant planar feature. Garnet (pyrope 35, Fe 50-60%) generally occurs as round to angular subhedral porphyroblasts. Plagioclase (An 30-50) and K-feldspar (orthoclase, 80-90) grains vary from equant to elongate parallel to the banding. A small proportion of grains of K-feldspar and plagioclase show signs of late alteration. Generally plagioclase seems to be more resistant to alteration than K-feldspar. Quartz grains are generally elongate within the banding and often define a lineation (fig 4.2). Prismatic sillimanite grains are also present and normally lie within the plane of banding. They sometimes define a lineation on the banding planes (S19).

4.2.1.3 Marble

Marbles were collected from two localities. The major minerals are calcite, dolomite, plagioclase feldspar, diopside, quartz and phlogopite. A foliation is weakly developed and in some cases weak compositional banding can be seen in the field (S52). Volumetrically calcite counts for about 94% of the samples. Feldspar, quartz and diopside are only present as scattered clusters (fig 4.3). Microstructurally marbles are usually coarse grained (2-5 mm) and the calcite show intense development of late, low temperature (thin) twins.

4.2.1.4 Metabasic rocks

In metabasic rocks a strong compositional banding is defined by mafic (hornblende & pyroxene) and felsic (quartz and plagioclase) horizons (fig 4.4). In relatively undeformed samples the grain boundaries are straight, the texture is

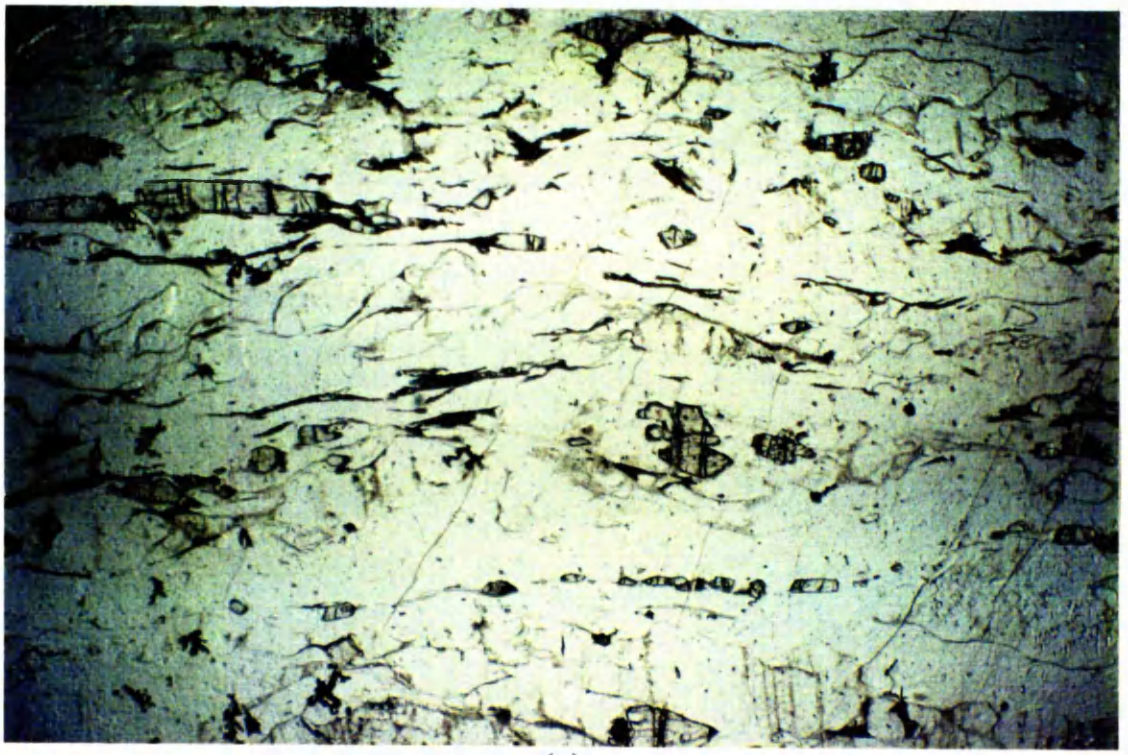

(a)

1 mm

(b)

Figure 4.2: Photomicrographs of a stronalite consisting mainly of biotite, plagioclase, quartz and sillimanite. (sample S19). There is a weak compositional banding but good grain shape foliation (a = plane polarised light, b = cross polarised light).

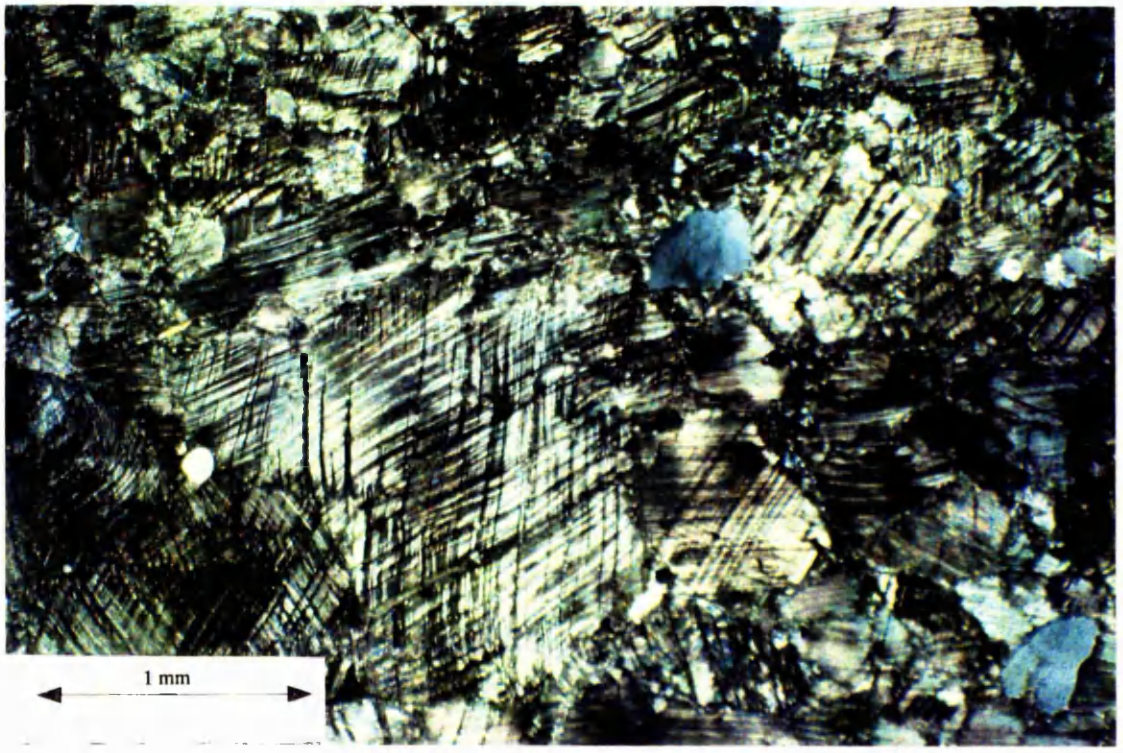

Figure 4.3: Photomicrograph of a marble (plane polarised light) consisting almost entirely of coarse grained calcite which heavily twined (sample S52A). There are also some minor quartz and plagioclase grains.

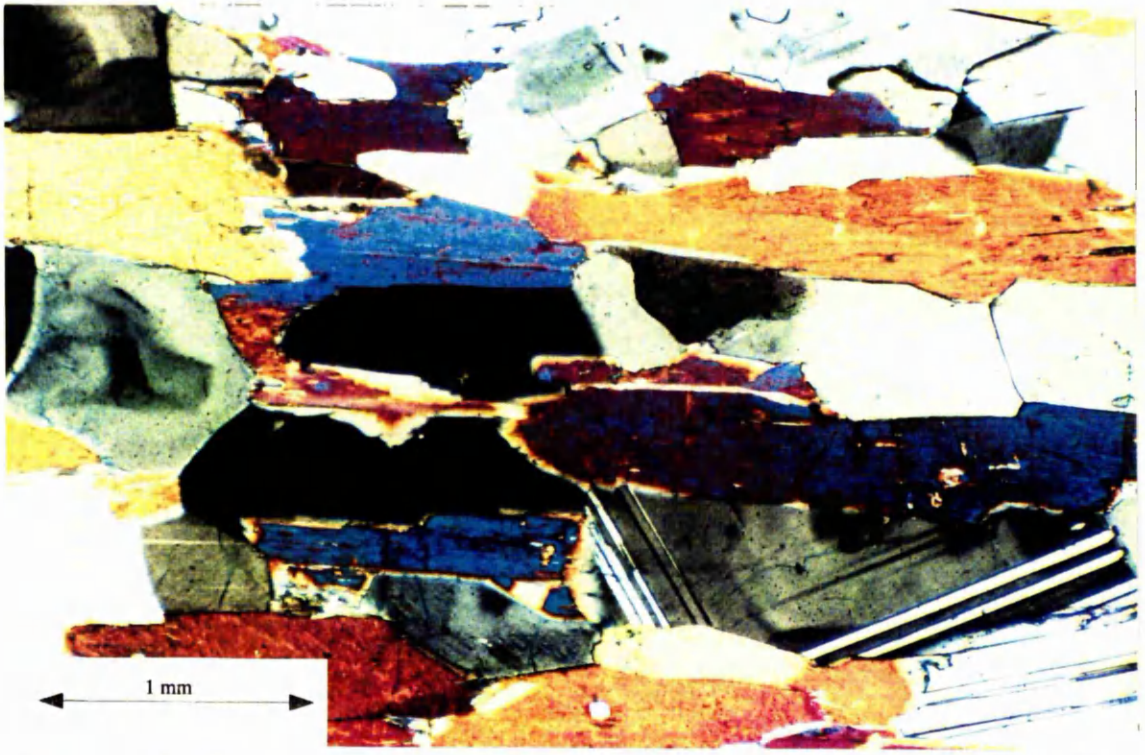

Figure 4.4: Photomicrograph (crossed polaris light) of an amphibolite showing strongly aligned, elongate hornblende crystals. The sample is composed mainly of hornblende and plagioclase (sample S15A).

granoblastic polygonal, and indicates a close approach to an equilibrium texture. Metabasic rocks are divided into two subgroups; (a) amphibolite facies metabasic rocks and (b) granulite facies metabasic rocks.

(a) The amphibolite facies metabasic rocks consist of plagioclase, green hornblende (pargasitic) and diopside with minor titanite and opaque minerals (fig 4.5). Hornblende occurs as flattened prismatic grains defining a strong foliation and lineation. The plagioclase grains are generally equant and variably plastically deformed.

(b) The granulite facies metabasic rocks consist of plagioclase, brown hornblende (magnesio-hornblende), orthopyroxene (Fs 24-43 & En 57-77) diopside (En 32-42 & Fs 14-18) and garnet (fig 4.6). Garnet is generally coarse grained and forms round to subhedral porphyroblasts (e.g. S28).

4.2.1.5 Ultrabasic rocks

Peridotites and pyroxenite were the only ultrabasic samples collected. In peridotites, the dominant constituent minerals are olivine, pyroxenes, and some amphiboles. The peridotites are extremely fresh with a coarse grained (average 1.8 mm) granoblastic polygonal texture (fig 4.7 & 4.8). The olivine (Fo 89-93) generally shows optical strain features and subgrains of olivine were present, particularly in the Premosella peridotite (fig 4.9). Alteration of olivine along the cracks has led to the formation of serpentinite. Pyroxenes in peridotites show little sign of plastic deformation but optical strain features such as undulose extinction are present. Diopside (En 40-45 & Fs 45-50) is the main clinopyroxene with little alteration and sometimes shows lamella twining. Enstatite is the main orthopyroxene and is normally more altered than diopside.

There are a number of pyroxenite bodies (clinopyroxenite, orthopyroxenite, websterite) in the IV zone but the majority of them were not suitable for sampling owing to alteration or pseudotachylite veining (fig 4.10). Samples from only one pyroxenite body were collected for this study. This sample contains about 8% plagioclase and 92% pyroxenes (fig 4.11). The sample is coarse grained with an equigranular, granoblastic polygonal texture. The clinopyroxene is diopside and the orthopyroxene is Enstatite.

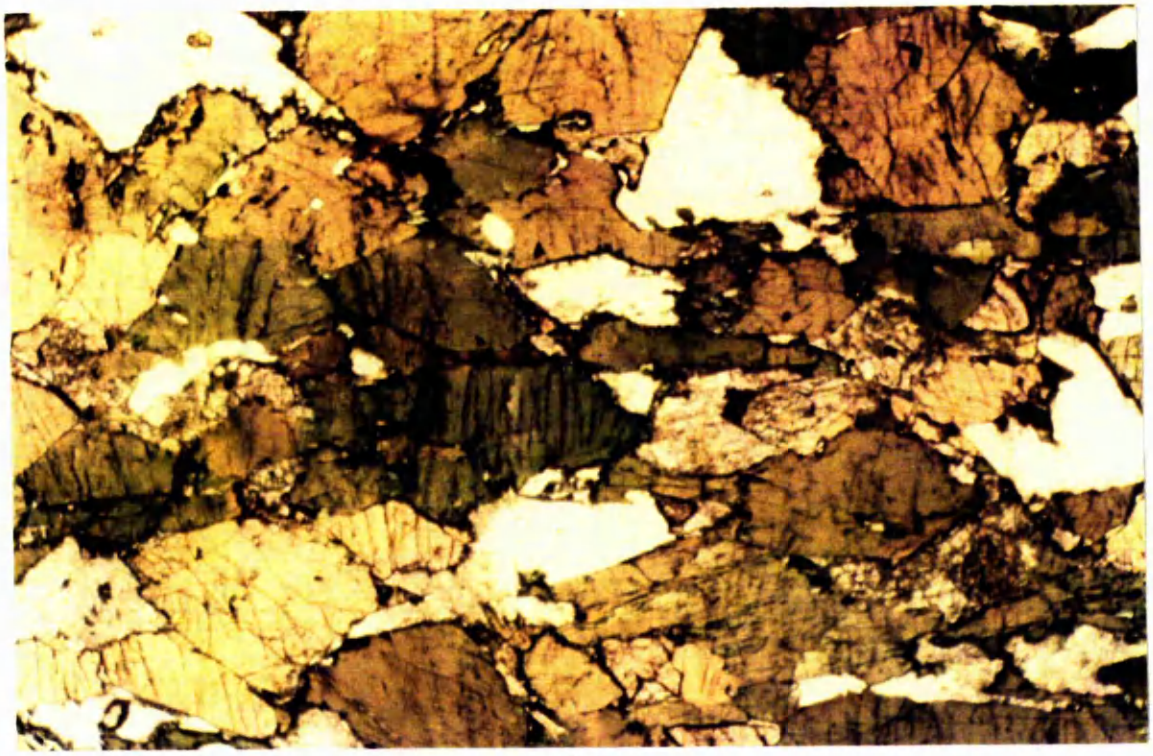

(a)

1 mm

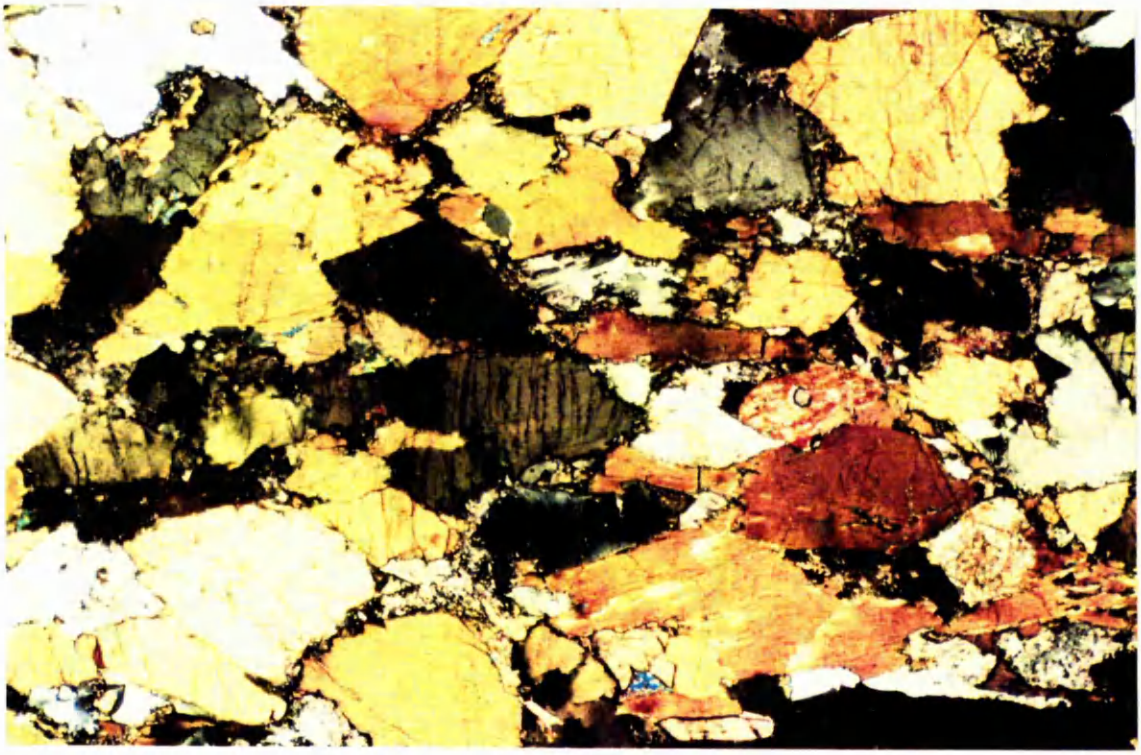

(b)

Figure 4.5: Photomicrographs of an amphibolite consisting mainly of hornblende and plagioclase (sample S35). Both lineation and foliation are defined by elongate and aligned amphibole grains (a = plane polarised light, b = cross polarised light).

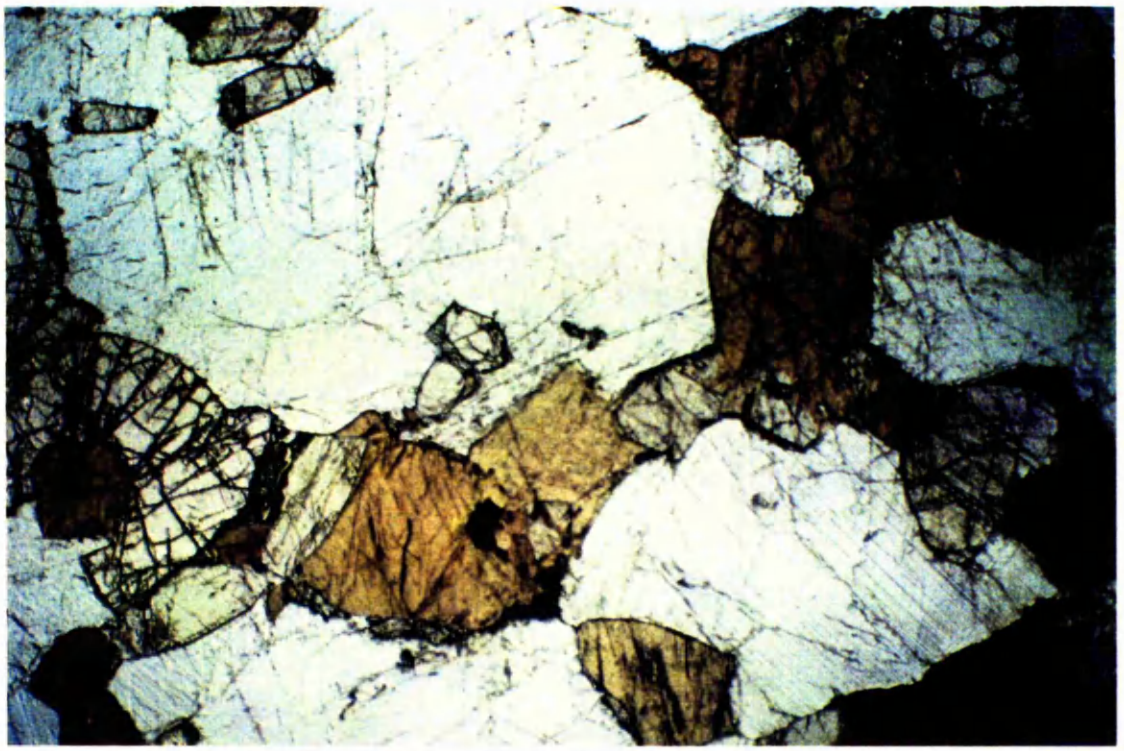

(a)

1 mm

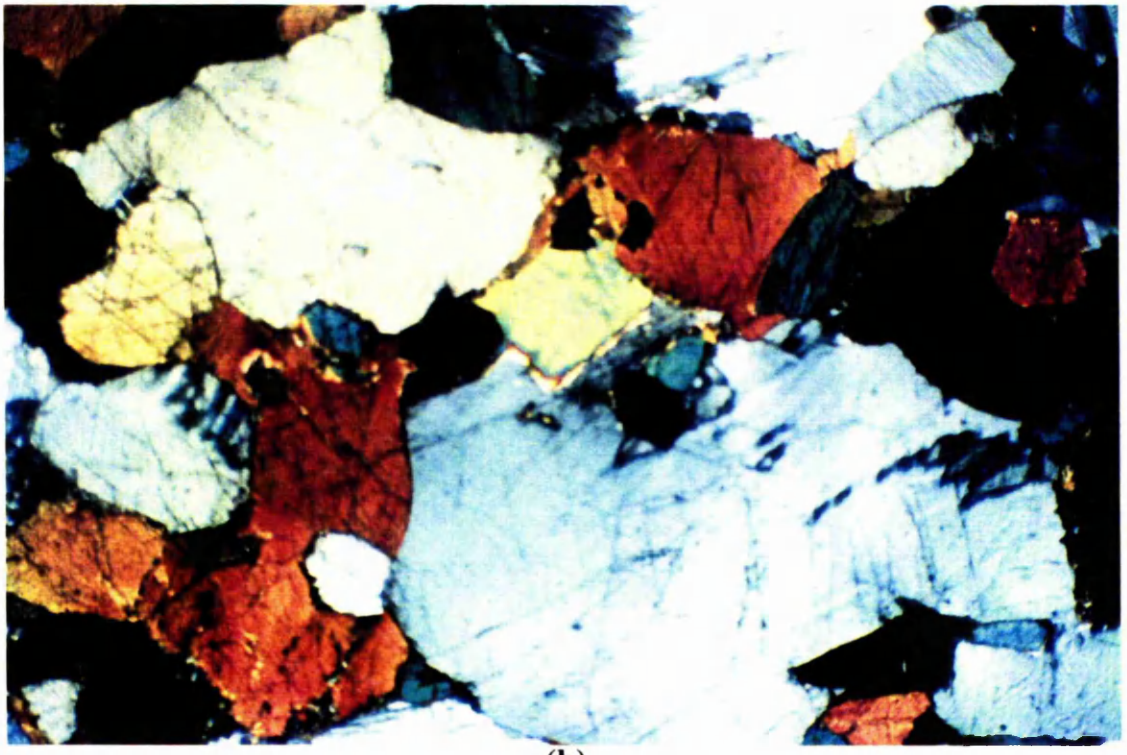

(b)

Figure 4.6: Photomicrographs of a granulite facies granofels ('pyroclasite') (a = plane polarised light, b = cross polarised light) consisting mainly of plagioclase, pyroxenes and garnet (sample S87). The texture is granoblastic polygonal.

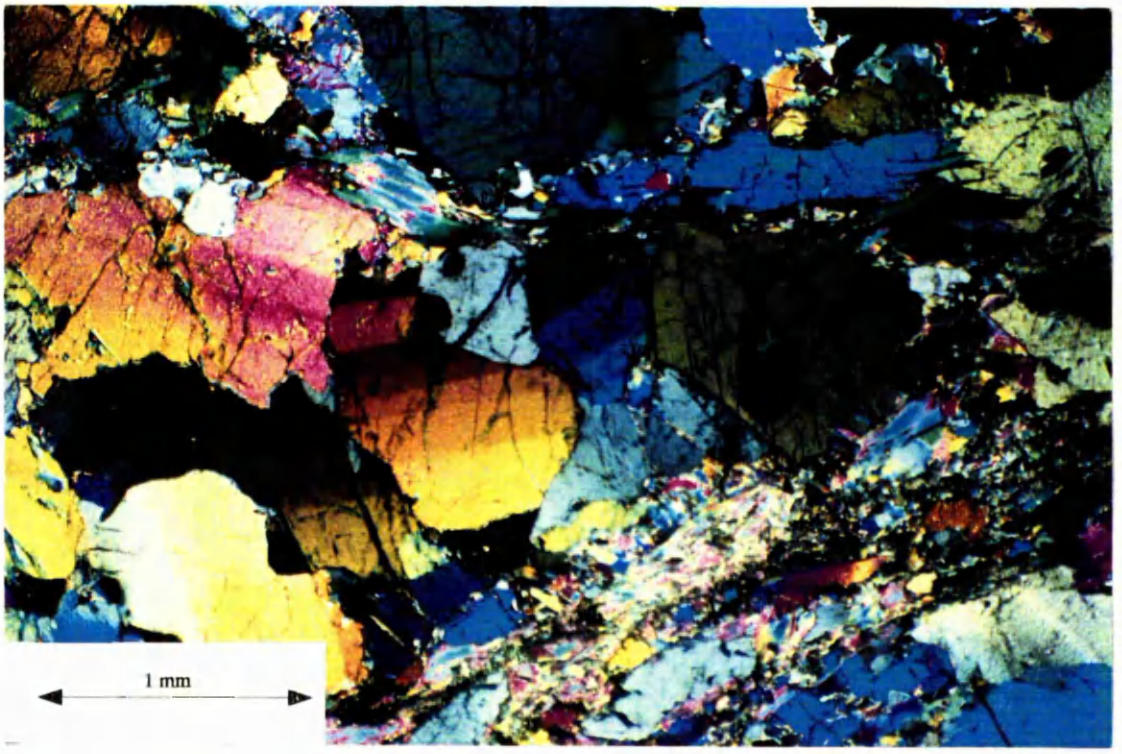

Figure 4.7: Photomicrograph of a phlogopite-rich peridotite (cross polarised light) consisting of olivine, phlogopite, hornblende and pyroxenes. Phlogopite defines a weak compositional banding (sample S60A).

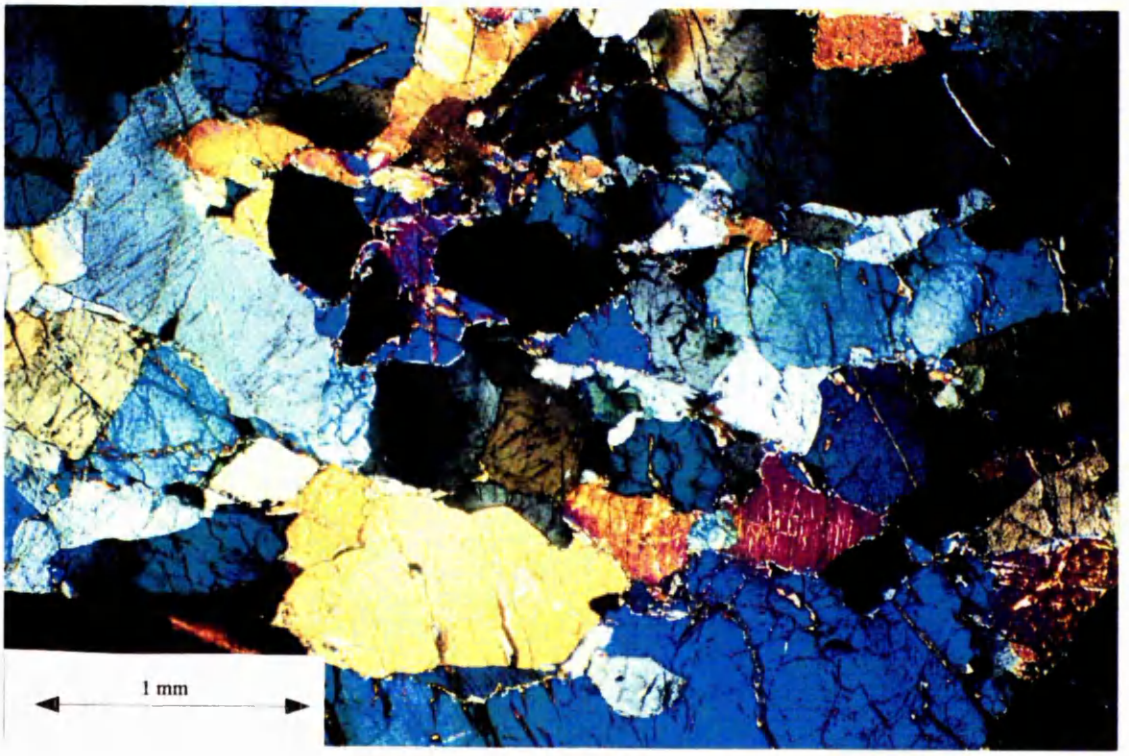

Figure 4.8: Photomicrograph (cross polarised light) of Balmuccia peridotite showing equigranular texture and weak elongation of olivine defining a foliation. There is sub-grains in some olivine grains.

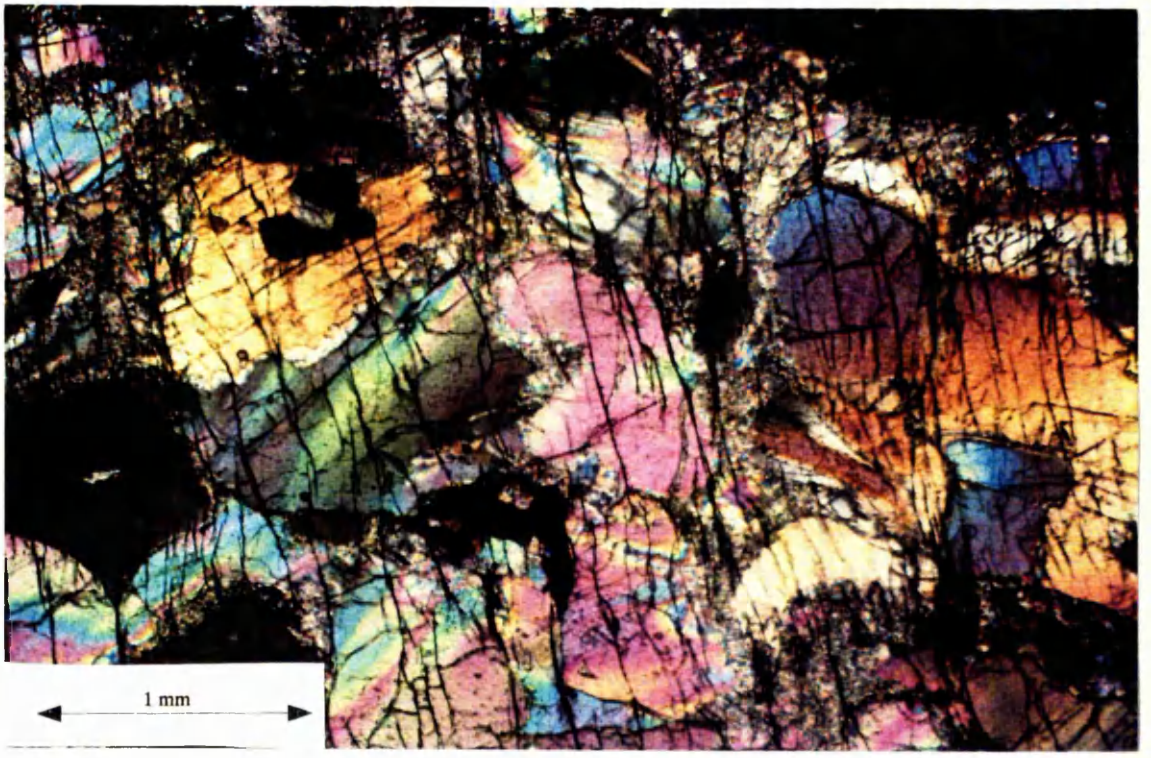

Figure 4.9: Photomicrograph of Premosella peridotite (sample S32A; cross polarised light). The sample consists mainly of olivine, pyroxenes and plagioclase. Olivine contains deformation bands and shows irregular recrystallization.

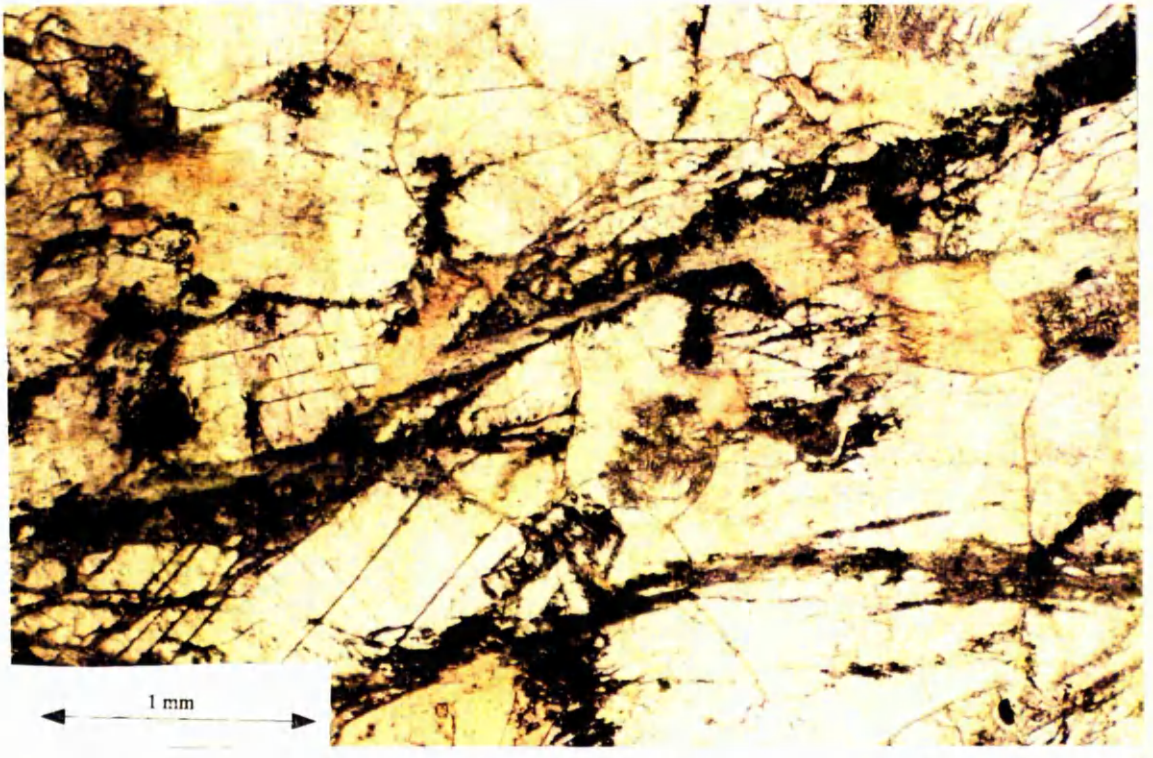

Figure 4.10: Photomicrograph of a pyroxenite (plane polarised light) consisting of pyroxenes and plagioclase. Pseudotachylite have been injected into the rock and virtually destroy the microstructure of the sample. There is also some cataclastic deformation and greenschist facies retrogression.. (sample S24A)

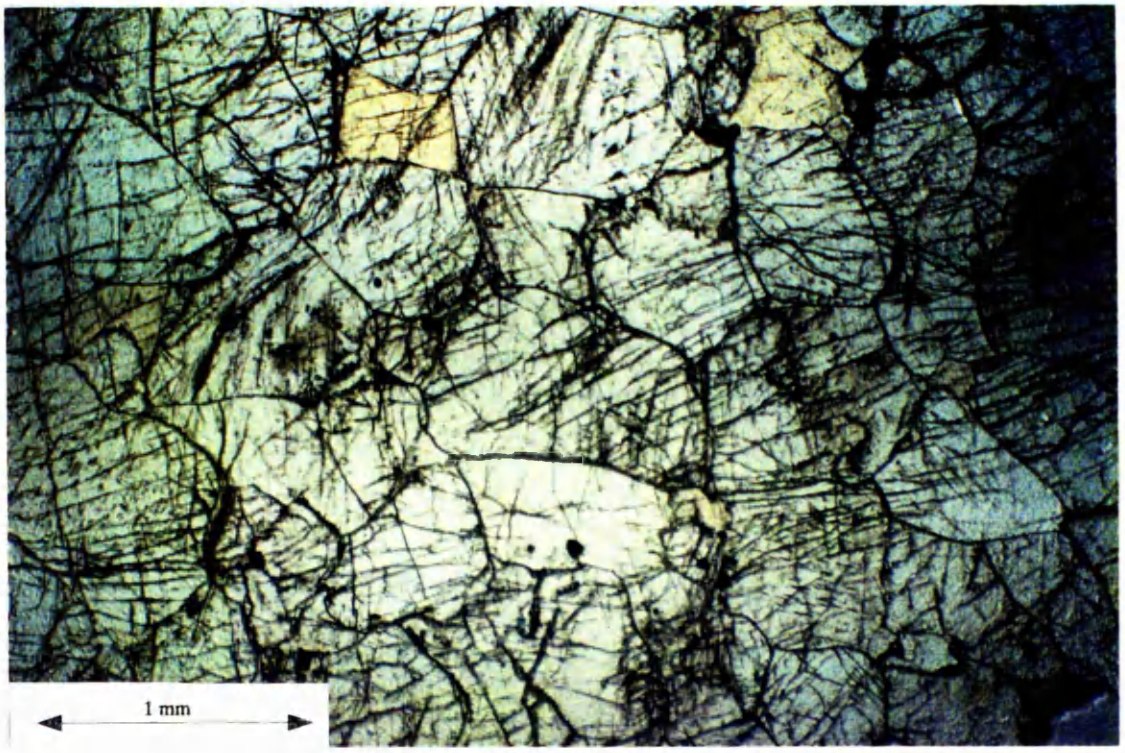

(a)

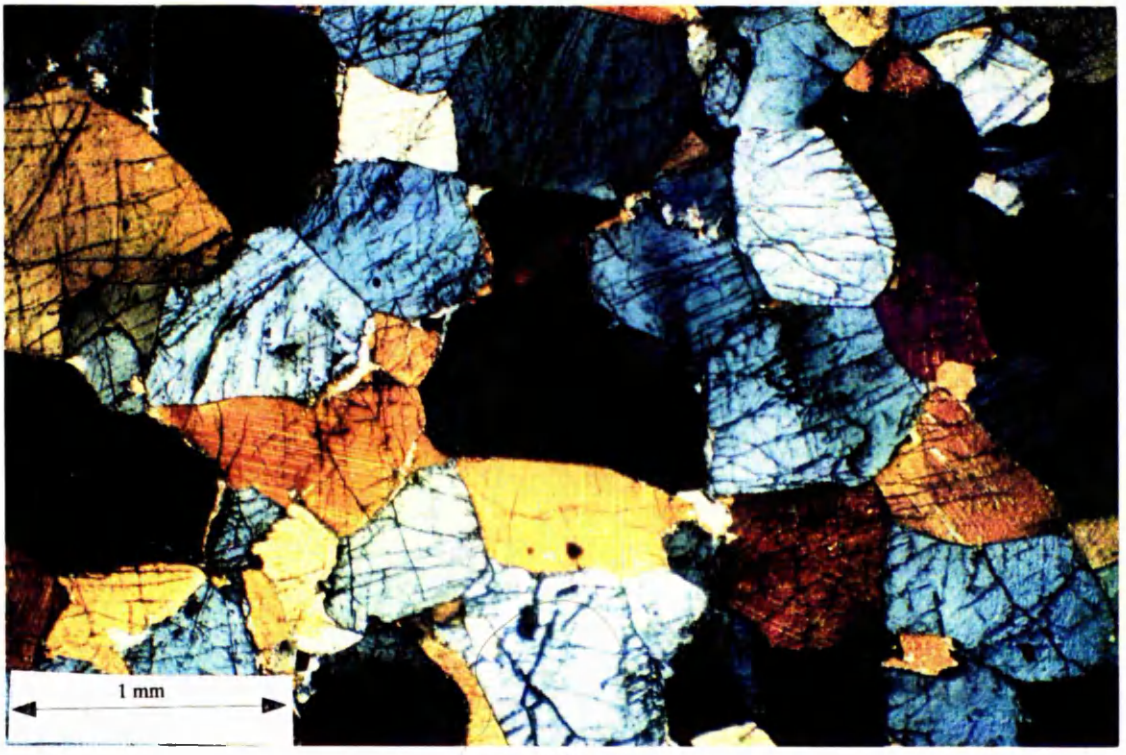

(b)

Figure 4.11: Photomicrographs of a pyroxenite sample from Rio del Ponte (S24A). The sample consists of clino- and orth- pyroxenes, plagioclase and amphibole and the texture is granoblastic polygonal (a = plane polarised light, b = cross polarised light).

4.2.2 Post-metamorphic-peak Microstructures

The peak thermal metamorphism produced near equigranular granoblastic textures. The major forms of post-metamorphic-peak structure are the development of mylonites along extensional shear zones, and of folds.

4.2.2.1 High temperature mylonites

High temperature shear zones occur within a variety of different lithologies in the IV zone, particularly within the granulite facies rocks (fig 4.12). All the high temperature shear zones show tectonic reduction in grain size (0.1-0.5 mm) due to dynamic recrystallization. In the high temperature shear zones deformation is isochemical and largely isomineralic, with only small changes in the mineral chemistry of individual phases being recorded between host and mylonitic rocks (Brodie 1980). Rutter & Brodie (1992) estimated the temperature range of 750°C to 500°C for the high temperature shear zones, based on the mineral assemblages and the radiometric cooling curve.

4.2.2.2 High temperature mylonite samples

A number of mylonite samples of different lithologies were collected for laboratory seismic investigation. Unfortunately it was later discovered that alteration and low temperature deformation (greenschist facies) had affected most of the high temperature mineral assemblage and the microstructures. Only samples from three high temperature shear zones were suitable for seismic measurements and they are described in the following sections.

i) Calcite mylonite from Val Cannobino

Calcite mylonite samples were collected from a shear zone cutting through a sequence of calcite and dolomite marbles in Val Cannobino. The shear zone is developed in calcite-rich strata as they have less resistance to deformation than dolomite. Calcite as the weakest phase accommodated the greatest part of the deformation, resulting in extensive grain size reduction and producing a fine grained matrix (fig 4.13). The mylonitic fabric is well developed in calcite-rich layers and cross-cuts the early

Figure 4.12: Photograph of a high temperature shear zone formed in metagabbro in Anzola quarry. The shear zone is about 5 meter wide and has a sharp boundary with the protolith metagabbro.

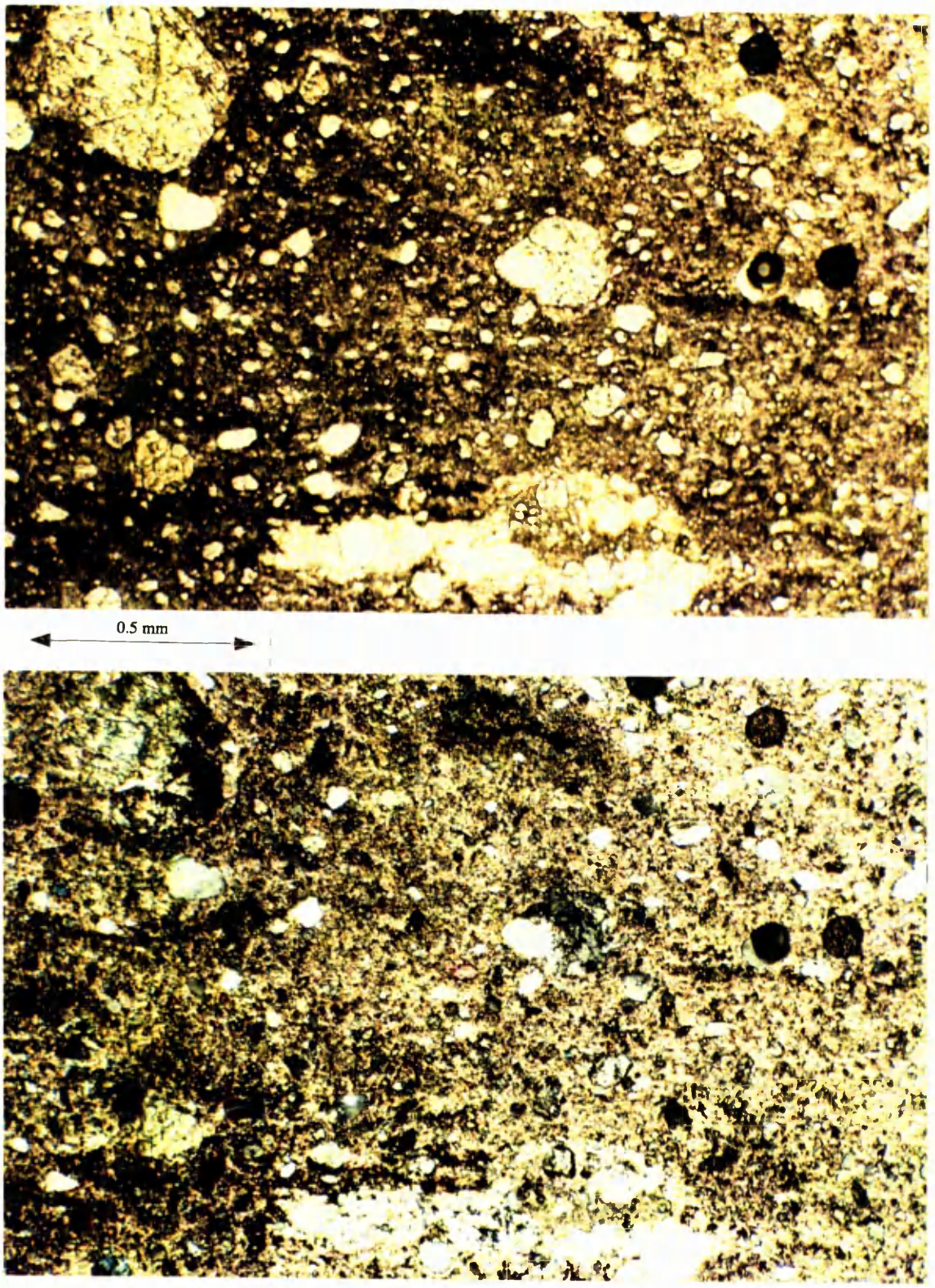

Figure 4.13: Photomicrographs of a calcite mylonite (top plane & bottom cross polarised light) showing extensive grain size refinement of calcites. (sample LCFA). The matrix consists of mainly calcite with plagioclase, quartz and diopside forming porphyroclasts.

metamorphic foliation. The primary metamorphic phases (plagioclase feldspar, diopside and quartz) form rounded clasts in a calcite-rich matrix. Coarser recrystallized grains of calcite have grown in the pressure shadow of these clasts.

ii) Metabasic mylonite from Anzola

Samples were collected from a shear zone approximately 5 meters wide formed in an amphibolite facies metagabbro near Anzola, Val d'Ossola (Brodie, 1981). The shear zone has sharp boundaries with the undeformed metagabbro. Both mylonite and the protolith are mainly composed of plagioclase and amphibole, with some pyroxenes and minor opaque minerals (Fe-Ti oxides and Fe sulphides; fig 4.14 & 4.15). The major foliation in the mylonite is compositional banding defined by segregation of plagioclase and amphiboles. There is a progressive reduction of grain size of all phases in the shear zone. The mylonite consists mainly of porphyroclasts of plagioclase and hornblende surrounded by fine grained recrystallized plagioclase and hornblende.

Both plagioclase feldspar and hornblende appear to have recrystallized dynamically to produce the finer grained matrix. However, as plagioclase is the weaker phase it had to be the main load bearing phase. Therefore the recrystallization must have started sooner, and progressed faster, for plagioclase than for hornblende. This may be why there are more porphyroclasts of hornblende than plagioclase. A possible alternative explanation is that the deformation mechanism changed from dynamic recrystallization to grain size sensitive flow once a sufficient large percentage of the plagioclase had recrystallized to the finer grain size (Brodie & Rutter 1987). There is a reduction in grain size of opaque minerals which is possibly due to cataclastic granulation.

iii) Metabasic mylonite from Gula

The Gula mylonite is one of the thickest mylonitic shear zones (about 30 m) in the IV zone. Part of the shear zone is exposed in Val Mastallone near to the village of Gula (see fig 3.1).

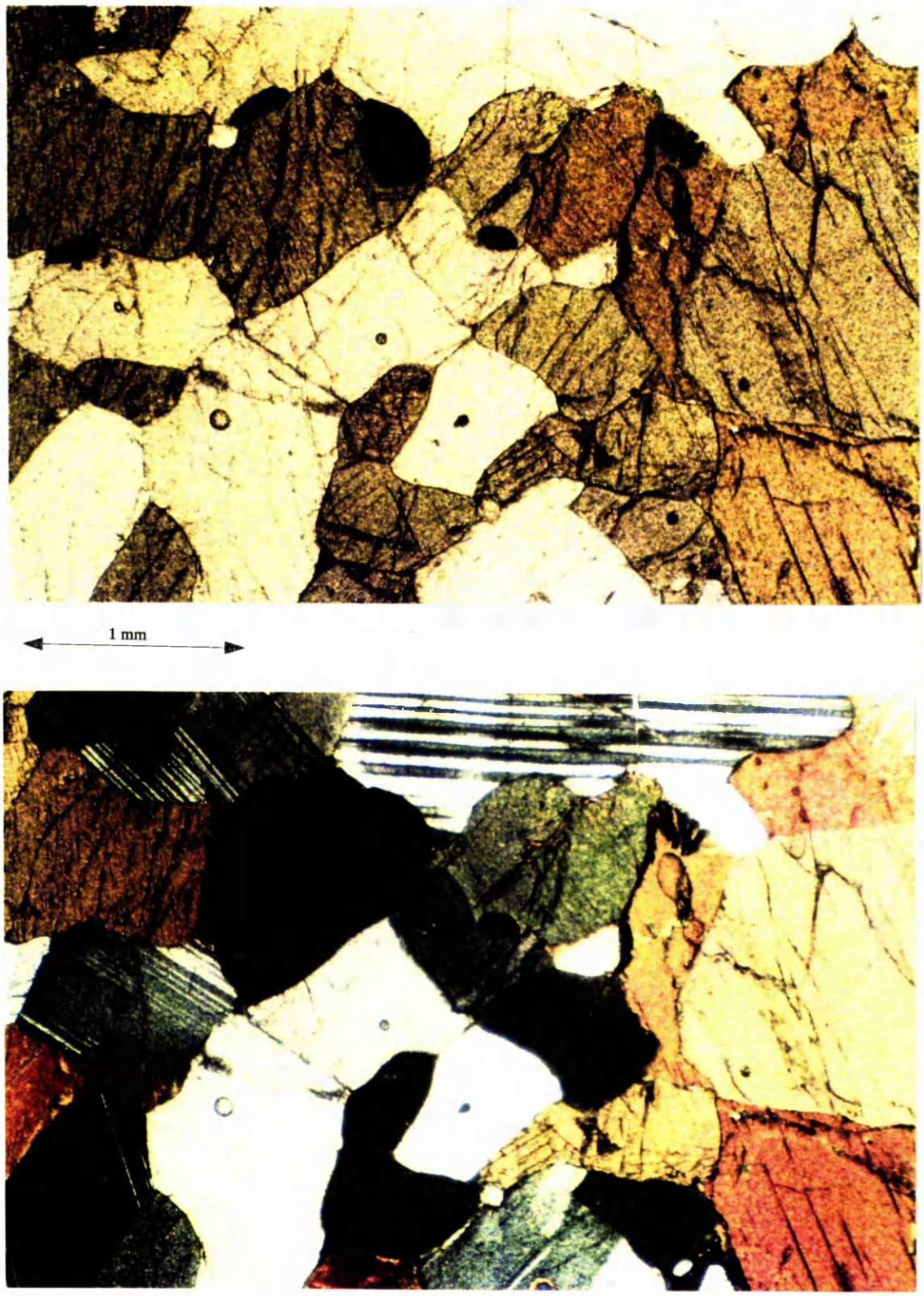

Figure 4.14: Photomicrographs of Anzola metagabbro (top plane & bottom cross polarised light) showing coarse grained granoblastic texture (sample B6A). The sample consists of hornblende and plagioclase with minor opaque phases.

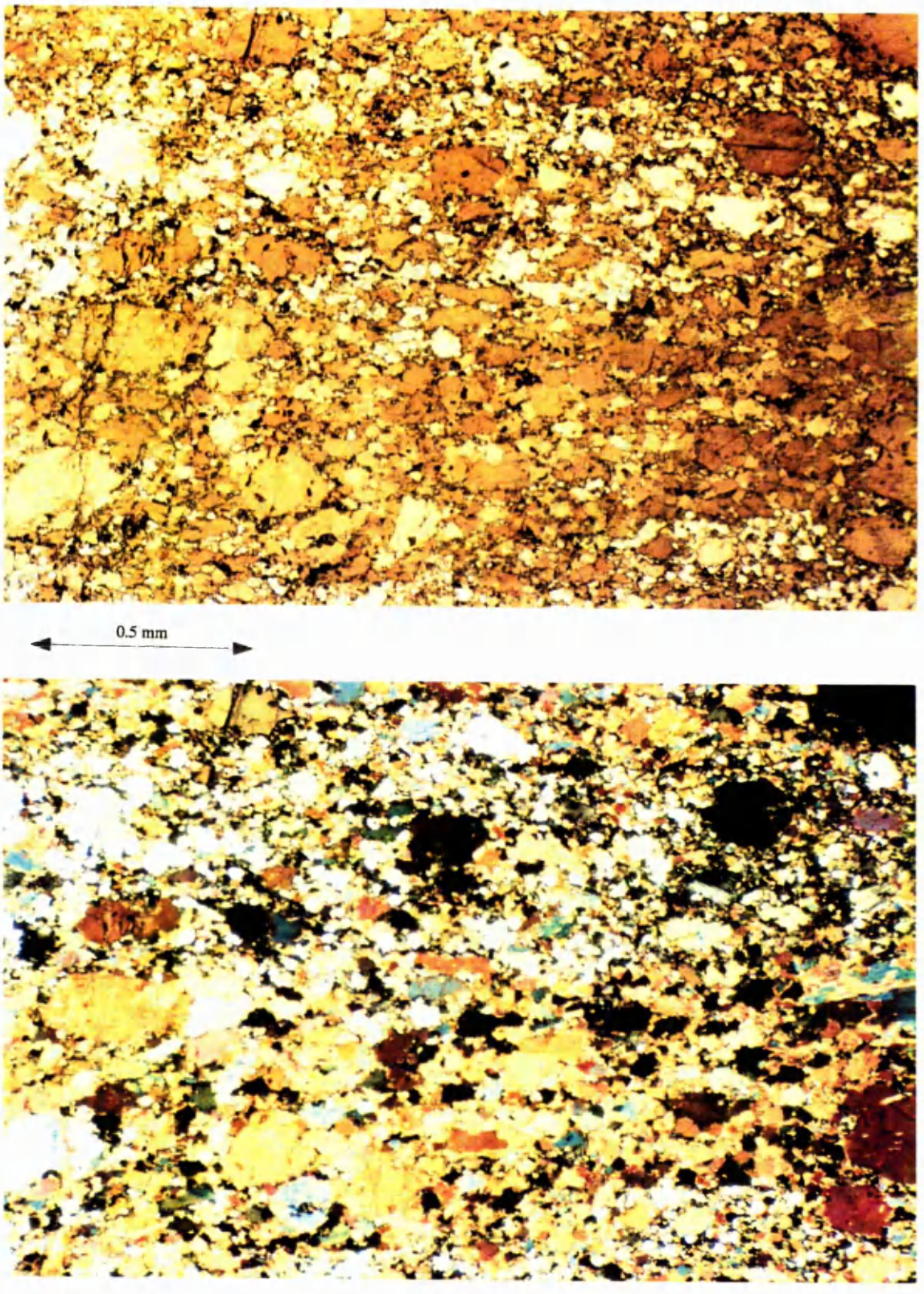

Figure 4.15: Photomicrographs of Anzola mylonite (top plane & bottom cross polarsed light) formed in metagabbro (B6A). There is extensive grain size reduction of both amphibole and plagioclase associated with the deformation. The sample is partly annealed and does not contain a strong mylonitic foliation. Hornblende grain appear to have a good crystallographic preferred orientation.

The protomylonite adjacent to the mylonite in the Gula area is coarse grained (<0.8 mm) with a granoblastic texture (fig 4.16). The major constituent minerals are biotite, plagioclase, amphibole and pyroxenes. Quartz seems to be very rare, but biotite is quite abundant. The composition of the rock is closer to metasedimentary than metabasic, but could have been possibly charnockitic or granitic. The amphiboles show optical strain features but they are not significantly plastically deformed. The plagioclase is moderately strained and there are some recrystallized plagioclase grains (>0.2 mm) along the grain boundaries.

In the mylonite the main constituent minerals are plagioclase, amphibole, pyroxenes, and quartz (fig 4.17). There is a weak compositional banding defined by segregation of plagioclase and mafic minerals (amphiboles and pyroxenes). Amphibole and pyroxenes seem to have been fractured and dragged out along the shear bands and are possibly recrystallized as well. Plagioclase shows intense grain size refinement (average 0.16 mm) associated with total dynamic recrystallization. Recrystallized plagioclase is larger in size (about 0.5 mm) away from mafic rich-bands and much smaller (about >0.1 mm) along the bands and close to mafic minerals. This implies that intergranular contamination due to the presence of mafic fragments prevents the growth of plagioclase. In contrast, in the areas away from mafic rich-bands the plagioclase crystals grow larger. There are some quartz grains present in the form of long ribbons (about 0.8 mm). Although generally the mylonite has metabasic composition, the presence of quartz possibly indicates a charnockitic composition for the original rock. The lack of biotite in the mylonite, in comparison with the protomylonite, can be only explained due to the shear zone intersecting primary compositional banding or a lithological boundary.

4.3 Modal Analysis

Model analysis of the samples was carried out using the SEM (table 4.2). The desired back-scattered image was displayed on the SEM CRT screen., and magnification, brightness and contrast adjusted until the individual phases could be clearly distinguished. The image was then captured by the Link Systems image

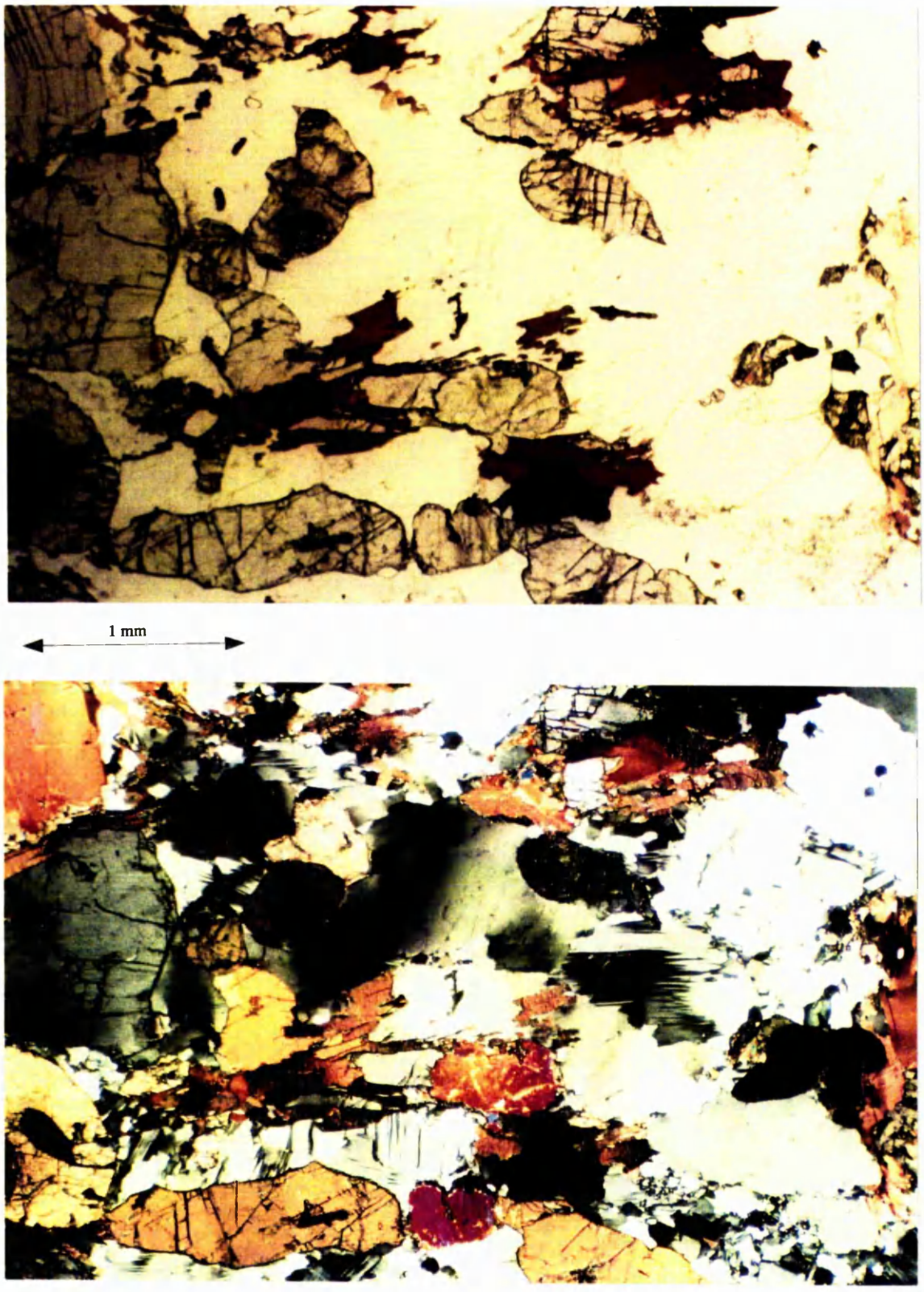

Figure 4.16: Photomicrographs of metasedimentary rock adjacent to the Gula mylonite (top plane & bottom cross polarised light). The sample (S66A) consists of biotite, amphibole, plagioclase and pyroxenes, and it has different composition to the Gula mylonite (S67A) which appears to have formed along a compositional boundary.

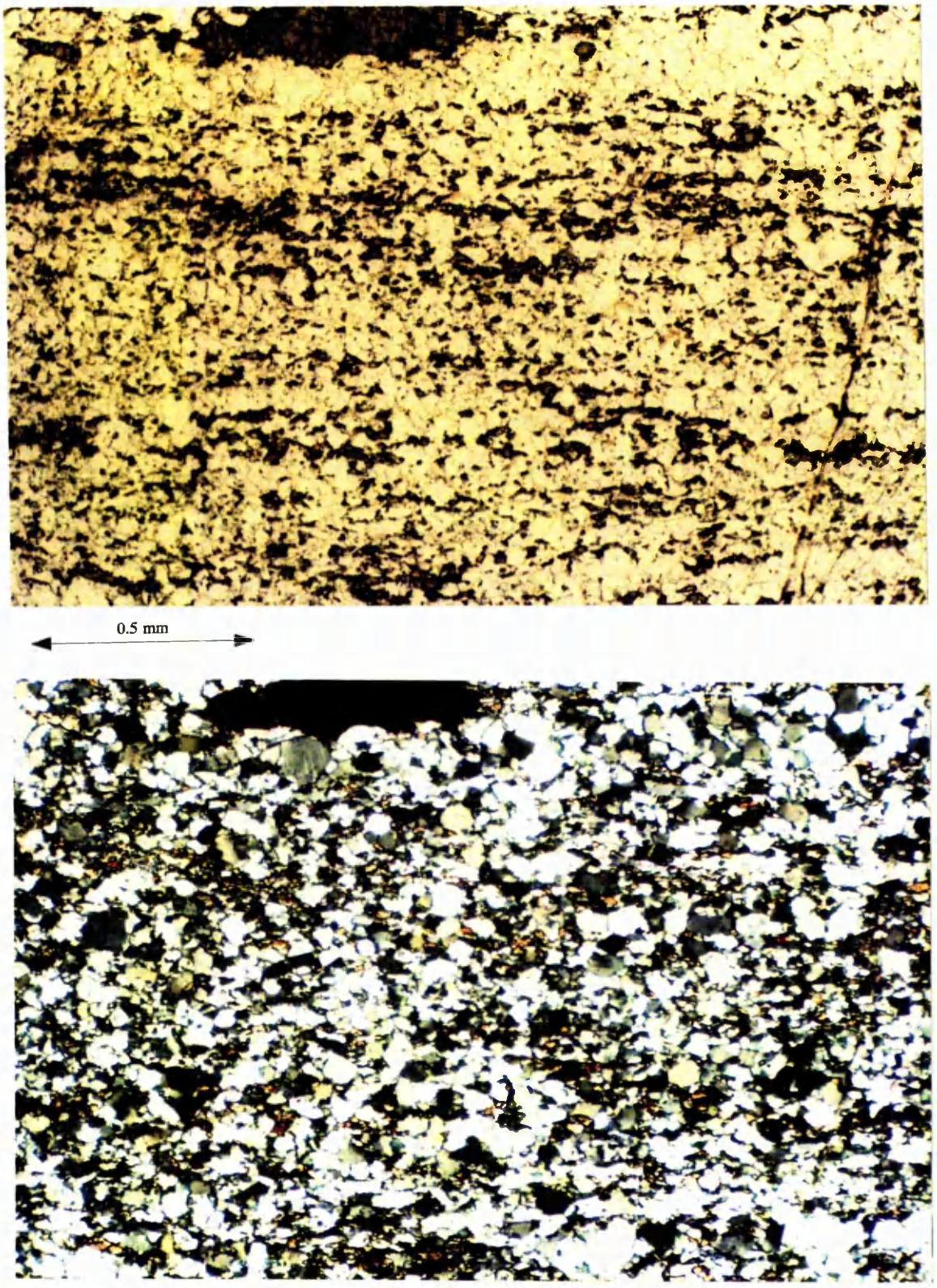

Figure 4.17: Photomicrographs (top plane & bottom cross polarised light) of Gula mylonite (sample S67A). It shows a weak compositional banding defined by segregation of plagioclase and mafic minerals. The mafic minerals (amphiboles and pyroxenes) are fine grained and seems to be at least partly deformed by cataclastic deformation. Plagioclase shows total recrystallization and grain size refinement, possibly associated with dynamic recrystallization.

Sample No	Ol	Cpx	Opx	Spl	Hbl	Phl	Pl	Gr	Bi/OP	Kf	Qz	Sil	Mus	Cal	Dol
S32A	80	10	6	4											
S89A	70	5	5		20										
S01A	55	11	32	2											
S60A	60	10	12	3	3	12									
S24A	4	49	43				4								
S63A		30	15			55									
S87A		7	8		38	30		17							
S88A		6	8		46	25		15							
S26A		26	18				56								
S28A		25	10				32	33							
B06		15	15		25		43		1				1		
B01		4	5		20		64		5				2		
S35A		7	4		30		47			3	9				
S69A		10	25				40	24	1						
S50A					28		45			7	10				
B17A					30		40		16	4			2		
S75A					40		60								
S41A			5		15		60		20						
S42A		5	5		10		55		25						
S74A							40	22		7	19	12			
S04			16				55	10		13	6				
S126A		5	5		20		50		8	15					
S135A		10	10		15		45			15					
S19A							40	16		14	25	5			
S72A							50	15	5	25					
S73A							40	10	3	12	30	3			
S74A					15		20	45		15	5				
S43A							45	15	20	15					
S129C							25	15	35	25					
S133A							40	10	10	25	15				
S52A							5				13		1	80	1
LCFA							10				2			82	6
B11A							13		13	28	36		10		
S99A							15		7	25	45		8		
S123A							21		15	7	42		15		
S92A							35		2	35	26		2		
S94A							26		1	35	37		1		

Table 4.2: Results of modal analysis of a selected samples. The result are rounded and their accuracy varies from sample to sample and depends on the difference in mean atomic weight of each phase and obtaining a high quality image. However, the accuracy has been found to be around 5% or better.

analyser. The image analyser designates eight colour bands, which are initially equally divided across the range of gray levels contained in the image. The grey levels are displayed as a graph of grey level against number of pixels, enabling concentrations of particular grey level ranges, corresponding to individual phases, to be seen as peaks on the graph. The range of grey levels designated to a particular colour band is then adjusted manually so that each phases is displayed by a different colour. The false colour image of the sample can be compared with the back-scattered image on the SEM screen to make detailed adjustments. The image analyser then calculates the area occupied by each colour, and presents this as a percentage of the total area of the image. These values correspond to the area of each phase on the image.

Depending on the heterogeneity and grain size of the sample, it is usually necessary to collect and evaluate a number of images, and to average the values obtained. Chemical zoning within phases can be a problem, especially if the grey levels overlap with those of other phases. Similarly, phases with similar or close mean atomic numbers can be difficult to distinguish from each other. In this case it may be necessary to analyse each field twice, with different brightness and contrast setting, in order to distinguish different groups of phases.

4.4 Mineral Alteration & Weathering

Alpine deformation is responsible for most of the greenschist to sub-greenschist facies retrogression seen in the rocks. Alteration is more prominent near faults and where rocks are more fractured such as shear zones. The secondary minerals generally have a random fabric (e.g. B17). The plagioclases vary in their susceptibility to alteration. Albite-rich plagioclase is relatively more resistant to alteration than anorthite-rich members of the series. Calcic plagioclase is altered to epidote, zoisite, white mica and carbonate. Plagioclase feldspar is often partially sericitized, being replaced by muscovite and carbonate or clay minerals. Weathering results in complex alterations of the feldspars forming clay minerals such as kaolinite. Biotite alters to chlorite. White muscovite is a mineral that is relatively resistant to alteration, however, it may undergo hydration or alter to clay minerals. Hornblende alters to chlorite, carbonate, epidote and

biotite. Clinopyroxene and orthopyroxene alter to actinolite and epidote. Olivines are commonly serpentinized along cracks, although alteration may proceed further and serpentinize the olivine completely (e.g. S60 and S 61).

Chapter 5

Techniques of Ultrasonic Velocity Measurement

5.1 Introduction

This chapter mainly describes the experimental program. It reviews common methods of generating elastic waves in laboratories for seismic velocity measurements of rocks. The newly set up experimental apparatuses for measuring the seismic velocity of rock samples at high pressure and temperature is then described in more detail. Towards the end of the chapter the validity, accuracy and the possible errors in evaluating seismic velocity are discussed.

5.2 Generation of Elastic Waves

Elastic waves are defined as mechanical vibrations that propagate in solids, liquids and gases. The elastic waves travel with different velocities that depend on the elastic properties and density of the medium through which they propagate. Elastic waves are generated naturally in the earth by Earthquakes. They produce waves of various kinds with a very wide range of frequency. Two types of these waves are of importance for geological and seismological studies. One is a compressional (variously termed as primary, P, dilatational, longitudinal or irrotational) wave and the other one is a shear (secondary, S, transverse or rotational) wave. Compressional waves have vibration parallel to the propagation direction, whereas shear waves have vibration normal to the propagation direction.

The common way of generating elastic waves for laboratory measurements is by the inverse piezoelectric effect. Piezoelectricity is a natural property of certain non-centrosymmetric crystalline materials. When mechanical pressure is applied to these materials, their crystalline structures become polarized and produce a voltage proportional to the applied pressure. The most widely used piezoelectric materials are grouped into two major categories; monocrystalline materials, such as quartz, and polycrystalline materials, such as lead zirconate titanate (PZT) or barium titanate (BT). The latter are commonly referred to as piezoelectric ceramics.

During a process known as 'Poling' the piezoelectric property is imparted to such ceramic materials (fig 5.1). After this process is completed, a voltage lower than the poling voltage changes the dimensions of the ceramic for as long as the voltage is applied (fig 5.2). Depending on the poling axis, mode of vibration and polarisation direction the ceramic either contracts or expands more along the poling axis than any other direction. This contraction or expansion would result in generation of elastic waves that could be of P or S type. For a compressional wave transducer this means maximising the thickness expansion and for shear wave transducer this means maximising the lateral distortion (fig 5.3).

5.2.1 Ultrasonic Waves and Transducers

P and S-waves are two modes of wave propagation normally used for seismic velocity measurements. Elastic waves of high frequency are used for laboratory velocity measurements due to the small size of samples. Elastic waves with frequency above the range of human hearing (i.e., 15-20 KHz) are known as ultrasonic waves. Modern ultrasonic techniques make it possible to generate ultrasonic waves with a frequency of several megahertz or even higher. Most non-destructive testing is carried out within the frequency range 1 to 10 MHz.

Any transducer has a characteristic frequency called a resonant frequency. The resonant frequency is that at which the thickness of the crystal between the electrodes is equal to half of a mechanical wavelength. Thus the relationship between the resonant frequency (f_o) and the mechanical wavelength (λ) is;

$$t = \lambda/2 = c/2f_o$$

$$f_o = c/2t \qquad (5.1)$$

where t is the thickness of the transducer and c is speed of sound in the transducer.

As explained earlier, many types of piezoelectric ceramic materials are manufactured. Each type satisfies the requirements of a particular application. For seismic velocity measurements of rock samples in this study PZT type was chosen. This

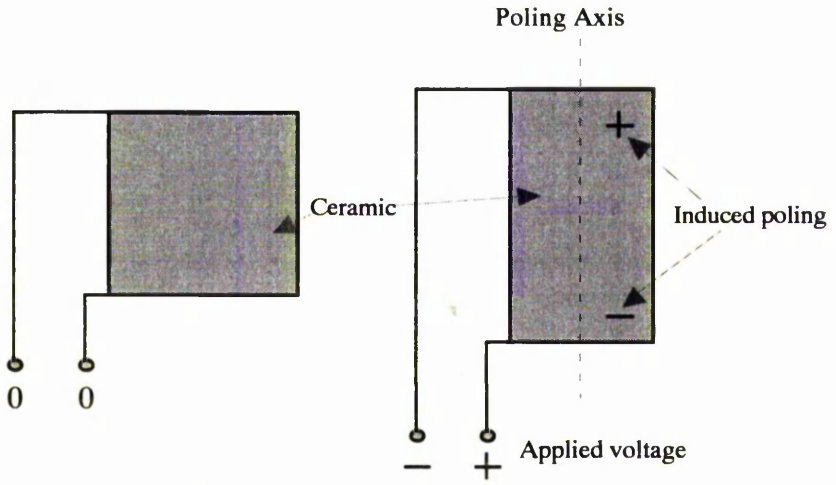

Figure 5.1: Demonstrating the effect of the poling process on a ceramic transducer element. The poling process changes the dimensions of a ceramic element. The scale is exaggerated to show the poling effect better.

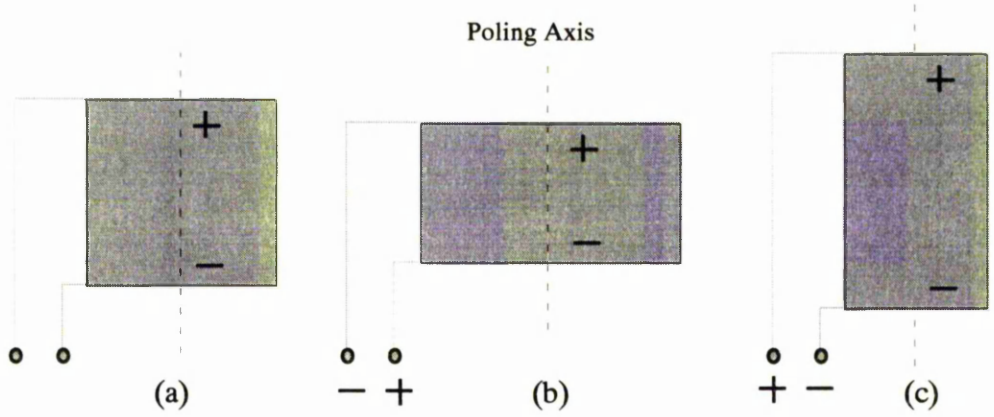

Figure 5.2: Piezoelectric action from applied voltages. a) no voltage applied, b) appled voltage of opposite polarity as poled element, c) applied voltage of same polarity as poled element.

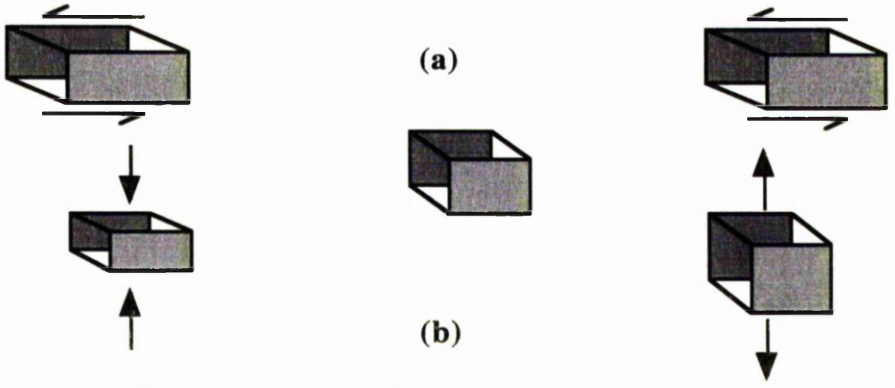

Figure 5.3: Illustrating the thickness shear (a) and thickness expansion (b) of piezoelectric plates under applied voltage resulting in creation of S and P waves. The arrows indicating the shearing, compression and contraction directions.

material has an extremely high mechanical quality and a low loss factor. Also it can be manufactured to any shape or size. Some important properties of PZT type ceramics are shown in table 5.1.

Density	7600 kg/m^3
Velocity of sound	4000 m/s
Curie temperature	300 °C
Resonant Frequency	1 MHz
Poisson's ratio	0.31

Table 5.1. Some properties of Lead Zirconate Titanate Ceramics (PZT-8) as specified by the manufacturer. Piezoelectric materials lose their piezoelectricity above the Curie temperature.

5.3 Methods of Laboratory Velocity Measurements

5.3.1 Common Techniques

In general two methods are employed for laboratory velocity measurements of rock samples. The first method measures *Group Velocity* and it is based on the timing of the propagation of the P and/or S-wave through a known length of a sample. The velocity is then calculated from transmission time (time-of-flight), and the specimen length. This method is carried out in the Time Domain. The second method is performed in the Frequency Domain and measures *Phase Velocity.* It relies on measurements of vibration resonance arising from standing elastic waves generated in the specimen. Frequencies at which resonance occurs are determined and phase velocities calculated from these frequencies. In non-dispersive media there is no difference between group velocity and phase velocity. However in dispersive media the difference is noticeable (see chapter 7). Field seismic experiments measure group velocity therefore it is desirable to measure the group velocity, in the laboratory.

5.3.2 Measuring Group Velocity in the Laboratory

There are two common methods for measuring group velocity in laboratories. One is known as the *Pulse Transmission Method* and the other one known as the *Pulse Echo Method.* In the case of pulse transmission method an ultrasonic transducer is

mounted at each end of a normally cylindrically shaped rock sample. By exciting one of the transducers with a steeply rising electrical pulse it is made to produces a mechanical vibration that propagates through the specimen to the other transducer. The second transducer then acts as a receiver and converts the mechanical motion to an electrical signal (fig 5.4.a). The electric signal is proportional to the mechanical motion and can be amplified and displayed on an oscilloscope. By measuring the time which is taken by the input signal to travel through the sample and knowing the length of the sample the velocity can be easily calculated using the following equation;

$$v = x/t \tag{5.2}$$

where x is the length of the sample and t is the travel time.

The pulse echo method is similar to the pulse transmission method but it uses only one transducer. The single transducer acts as both transmitter and receiver. It is normally mounted at one end of a cylindrically shaped sample, which has the other end a material with different impulse response (the product of velocity and density) than the rock sample. The signal emitted from the transducer travels through the sample, and at the boundary with the sample backing material it is reflected. The same transducer receives the reflected pulse. The travel time of the pulse that travels twice the length of the sample is then used for calculating the velocity (fig 5.4.b). The following expression shows the relationship between the velocity of the sample (v) and the travel time (t).

$$v = 2x/t \tag{5.3}$$

5.4 Experimental Apparatuses

5.4.1 Introduction

The design, construction and assembly of an experimental apparatus that is capable of measuring seismic P-and S-wave velocities at both elevated pressures and temperatures was the first and the most time consuming part of this work. Previously, there was no such apparatus at the Manchester Rock Deformation Laboratory. So most of the time during this research was spent on development, testing and improvement of the seismic apparatus.

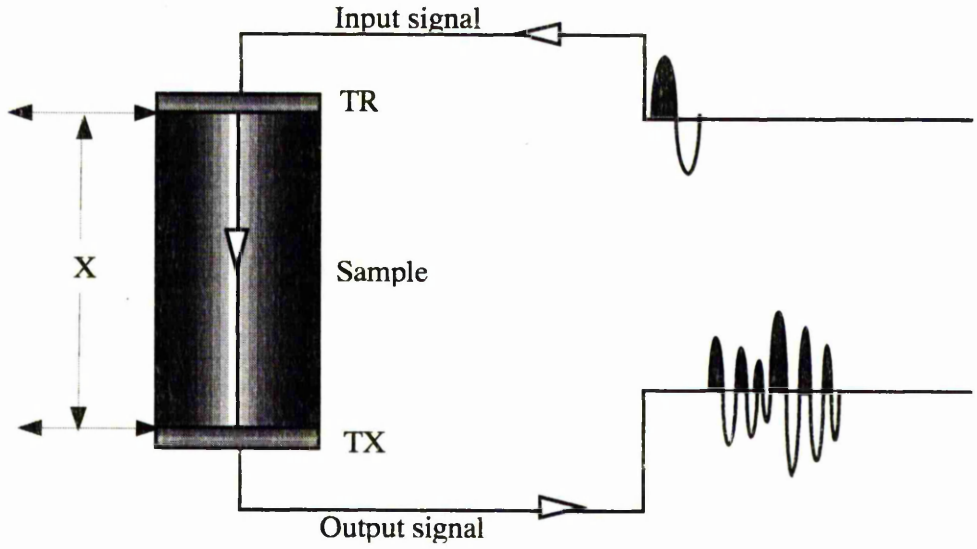

(a)

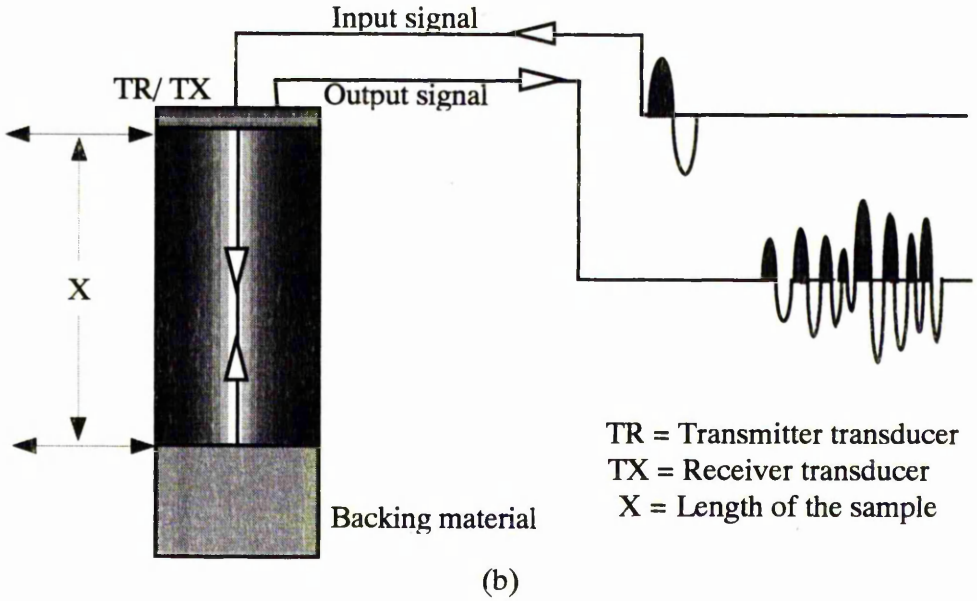

(b)

Figure 5.4: Schematic diagram of (a) pulse transmission method (b) pulse echo method.

It was decided to adapt a pressure vessel, using oil as confining medium, for room temperature, high pressure measurements and a Paterson gas medium apparatus for combined high temperature and high pressure measurements. Any apparatus capable of measuring seismic velocity of rocks at both high pressure and temperature normally consists of three major parts; (a) the high pressure and high temperature systems, (b) piezoelectric assembly and (c) control and recording instruments.

5.4.2 Oil medium apparatus

The oil medium apparatus was designed to generate confining pressure up to 500 MPa by means of an air operated hydraulic pump and an intensifier/separator. The apparatus uses low viscosity oil as the confining medium and is subsequently referred to as the 'oil rig'. It consists of three major parts, (a) the pressure vessel, (b) the air operated hydraulic pump and (c) the hydraulic intensifier/separator (fig 5.5). The air pump supplies ordinary hydraulic oil at pressure up to 70 MPa to one side of the separator/intensifier, which has a hydraulic ratio of 10:1. Thus the intensifier is capable of generating pressures up to 700 MPa. It is therefore used well within its capability. High pressure oil generated by the combined action of the air pump and the intensifier is then led to the pressure vessel through a 700 MPa rated pipe. A low viscosity oil is required for use at pressures in excess of 200 MPa so that, despite the increase in viscosity of oil with pressure, the oil continuous to flow at high pressure. This system is capable of generating confining pressures as high as 500 MPa in a matter of minutes. Three Bourdon tube gauges and one pressure transducer (max. 700 MPa) are used for monitoring the input and output pressures of the intensifier, connecting pipes and the pressure vessel.

5.4.2.1 Pressure vessel

The pressure vessel is a hardened, thick-walled steel cylinder, about 125 mm in wall thickness, 500 mm long and 300 mm in diameter. The bore in the middle is 350 mm long, 50 mm in diameter and has an internal volume of 687 cm^3. It is connected to the pressure generator part of the system through a closure plug and a high pressure pipe

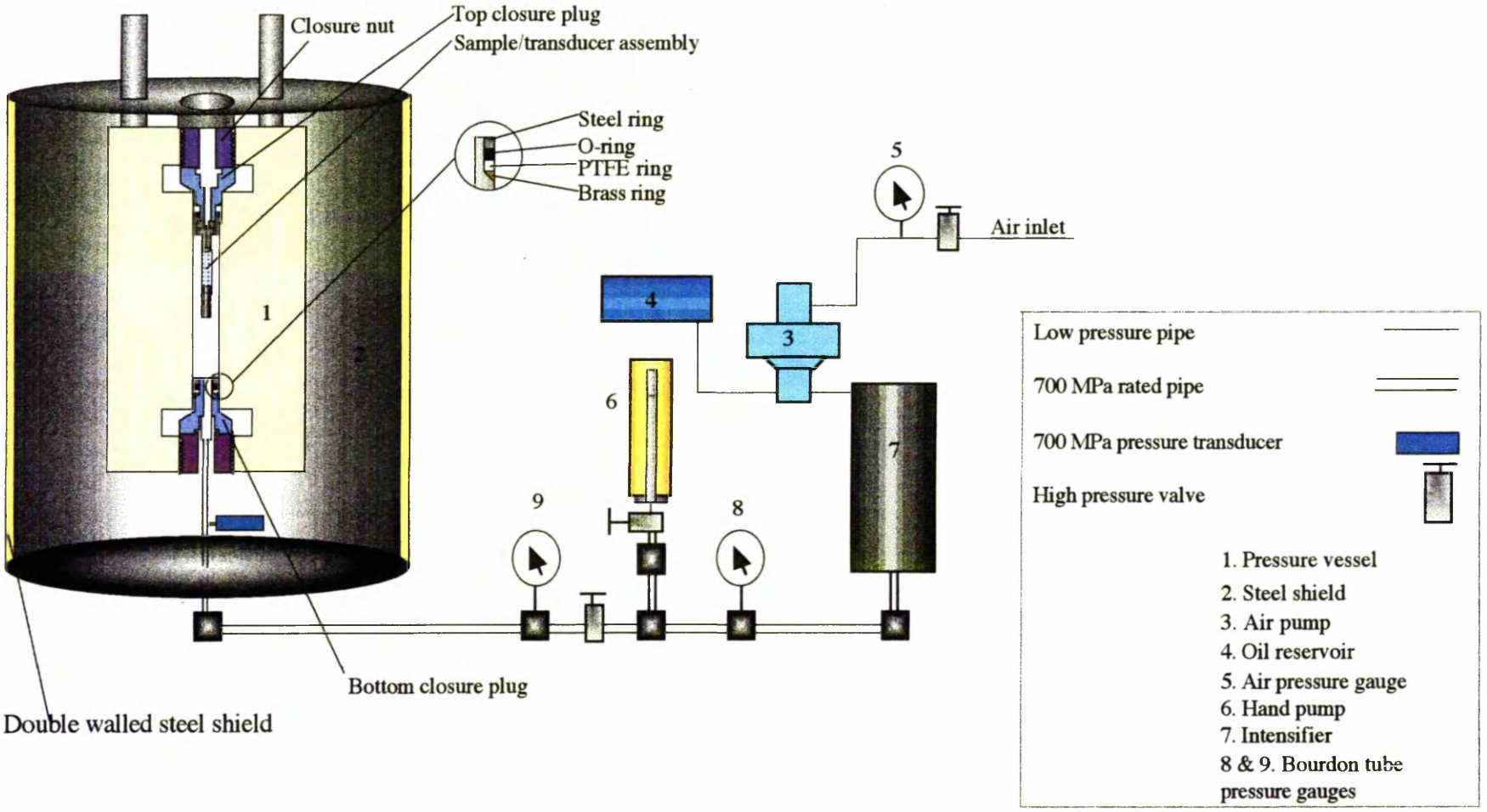

Figure 5.5: Schematic diagram of oil medium apparatus showing the different parts of the high pressure hydraulic system. The scale is exaggerated to show all the major parts.

from the bottom. The specimen/transducer assembly is introduced from the top into the vessel. The combined actions of the closure plug and series of o-rings seal the vessel from the top. The vessel is secured inside a double walled steel shield to form a safety enclosure (see figure 5.5).

5.4.2.2 Air driven pump and intensifier

High pressure air (0.6 MPa) is connected to the air operated hydraulic pump through a regulator, filter and lubricator. The air driven hydraulic pump pressurises the low pressure oil side of the 1/10 ratio intensifier to about 500 MPa.

5.4.2.3 Pressure control and monitoring

An Intersonde HP28 pressure transducer was placed at the bottom of the pressure vessel to measure the confining pressure applied to the specimen. This transducer has a working range of 0-700 MPa and used a 12 V DC supply to power a Wheatstone bridge. A Eurotherm digital indicator was used to display the pressure value, supply the necessary DC voltage for the HP28 pressure transducer and to down load the pressure reading to the controlling computer through a digital serial link. In addition, two Bourdon tube pressure gauges were connected to the pressure line. These gauges were used during the pressurisation of samples to give a direct visual indication of confining pressure.

5.4.2.4 Sample emplacement and operating procedures

The sample/transducer assembly is described in section 5.4.4. The whole assembly is connected to the end of the vessel upper closure plug. The seal comprises a viton rubber 'O' ring, backed by a square section PTFE ring and a brass mitre ring. The plug is forced down the vessel's bore and kept in place by large closure nut above it (see figure 5.5).

Once the sample/transducer assembly has been placed inside the pressure vessel and the necessary electric connections have been made, it is ready for pressurising. The pressurising procedure starts by using a hydraulic hand pump to push the intensifier

piston to one end of its stroke. The air pump then can be switched on to generate pressure at the low pressure side of the intensifier. In turn, the intensifier produces 10 times more pressure at its high pressure side which is connected to the pressure vessel. The intensifier piston normally reaches the end of its stroke before obtaining the necessary pressure (about 500 MPa). Therefore it is necessary to restroke and repeat the above procedure several times.

5.4.3 Paterson Apparatus

Combined high pressure & high temperature velocity measurements were performed on a Paterson Deformation Apparatus. This apparatus is a tri-axial testing machine that is internally heated and uses argon gas as the confining medium. It will subsequently be referred to as the 'gas rig' (fig 5.6). The apparatus was originally designed for experimental rock deformation at high pressure (500 MPa) and temperature (1200 °C). The rig consists of three major parts. A deformation system, a high temperature system and a mechanical/electronic controlling system. The deformation system on its own consists of two sub-systems. One produces axial load on a cylindrically shaped specimen (up to 15 mm in diameter and 40 mm in length), and the other provides confining pressures up to 500 MPa around the specimen.

The ultimate aim of the present developments are to measure seismic velocity of rock samples during deformation but due to the extensive amount of work and limited time available this aim was not realised during the present study. Therefore the Paterson rig was prepared so as to measure seismic velocity of rock samples only under hydrostatic conditions, at high temperature (up to 700 °C) and at confining pressure up to 500 MPa.

5.4.3.1 Preparing the Paterson apparatus for high temperature seismic velocity measurements

There are two major problems facing high temperature velocity measurements. The first one is overheating of the transducers. The transducers lose their piezoelectric property if their temperature exceeds the Curie temperature. In the case of PZT-8

transducers the Curie temperature is 300°C. Even at lower temperatures there is a risk of cracking the transducers by thermal shock. The second problem is taking the necessary electric connections outside the vessel without them being damaged by temperature or pressure.

Section 5.4.4.2 describes the design of the sample/transducer assembly for high temperature measurements. The unique design of the assembly eliminates the above mentioned problems.

5.4.3.2 Operating procedures

Operating the Paterson gas rig for seismic velocity measurements is described in two steps. Firstly the application of the necessary pressure and secondly of the required temperatures.

Figure 5.7 illustrates the gas flow scheme, valves and switches used during pressurising. Commercial high purity Argon gas is drawn from a standard (25 MPa) gas bottle, and the pressure is raised by a gas booster and a ratio intensifier. The compressed air powered gas booster can raise the confining pressure to between 120 to 140 MPa, depending on the initial pressure of the gas bottle. To achieve even higher pressures it is necessary to use the intensifier. The gas booster is first switched off and disconnected from the rest of the system by closing the appropriate valves. The intensifier can provide additional pressure possibly up to maximum of 400 MPa before the intensifier piston reaches the end of its stroke. Confining pressures higher than 400 MPa require recycling of the system. This means closing off the pressure vessel and pushing the intensifier piston up by opening the oil reservoir valve and following the above procedure again.

An internal furnace provides necessary temperatures up to 700 °C. The furnace has three windings with separate controls. The three control settings can be adjusted to minimise thermal gradients along the sample. The required settings for a given specimen temperature were found by measuring the thermal profile across a hollow dummy sample of alumina, as described in section 5.7.3.

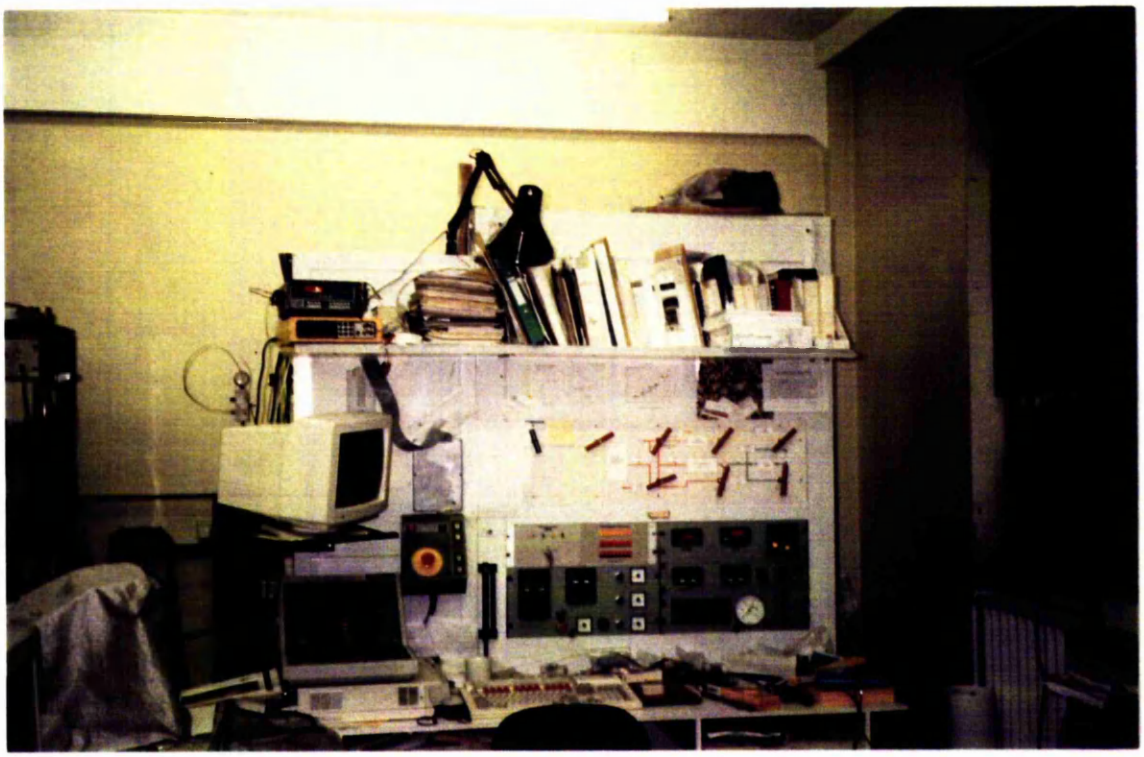

Figure 5.6: An external view of Paterson deformation apperatus.

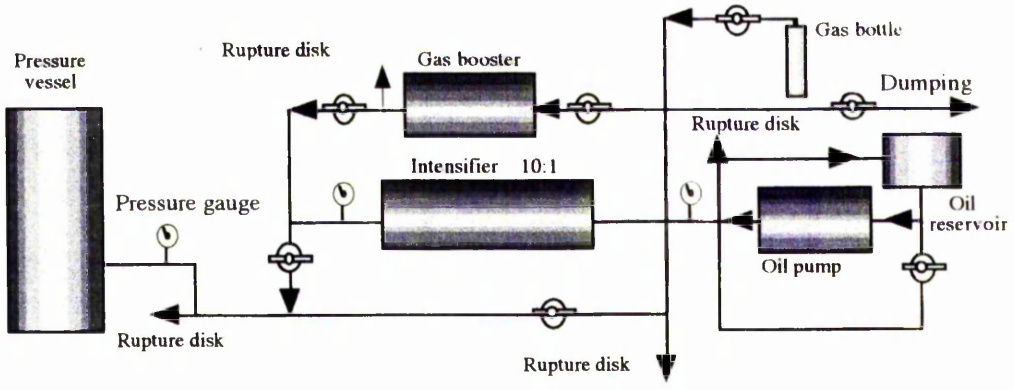

Figure 5.7: Gas flow scheme on Paterson apperatus, showing the valves and rupture disks position on gas line used for hydrostatic pressure application.

5.4.3.3 Pressure and temperature monitoring

The confining pressure is measured using a HP28 pressure transducer placed in the pressure line. The transducer has a maximum working pressure of 0-700 MPa and requires a 10 V DC power supply to provide an output of 0.018 mV per MPa.

The specimen temperature was measured by a nickel-chromium/nickel-aluminium (type K) thermocouple, which touched the top of the specimen after passing through the hollow top piston, transducer and top buffer rod (see figure 5.12). The temperature reading recorded was therefore for the top of the 30 mm long specimen.

5.4.4 Transducer/sample Assembly

Several different designs of sample and transducer assemblies were constructed and evaluated during the course of this work. Finally five designs were found to be more suitable for the aims of this research. Four transducer assemblies were made for room temperature and high pressure measurements and one assembly was produced for combined high pressure and high temperature measurements. For all transducer/sample assemblies it was essential to ensure that the following requirements were fulfilled.

i) The transducers should be kept as safe from possible damage by pressure or high temperature

ii) The electric connections need to be screened against electric and electromagnetic noise.

iii) Perfect mechanical coupling between the transducer and the sample and the transducer and the backing plate is needed to direct most of seismic energy into the sample.

iv) The assembly should be designed in such a way as to make sample changing as easy and quick as possible.

5.4.4.1 Transducer/sample assemblies for HP & room temperature measurements

A total of four different sample/transducer assemblies were designed and constructed for high pressure room temperature seismic velocity measurements. Two assemblies were designed to measure P-and S-waves on 15 mm diameter cores. One

assembly was designed to measure P-and S-wave velocity of 20 mm diameter core simultaneously. Finally, one assembly was constructed to measure possible splitting of shear waves.

Figure 5.8 is a the schematic diagram of the 15 mm and 20 mm transducer assemblies. The discs of piezoelectric material of 12 and 20 mm diameter and 1 mm thickness were secured inside a steel piston. To make the electric connection a steel piece was machined in such a way as to make a flat connection with the bottom of transducer and also to reflect any signal which may emit from the back of the transducer. A piece of pyrophyllite which was hard fired was used to meet the following two requirements:

i) to act as an insulator to avoid any contact between the electrodes and transducer and the steel piston.

ii) to suppress possible signals emitted from the back of the transducer which are not reflected by the connector-reflector disk.

Figure 5.9 illustrates the wire connection for the top and bottom piston. It consists of a 0.5 mm diameter iron wire soldered to the connector-reflector disk backing the transducer. A heat shrink sleeve covers the wire and an earthed brass tube slides over it to screen against any electrical noise.

In the case of dual transducer assemblies (P&S and S&S), transducers were cut in half to form two semicircles. S transducers were cut along the polarisation direction for P&S assembly and parallel and perpendicular to the polarisation direction for the S & S assembly (fig 5.10). The same design of signal transducer assembly was used for the dual assembly with one exception. The cone-shape metal backing connection was cut in half along its cone axes. This provided two separate half cone metal backings which were separated by an insulating strip. The half cone metal backings were in turn connected to separate wires similar to the way described earlier. This allows operation the semicircular transducers individually (see figure 5.8).

In case of the P & S assembly P-wave and S-wave velocities were measured simultaneously. Although S & S assembly was tested for measuring shear wave

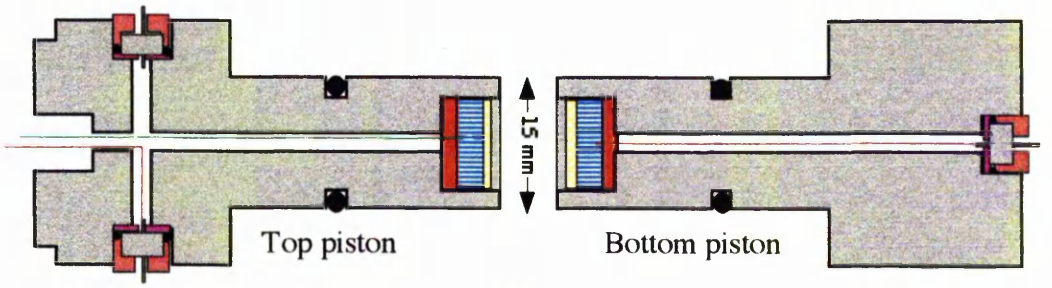

(a)

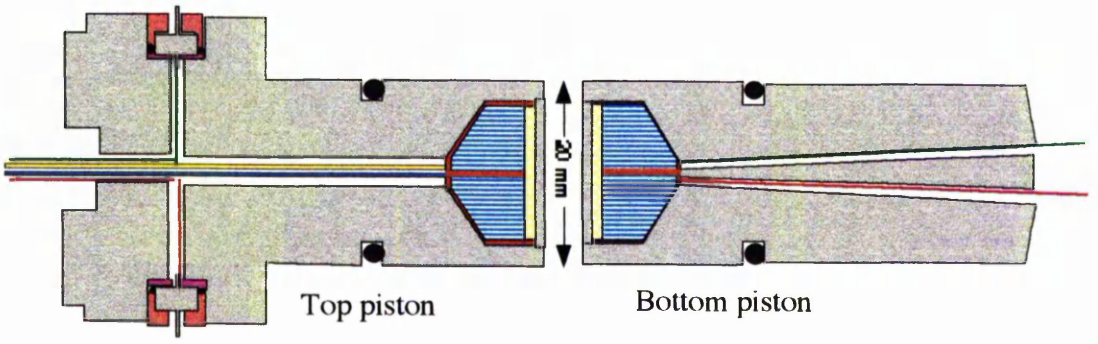

(b)

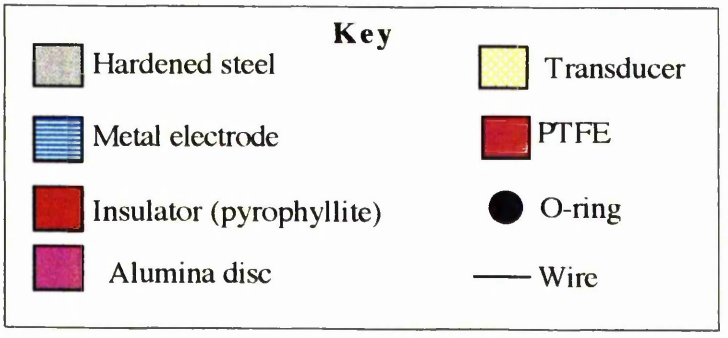

Figure 5.8: A cross section view of pistons containing ceramic transducers for use at room temperature. (a) Top and bottom pistons for 15 mm diameter core size (b) top and bottom pistons for 20 mm diameter cores and simultaneous P and S measurements.

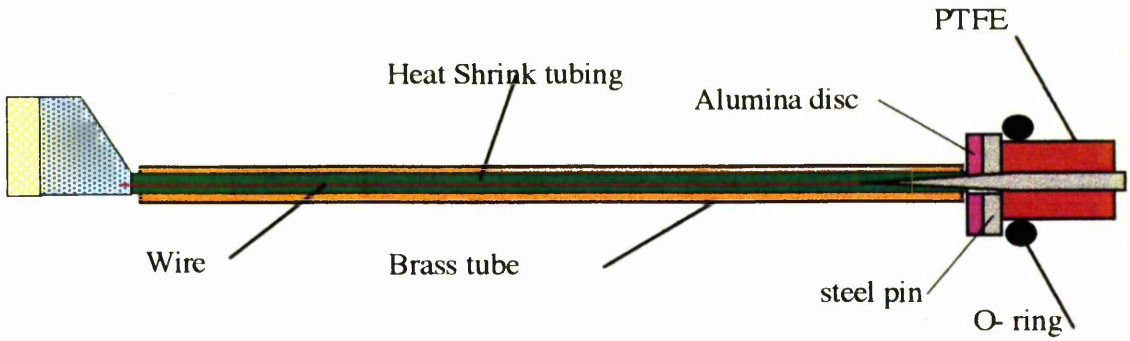

Figure 5.9: Schematic diagram showing the wire connection from the electrode backing the transducer to the outside part of the piston. The O-ring prevents the oil from penetrating inside the piston. The scale is exaggerated to show the details.

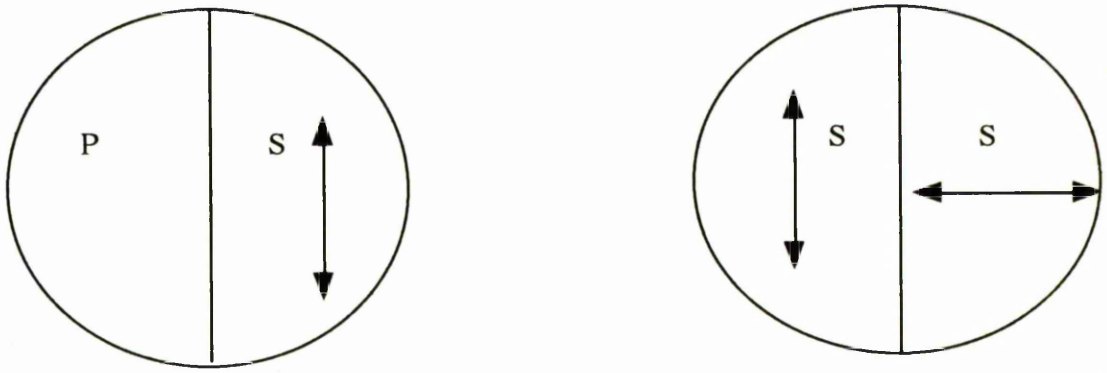

Figure 5.10: Plan view of piezoelectric ceramics which were cut in half to make two semicircles, used for dual transducer assemblies. In case of the S & S dual assembly the shear transducers were cut such that their polarisation directions were perpendicular to each other.

splitting but due to time constraints no systematic measurements of shear wave splitting were carried out.

Figure 5.11 shows a schematic diagram and a picture of the 15 mm assembly. The rock sample and the two pistons are held together by sliding a rubber tube over them. There is an o-ring near to the end of each piston which prevents the penetration of oil into the rubber tube. The whole assembly is a little loose when assembled but under pressure it straightens up to ensure perfect acoustic coupling between pistons and the sample.

5.4.4.2 Transducer / sample assembly for high pressure / temperature measurements

The high temperature/high pressure assembly consists of two pistons containing the receiver and the transmitter transducers, two buffer rods, the rock sample, the iron jacket and appropriate electrical connections (fig 5.12).

The transducer assembly and the connections are similar to the low temperature assembly. The connection from the bottom transducer was designed in such a way as to form a spring-loaded connection between the side of the piston and two semi-circular gold covered segments at the bottom of the furnace when the assembly is inserted into the pressure vessel. The gold ring segments are welded to two insulated platinum wire connections which pass through the insulation in the body of the furnace. This ensures that the connections do not become hot. There are six connection leads which come through the top closure of the pressure vessel, normally used for temperature measurement and control and the live furnace leads. Two of these connections were replaced by the bottom acoustic transducer connections. The top transducer was placed at the low pressure, low temperature side of the vessel closure, therefore there was no problem with making the electrical connections.

The top piston is made from hardened steel with a 1 mm axial hole. This hole is normally only for the thermocouple to pass through. A PZT-8, 1 MHz and 15 mm diameter transducer is placed on the flat low pressure side of the top piston. A copper plate connected to a brass tube acts as the "live" electrode. This is connected to the exterior by a 1.3 mm diameter brass tube. A 0.5 mm diameter Cr/Al thermocouple

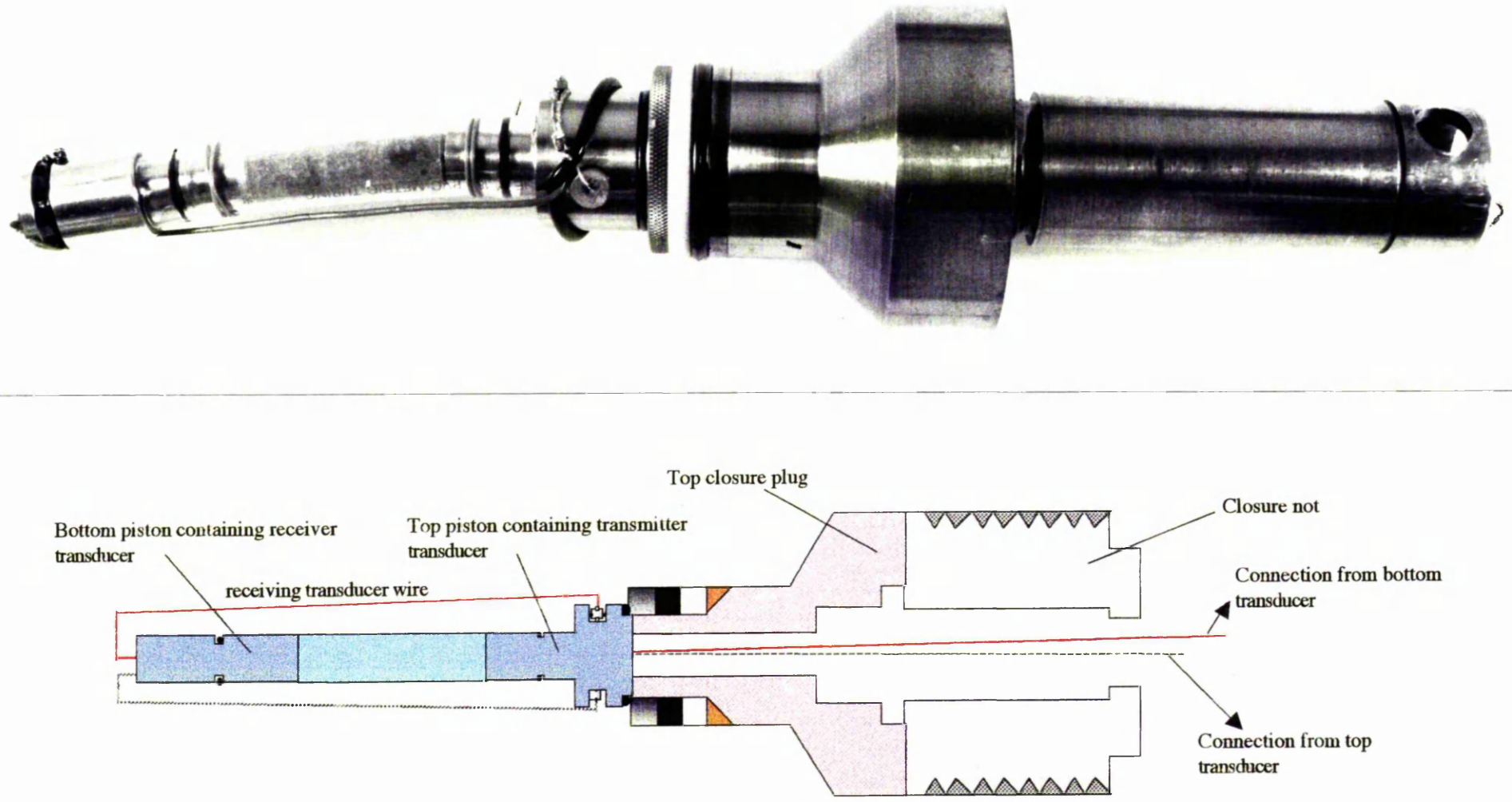

Figure 5.11:(top) A Photograph of the transducer/sample assembly showing the sample sandwiched between the two pistons and a rubber tube slid over it. (bottom) Simple illustration of the top plug closure and transducer/sample assembly

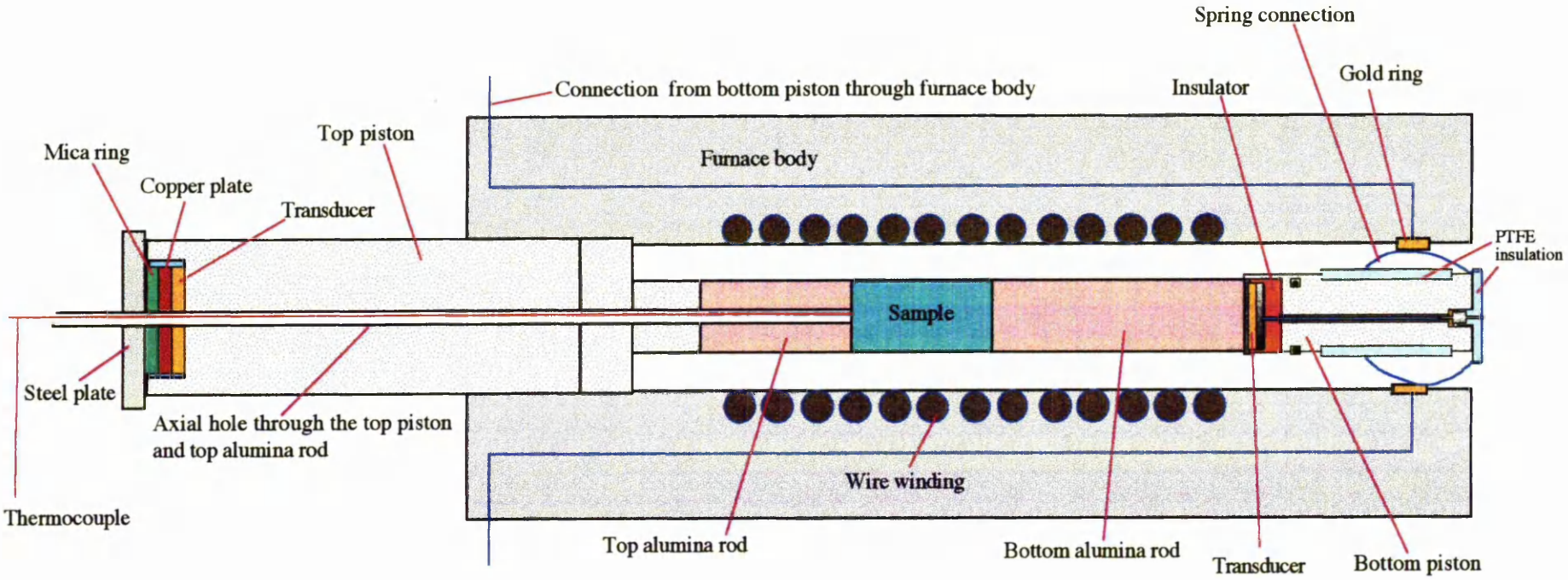

Figure 5.12: Schematic drawing of the furnace inside the gas rig pressure vessel, showing the sample/ transducer assembly and its different parts. The assembly is about 300 mm in length and 50 mm in diameter.

passes through this tube, the transducer and down the hollow piston until it contacts the top of the sample (see fig 5.12). The top closure plug, which screws on to the top of the piston and an intervening metal plate, forces the copper electrode, transducer and the steel piston together, producing a mechanical coupling. A mica sheet was used as insulator between the copper disk and the metal disc upon it. After pressurising the vessel the top piston is forced outwards. This produces extra axial load on the transducer, metal backing and the piston to ensure perfect coupling.

In order to keep the transducer away from elevated temperature, it was necessary to use two recrystallized alumina (Al_2O_3, 99.5 %) buffer rods, to increase the length of the assembly. This kept the transducers outside the furnace. Alumina buffer rods were chosen because of their extremely high seismic velocity (10 km/s), high melting point (table 5.2) and fairly low thermal conductivity. The top alumina rod has a hole through it aligned with the hole in the top piston to accommodate the sample thermocouple.

Principal Constituent	Al_2O_3	99.7
Apparent Density	g/cm^3	3.7-3.95
Grain Size	μm	10-20
Total Porosity	%	0
Hardness	N/mm^2	23000
Compressive Strength	N/mm^2	3000
Melting Point	°C	2030
Specific Heat	J/gK	850
Thermal Conductivity at 100°C	W/mK	25-30
Compressional Velocity	km/S @ 1 kbr	10.404

Table 5.2 Some physical properties of the aluminium oxide ceramic (recrystallized alumina rod) as specified by the manufacturer. Seismic velocities for this material were measured at elevated pressure and room temperature using the oil rig apparatus.

Figure 5.13 shows the sample, alumina and pistons assembly. The cylindrical shaped rock sample, sandwiched between the two alumina pistons is placed inside an 0.25 mm wall thickness iron jacket and the two pistons are pushed into each end of the metal jacket. The O-ring on the bottom piston seals the jacket at the bottom and the combination of an O -ring and a gland nut seals the jacket at the top.

Figure 5.13: A photograph of transducer/sample assembly for high temperature and high pressure compressional velocity measurements. The picture shows the top and bottom pistones and the iron jacket which is slid over the sample and two alumina bars (Centimetric scale bar)..

Heat treated alumina paper was wrapped around the metal jacket before placing the assembly inside the vessel. This helps ensure homogeneous distribution of the temperature along the sample. This alumina paper is held in place with three curved plates of zirconia, to minimise heat loss.

5.4.5 The Electronic Part of the Seismic System

Figure 5.14 illustrates the connections and the electronic instruments. A signal generator produced a single cycle 1 MHz sine wave with 5 ms repetition rate. The signal (with 7 V peak to peak amplitude) from the signal generator was then amplified using a power amplifier to a 50 V or 100 V peak to peak signal. The amplified signal is transmitted to the assembly along a 1 mm coaxial cable. The bottom transducer acted as a receiver. Its signal was displayed on a 300 MHz dual channel LeCROY Oscilloscope. The arrival time of the signal can be measured either on the scope, or can be down-loaded to the computer and then stored for further processing.

5.4.5.1 Signal generator

A Thurlby TG1304, 13 MHz programmable Function Generator was used to generate a single cycle 1 MHz sine wave needed for exciting the transducers.

5.3.5.2 Oscilloscope

A LeCROY 9310/14 series digital oscilloscope was used for displaying signals. The scope is a 300 MHz dual channel instrument capable of performing various kinds of arithmetic and analyses on the digital signal (e.g. signal averaging, Fast Fourier Transform etc.). The instrument also has a RS-232-C remote control port, as well as the GPIB (IEEE-488) interface bus. The latter was used to interface the oscilloscope directly to the Acorn 410/4 computer.

5.4.5.3 Amplifier

A power amplifier was designed and constructed to amplify the input signal. The sine wave source signal of 1 MHz frequency and 7 V peak to peak was amplified to

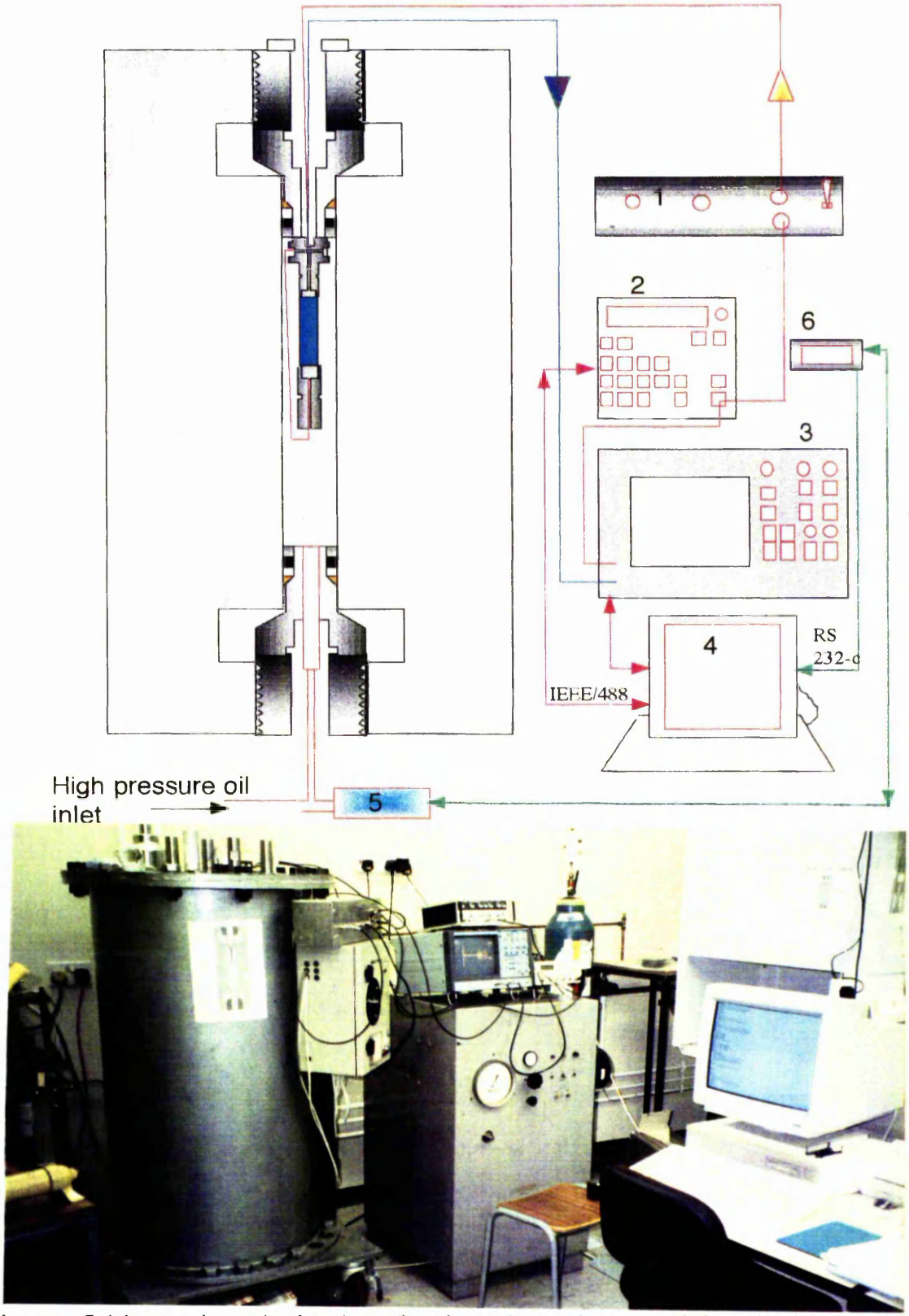

Figure 5.14: a) schematic drawing of various electronic parts of the seismic system and their interfacing. b) Picture of Oil medum apparatus and electronic instruments. [1) amplifier, 2) Function generator 3) Oscilloscope 4) Computer 5) pressure transducer 6) digital pressure indicator].

50 V peak to peak before being feed to the transmitter transducer. The dynamic range of the return signal is normally expected to be in excess of 80 dB. Therefore there was no need to amplify the receiver signal.

5.4.5.4 Computer

Due to the large number of velocity measurements required for the research (many thousands) it was necessary to record each waveform individually for possible future processing and measurements. All electronic instruments except the amplifier were interfaced with an Acorn 410/4 personal computer via both IEEE or serial links. This allows the computer to monitor and record all the activity of the individual instruments. A computer program was written in the BBC BASIC language (appendix 2) to provides the following features (fig 5.15);

i) Monitoring the activity of the Function Generator and LeCroy Oscilloscope

ii) Down loading waveforms from the LeCroy oscilloscope to a personal computer

iii) Down loading the pressure reading of the pressure transducer

iv) Manipulating the waveform such as signal averaging, signal expansion, saving and re-loading of the waveforms

v) Time and amplitude measurements

vi) Fast Fourier Transform (including amplitude and phase spectrum and digital filtering).

5.5 Data Logging Procedures and Processing

As mentioned in the previous section data logging software was written. The program is capable of down loading the pressure, the temperature and the waveform automatically with a user-defined rate of logging or selective data logging. In the latter case by using the mouse the user clicks on an icon to download the data. Each waveform along with the other related data such as pressure, temperature and any other information related to that test (e.g., sample number, sample length, data, etc.) is saved as text-formatted data file. This allows the data to be transferred to other types of computer if necessary, and to other software, e.g. spreadsheet. The waveform data is

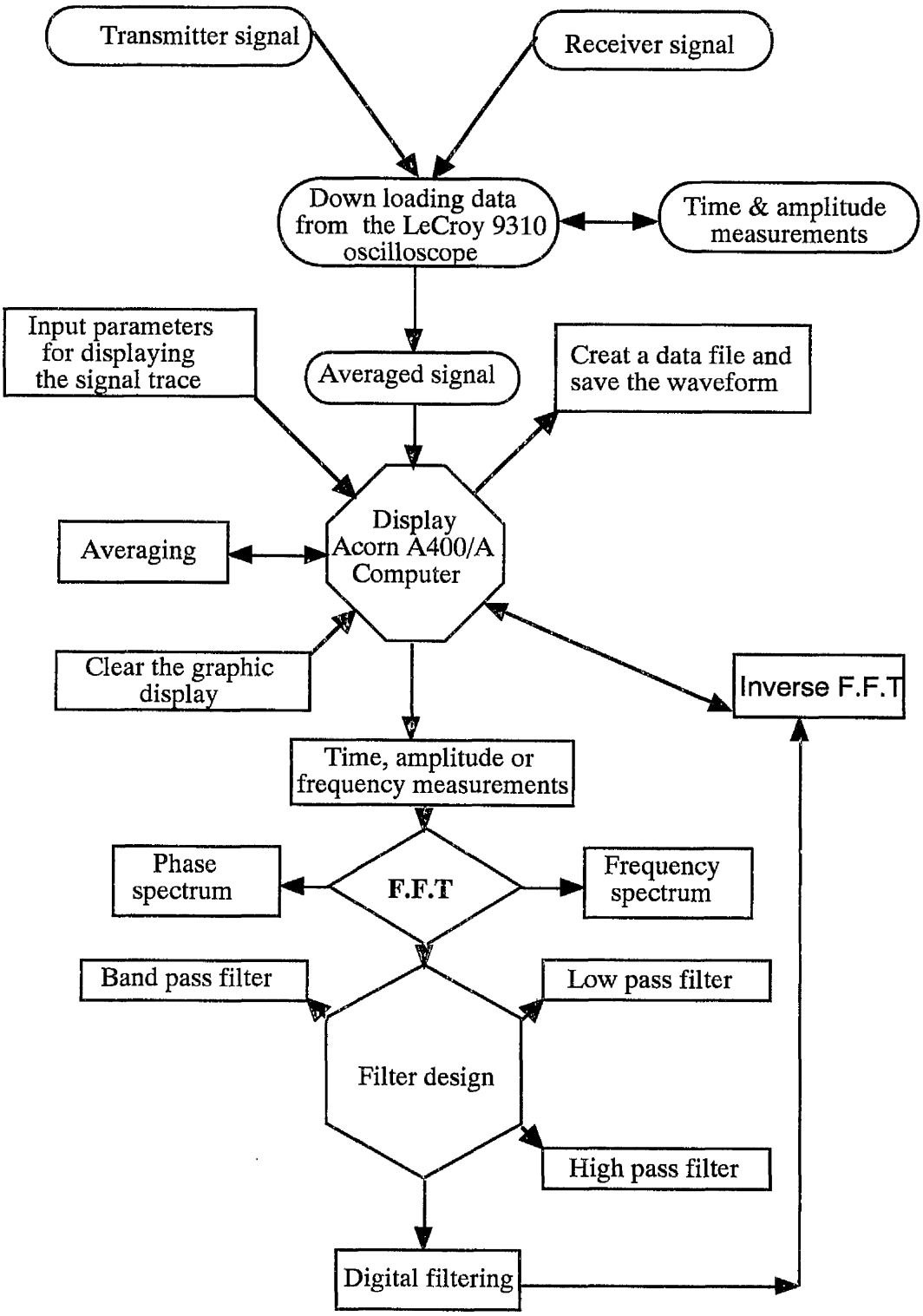

Figure 5.15: Flow chart of the seismic program. (F.F.T = Fast Fourier Transform)

recorded in a single column. The first five records contain information describing the sample and records six and seven contain information concerning the pressure and temperature.

5.6 Improving the Signal

Rocks have high attenuation factor for seismic energy, therefore it is important not only that as much energy as possible is transmitted into the sample, but also to protect it from interference by unwanted signals or random noise.

5.6.1 Transducer Backing

If the transducer is exited with a single pulse, it will continue to change its thickness for a short time thereafter. This phenomenon is known as ringing (Allocca et al., 1984). To have a clean signal it is important to suppress ringing. Transducers should be mechanically damped in order to reduce ringing and spurious echoes from inside the transducer. The backing material should have high density and be highly absorbent to ensure a reasonable bandwidth and to reduce the ringing effect. The subject of the backing material is thoroughly discussed by Silk (1984). He explains how to choose a backing material, based on the acoustic impedance of the piezoelectric plate and, describes some well-known backing materials. Pyrophyllite hardened by firing to 1000°C was used in the present study as the backing material and to provide electrical insulation and performed very well.

5.6.2 Cables and Connections

It is well established that cables may pick-up noise signals when subjected to shock and vibration. This noise maybe due to the proximity of an electromagnetic field, radio frequency transmitters or static disturbance (Perls, 1952). To avoid these problems precaution should be taken by means of effective grounding, shielding and use of low impedance coaxial cables. Screened wires were used wherever possible to minimise noise and other unwanted pick up.

5.6.3 Amplifying and Averaging the Signal

Both the input and output signal can be amplified as long as the signal to noise ratio remains high. It is important to use the same amplification and gain for all tests as the position of the first break is gain-dependent. All tests were carried out using 50 V peak to peak input signal in case of the oil rig system and 100 V p-p for the gas rig seismic system. To improve further the signal to noise ratio, the seismic waveforms were averaged in real time for over 2000 times on the oscilloscope.

5.7 Testing Procedure

5.7.1 System Calibration

There were two sets of calibrations to be carried out. First to calibrate the pressure and temperature monitoring instruments, second to measure the total time delay. The total time delay is the time taken by the signal to travel outside the sample.

5.7.2 Calibration of Pressure Transducers

The oil rig pressure transducer used for monitoring the confining pressure was bought brand new. It was calibrated against a Bourdon tube gauge. The calibration results were in excellent agreement with manufacturers calibration (fig 5.16).

An Intersonde HP28 high pressure transducer was used for monitoring the confining pressure of the gas rig. Its calibration was checked before the first high temperature test, using a Heise gauge (fig 5.17). It was found to be consistently reading 0.12 mV too low and this was accounted for.

5.7.3 Temperature Monitoring

A brand new 0.5 mm diameter, type K thermocouple was used for temperature monitoring. The thermocouple measures the temperature at the top of the specimen. Thermal convection inside the pressure vessel results in a temperature variation along the

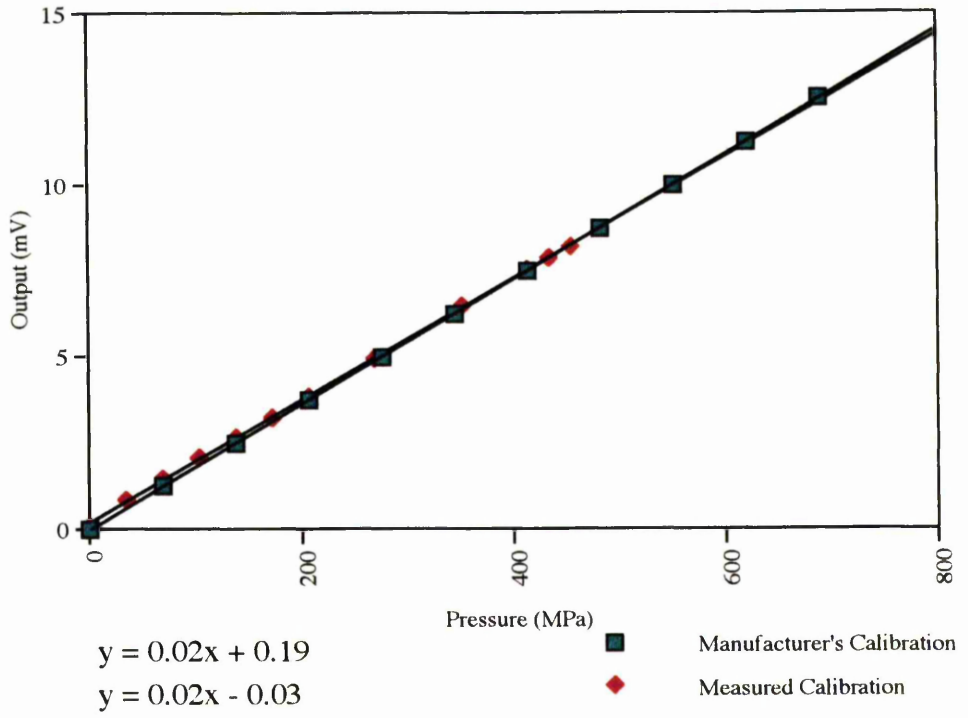

Figure 5.16: Plot of output from the pressure transducer (HP28/ serial no: 10724) in mV versus the pressure reading in MPa on the Bourdon tube gauge and the output in mV from the transducer per MPa according to manufacturer.

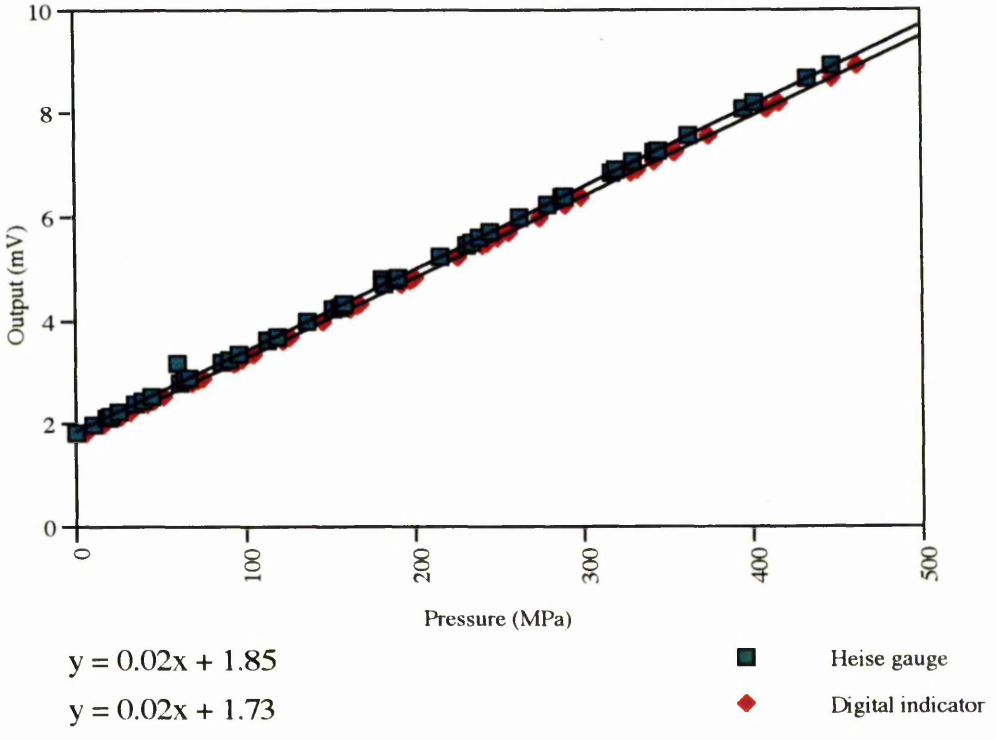

Figure 5.17: Plot of Output reading of pressure transducer in mV versus the pressure reading on a Heise gauge and on the pressure transduce in MPa.

sample. The thermal profile along the length of a dummy sample was measured in order to measure the temperature variation along the sample. A 30 mm long alumina rod with a 1 mm diameter axial hole in its centre was used for estimating the thermal profile along the sample and to find the position of the hot zone. Temperature was measured at 5 different positions simultaneously along the dummy sample using a spaced array of thermocouples along the hole in the middle of the dummy sample with a real time computer graphical display. The drive to each furnace binding could be independently adjusted to optimise the thermal profile at each temperature. Figure 5.18 shows the variation in temperature along the length of the dummy sample. It is evident that the maximum temperature difference along the sample does not exceed 10 °C at 300 °C peak temperature and 25 °C at 700 °C. The maximum obtainable temperature (700 °C) and the degree of control over the thermal profile are limited by maximum available input power set against heat-loss by convection and conduction along the sample assembly.

5.7.4 Measuring the total delay time

Electronic instruments and cable connections introduce some time delay for the transmitted signal. Additionally time taken by the signal outside the specimen must be deducted from the total travel time in order to calculate the velocity. Two different methods were used for measuring the total delay time of the seismic systems on the oil rig and on the gas rig.

5.7.4.1 Measuring the total delay time of the oil rig seismic system

The best way to measure the total time delay is by measuring the travel time through sets of alumina rods (dummy specimens) of different lengths and extrapolating to zero length. A long alumina rod of high purity (99.7%) was machined and cut to required diameter and different lengths. Figure 5.19 shows the plots of total travel time versus the length of alumina rods. By extrapolating the plot to zero length the total delay times of the different transducer assemblies were obtained.

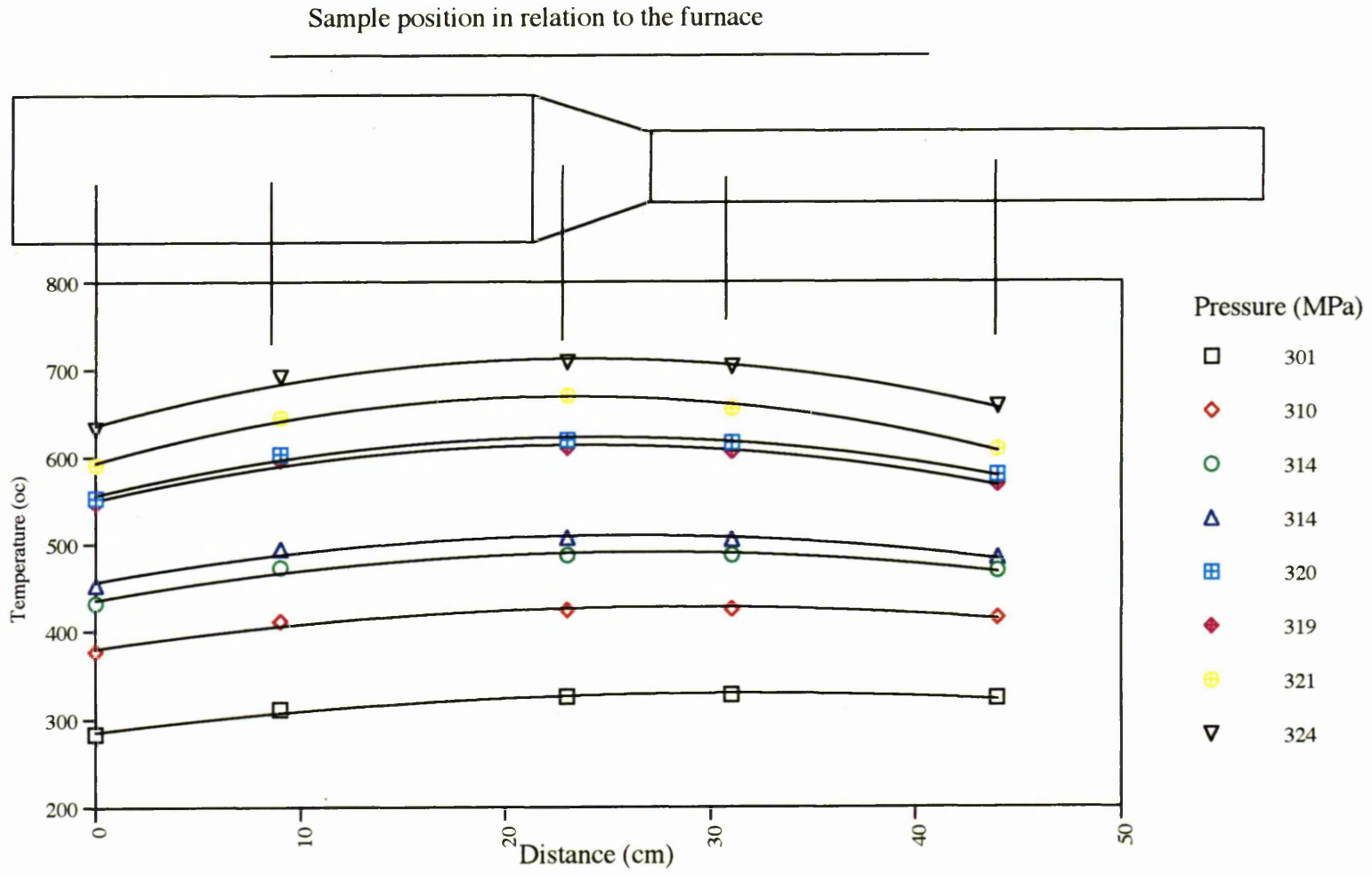

Figure 5.18: Plot of temperature reading of five thermocouples at varius pressure (in MPa) versis their distance along the dummy sample. The drawing above the plot is of the dummy sample and the vertical lines indicating the position of the thermocouples. The sample position with respect to the thermocouple positions is shown.

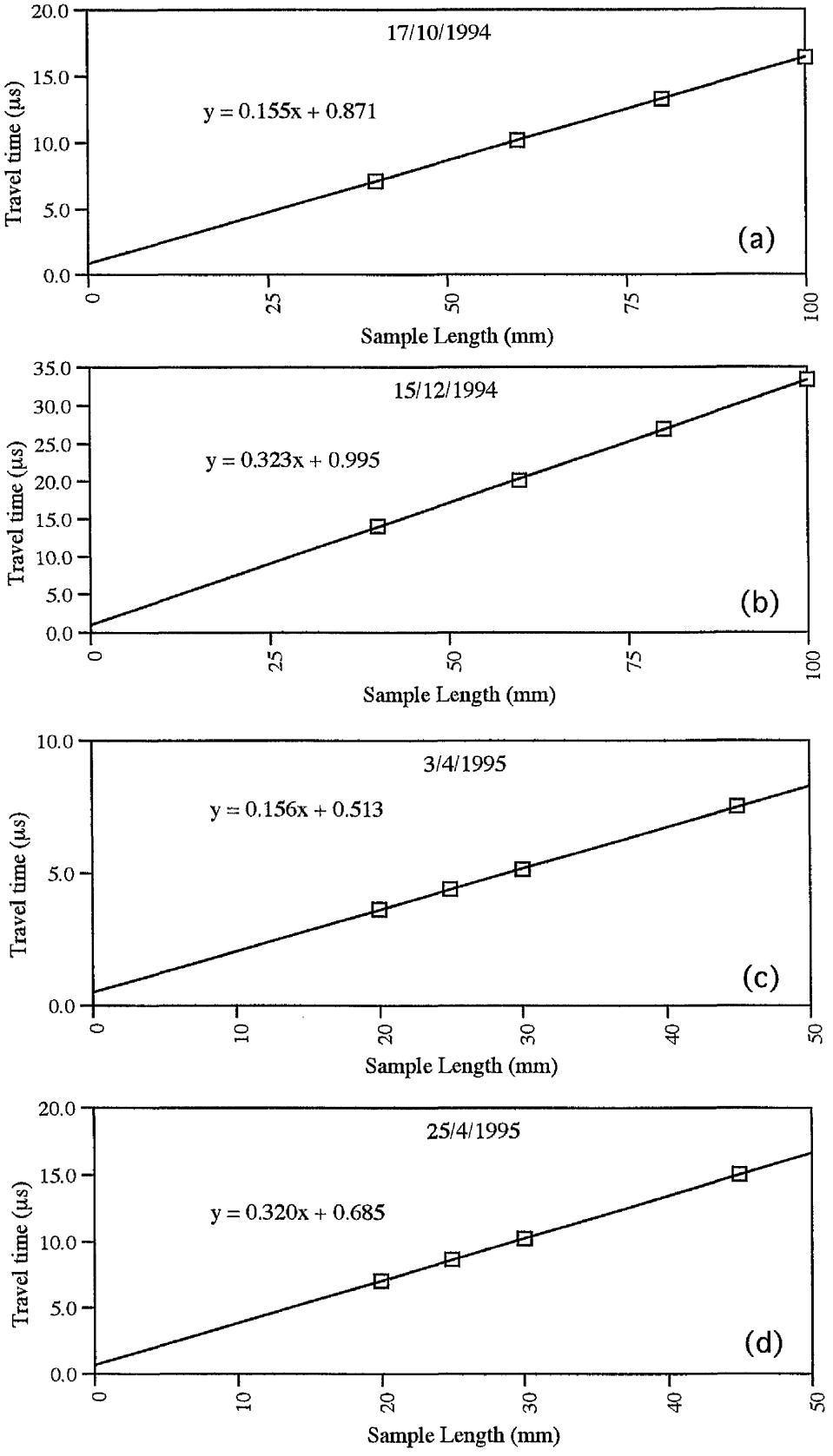

Figure 5.19: Total delay time of room temperature and high pressure seismic velocity measurments system using different transducer assemblies. The intercept of the best fit line with the Y axis would give the total delay of the seismic system. (a) using the 15 mm P-wave assembly. (b) using 15 mm S-wave assembly. (c) using the P-wave one inch assembly and (d) the 1 inch S-wave assembly.

5.7.4.2 Measuring the total time delay of the gas rig seismic system

Figure 5.12 shows the sample/transducer assembly for high temperature, high pressure measurements. The signal emitted from the transmitter transducer (in the bottom piston) travels through many different materials. It travels through a 1 mm thick steel disk, a 90.61 mm long alumina rod, the specimen (about 35 mm), the top alumina rod (42.54 mm in length) and finally through the top steel piston (79.05 mm in length) before reaching the receiver transducer. The total transmission time (t_t) of the signal is equal to the transmission time through the sample (t_S) plus the transmission time through the rest of the assembly (t_d). As the measurements are carried out at high pressure and temperature the transmission time can be described by the following equations:

$$t_t = t_s + t_d \tag{5.4}$$

where ;
t_t is the total measured travel time at a given P & T
t_s is travel time through the sample at a given P & T
t_e is travel time through materials other than specimen at a given P & T

Assuming a linear variation of travel time with pressure and temperature and no second order effects, then the equation 5.4 can be rewritten as follows;

$$\left(\frac{\partial t_t}{\partial P}\right)T + \left(\frac{\partial t_t}{\partial T}\right)P + C = \left[\left(\frac{dt_s}{\partial P}\right)T + \left(\frac{\partial t_s}{\partial T}\right)P + C'\right] + \left[\left(\frac{\partial t_d}{\partial P}\right)T + \left(\frac{dt_d}{\partial T}\right)P + C''\right] \tag{5.5}$$

where at a given pressure and temperature;

$$t_t = \left(\frac{\partial t_t}{\partial P}\right)T + \left(\frac{\partial t_t}{\partial T}\right)P + C$$

$$t_S = \left(\frac{dt_s}{\partial P}\right)T + \left(\frac{\partial t_s}{\partial T}\right)P + C'$$

$$t_d = \left(\frac{\partial t_d}{\partial P}\right)T + \left(\frac{dt_d}{\partial T}\right)P + C''$$

$\left(\frac{\partial t_t}{\partial P}\right)$ is the pressure coefficient of total transmission time at a given temperature

$\left(\frac{\partial t_t}{\partial T}\right)$ is the temperature coefficient of the total transmission time at a given pressure

$\left(\frac{dt_s}{\partial P}\right)$ is the pressure coefficient of transmission time through the specimen at a given temperature

$\left(\frac{\partial t_s}{\partial T}\right)$ is the temperature coefficient of transmission time through the specimen at a given pressure

$\left(\frac{\partial t_d}{\partial P}\right)$ is the pressure coefficient of transmission time outside the specimen at a given temperature

$\left(\frac{dt_d}{\partial T}\right)$ is the temperature coefficient of the transmission time outside the specimen at a given pressure

C, C' & C'' are constants.

To calculate the travel time through the specimen at various pressures and temperatures the equation (5.5) can be rearranged as follow;

$$\left(\frac{dt_s}{\partial P}\right)T+\left(\frac{\partial t_s}{\partial T}\right)P+C' = \left[\left(\frac{\partial t_t}{\partial P}\right)T+\left(\frac{\partial t_t}{\partial T}\right)P+C\right]-\left[\left(\frac{\partial t_d}{\partial P}\right)T+\left(\frac{dt_d}{\partial T}\right)P+C''\right] \qquad (5.6)$$

If the delay time is known then the travel time through the specimen can be easily calculated from the measure d time. Once the delay time is calculated for a given pressure and temperature, it will be the same for all measurements at that pressure and temperature, provided no modifications have been made to the assembly.

To calculate the delay time we need a specimen with a known linear velocity over a range of pressures and temperatures. From the P-wave velocity the travel time of compressional wave through the specimen (t_S) then was calculated. Knowing the travel time through the specimen (t_S) then the total delay can be calculated by subtracting the total transmission time (t_t) of the signal from the travel time through the specimen (t_S) at a given pressure and temperature.

To use this method to find the total delay a material whose velocity is known accurately at a wide range of P & T was needed. The pressure and temperature dependence of some metallic materials such as aluminium or steel are known. However it was decided not to use them for two main reasons. One is because of impurity effects and compositional variation of metallic materials which can have noticeable effects on their elastic properties. The second reason was the high thermal conductivity of metals (e.g. copper=390 W/m K; aluminum=220 W/m K at 0°C; after Lide, 1994) in comparison with rocks (e.g. granite 2.2 W/m K; limestone 2.0 W/m K; average for calcite single crystal 5.05 W/m K at 0°C; after Lide 1994), which would produce a different thermal profile across the sample assembly. Therefore when the dummy sample is replaced by the real rock, it is likely that a different thermal profile would form and consequently cause some change in total travel time.

After some research it was decided to use a calcite single crystal for calibration for the following three reasons:

i) known high pressure and high temperature elastic stiffness

ii) high purity sample material readily available

iii) better analogue of real rocks than metals in terms of having thermal conductivity much closer to rocks than metals.

Calibration of the high temperature and high pressure seismic compressional velocity measurement system therefore was carried out according to the following five steps.

1) A high purity single crystal of calcite was cored along its "*r* " direction (normal to cleavage; fig 5.20). After several attempts a good core, 34.25 mm in length and 14.76 mm in diameter was obtained.

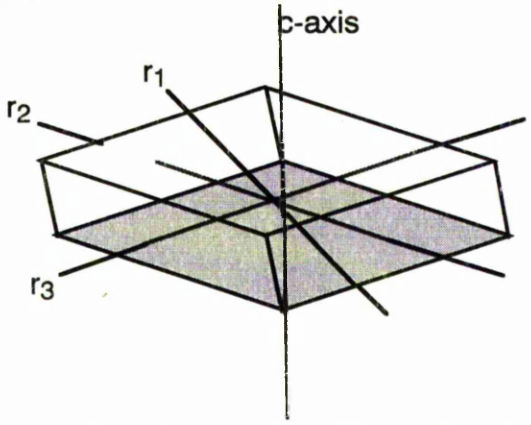

Figure 5.20: Schematic illustration showing the rhombohedral unit cell for calcite and the relationships between the c-axes, the poles to the cleavage planes and rhombohedral axes r_1, r_2, r_3.

2) The compressional velocity matrix for a single crystal of calcite was calculated from its elastic stiffness tensor (Dandekar, 1968) using the Mainprice seismic velocity method (1990) at a range of pressures (Max. 600 MPa) and temperatures (Max. 500°C).

Figure 5.21 & 5.22 show the calculated seismic P-wave velocities of a single crystal of calcite over a complete sphere at various temperatures and pressures. From the calculated velocity the expected P-wave travel time was estimated for the calcite core

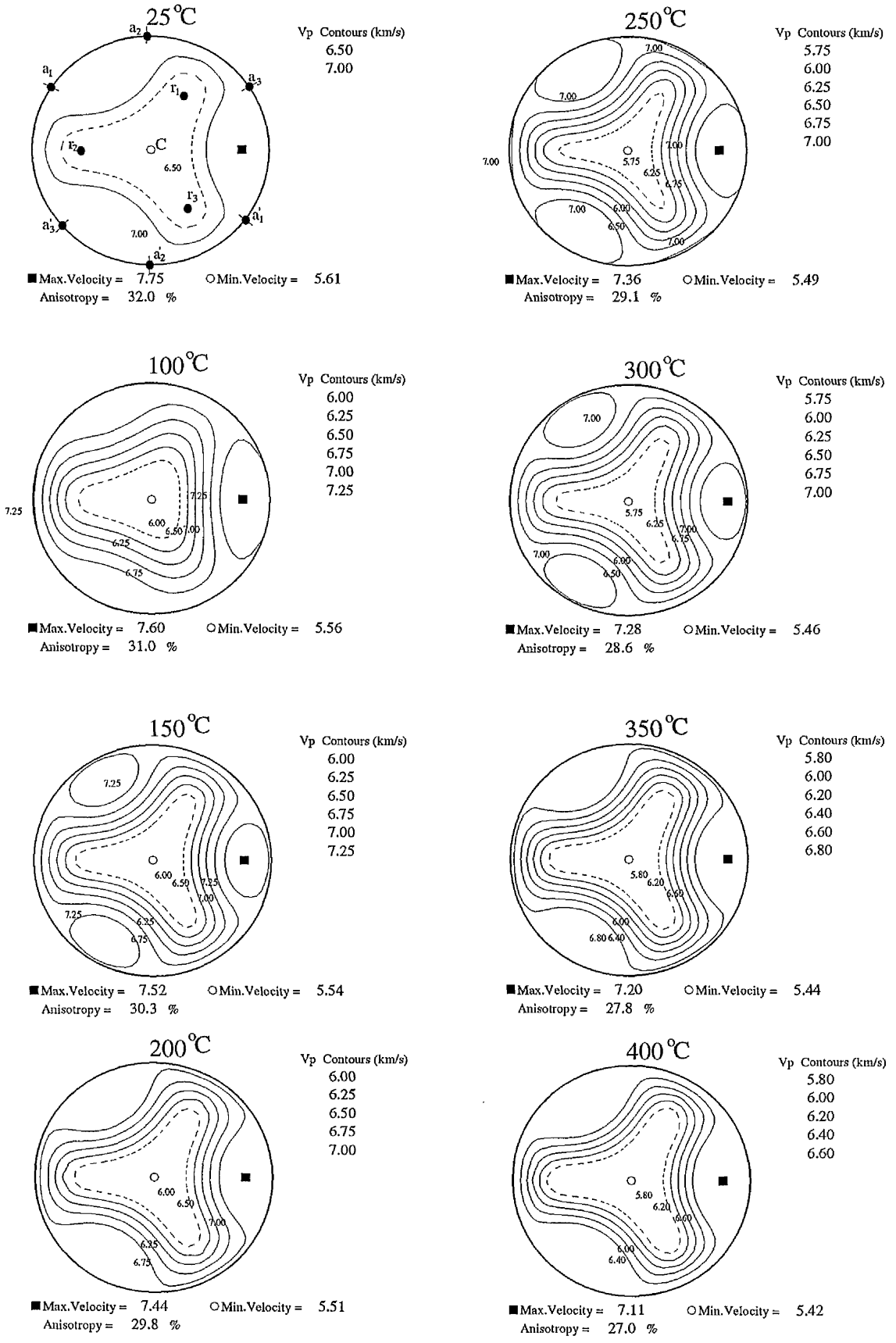

Figure 5.21: Calculated compressional velocity for a single crystal of calcite at various temperature and room pressure. The position of c- & a-axes and poles to the cleavage planes (r) are also marked on the first plot.

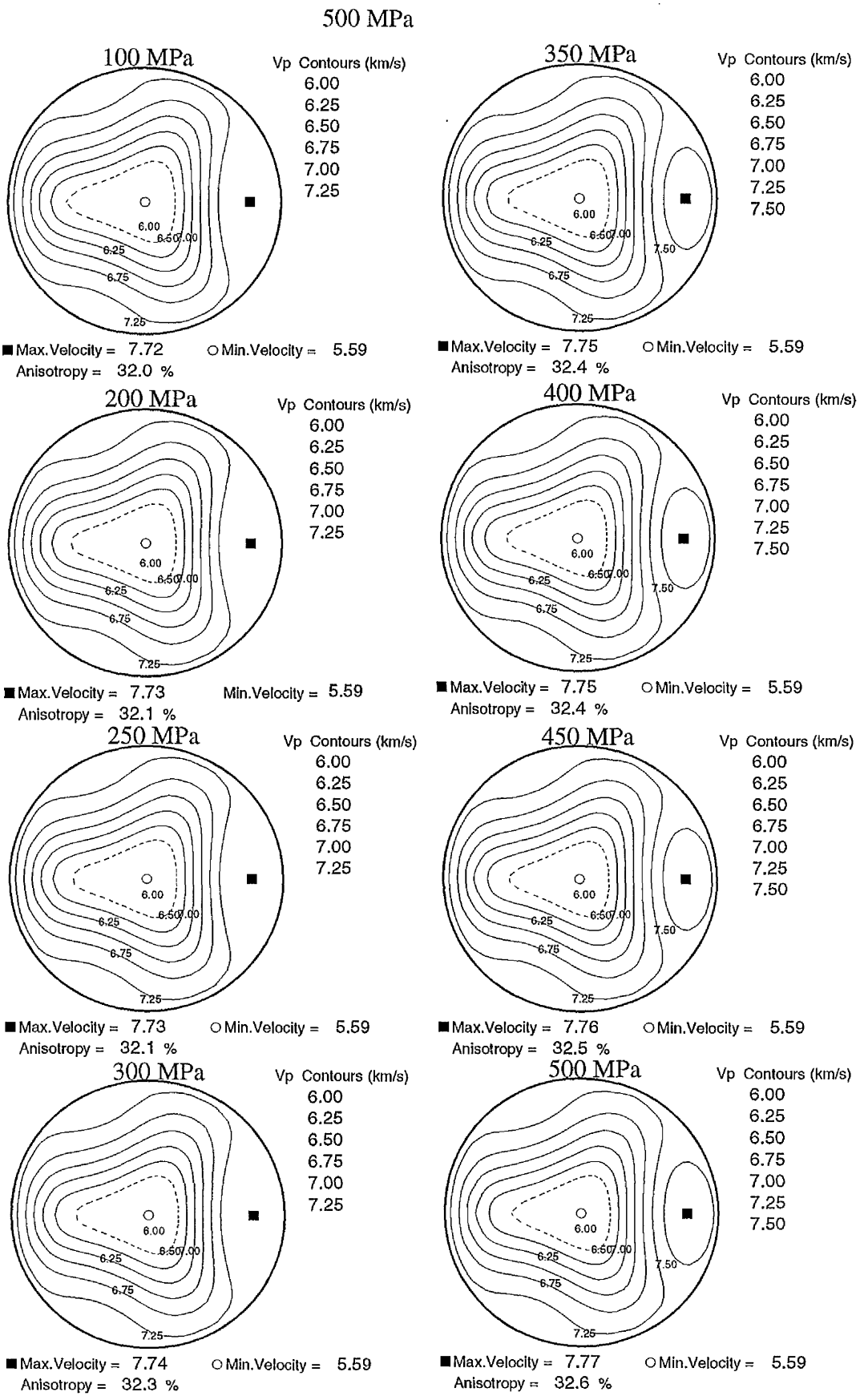

Figure 5.22: Calculated compressional velocity for a single crystal of calcite at various pressure and room temperature. The position of c- & a-axes and poles to the cleavage planes (r) are the same as first plot in the figure 5.21.

drilled along the pole to a cleavage plane at the range of pressure (fig 5.23a) and temperature (fig 5.23b).

3) The compressional wave velocity of the calcite core was measured at elevated pressure and room temperature using the oil rig system. An excellent agreement was obtained between measured and estimated velocities over the same pressure range from stage 2. This was done purely to demonstrate the validity of the calculated velocities (fig 5.24).

4) The total travel time of the assembly containing the calcite single crystal core was then measured at pressures from 300 MPa to 500 MPa and temperatures from 0 to 600°C. It was important to increase the pressure first to prevent any thermal cracking of the sample. Figure 5.25 shows the measured travel time at a range of pressures and temperatures. Using the least squares method the best fit line was calculated for the two plots. The slope of the best fit line for plot of travel time versus confining pressure (fig 5.25 a) gives the pressure coefficient of the total transmission time (*dt/dp*). The slope of total travel time versus temperature plot (fig 5.25b) gives the temperature coefficient of the total transmission time.

5) Finally, the equation (5.6) can be rearranged in the following way to have the total delay time on one side an the rest of the equation on the other side.

$$\left(\frac{\partial t_d}{\partial P}\right)T+\left(\frac{dt_d}{\partial T}\right)P+C'' = \left[\left(\frac{\partial t_t}{\partial P}\right)T-\left(\frac{dt_s}{\partial P}\right)T\right]+\left[\left(\frac{\partial t_t}{\partial T}\right)P-\left(\frac{\partial t_s}{\partial T}\right)P\right]+\left[C-C'\right] \qquad (5.7)$$

All the parameters on the right side of the equation (5.7) are known from steps 3 and 4.

$\left(\frac{\partial t_t}{\partial P}\right)T$=5.56×10^{-4} (s/MPa)

$\left(\frac{dt_s}{\partial P}\right)T$=8×10^{-5} (s/MPa)

$\left(\frac{\partial t_t}{\partial T}\right)P$=1.59×10^{-3} (s/°C)

$\left(\frac{\partial t_s}{\partial T}\right)P$=1.22×10^{-3} (s/°C)

C= 31.58 (s)

C'= 4.62 (s)

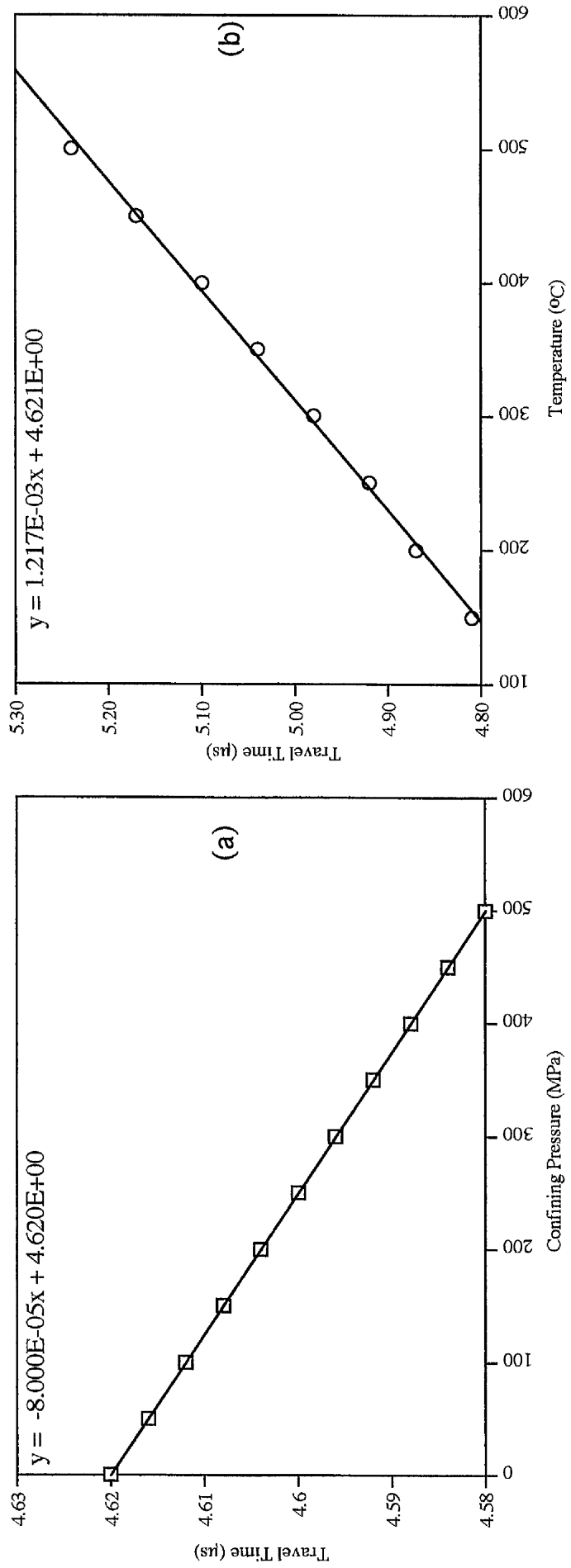

Figure 5.23: Estimated travel time of compressional wave through 34.25mm length of the calcite core at various pressures (a) and temperatures (b) The slope of the line in graph (a) gives the pressure coefficient of transmission time for the calcite core. The slope of the line in graph (b) gives the temperature coefficient of transmission time throught the sample.

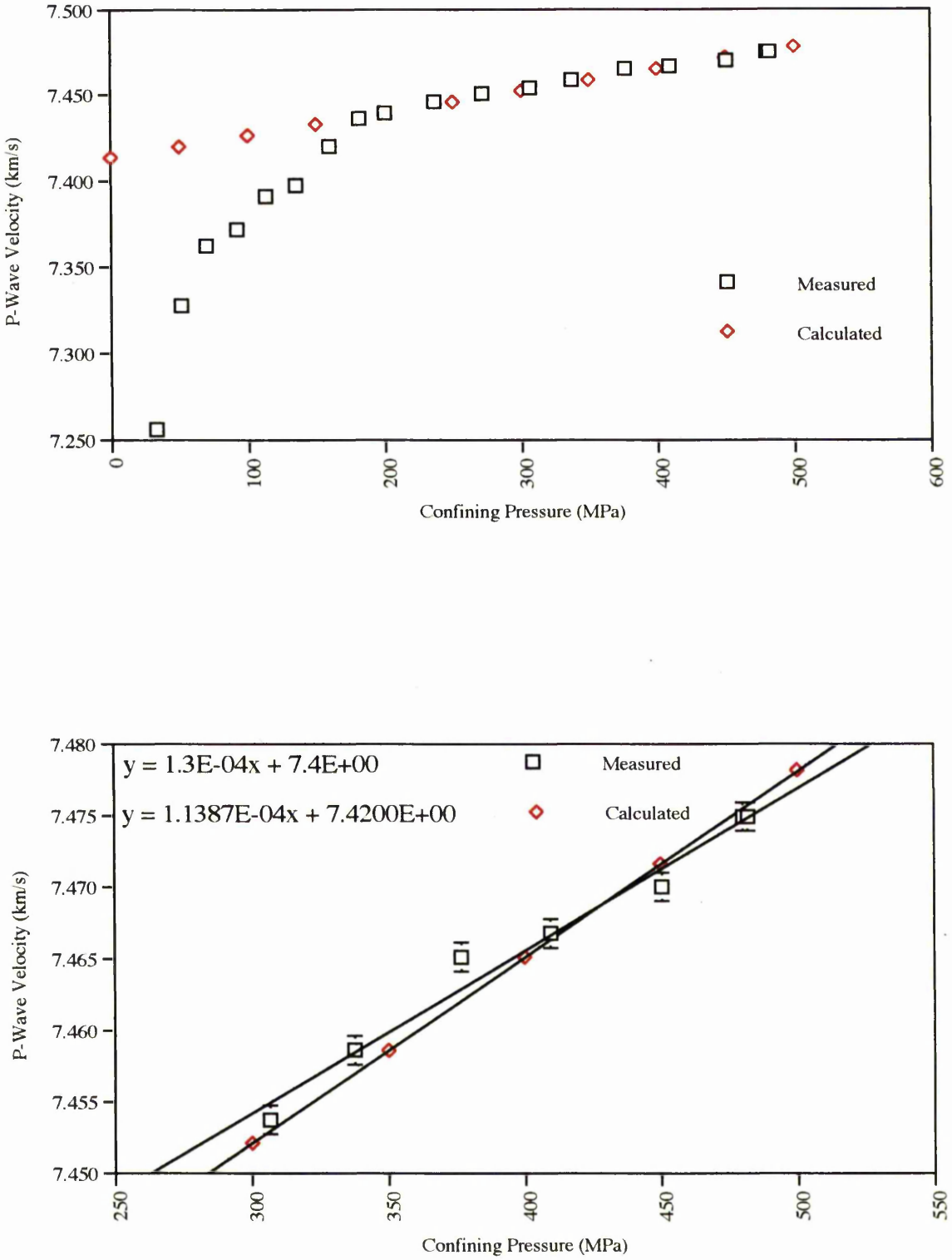

Figure 5.24 : Measured and calculated compressional velocity versus confining pressure for a calcite single crystal at the direction normal to the cleavage plane (top plot).The least squares method was used to find the best fit line through the velocity points measured above 300 MPa confining pressure.

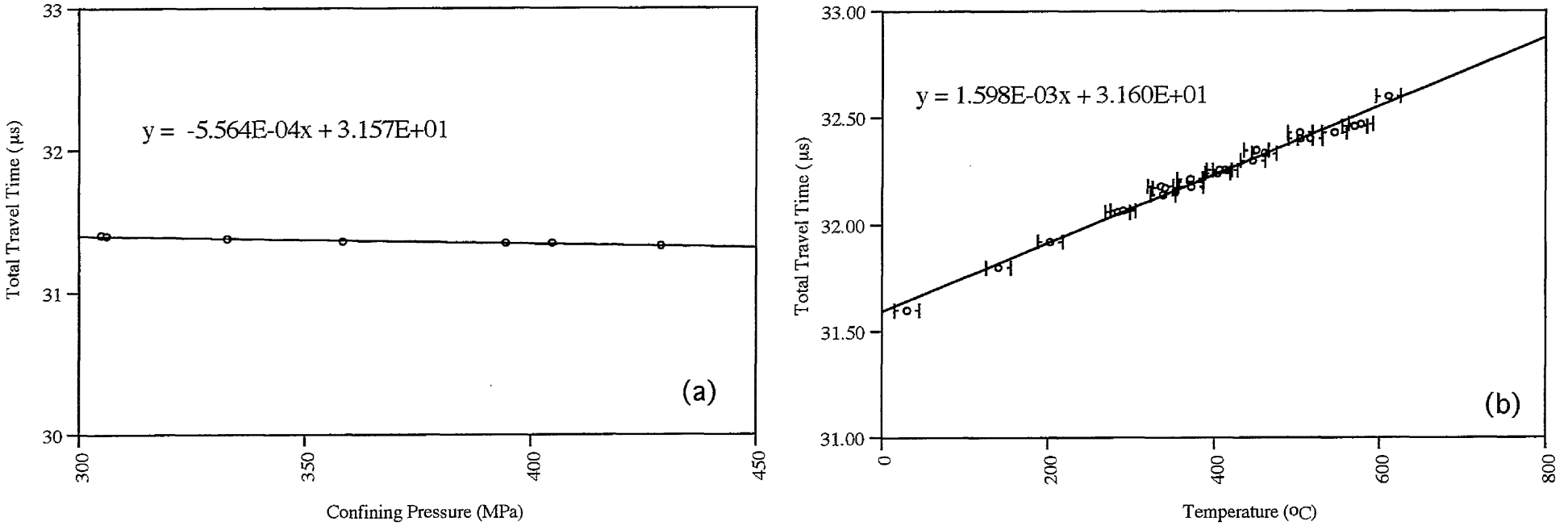

Figure 5.25: Measured total transmission time for compressional wave through high temperature/pressure assembly at various pressures (plot a) and temperatures (plot b). Slope of the line on graph (a) is the pressure coefficient of the total transmission time and the slope of the line on the graph (b) is the temperature coefficient of the total transmission time. The horizontal error bars in plot (b) are for the uncertainty in measured temperature of the sample (see section 5.8.5).

By substituting the above known parameters into the equation (5.7) the delay time of the system was calculated at any required pressure or temperature during measurements of rock samples.

5.7.5 Velocity Measurements

To ensure the measured velocities are for the compressional and shear waves, testing the system is essential. The most convenient method is calibration with the use of high purity aluminium or steel bars. The velocity of compressional waves in aluminium metal is 6320 ms^{-1} and the shear wave velocity is 3100 ms^{-1} (Kolsky. 1963). The compressional and shear velocities of number of aluminium metal bars of high purity was measured with all different transducer assemblies. A close agreement between the measured velocity and the ones by Kolosky (1963) have found (table 5.3).

Length of alumina bar	**99.99 (mm)**	**79.97 (mm)**	**59.96 (mm)**	**40.01 (mm)**
15 mm P-wave assembly	6322 (m/s)	6336 (m/s)	6330 (m/s)	6337 (m/s)
15 mm S-wave assembly	3130 (m/s)	3145 (m/s)	3120 (m/s)	3125 (m/s)
Length of alumina bar	**19.96 (mm)**	**24.92 (mm)**	**30.01 (mm)**	**44.93 (mm)**
P-wave, 1 inch assembly	6324 (m/s)	6315 (m/s)	6336 (m/s)	6312 (m/s)
S-wave, 1 inch assembly	3135 (m/s)	3120 (m/s)	3115 (m/s)	3130 (m/s)

Table 5.3: Measured compressional and shear velocities of a set of aluminium bars of various lenght at room pressure and temperature using different transducer assembly.

The disagreement between measured velocities in all cases and with results from Kolosky (1963) is less than 1 % which is within the uncertainty of method.

5.8 Evaluation of Error and Accuracy in Measuring Seismic Velocity

Error associated with velocity measurements can have a number of sources;

i) uncertainty in measuring travel time (leads to inaccurate estimation of delay time as well as measuring first arrival time).

ii) uncertainty associated with measuring sample length and sample length changes due to pressure or temperature variations.

iii) uncertainty associated with position of first arrival.

5.8.1 Possible Errors in Measuring the Total Delay Time of the Seismic System

Section 5.7.3 describes the method of measuring the total time delay. The delay was measured at least to the ±0.01 (μs) & ±0.02 (μs) at the room temperature for P and S assembly respectively. If a part of seismic system was changed or modified (e.g. changing cable connections or modifying a part of the transducer assembly) the calibration for measuring the total system delay was repeated.

5.8.2 Possible Error in Measuring Time

To determine the velocity of a core, the time between the electrical trigger pulse to a timing point or time-pick corresponding to the first arrival of the received waveform is measured. The first arrival can be defined as either the first break, the position of the maximum of the first peak or the point of maximum slope prior to the first peak. For all P-wave measurements the first break was chosen as the picked time. In case of S-wave measurements as a P component wave was sometimes seen arriving prior to the S-wave, and in some case this made the picking of the S-wave first break difficult. The uncertainty in evaluating the travel time was ±0.01 (μs) for P-wave and ±0.015-0.02 (μs) for S-wave.

5.8.3 Measuring the Length of the Sample

Cylindrical core samples were cut to the required length and their ends were squared. The ends of the cores were lapped parallel to fine tolerances (±0.01 mm). A digital vernier calliper gauge was used for measuring the length of the core to ± 0.01 mm.

The length measurements were carried out under room pressure and temperature conditions. Under high confining pressures and temperature there will be some length

changes depending on the compressibility (k) and thermal expansion of the sample. With the existing set up it was not possible to measure the amount of such changes, however Christensen (1965) states that the error arising from length changes for low porosity rocks (metamorphic and igneous) is less than 1% over working pressure.

5.8.4 Possible Error in Velocity Evaluation

The following equation was used to estimate the overall error associated with each velocity measurement:

$$\left(\sigma_V/V\right)^2 = \left(\sigma_X/X\right)^2 + \left(\sigma_t/t\right)^2 \qquad (5.8)$$

where σ is the uncertainty (e.g. standard deviation), V is velocity t is travel time and X is length of the sample.

Knowing that the sample length was never shorter than 30 mm or longer than 50 mm, and that the measured P-wave velocity was between 8.4 km/s and 5.5 km/s, the propagating error through velocity measurements can be calculated using the above equation. As expected, such a calculation reveals (table 5.4) that the error is higher for a short sample with a high velocity and lower for a long sample with a low velocity.

Vp (km/s)	Sample length (mm)	error (±) km/s
8.4	30	0.0037
8.4	50	0.0022
5.5	30	0.0021
5.5	50	0.0013

Table 5.4: Maximum and minimum error associated with all measurements of seismic velocities at room temperature and high pressure.

5.8.5 Possible Error in Pressure and Temperature Reading

Pressure was measured to a resolution of ±0.1 MPa using a pressure transducer. The pressure transducer is connected to a digital display and to the computer. The pressure reading was down loaded automatically preventing any human error in recording it. As the pressure was increased or decreased, sufficient time must be allowed for the pressure to equilibrate and for the effects of adiabatic temperature

fluctuation to dissipate. It was found that 10 to 15 minutes is enough for these effects to disappear.

Although temperature at the top of the sample was measured to ±0.1 °C, this does not necessarily correspond to an accurate estimation of the sample temperature. Base metal thermocouples are probably accurate to about ±3 °C at 700 °C. Error in estimating the thermal gradient along the sample can arise from difference between the sample, calibration, geometry and changes of furnace characterisations with time. As a result, reported test temperatures are likely to be correct to only ±3 °C at the tip of the thermocouple (top of sample) and +0/-20 °C at the bottom of the sample at 700 °C , and correspondingly better at lower temperature. The bottom of the sample is always expected to be cooler than the top, and the middle may be up to 10 °C hotter.

5.8.6 Reproducibility

The seismic velocity measurements were very reproducible at high pressure (typically ±0.015 km/s; table 5.3) and high temperatures (typically ± 0.025 km/s; see chapter 7). However there are two exceptions:

i) For the samples with high initial crack density most of the cracks are closed but not all of them are reopened as the pressure was released (i.e. thermal cycling repairs damage to specimens). This results in higher velocity at the low pressure range (between 0 and 200 MPa) for the second thermal of measuring the same cores (see chapter 6 for more details).

ii) It was also observed that velocity decreases at low temperature during heating up but not during cooling down. This was attributed to thermal cracking during the heating stage and possible crack healing or repairing after it is been at high temperature for some time. This effect is discussed in more detail in chapter 7.

Chapter 6

Experimental Results:

(Room Temperature & High Pressure Velocity Measurements)

6.1 Introduction

This chapter presents the results of velocity measurements for over 30 representative rock types from the Ivrea-Verbano zone and the Serie dei Laghi at room temperature and elevated pressures.

P-wave velocity was measured for at least three orthogonal cores from each geological unit (see fig 3.20). For highly heterogeneous lithologies the aim was to measure the velocity of more than three cores. Due to time constraints, S-wave velocity was measured only along the A direction (normal to the foliation) for all samples. However, for some rocks with high V_p anisotropy, the S-wave measurements were carried out for all three orthogonal directions.

The velocity of each core was measured at 15 or more different pressures ranging from about 20 MPa to 500 MPa. Due to the large number of seismic velocity measurements made, the results are tabulated as velocity data extrapolated back to room pressure and temperature and the plots of velocity versus pressure are presented in appendix 3. Towards the end of the chapter, the measured seismic velocities and density for each rock type were used in attempt to find correlations between those parameters and lithology.

6.2 Velocity Measurements at Room Temperature and Elevated Pressure

P and S waves velocity measurements at elevated confining pressures and room temperature were carried out using the oil medium apparatus described in chapter 5. The sample was first pressurised to about 500 MPa. Normally, about 10 to 15 minutes was needed to obtain a stable reading of the confining pressure. Therefore it was decided to wait about 15 minutes every time the pressure was increased or decreased so that a condition of equilibrium can be achieved between the sample and the confining medium.

Velocity measurements were made at various pressures from 500 MPa down to room pressure. The travel time of the 1 MHz pulse through the specimen was obtained by subtracting the delay time of the system from the total measured travel time (see chapter 5). The velocity and density data presented in this chapter are not corrected for the changes of sample length with pressure. Christensen (1965) showed that this effect is less than 1% for low porosity metamorphic rocks.

Figure 6.1 shows the results of velocity measurements at various pressures for some of the samples. For almost all samples the velocity versus pressure curves can be divided into two parts. The first part of the curve at low pressure, ranging from 0 to about 200 MPa, shows a rapid increase in velocity. This sharp increase of velocity at low pressure range is attributed to microcrack closure (e.g. Kern 1982). Above about 200 MPa the relationship between velocity and confining pressure becomes nearly linear. For almost all samples at pressures above 300 MPa such a linear relationship between pressure and velocity was observed. Since it is known that seismic velocities are proportional to the elastic moduli, this trend confirms the expected linear pressure dependence on the elastic moduli and density of the mineral components. Using the least squares method a best fit line for the velocity points above 300 MPa was found (fig 6.2). The intercept of the line with the velocity axis would give the velocity of the sample at room pressure and temperature for the direction of the core assuming no microcracking. The slope of the line defines the pressure derivative of velocity. By extrapolating the best fit line to the higher pressure the velocity of the sample at pressures above 500 MPa can be estimated.

Since some of the rocks are anisotropic for seismic velocities, by measuring the seismic P and S wave velocities along at least three orthogonal directions (fig 6.3), the seismic anisotropy can be calculated using the following equation;

$$Anisotropy(\%) = \frac{2(V_{\max} - V_{\min})}{(V_{\max} + V_{\min})} \times 100\% \qquad (6.1)$$

where V_{max} is the maximum measured velocity along one direction and V_{min} is the minimum velocity along another direction for a sample.

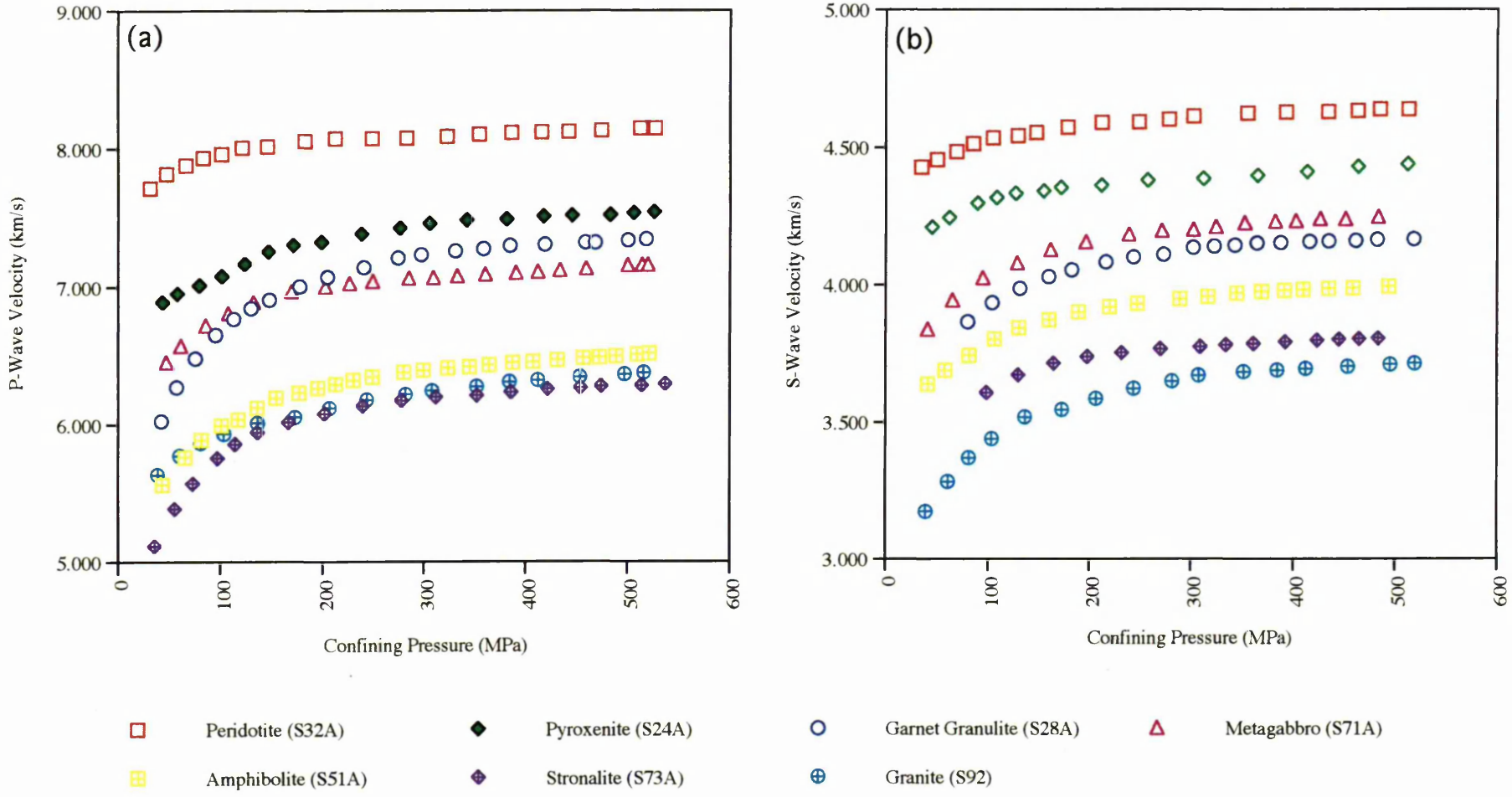

Fig 6.1: Velocities of (a) compressional and (b) shear waves for a selection of rock types as a function of confining pressure up to 550 MPa. All the measurements are for the direction normal to the foliation.

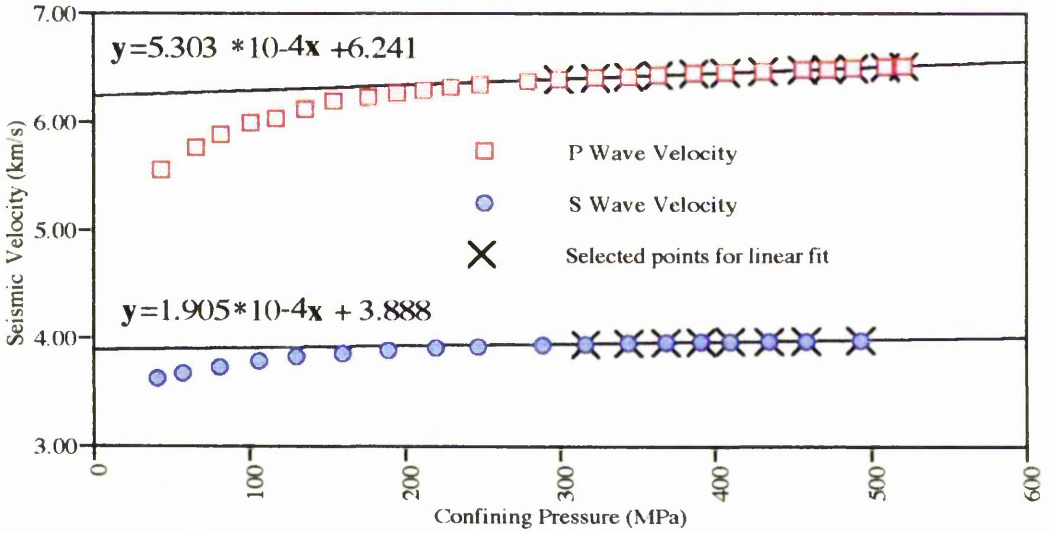

Figure 6.2: Plot of seismic velocities against confining pressure, showing the velocity points selected to calculate the best fit line. The equations above the lines give the slope and the intercept of the line with the velocity axes.

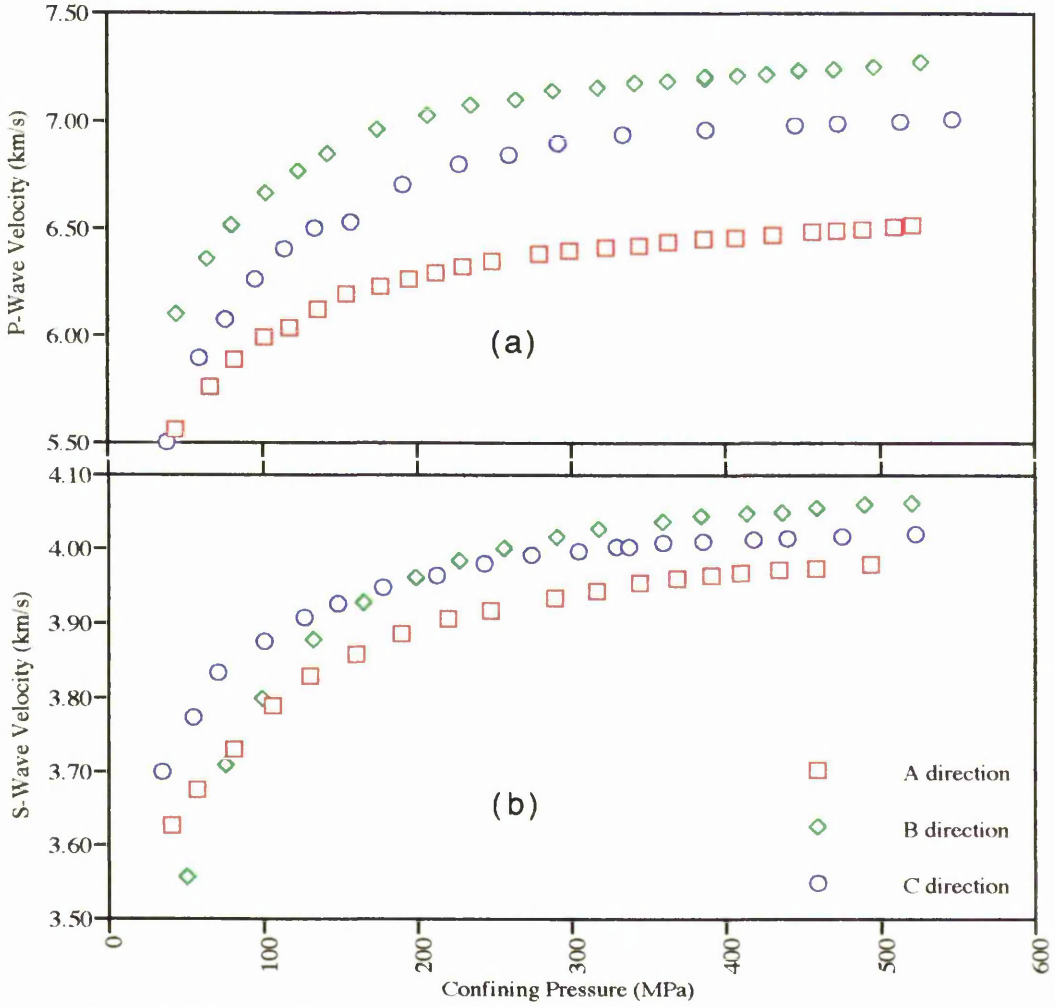

Figure 6.3: Velocities of (a) compressional and (b) shear waves at elevated pressure and room temperature for an amphibolite sample (S50) measured along three orthogonal directions.(A) is the direction normal to the foliation, (B) is the direction parallel to the foliation plane and parallel to the lineation and (C) is the direction parallel to the foliation plane and normal to the lineation.

The calculated anisotropy may be less than the true anisotropy because the measured maximum and minimum velocity values do not necessary correspond to the absolute extreme velocities of the rocks. The true maximum and minimum velocities could be along directions other than the three orthogonal core directions. However, as the three core directions were selected with respect to the microstructures of the rock, it is more likely that they are closest to the true maximum and minimum velocities.

6.2.1 Velocity of Ultramafic Rocks

Table 6.1 and 6.2 present the measured V_P and V_S of four ultramafic rocks. The velocity data given are extrapolated to room pressure. Balmuccia and Premosella peridotites (see table 6.2) show V_P velocities above 8.0 km/s and V_S velocity more than 4.6 km/s with Premosella peridotites showing the highest averaged V_P (8.10 km/s) and V_S (4.63 km/s). The higher seismic velocities of the Premosella peridotites can be attributed to the higher olivine contents.

Phlogopite-rich peridotites from Finero show a wide range of seismic V_P ranging from 7.42 to 8.33 km/s and Vs ranging from 4.15 to 4.72 km/s when extrapolated to room P and T conditions. This wide velocity range could be due to the following three factors;

(i) variation in olivine content, which is the most abundant high velocity phase relative to phlogopite and other slower phases.

(ii) possible crystallographic preferred orientation of olivine or phlogopite or.

(iii) some combination of both.

Figure 6.4 shows the P-wave velocity of four phlogopite-rich peridotites cores with the same orientation (parallel to the foliation plane) but different amounts of phlogopite (no accurate quantitative measurements of phlogopite contents was obtained). A maximum variation in compressional velocity near to 0.6 km/s was observed, which is attributed to variation in phlogopite/olivine ratio. Finero peridotites show (a) lower seismic velocities and (b) higher seismic anisotropy than the other two peridotites (Balmuccia (S01) and Premosella (S32), see table 6.1)

Lithology & Sample No	Density gr/cm3	Vp km/s	AvVp km/s	dvp/dp (*10^{-4}) km/s/MPa	Av dVp/dp (*10^{-4}) km/s/MPa	Anisotropy %
Peridotite						
S01A	3.280	7.906	**7.917**	3.106	**2.880**	
S03A	3.282	7.928		2.653		
S01B	3.308	8.287	8.287	2.082	2.082	
S01C	3.295	8.103	8.103	4.392	4.392	
Average	**3.291**		**8.102**		**3.118**	4.57
Peridotite						
S32A	3.309	8.000	**7.985**	2.827	**2.206**	
S32A'	3.300	7.969		1.584		
S32B	3.303	8.369	8.369	1.584	1.584	
S32C	3.290	8.253	8.253	2.890	2.890	
Average	**3.301**		**8.202**		**2.227**	4.70
Phlog-Peridotite						
S60A	3.251	7.454	7.454	3.630	3.215	
S60B	3.245	8.079	8.079	2.921	4.367	
S60C	3.253	7.781	7.781	1.785	3.588	
S118'A	3.213	7.528		3.850		
S118A	3.221	7.418		4.146		
S119A	3.242	7.530		3.598		
S120A'	3.256	7.588		2.578		
S118B	3.248	7.622		4.430		
S120B	3.251	7.994		4.303		
S118C	3.252	7.607		3.588		
Average	**3.242**		**7.771**		**3.723**	8.05
Hbl-Peridotite						
S89A	3.167	8.021	8.021	2.509	2.509	
S89B"	3.185	8.093	8.093	1.563	1.563	
S89C	3.247	8.203	8.203	2.569	2.569	
Average	**3.200**		**8.106**		**2.214**	2.24
Pyroxenite						
S24A	3.208	7.359	7.359	3.502	3.502	
S24B	3.213	7.421	**7.430**	5.958	**4.307**	
S24'B	3.220	7.439		2.655		
S24C	3.249	7.543	7.543	2.633	2.633	
Average	**3.223**		**7.444**		**3.481**	2.47

Table 6.1: Measured density, compressional velocity and pressure coefficient of P-wave velocity of ultramafic samples. The bold values are the averaged of a number of measurements. Samples. 'Av Vp' is averaged compressional velocity for three orthogonal directions, 'dVp/dP' is the pressure coefficient of compressional velocity and 'Av dVp/dP' is the averaged of pressure coefficient of compressional velocity for three orthogonal directions. S60's are the best representatives of heterogeneous phlogopite-rich peridotite (shaded in grey). Similar symbols have been used for all tabulated velocity data.

Lithology & Sample No	Density gr/cm3	Vs km/s	Av Vs km/s	dVs/dp (*10^{-4}) km/s/MPa	Av dVs/dp (*10^{-4}) km/s/MPa	Anisotropy %
Peridotite						
S01A	3.280	4.450	4.450	1.550	1.550	
S01B	3.308	4.670	4.670	0.754	0.754	
S01C	3.295	4.597	4.597	1.782	1.782	
Average	**3.294**		**4.634**		**1.362**	4.8
Peridotite						
S32A	3.309	4.580	4.580	1.144	1.144	
S32B	3.303	4.684	4.684	0.624	0.624	
S32C	3.290	4.615	4.615	1.055	1.055	
Average	**3.301**		**4.632**		**0.884**	2.2
Phlog-Peridotite						
S60A	3.251	4.158	**4.407**	1.775	**1.752**	
S118A	3.221	4.590		0.961		
S120A	3.271	4.472		2.521		
S60B	3.245	4.500	**4.545**	1.166	**1.595**	
S118B	3.248	4.446		1.341		
S120B	3.252	4.511		2.351		
S121B	3.291	4.723		1.520		
S60C	3.253	4.294	4.294	1.630	1.630	
Average	**3.254**		**4.415**		**1.659**	5.7
Pyroxenite						
S24A	3.208	4.555	4.555	1.855	1.855	
S24B	3.213	4.605	4.605	1.150	1.150	
S24C	3.249	4.615	4.615	1.115	1.115	
Average	**3.223**		**4.592**		**1.373**	1.31

Table 6.2: Measured shear wave velocity and density for a number of ultramafic rocks. Pressure coefficient of shear wave velocity is also displayed. The bold numbers are averaged values of number of measurements. The symbols are the same as table 6.1.

(a) Although similar seismic velocity measurements have been obtained by Fountain (1976), the calculated velocity for the same rock by Zappone (1992), based on model proportion data and single crystal petrofabric elastic properties, indicates a much lower compressional and shear velocities. This highlights the significant effect of microstructures (in this case the discontinuous bands of phlogopite and their laminated structure as well as the relative continuity of olivine crystals along the propagation path of ultrasonic wave) on propagating ultrasonic waves (such effects are not accounted for in calculated velocity). It seems likely that in the ultrasonic measurements the fine P-wave arrival, upon which the measured velocity is based, is for the fast path way through olivine crystal alone, even with the aid of diffraction around phlogopite crystals.

Figure 6.5 shows schematic diagrams of a two phase aggregate with four different microstructures. There are different paths for propagation of the ultrasonic wave through the aggregate which may result in various seismic velocities. For example in diagram A the seismic wave has no option except to travel through both phases but in diagram B the seismic wave may travel mainly through the faster phase and will certainly control the first arrival. If this is the case then one would obtain a higher measured velocity than calculated or possibly measured on a bigger scale (e.g. in-situ low frequency measurements). The last two diagrams show microstructures for which the seismic velocity (first arrival) will be influenced mainly or wholly by the darker phase due to its higher volume fraction. The behaviour will be as if the light phase was not present.

The above example shows the significant effect of microstructures on the results of seismic velocity measurements on rocks containing two or more phases and a limitation of laboratory velocity measurements which highlights the scaling problem associated with such measurements.

(b) The high seismic anisotropy of the Finero peridotite is similar to mica rich rocks such as biotite schist (e.g. B11 & S99, see table 6.7). Considering the similarity in crystal structure of biotite and phlogopite it is justifiable to infer the phlogopite to be mainly responsible for the higher seismic anisotropy.

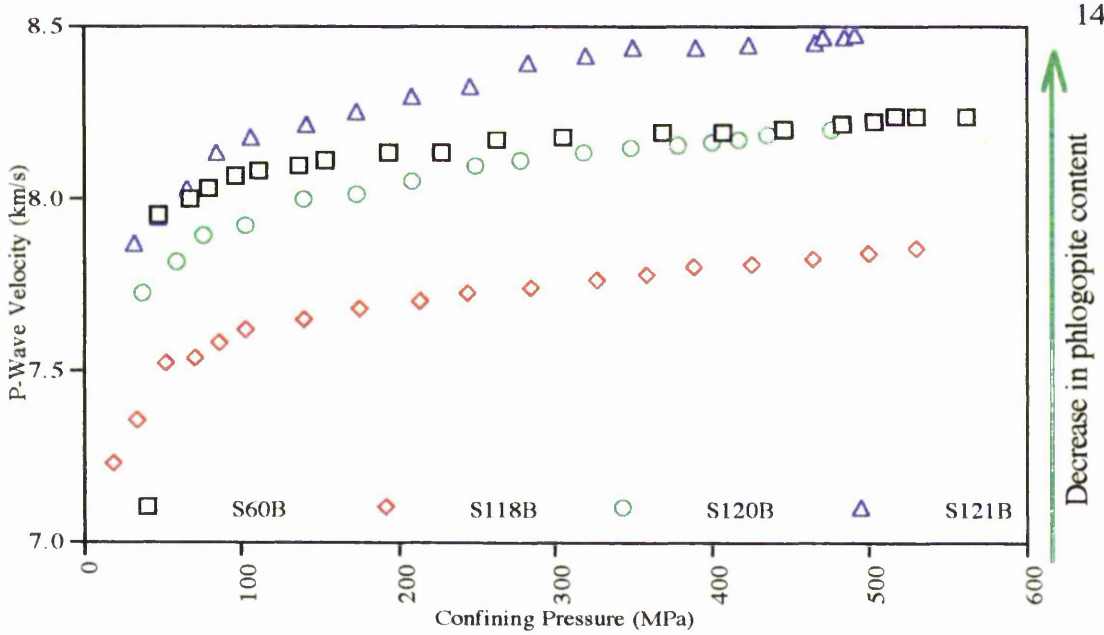

Figure 6.4: Compressional velocity/pressure plot for cores of phlogopite-rich peridotites. All the cores are for the direction parallel to the foliation plain and parallel to lineation.

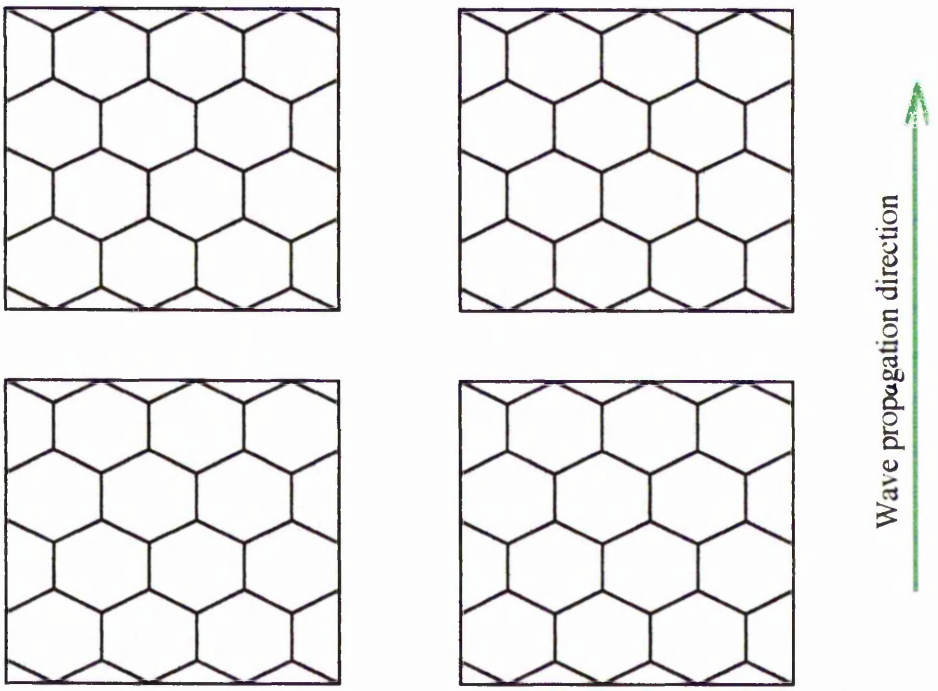

Figure 6.5: Cartoon diagrams of a two phase aggregate with different microstructure. (A) horizontal compositional banding, (B) vertical compositional banding, (C) discontinuous horizontal bands & (D) random microstructure.

There are a number of pyroxenite bodies in the IV zone and some of them are associated with the peridotites. However, the high concentration of pseudotachylite veins common in these rocks made it virtually impossible to obtain a fresh sample. Samples from only one pyroxenite body were suitable for velocity measurements and that shows an averaged Vp of 7.444 km/s and Vs of 4.592 km/s.

6.2.2 Velocity of Metabasic Rocks

Metabasic rocks here comprise a very wide range of rock types, such as amphibolites, mafic granulites and metagabbroic rocks. Table 6.3 and 6.4 show the results of measurements and calculated velocities (Vp & Vs respectively).

Two amphibolite samples (S35 & S50) show an averaged Vp of 6.710 km/s and 6.684 km/s and shear wave velocities of 3.726 to 3.971 km/s. Both samples show high seismic velocity anisotropy which reflects the strong velocity anisotropies of hornblende and plagioclase. All amphibolites have relatively high seismic anisotropy, with their highest seismic velocities for the direction parallel to the foliation (B direction) and the lowest velocities for the direction normal to the foliation (A direction). Figure 6.6 shows plots of compressional velocity versus confining pressure for two amphibolite rocks (S35 & S50). They both rock display large seismic velocity anisotropy with one having orthogonal anisotropy pattern (S50) and the other one a transverse isotropic pattern (S35).

It was observed on the polished sections of these amphibolites that the majority of the hornblendes are oriented with their long axes (crystallographic c-axis) on the foliation plane. Examining the maximum and minimum velocity directions of single crystal of hornblende would show that the high and low velocity direction of hornblende corresponds well with the measured high and low velocity directions of the samples (fig 6.7). Thus, well oriented hornblendes are probably largely responsible for the observed high velocity anisotropy.

The granulites have higher seismic velocities than the amphibolites, ranging from 6.73 km/s to 7.08 km/s for Vp and from 3.826 km/s to 4.146 km/s for Vs (fig 6.8).

Lithology & Sample No	Density gr/cm3	Vp km/s	Av Vp km/s	dVp/dp (*10^{-4}) km/s/MPa	Av dVp/dp (*10^{-4}) km/s/MPa	Anisotropy %
Amphibolite						
S35A	3.035	6.440		5.878		
S35A'	3.032	6.440	**6.445**	6.144	**5.599**	
S36A	3.033	6.455		4.775		
S35B	3.062	6.805	**6.812**	6.010	**5.980**	
S35'B	3.050	6.819		5.949		
S35C	3.043	6.805	**6.874**	6.364	**6.569**	
S35C"	3.044	6.943		6.773		
Average	**3.043**		**6.710**		**6.049**	6.44
Amphibolite						
S50A	2.954	6.241	6.241	5.303	5.303	
S50B	2.976	6.992	**7.014**	5.416	**4.952**	
S50'B	2.986	7.035		4.488		
S50C	2.972	6.796	6.796	4.081	4.081	
Average	**2.972**		**6.684**		**4.779**	11.7
2 PX Granulite						
S63A	3.055	6.848	6.848	6.809	6.809	
S63B	3.061	7.077	7.077	4.533	4.533	
Average	**3.058**		**6.963**		**5.671**	3.29
2 PX Granulite						
S70A	3.045	6.550	6.550	6.190	6.190	
S70B	3.033	6.622	6.622	7.155	7.155	
S69C	3.051	6.978	6.978	4.622	4.622	
Average	**3.043**		**6.717**		**5.989**	6.33
Metabasic						
S88A"	3.175	6.893	6.893	4.995	4.995	
S88B'	3.181	7.004	7.004	5.364	5.364	
S88C'	3.158	6.833	6.833	5.363	5.363	
Average	**3.170**		**6.910**		**5.241**	2.47
Px Granulite						
S87A	3.162	6.728	6.728	6.400	6.400	
S87C	2.998	6.889	6.889	5.155	5.155	
A v e r a g e	**3.080**		**6.809**		**5.778**	2.36
Metagabbro						
S26A	2.889	6.799	**6.682**	6.372	**8.085**	
S26A'	2.915	6.564		9.798		
S26B	2.947	6.851	6.851	6.436	6.436	
S26C	2.923	6.872	6.872	7.329	7.329	
Average	**2.919**		**6.802**		**7.283**	2.81

Table 6.3: Density, compressional velocity and pressure coefficient of velocity of some metabasic rocks at room pressure and temperatures. The bold values are the averages of number of measurements. Symbols are the same as table 6.1.

Lithology & Sample No	Density gr/cm3	Vp km/s	Av Vp km/s	dVp/dp (*10^{-4}) km/s/MPa	Av dVp/dp (*10^{-4}) km/s/MPa	An %
Metagabbro						
S28A	3.333	7.100	7.100	4.805	4.805	
S28B	3.116	6.980	6.980	4.330	4.330	
S28C	3.077	7.090	7.090	3.372	3.372	
Average	**3.175**		**7.057**		**4.169**	1.70
Metagabbro						
S71A"	2.848	6.927	6.927	4.505	4.505	
S71B	2.829	6.865	6.865	3.844	3.844	
S71C	3.009	6.897	6.897	7.506	7.506	
Average	**2.895**		**6.896**		**5.285**	0.90
Diorite						
S75A	2.911	6.911	6.911	3.665	3.665	
S75B	2.887	6.731	6.731	4.339	4.339	
S75C	2.982	6.855	6.855	3.695	3.695	
Average	**2.927**		**6.832**		**3.900**	2.64
Diorite						
S41A	2.863	6.411	6.411	3.636	3.636	
S41B	2.873	6.426	**6.424**	4.497	**4.578**	
S41B'	2.871	6.422		4.659		
S41C	2.875	6.209	6.209	6.170	6.170	
Average	**2.871**		**6.348**		**4.795**	3.40
Xenolith in diorite						
S42A	2.914	6.441	6.441	5.673	5.673	
S42B	2.878	6.330	**6.352**	5.929	**5.669**	
S42B`	2.880	6.373		5.409		
S42C	2.889	6.411	**6.442**	5.856	**5.555**	
S42C`	2.925	6.472		5.253		
Average	**2.897**		**6.411**		**5.632**	1.41
Metagabbro						
B6A	3.096	6.871	6.871	5.407	5.407	
B6B	3.112	7.226	7.226	3.556	3.556	
B6C	3.173	7.086	7.086	4.309	4.309	
Average	**3.127**		**7.061**		**4.424**	5.04
Sheared						
B1A	3.090	6.832	**6.819**	2.571	**2.877**	
B1A'	3.088	6.806		3.183		
B1B	3.082	6.892	**6.902**	3.110	**2.878**	
B1B'	3.086	6.911		2.646		
B1C	3.095	6.758	**6.752**	4.439	**4.618**	
B1C'	3.09	6.745		4.796		
Average	**3.089**		**6.824**		**3.458**	2.20

Table 6.3: contd.

Lithology & Sample No	Density gr/cm3	Vs km/s	Av Vs km/s	dVs/dP (*10^{-4}) km/s/MPa	Av dVs/dp (*10^{-4}) km/s/MPa	Anisotropy %
Amphibolite						
S35A	3.060	3.726	3.726	1.776	1.776	
S35B	3.062	4.105	4.105	3.150	3.150	
S35C	3.043	4.105	3.990	3.250	3.250	
Average	**3.055**		**3.726**		**2.725**	9.679
Amphibolite						
S50A	2.954	3.805	**3.83**	2.795	**2.357**	
S51A	2.983	3.855		1.919		
S51B	2.976	4.115	4.115	1.897	1.897	
S51C	2.972	3.969	3.969	1.040	1.040	
Average	**2.971**		**3.971**		**1.765**	7.174
2 PX Pyroxenite						
S70A	3.045	3.826	3.826	3.236	3.236	
S70B	3.033	3.985	3.985	3.350	3.350	
Average	**3.039**		**3.826**		**3.236**	4.071
Metagabbro						
S26A	2.889	3.768	3.768	2.673	2.673	
Average	2.889		3.768		2.673	=
Metagabbro						
S28A	3.333	4.090	4.090	1.450	1.450	
S28B	3.116	3.782	3.782	1.626	1.626	
S28C	3.077	3.941	3.941	1.286	1.286	
Average	**3.175**		**3.938**		**1.454**	7.825
Metagabbro						
S71A"	2.848	4.134	4.134	2.391	2.391	
S71B	2.829	4.050	4.105	4.050	2.110	
Average	**2.839**		**4.120**		**2.251**	0.704
Diorite						
S75A	2.911	3.910	3.910	2.905	2.905	
Average	2.911		3.910	2.905		=
Diorite						
S41A	2.863	3.267	3.267	2.433	2.433	
Average	2.863		3.267		2.433	=
Metagabbro						
B6A	3.133	4.153	4.153	1.532	1.532	
B6C	3.096	4.104	4.104	2.9	2.900	
Average	**3.115**		**4.129**		**2.216**	1.187
Sheared						
B1A	3.088	3.977	3.977	1.178	1.178	
B1B	3.086	3.981	3.981	1.407	1.407	
B1C	3.095	3.952	3.952	1.645	1.645	
Average	**3.090**		**3.970**		**1.410**	0.731

Table 6.4: Density and shear wave velocity of metabasic samples at room temperature and pressure. Bold values are the average of number of measurements. Symboles are the same as table 6.1.

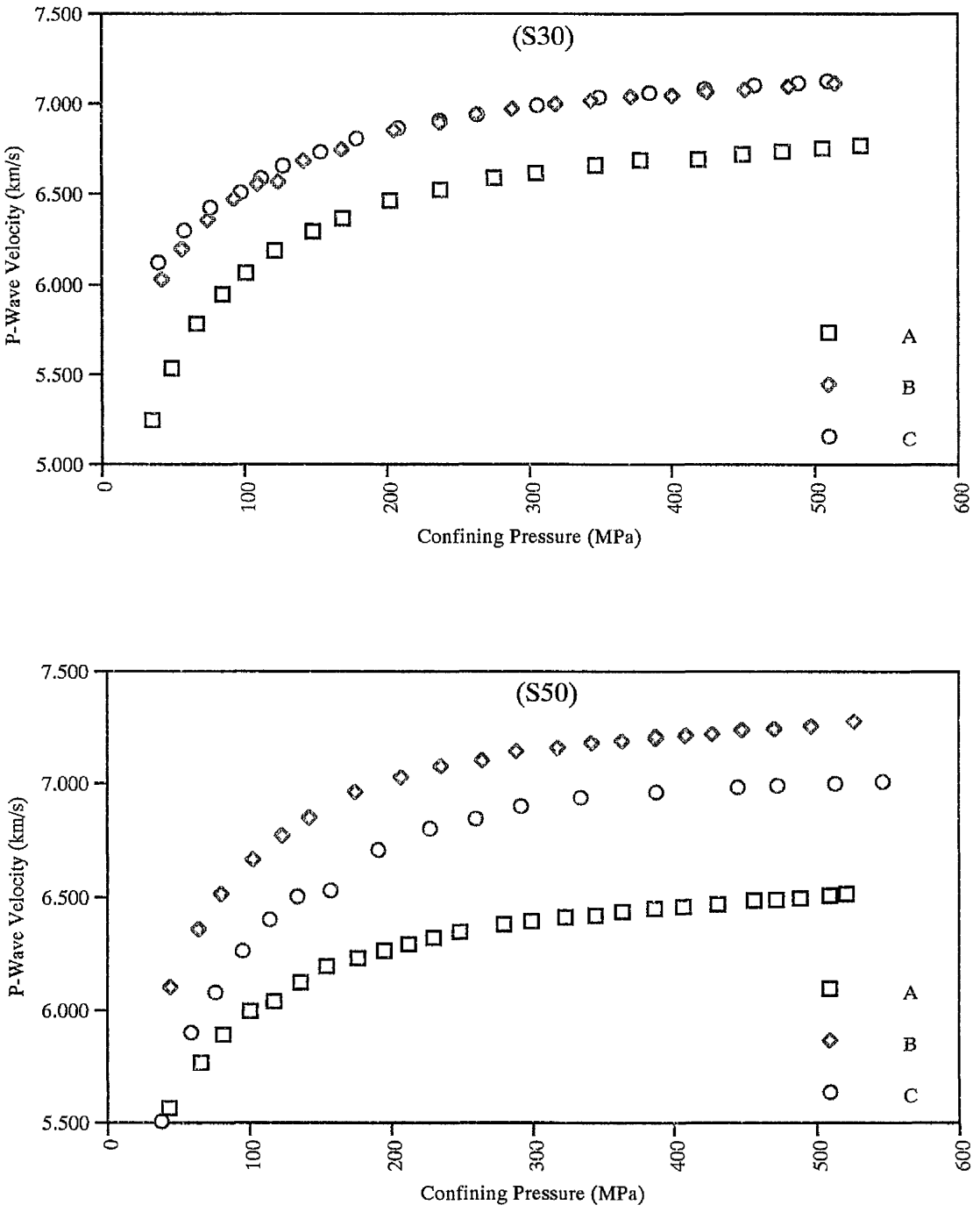

Figure 6.6: Plots of compressional velocity as a function of confining pressure for two amphibolite rocks. Velocity measurements were conducted on three orthogonal cores for each rock.

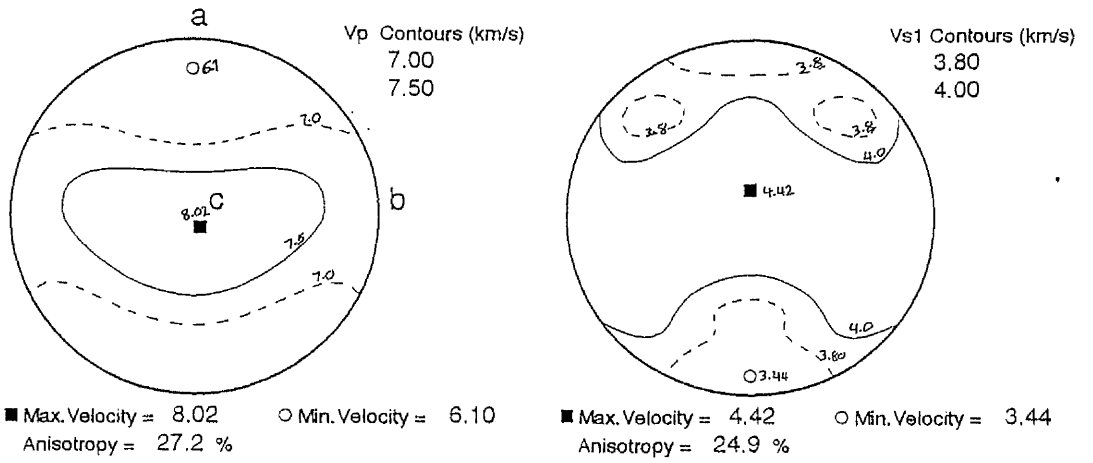

Figure 6.7: Calculated compressional and shear waves velocities of hornblende single crystal. Crystallographic axes (a, b, c) have also been shown.

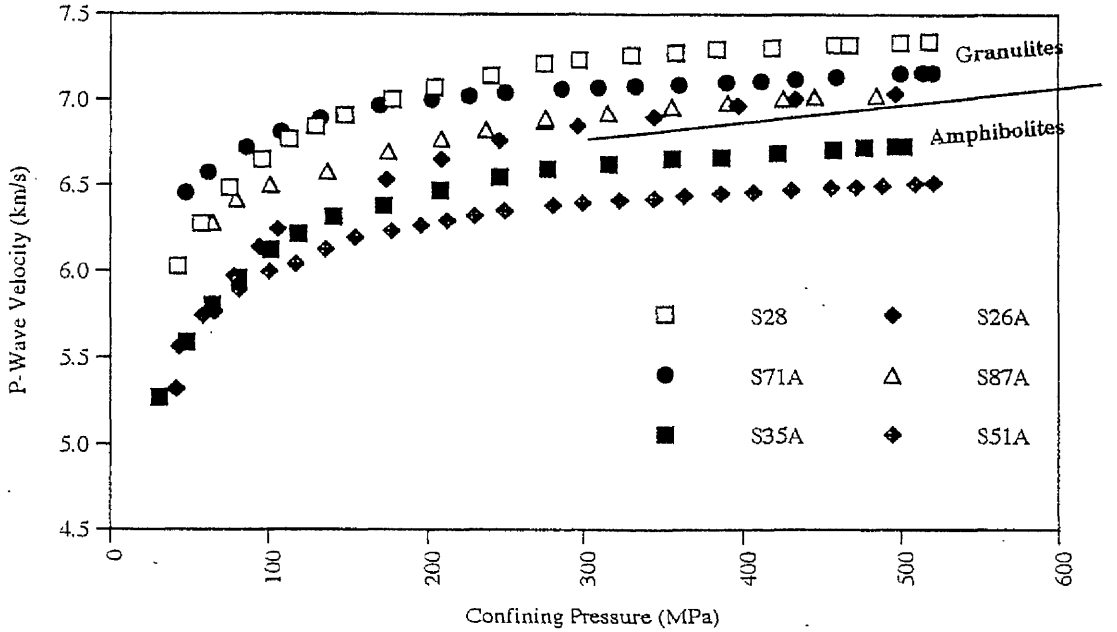

Figure 6.8: Compressional velocities for a number of amphibolite and granulite samples in the direction normal to the foliation. All granulites show higher V_P than amphibolites.

Granulites have lower seismic anisotropy than amphibolites. This could be due to either of the following factors or combination of them.

i) High garnet content which is an isotropic crystal

ii) Relative lack of strongly oriented, anisotropic phases such as pyroxenes.

Metagabbroic rocks in general show high seismic Vp (ranging from 6.68 to 7.23 km/s) and Vs (ranging from 3.77 to 4.14 km/s). Most metagabbros show similar seismic velocities and densities to granulites, making it difficult to distinguish them on the basis of these properties. Sample B6 is a banded metagabbro that shows similar seismic velocities (averaged V_P of 7.061 and V_S of 4.129 km/s) to most metagabbros but higher seismic Vp and Vs anisotropy than most of them. This is possibly due to the distinctive fine scale compositional banding present in this metagabbro. Sample B1 was collected from a high temperature shear zone formed in the Anzola metagabbro (sample B6). Both V_P and V_S of the sheared rock are lower than those of the protolith (B6, fig 6.9). It also has lower seismic anisotropy than the metagabbro. There will be more discussion on the seismic properties of shear zones in the next chapter.

The seismic velocities of three dioritic samples were also measured. Sample S75 is a coarse grained granoblastic diorite having an averaged seismic Vp of 6.832 km/s and a Vs of 3.910 km/s. It has a higher compressional velocity than the other two diorites (S41 & S42). This is due to higher biotite and lower hornblende content in samples S41 and S42, because biotite has lower seismic velocities than hornblende (see section 6.3.3).

6.2.3 Velocities of Metasedimentary Rocks

What are here referred to as metasediments cover a very wide range of rock compositions. It is therefore not surprising that the compressional velocity of these rocks show a wide range of values, from 6.19 km/s (S73) to 6.88 km/s (S126).

Tables 6.5 and 6.6 show the seismic Vp and Vs of 10 different metasediments. Stronalite and kinzigite are the dominant metasedimentary rock types. The seismic velocities of stronalite range from a minimum of 6.128 km/s to a maximum of 6.787 km/s and shear wave velocities range from 3.721 to 4.076 km/s. The highest velocities

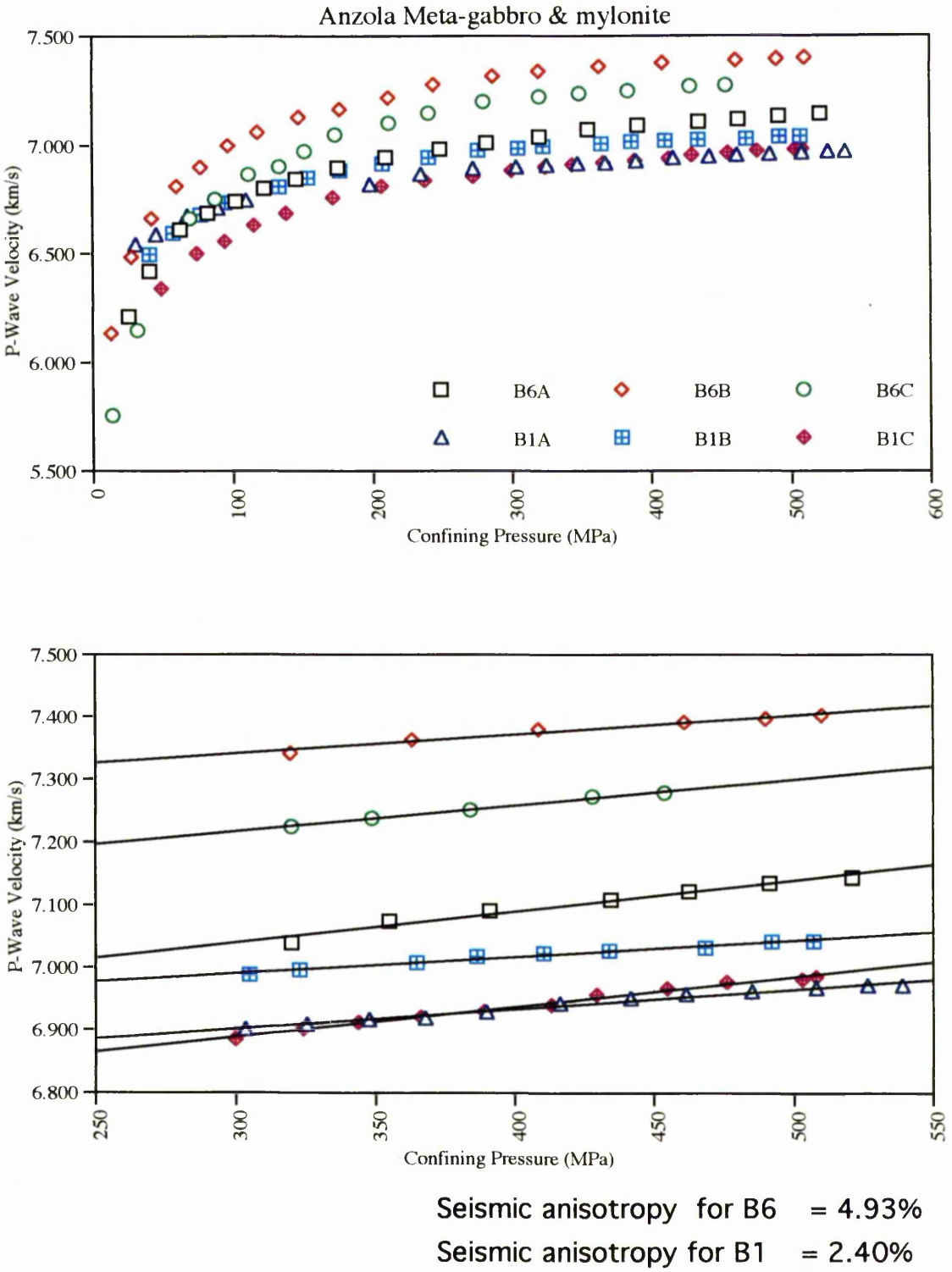

Figure 6.9: Plot of seismic compressional velocity as a function of confining pressure for cores of metagabbro protolith (B6) and its mylonite (B1). The top plot shows the velocity measurements over a full pressure range from 20 MPa to 530 MPa. The bottom plot only shows the velocity points above the 300 MPa confining pressure. The velocity measurements above 300 MPa was used to find the best fit line through them.

Lithology & Samle No	Density gr/cm3	Vp km/s	Av Vp km/s	dVp/dP (*10^{-4}) km/s/MPa	Av dVp/dp (*10^{-4}) km/s/MPa	Anisotropy %
Px Stronalite						
S4A	3.024	6.536	6.536	4.336	4.336	
S4B	2.968	6.643	6.643	3.201	3.201	
S4C	2.999	6.475	6.475	6.407	6.407	
Average	**2.997**		**6.551**		**4.648**	**2.56**
Stronalite						
S19A'	2.870	6.577	**6.478**	2.629	**4.692**	
S19A	2.888	6.378		6.755		
S19B	2.881	6.787	6.787	6.776	6.776	
S19C	2.970	7.054	7.054	5.629	5.629	
Average	**2.902**		**6.773**		**5.699**	**8.52**
Stronalite						
S72A	2.637	6.154	6.154	4.306	4.306	
S72B"	2.631	6.337	6.337	4.221	4.221	
S72C	2.632	6.128	6.128	4.757	4.757	
Average	**2.633**		**6.206**		**4.428**	**3.35**
Stronalite						
S73A	2.779	6.069	6.069	4.296	4.296	
S73B	2.813	6.452	6.452	3.852	3.852	
S73C	2.764	6.042	6.042	6.190	6.190	
Average	**2.785**		**6.188**		**4.779**	**6.56**
Kinzigite						
S43A	2.890	6.476	**6.200**	4.457	**6.048**	
S43A`	2.800	6.250		6.657		
S43A``	2.720	5.873		7.029		
S43B'	2.720	6.580	6.580	4.371	4.371	
S43C	2.697	6.558	6.558	5.000	5.000	
Average	**2.765**		**6.446**	**5.503**	**5.140**	**5.95**
Marble						
S52A'	2.691	6.333	**6.312**	0.514	**1.069**	
S52A"	2.700	6.318		0.783		
S52A'	2.704	6.285		1.910		
S52B	2.676	6.833	6.833	0.619	0.619	
S52C	2.684	6.555	6.555	1.236	1.236	
Average	**2.691**		**6.567**		**0.975**	**7.93**
Calcite Mylonite						
LCFA	2.85	6.488	6.488	2.825	2.825	
LCFB	2.851	6.579	6.579	3.541	3.541	
LCFC	2.883	6.700	6.700	4.524	4.524	
Average	**2.819**		**6.589**		**3.630**	**3.22**
Metasediment						
S74A	2.996	6.650	6.650	3.493	3.493	
S74B	3.079	6.633	**6.559**	6.070	**4.725**	
S74B`	3.062	6.484		3.379		
S74C`	2.998	6.629	6.629	4.925	4.925	
Average	**3.034**		**6.613**		**4.381**	**1.39**
Charnacite Mafic						
S126A	2.815	6.984	6.984	4.903	4.903	
S126B	2.805	6.91	6.910	2.964	2.964	
S126C'	2.835	6.842	**6.733**	3.747	**3.406**	
S128C	2.755	6.623		3.064		
Average	**2.803**		**6.876**		**3.758**	**3.67**
Charnecite felsic						
S129C	2.715	6.243	**6.264**	3.458	**3.423**	
S129C'	2.725	6.284		3.388		
Average	**2.720**		**6.264**		**3.423**	
Migmatite Felsic						
S131A	2.834	6.423	**6.234**	4.467	**5.049**	
S133A	2.678	6.125		5.167		
S134A	2.65	6.154		5.513		
S133B"	2.657	6.184	6.184	3.532	3.532	
Average	**2.705**		**6.209**		**4.291**	**0.81**
Migmatite Mafic						
S135A	2.974	6.833	6.833	2.491	2.491	
S135B"	2.899	6.759	6.759	3.092	3.092	
Average	**2.937**		**6.796**		**2.792**	**1.09**

Table 6.5:Measured density, compressional velocity and pressure coefficient of velocity of metasedimentary samples. The bold values are the averaged of a number of measurements. The symbols are the same as table 6.1.

Lithology & Samle No	Density gr/cm3	Vs km/s	Av Vs km/s	dVs/dP (*10-4) km/s/MPa	Av dVs/dp (*10-4) km/s/MPa	An %
Px Stronalite						
S4A	3.024	3.836	3.836	2.008	2.008	
S7A	2.968	3.871	3.871	1.311	1.311	
Average	**2.996**		**3.854**		**1.660**	**0.908**
Stronalite						
S19A	2.888	3.853	3.853	0.823	0.823	
S19B	2.881	4.061	4.061	2.839	2.839	
S19C	2.970	4.076	4.076	2.902	2.902	
Average	**2.913**		**3.997**		**2.188**	**0.369**
Stronalite						
S73A	2.779	3.721	3.721	1.785	1.785	
Average	**2.779**		**3.721**		**1.785**	=
Kinzigite						
S43A	2.890	3.508	3.508	4.000	4.000	
S43B	2.900	3.927	3.927	3.400	3.400	
S43C	2.697	3.547	3.547	4.600	4.600	
Average	**2.829**		**3.661**		**4.000**	**11.271**
Marble						
S52B	2.676	3.430	3.430	0.623	0.623	
Average	**2.676**		**3.430**		**0.623**	=
Calcite Mylonite						
LCFA	3.605	3.605	3.605	1.168	1.168	
LCFB	3.707	3.707	3.707	2.957	2.957	
LCFC	3.697	3.697	3.697	0.993	0.993	
Average	**3.670**		**3.670**		**1.706**	**2.790**
Metasediment						
S74A	2.996	4.255	4.255	1.242	1.242	
Average	2.996		4.255		1.242	=
Charnockite						
S129C	2.725	3.896	3.896	1.0022	1.002	
S128C	2.72	3.879	3.879	2.209	2.209	
Average	**2.723**		**3.888**		**1.606**	=
Migmatite						
S133A`	2.678	3.784	3.784	2.371	2.371	
S135A`	2.899	3.776	3.776	2.286	2.286	
Average	**2.789**		**3.780**		**2.329**	=

Table 6.6: Measured shear wave velocity and density of a number of metasedimentary rocks at room pressure and temperature. The symbols are the same as table 6.1.

were measured for garnet-rich stronalite (S19) and pyroxene-rich stronalite (S04) and the lowest was for quartz-rich stronalites (S72 & S73).

Kinzigite samples showed lower seismic velocities (Vp ranging from 5.87 km/s to 6.58 km/s & Vs ranging from 3.51 to 3.93 km/s) than most but higher seismic anisotropy (about 12 %). This low velocity can be attributed to lower garnet and plagioclase and higher quartz and phyllosilicate fractions. Almost all primary phyllosilicate are oriented along the foliation plane and show strong CPO. This can account for the high seismic anisotropy of the kinzigites and also of most mica rich rocks (e.g. mica schists, sample B11).

Marbles are quite abundant as extensive bands and lenses in the low grade part of the northern half of the IV zone, interlayered with kinzigite and stronalites. Sample S52 is a coarse grained calcite marble showing high seismic Vp (6.567 km/s) and Vs (3.40 km/s). Sample LCF is a fine grained calcite mylonite. It has similar compressional velocity (6.589 km/s) and higher shear wave velocity to S52. Considering both samples have very similar modal composition (more than 90% calcite). The difference in their seismic velocities could only be due to the differences in their crystallographic and shape fabric (see section 6.3.2.2).

Charnockites and migmatites are important volumetrically in the southern part of the IV zone. Their seismic velocities show a very wide range, directly reflecting the heterogeneity of these two rock types. Based on the amount of mafic minerals they contain, these rocks can be divided into two group either rich or poor in mafic minerals. Seismic velocity directly reflects such a subdivision. Figures 6.10 and 6.11 shows velocity pressure plots for a number of charnockites and migmatites in various directions.

6.2.4 Velocities of Rocks from the Serie dei Laghi

Table 6.7 and 6.8 shows the results of seismic Vp and Vs measurements for 6 rock types from the SdL. For all these rocks the Vp ranges from a maximum of 6.12 km/s (schist B11) to minimum of 5.82 km/s (Gneiss S58).

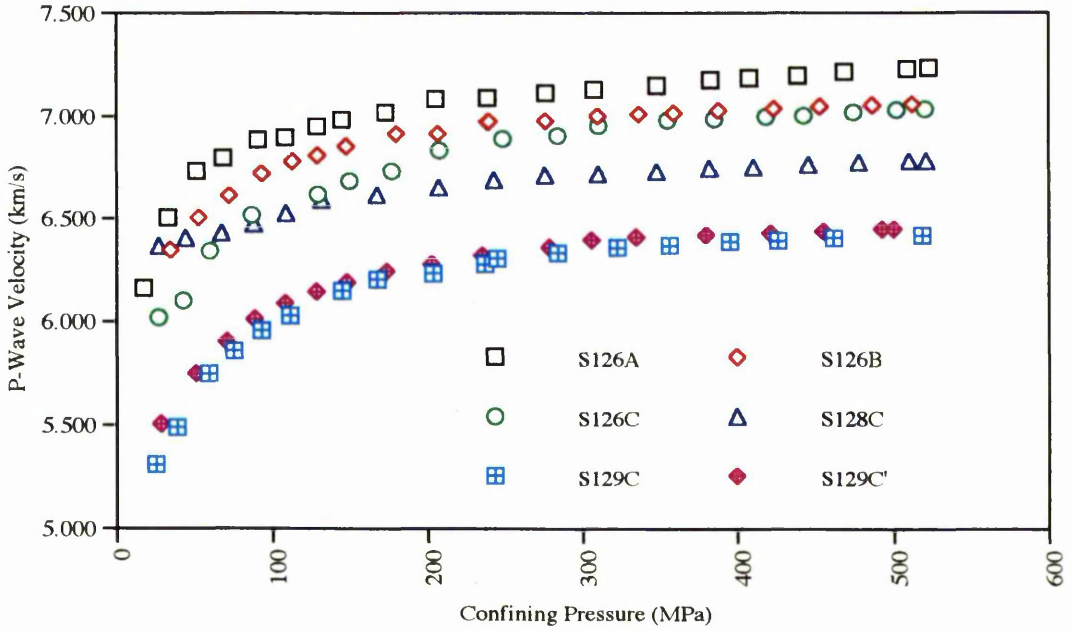

Figure 6.10: Compressional velocities at confining pressures up to 530 MPa for Charnockite samples. There is a wide variation in seismic velocity associated with this rock type. This is attributed to the significant variation in mineralogy.

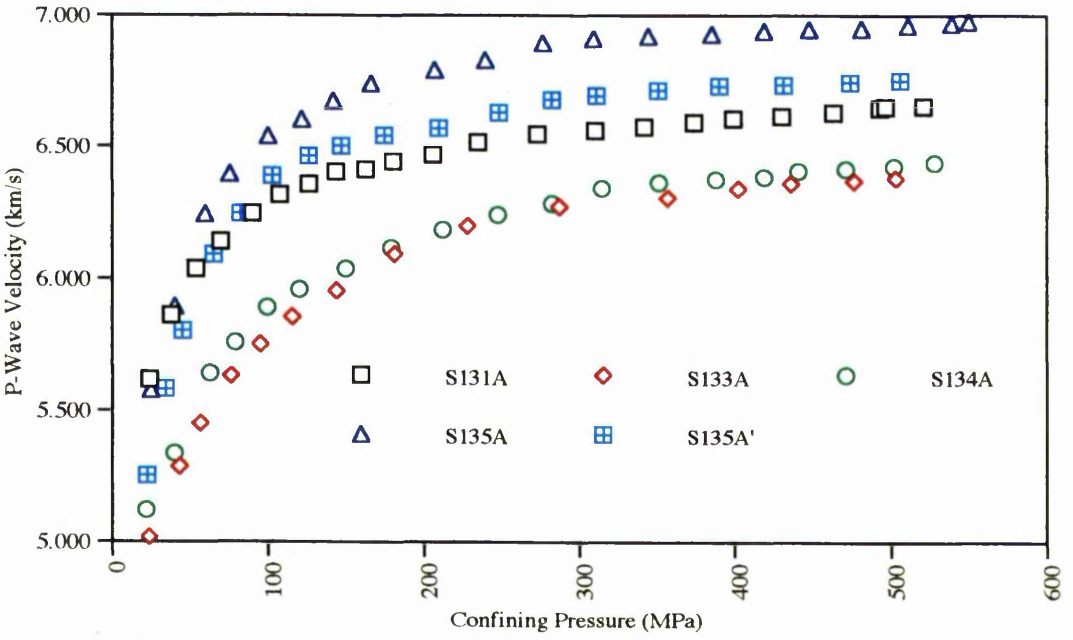

Fig.6.11: Plot of compressional velocity as a function of confining pressure up to maximum 540 MPa for number of migmatites cores. The measurements are for the direction normal to the foliation plane.

Lithology & Samle No	Density gr/cm3	Vp km/s	Av Vp km/s	dVp/dP (*10^{-4}) km/s/MPa	Av dVp/dp (*10^{-4}) km/s/MPa	Anisotropy %
Ceneri Gneiss						
S59A	2.715	5.613	5.613	5.300	5.300	
S59B	2.701	5.897	5.897	4.742	4.742	
S59C	2.708	5.965	5.965	3.782	3.782	
Average	**2.708**		**5.825**		**4.608**	**6.08**
Gneiss						
S11A	2.692	5.653	**5.648**	3.922	**3.842**	
S12A	2.690	5.642		3.761		
S11B	2.713	6.383	6.383	4.239	4.239	
S11C	2.631	5.988	5.988	5.337	5.337	
Average	**2.682**		**6.006**		**4.473**	**12.2**
Orthogneiss						
S123A"	2.616	5.719	5.719	4.154	3.838	
S123B	2.658	5.990	5.990	5.355	4.337	
Average	**2.637**		**5.855**		**4.088**	**4.63**
Schist dei Laghi						
S99A'	2.790	5.500	**5.560**	6.562	**5.908**	
S99A	2.793	5.570		5.384		
B11A"	2.871	5.611		5.779		
S99B	2.743	6.504	**6.577**	4.993	**5.441**	
B11B	2.781	6.650		5.888		
S99C	2.716	6.313	**6.177**	3.04	**4.467**	
B11C	2.807	6.040		5.894		
Average	**2.784**		**6.377**		**4.954**	**16.8**
W-Granite						
S92	2.608	6.049	**6.035**	6.460	**6.455**	
S93	2.607	6.010		7.755		
S53A	2.605	6.046		5.149		
S53B	2.61	6.101	6.101	4.871	4.871	
S53C	2.606	6.150	6.150	4.218	4.218	
Average	**2.607**		**6.095**		**5.181**	**1.89**
P-Granite						
S94	2.604	5.955	5.955	8.122	8.122	
S96	2.585	5.964	5.964	7.033	7.033	
S98	2.587	5.904	5.904	7.778	7.778	
Average	**2.592**		**5.941**		**7.644**	**1.01**
Grt-Amphibolite						
B17A	2.991	6.454	6.454	3.873	3.873	
B17B	2.99	7.143	**7.143**	4.534	**4.379**	
B17B``	2.987	7.143		4.223		
B17C	2.984	6.605	6.605	6.289	6.289	
Average	**2.988**		**6.734**		**4.847**	**10.1**

Table 6.7: Density, compressional velocity and pressure coefficient of velocity for a number of rocks from Serie dei Laghi. The bold values are the average of a number of measurements. The symbols are the same as table 6.1.

Lithology & Samle No	Density gr/cm3	Vs km/s	Av Vs km/s	dVs/dP (*10^{-4}) km/s/MPa	Av dVs/dP (*10^{-4}) km/s/MPa	An %
Ceneri Gneiss						
S59A	2.715	3.495	3.495	1.933	1.933	
S59B	2.701	3.520	3.520	1.925	1.925	
Average	**2.708**		**3.495**		**1.933**	0.71
Orthogneiss						
S123A"	2.658	3.435	3.435	1.010	1.010	
S123B	2.679	3.508	3.508	1.575	1.575	
Average	**2.669**		**3.472**		**1.293**	2.10
Schist dei Laghi						
S99A'	2.793	3.353	**3.335**	2.055	**2.479**	
S99A	2.790	3.316		2.902		
S99`B	2.743	3.415	3.415	2.152	2.152	
S99C	2.716	3.615	3.615	1.531	1.531	
Average	**2.761**		**3.455**		**2.054**	8.07
Schist dei Laghi						
P-B11A	2.836	3.137	3.137	4.907	4.907	
P-B11C	2.807	3.248	3.248	3.569	3.569	
Average	**2.822**		**3.193**		**4.238**	3.48
W-Granite						
S92	2.608	3.610	3.610	2.030	4.174	
S93	2.607	3.595	3.595	4.174	4.174	
Average	**2.608**		**3.603**		**4.174**	0.42
P-Granite						
S94	2.604	3.547	3.547	3.859	3.859	
S96	2.585	3.592	3.592	2.331	2.331	
S98	2.587	3.676	3.676	1.522	1.522	
Average	**2.592**		**3.605**		**2.571**	3.57
G-amphibolite						
B17A	2.991	3.928	3.928	1.476	1.476	
B17B	2.984	4.522	4.522	2.505	2.505	
Average	**2.988**		**4.225**		**1.991**	14.06

Table 6.8: Density and shear wave velocity for a number of rocks from Serie dei Laghi. Velocity and density values are for room pressure and temperature conditions. Cores from two granites were collected at different but arbitrary directions due to lack of visible foliation or lineation. The symbols are the same as table 6.1.

Mica schists, paragneisses and orthogneisses are the dominant rock types in the SdL. They all have similar compressional and shear velocities but different velocity anisotropy. This difference in their seismic anisotropy is mainly due to variation in degree of the preferred orientation of phyllosilicate minerals such as biotite and muscovite.

Granites have similar seismic velocities to the other rock units in the SdL. Both show very small seismic anisotropy, reflecting the lack of mineral preferred orientation. The very low seismic anisotropy of granites is an indication that they are post metamorphic-peak intrusive that have not been deformed. Baveno Pink granite shows slightly lower seismic velocities than the White granite. This velocity difference can be attributed to differences in modal composition.

6.3 Discussion

All the velocity measurements which have been presented were carried out on dry rocks, and at high confining pressure in order to eliminate the effect of pore fluid pressure and microcracks. The remaining parameters which could have affected the velocity measurements are:

(i) confining pressure,

(ii) density changes due to pressure,

(iii) fabric (crystallographic and shape fabric),

(iv) mineral composition,

(v) temperature.

The effects of the last of these will be discussed in the next chapter. In this section the main focus of discussion will be on two points:

1) what would be the effect of the above mentioned parameters on seismic velocity.

2) how seismic velocity can be used to characterise lithology.

6.3.1 Velocity/pressure Relationships

Pressure not only changes the density of a sample due to changes in its volume

but also causes a change in elastic properties of the sample. Both changes will have direct effects on seismic velocity of the sample.

6.3.1.1 Elastic moduli/ pressure relations

The general velocity increase with pressure in the low pressure range (from 0 to about 250 MPa) has been observed in all studies on high pressure velocity measurements. This increase has been attributed to compaction of pore space and in particular the planar microcracks. For loose aggregates in which the component parts (e.g. mineral grains) do not fit perfectly together, confining pressure may produce stresses in the individual parts and along the grain boundary which are far from homogeneous. As the pressure increases, more pores and cracks become closed, the aggregate becomes more compact and the stress and strain distributions within become more homogeneous.

At higher confining pressure (above 250 to 500 MPa) all samples show a linear relationship between velocity and pressure, indicative of the intrinsic pressure effect on the density and stiffness of the rocks. All the measured samples show an increase in seismic velocities with pressure.

Assuming that the linear relation between velocity and pressure exist at higher pressure than 500 MPa, one can extrapolate the measured velocity data to higher confining pressure (around 700 to 1000 MPa). This would provide velocity values more appropriate to lower crustal conditions. Figures 6.12 shows plots of compressional velocities of different rock types versus confining pressure up to 1000 MPa. Clearly, at higher confining pressure some rocks display velocity relations with respect to each other that are different from the low pressure relationships.

6.3.1.2 Density and pressure

The decrease in volume of rock caused by pressure would result in increase in density of the sample. Such decrease in volume of rocks can be calculated from their compressibilities. There are direct and indirect methods of measuring the compressibility. The compressibility (K) of a sample can be calculated from compressional and shear velocities and density (ρ) using the following equation.

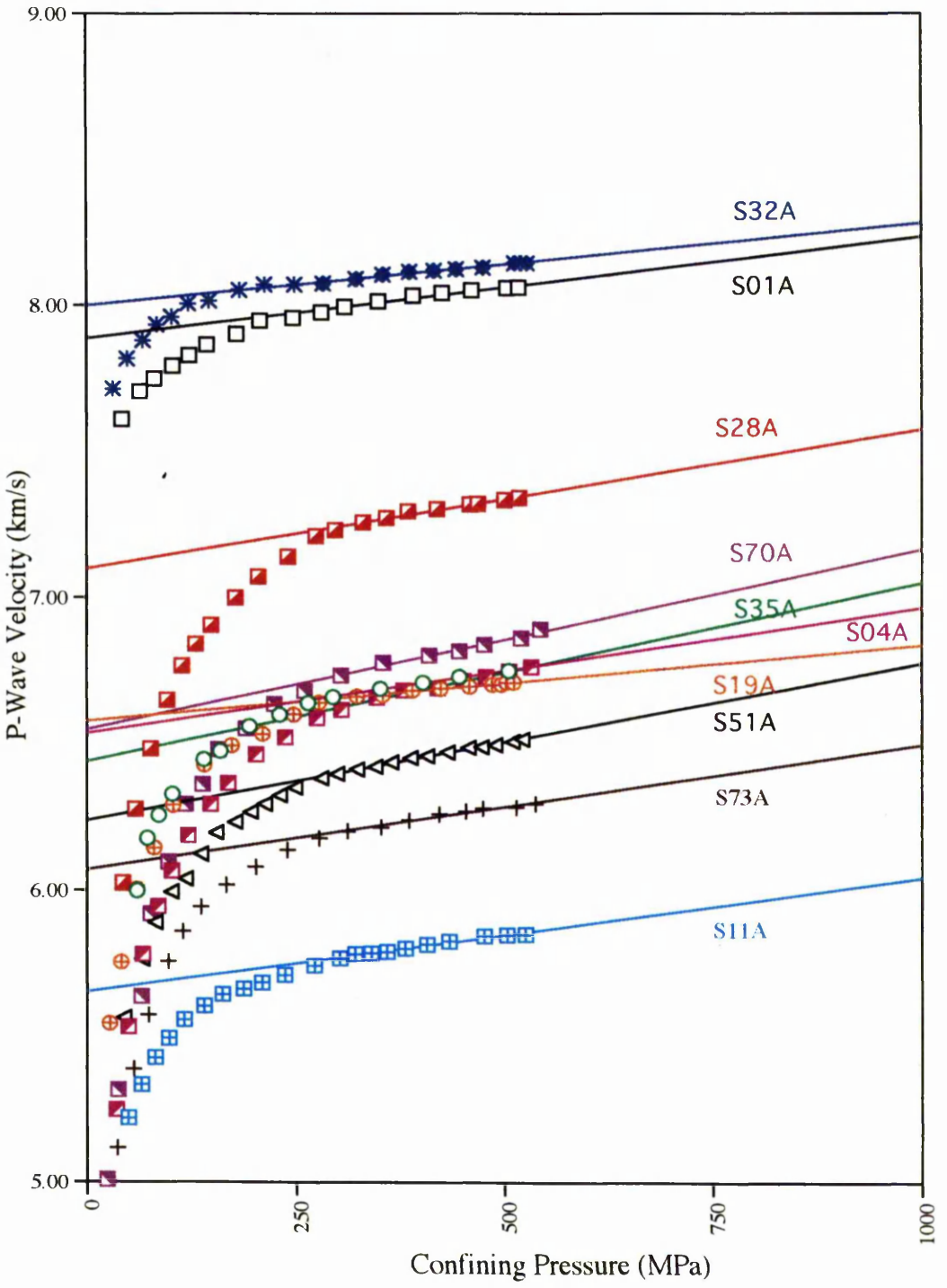

Figure 6.12: Plot of compressional velocity as a function of confining pressure for number of rocks. All the measurements were conducted on cores with the same orientation (normal to the foliations). Velocity points above 300 MPa were used to extrapolate the velocity values to higher confining pressure assuming a linear velocity/pressure relationships.

$$K = \rho\left(V_p^2 - {}^{4V_s^2}/_{3}\right) \tag{6.2}$$

The compressibility values for each rock type then can be used to calculate the change in density ($\rho^{(P)}$) with pressure (assuming no change of compressibility with pressure and an isotropic compressibility) using the following equation.

$$\rho^{(P)} = \rho'(1 + KP) \tag{6.3}$$

where ρ' is the surface density, K is compressibility and P is the confining pressure. Equation 6.2 was used to calculate the compressibility of each rock type. Further, equation 6.3 was used to calculate the variation in density of the samples over a range of pressure (table 6.9).

The results of calculated compressibility shows higher values for mafic-rich rocks and lower for more felsic-rich ones. This indicates a higher effect of pressure on the density of the mafic rocks than felsic ones. Figure 6.13 shows an increase of density of a number of rocks with pressure. For example, ultramafic sample shows an increase density around 1.7 % over a pressure range from 0 MPa to 500 MPa whereas for the same amount of change in pressure only 0.9 % change in density is observed for the granite.

From the above observations it can be suggested that in lower crust such as the IV zone, as the composition of the crust becomes more mafic towards the base of the crust, change of density with pressure becomes significant (see chapter 8). Although, it should be pointed that increase in lithospheric pressure is normally also associated with increase in temperature. Temperature has the opposite effect to that of pressure on the density. Thermal expansion causes volume increase and therefore decrease in density. Thus one should consider the combined effect of pressure and temperature on the density of the lower crustal rocks. See chapter 8 for more on the change of density of the samples with both pressure and temperature.

6.3.2 Fabric and Seismic Velocity

Difference in seismic velocity of rocks measured in various directions is an indication of seismic anisotropy. In a polycrystalline rock seismic anisotropy arises

Sample No	Lithology	Av Vp	Av Vs	K	Density (g/cm3)					
		km/s	km/s	MPa	0	100	200	300	400	500
S01	Peridotite	8.102	4.634	121.80	3.29	3.30	3.32	3.33	3.34	3.35
S32	Peridotite	8.202	4.632	127.64	3.30	3.31	3.33	3.34	3.35	3.36
S60	Peridotite	7.771	4.476	109.31	3.25	3.26	3.27	3.28	3.29	3.30
S24	Pyroxenite	7.444	4.492	91.88	3.22	3.23	3.24	3.25	3.26	3.27
S70	2Px granulite	6.717	3.826	77.90	3.04	3.05	3.06	3.07	3.07	3.08
S28	Gr granulite	7.057	3.938	92.47	3.18	3.18	3.19	3.20	3.21	3.22
S71	Meta gabbro	6.896	4.12	72.15	2.90	2.90	2.91	2.92	2.92	2.93
B6	meta gabbro	7.061	4.129	84.82	3.13	3.14	3.14	3.15	3.16	3.17
B1	Sheared metabasic	6.824	3.97	78.93	3.09	3.10	3.10	3.11	3.12	3.13
S35	Amphibolite	6.71	3.726	80.68	3.04	3.05	3.06	3.07	3.08	3.08
S50	Amphibolite	6.684	3.971	70.29	2.97	2.98	2.99	2.99	3.00	3.01
S41	Diorite	6.348	3.267	74.84	2.87	2.88	2.89	2.89	2.90	2.91
S75	Diorite	6.832	3.91	76.96	2.93	2.93	2.94	2.95	2.96	2.97
S04	Px stronalite	6.551	3.854	69.26	3.00	3.00	3.01	3.02	3.02	3.03
S19	Stronalite	6.773	3.997	71.31	2.90	2.91	2.92	2.92	2.93	2.94
S73	Kinzigite	6.188	3.721	55.23	2.79	2.79	2.80	2.80	2.81	2.81
S74	Meta sediment	6.613	4.255	59.44	3.03	3.04	3.05	3.05	3.06	3.06
S52	Marble	6.567	3.43	73.84	2.69	2.70	2.71	2.71	2.72	2.73
LCF	Sheared marble	6.589	3.67	71.76	2.82	2.83	2.83	2.84	2.85	2.85
S129	Felsic charnockite	6.264	3.888	51.90	2.72	2.73	2.73	2.74	2.74	2.75
S135	Mafic migmatite	6.796	3.78	79.69	2.94	2.94	2.95	2.96	2.97	2.98
S59	Gneiss	5.825	3.5	47.65	2.71	2.71	2.72	2.72	2.73	2.73
S123	Orthogneiss	5.855	3.47	48.06	2.64	2.64	2.65	2.65	2.66	2.66
S99	Schist de laghi	6.117	3.45	60.16	2.79	2.80	2.80	2.81	2.82	2.82
B11	Schist	6.11	3.19	67.01	2.82	2.83	2.83	2.84	2.85	2.85
B17	Gr amphibolite	6.734	4.225	64.38	2.99	2.99	3.00	3.01	3.01	3.02
S92	White granite	6.095	3.19	61.48	2.61	2.61	2.62	2.63	2.63	2.64
S96	Pink granite	5.941	3.6	46.70	2.59	2.60	2.60	2.61	2.61	2.62

Table 6.9: Average seismic velocities and density were used to calculate the compressiblity of different rocks. The calculated compressibility then was used to calculate density of the samples at 100, 200, 300, 400 and 500 MPa confining pressure. It was assumed that there is no change in compressibility with pressure.

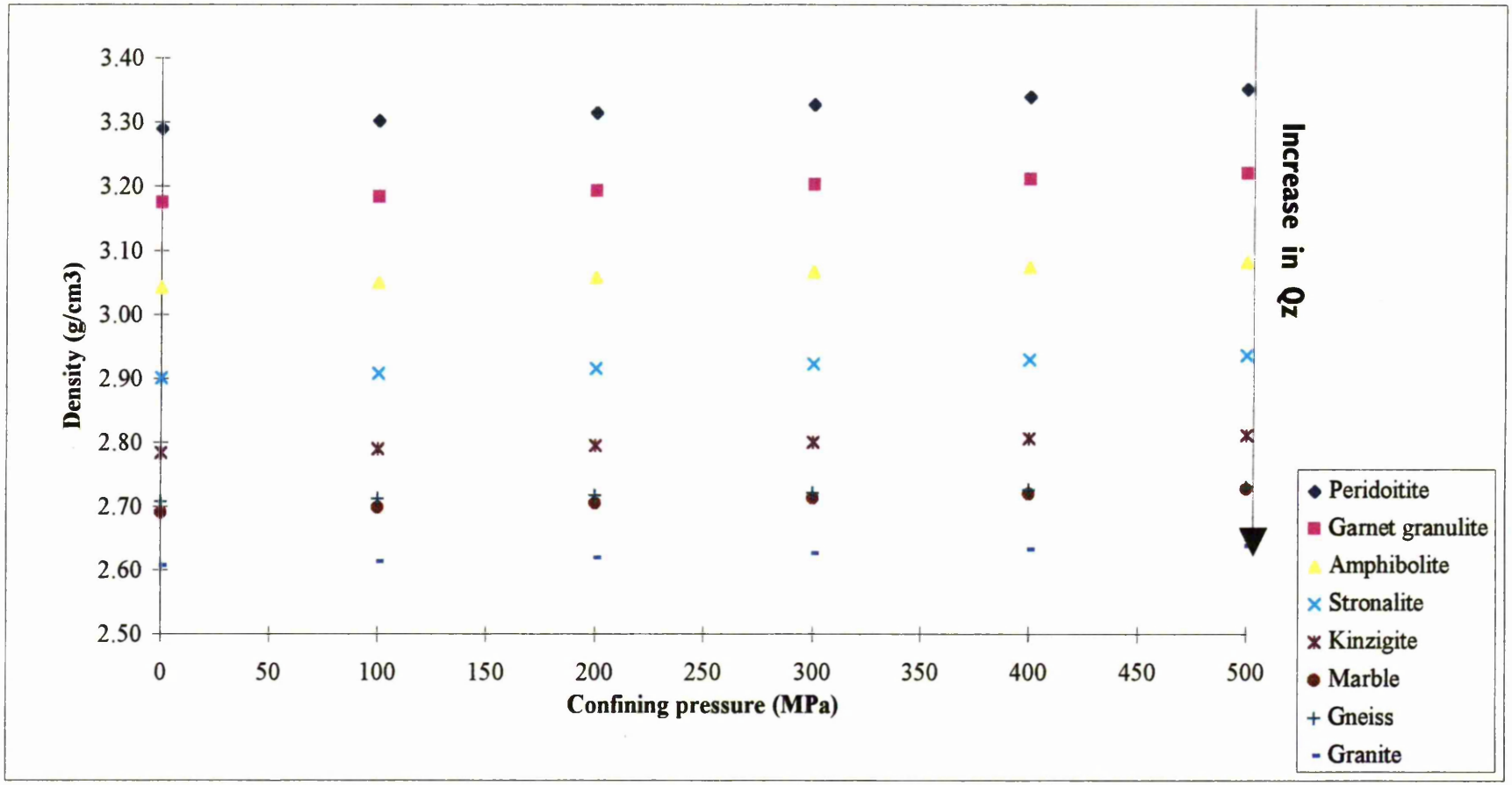

Figure:6.13: Plot of density as a function of confining pressure for a number of rocks. All rocks show an increase in density with pressure and at room temperature.

from various sources; (1) intrinsic anisotropy of minerals (2) crystallographic preferred orientation of minerals (3) preferred crack orientations (4) shape fabric or texture (e.g. elongated minerals or fine layering) (5) any combinations of above. The result of experimental studies on the samples from IV zone (this study) and some other lower crustal rocks (e.g. Christensen, 1989; Fountain et al., 1990) indicates that at low confining pressures microcracks contribute to seismic anisotropy significantly. At pressure well above 200 MPa where most microcracks are closed the observed anisotropy is believed to be due mainly to crystallographic preferred orientation of constituent minerals (fig 6.14). The measured seismic anisotropy is highest in foliated rocks and mainly due to alignments of phyllosilicate (e.g. schist, kinzigites) and hornblende (e.g. amphibolites).

6.3.2.1 Seismic anisotropy of mineral single crystals

Most minerals show various degrees of elastic anisotropy which is closely linked to their crystal symmetry. Figure 6.15 shows the calculated seismic compressional and shear velocity of number of minerals. Phyllosilicate, such as biotite and muscovite, show the highest seismic anisotropy, which reflects their crystallographic structure. Garnet, on the other hand displays virtually no seismic anisotropy, which is due to its cubic crystal structure.

6.3.2.2 Formation of CPO

In a polycrystalline aggregate where the individual grains are randomly oriented, and there is no shape fabric, one would not expect any seismic anisotropy. However if there is a crystallographic fabric then the degree of seismic anisotropy depends on two major parameters;

i) the degree of mineral anisotropy.

ii) the crystallographic preferred orientation (CPO) and the pattern of minerals produced by deformation for each crystalline phase.

In chapter 4 it was shown that many of the samples used for velocity measurements have strong shape or crystallographic fabric. The combination of the

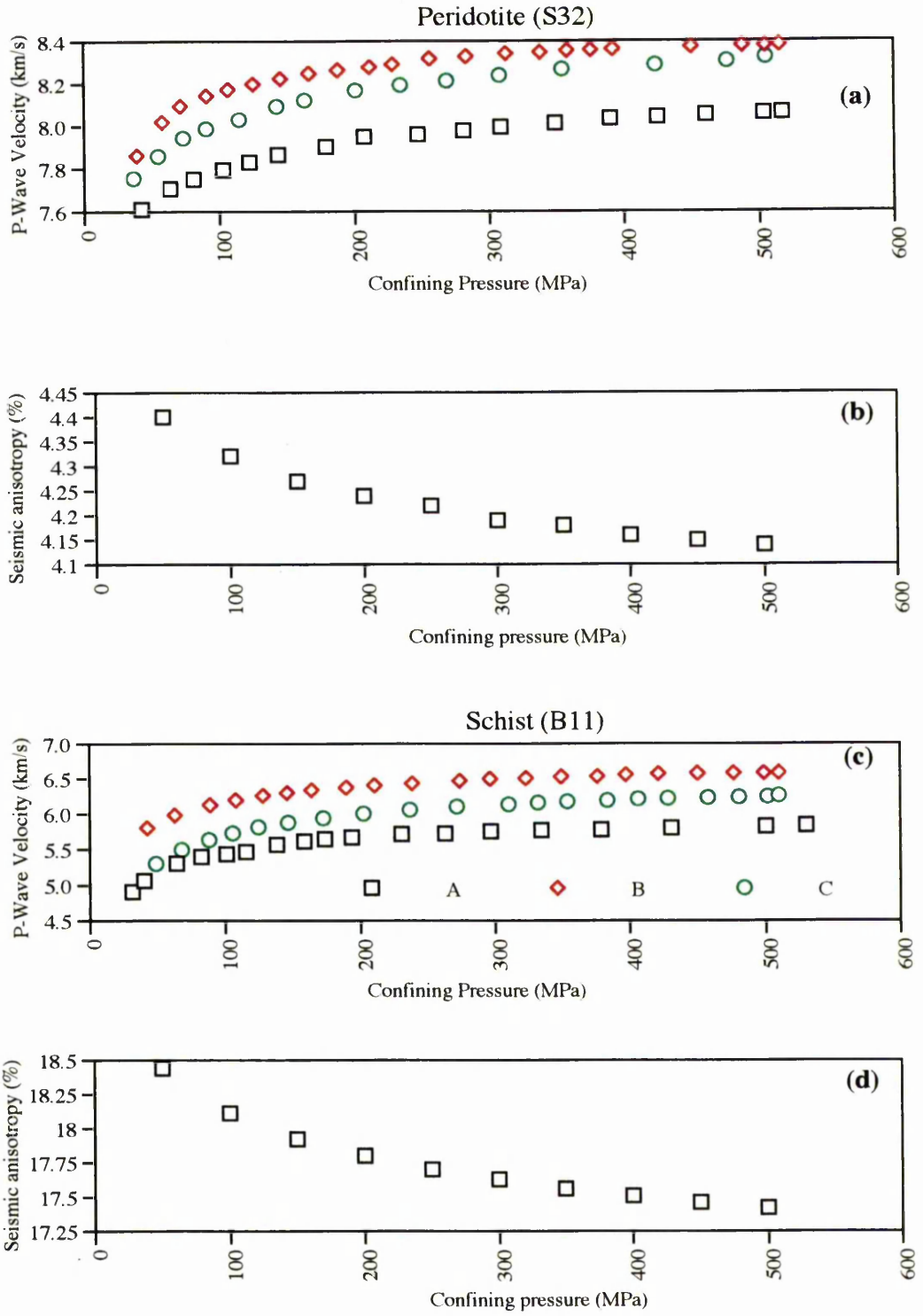

Figure 6.14: Plots of seismic velocity and seismic anisotropy as a function of pressure for two different samples. The plots (a & c) show compressional velocity versus confining pressure curves for three orthogonal cores. The plots (b & d) show the decrease in seismic anisotropy with increasing pressure for the same samples as a and c.

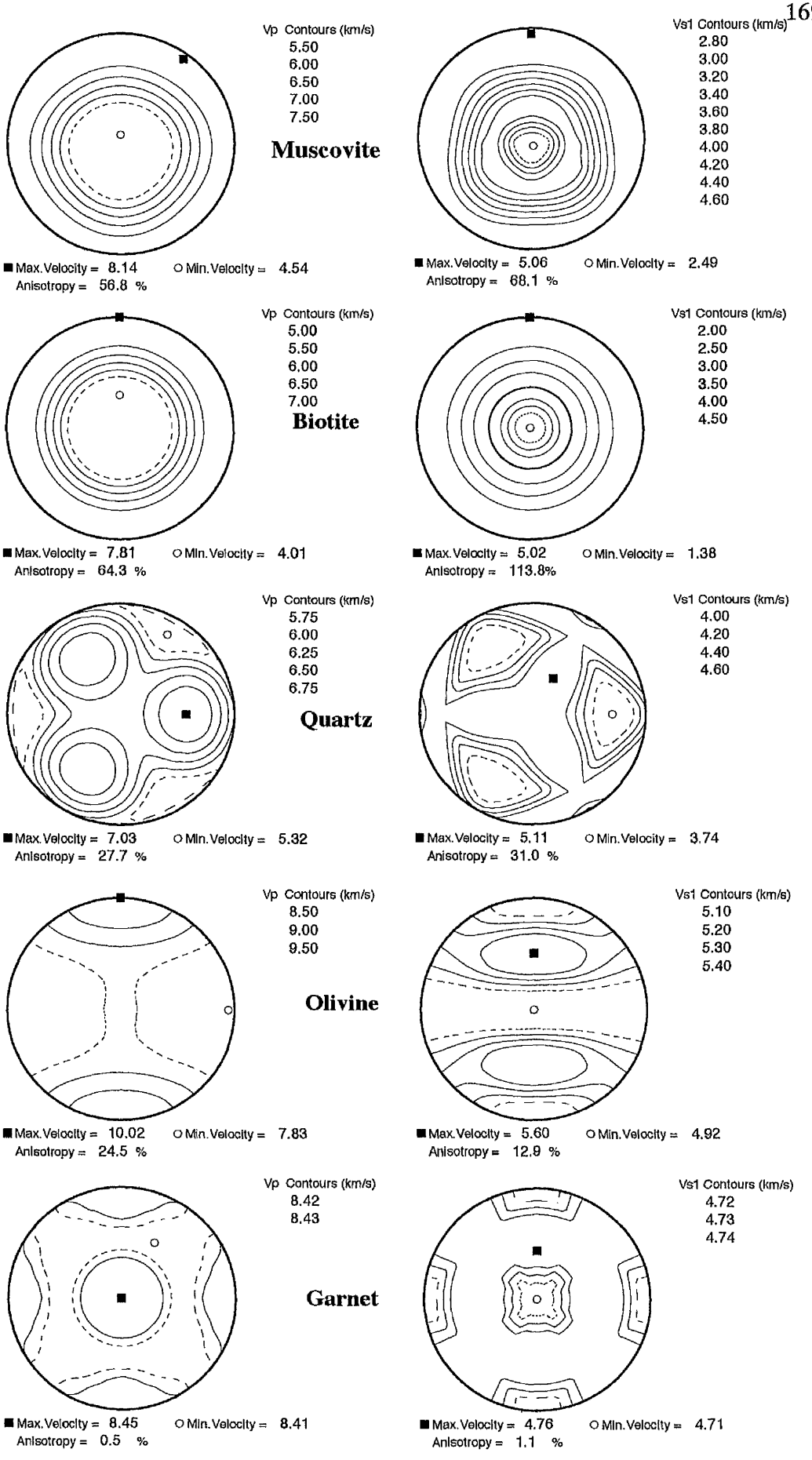

Figure 6.15: Calculated seismic compressional, shear waves velocities and seismic anisotropies (P-wave and S-wave velocity anisotropy) for a number of minerals.

CPO and anisotropic single crystal properties results in a three dimensional variation in rock properties. To evaluate this variation as explained before the seismic measurements were carried out in three orthogonal directions under hydrostatic pressure.

In order to study the effect of grain shape on the seismic velocity and seismic anisotropy a comprehensive study and analysis of the grain size, grain shape, volume fraction of each phase and their relative relationship are needed. This matter has not been pursued during the course of this study. However in order to explore further the importance of CPO on seismic properties of rocks, the crystallographic orientation of calcite grains in a mylonite sample (LCF) were measured using the texture goniometer method and later its seismic velocities where calculated and compared with the measured velocity values.

Importance of crystallographic preferred orientation on seismic anisotropy

The calcite mylonite (LCF) is characterised by a monoclinic fabric showing strong mineral preferred orientation of calcite c-axes (Figure 6.16). The fabric is of the type expected for low temperature, high stress deformation when twinning is active. By comparison with the results of experimental rock mechanics (Rutter et al., 1994), twinning deformation is expected to have occurred in the initial deformation of the protolith. Dynamic recrystallisation by twin boundary migration would remove the twins without changing the fabric, and eventually lead to grain-size refinement as deformation progresses (see fig 3.3).

A block of the calcite mylonite (LCF) was cored in seven different directions and the compressional velocity of each core was measured at elevated confining pressure (fig 6.17). Further the c-axis orientation of the calcites were used in conjunction with the elastic stiffness matrix of the calcite single crystal (Dandekar 1967 &1968) to calculate the seismic velocity of the sample (fig, 6.18). A good agreement was obtained with the velocity measurements (fig 6.19).

Considering that the calcite mylonite sample consists of mainly calcite (>96%) and the velocity experiments were carried out at high pressure to eliminates the effects of

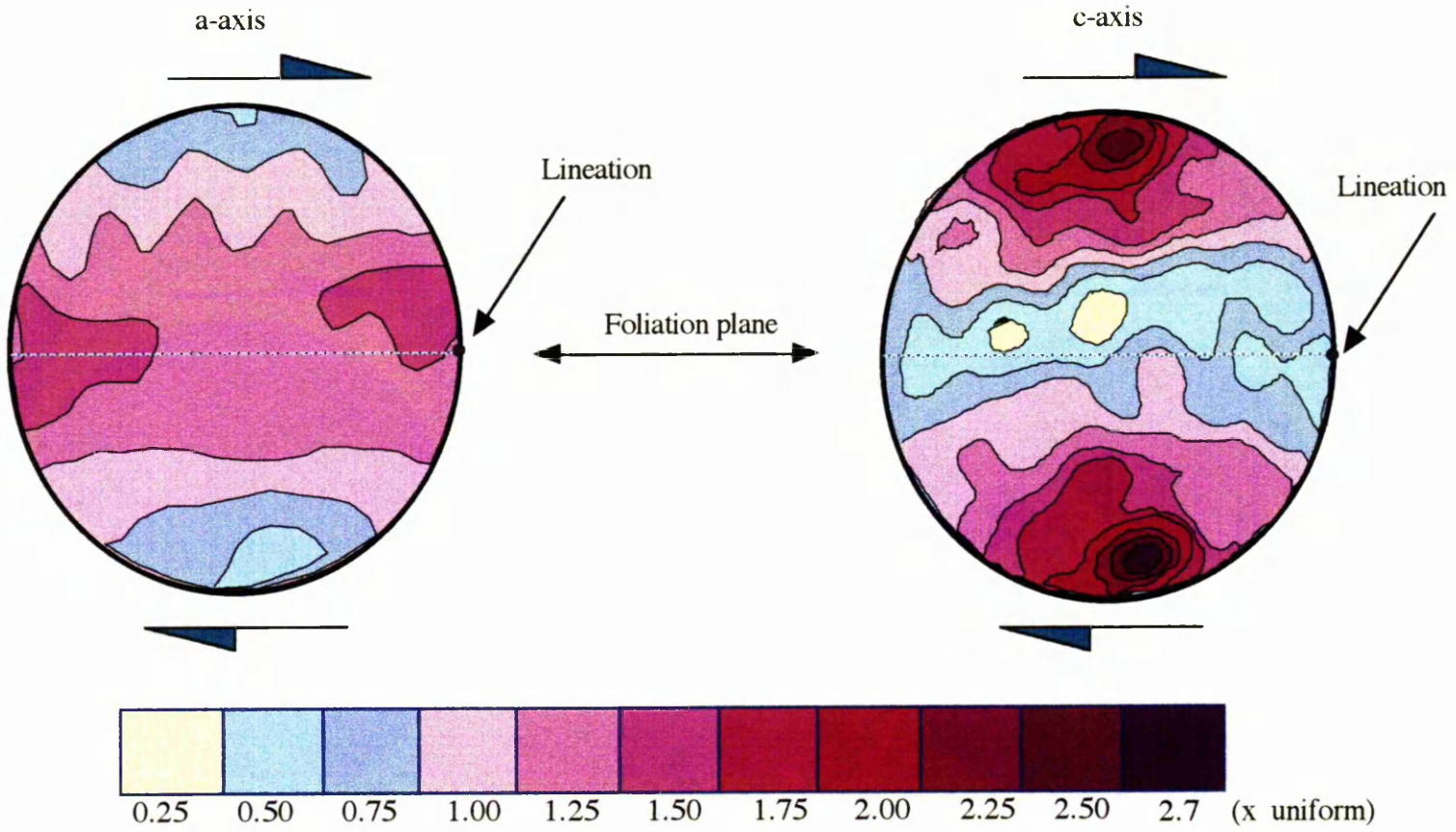

Figure 6.16: Calcite 'a' and 'c' axes pole figure of calcite mylonite from Val Cannabino. The fabric is a typical of high stress low, temperature (c-max type). The plots are equal area and upper hemisphere.

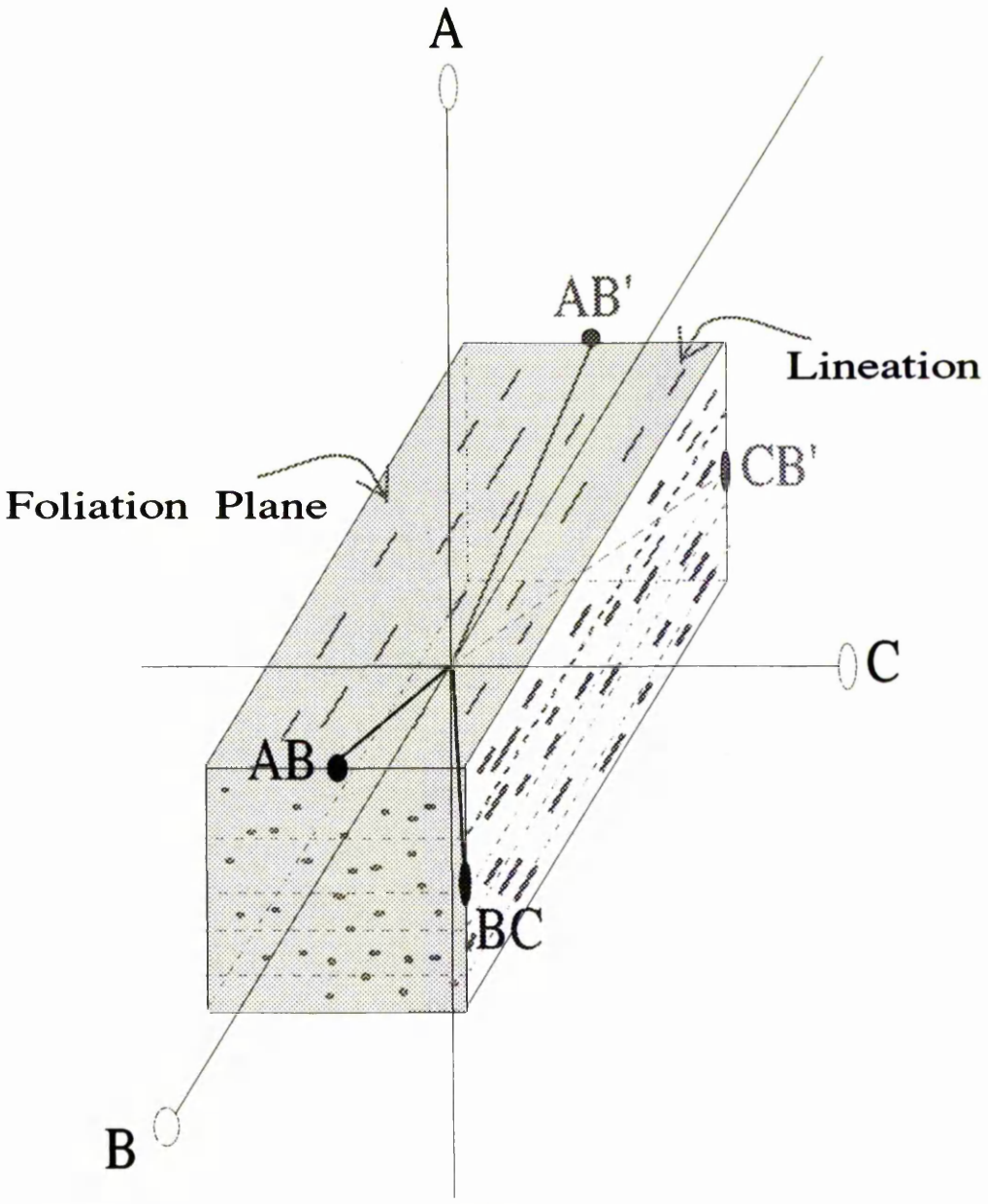

Figure 6.17: Orientation of the cores with respect to the foliation and lineation.

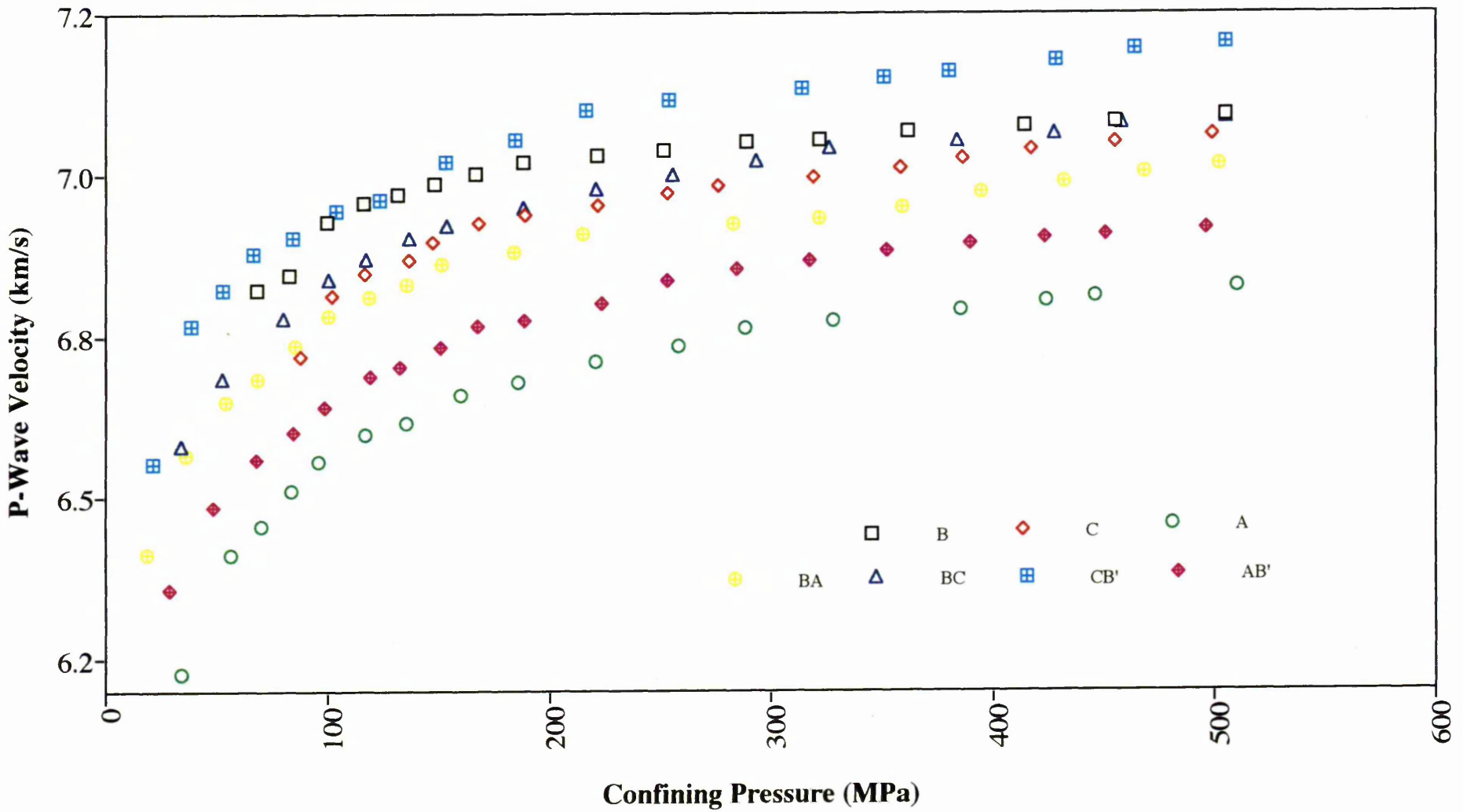

Figure 6.18 : Plot of compressional velocity as a function of confinig pressure for seven cores of calcite mylonite at various directions (see figure 6.17).

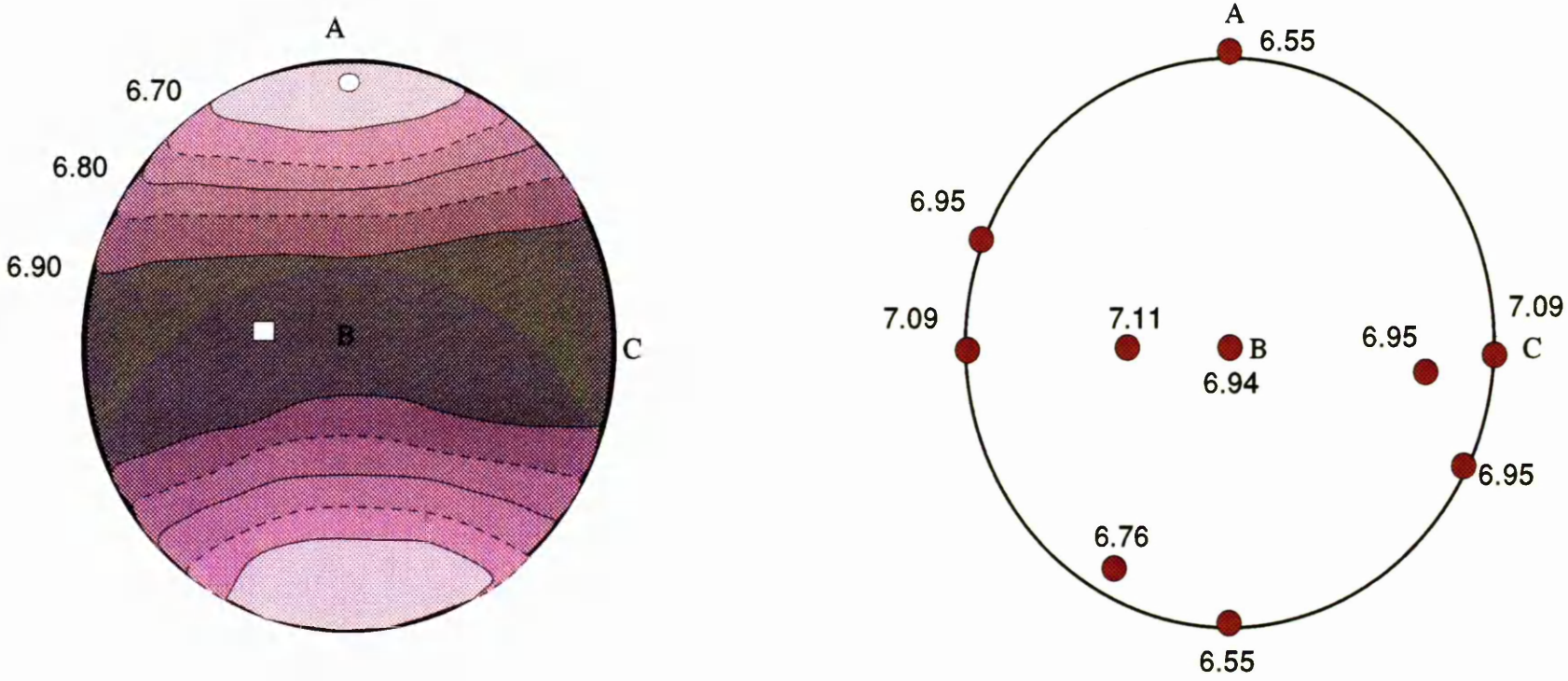

Figure 6.19: Showing the variation of compressional velocity with orientation for a calcite mylonite (LCF). Left: velocities calculated from the crystallographic fabric measured by X-ray texture goniometry, Right: velocities measured along cores. A, B and C indicate the kinematic axes (see fig 3.20).

microcracks, the observed measured and calculated seismic anisotropy therefore reflects the CPO of the calcite grains.

A seismic anisotropy of about 7.88% and 5% was obtained from the measured and calculated velocity respectively at ambient conditions. The maximum velocity is for the direction parallel to the foliation and about 50 degrees to the lineation direction. The minimum velocity value is in the direction normal to the foliation. There is a clear relationship between the crystallographic and velocity fabric. In calcite the maximum V_P corresponds to the maximum in the a-axes pole figure and the minimum Vp corresponds to the maximum in the c-axes pole figure (see fig 5.22 chapter 5).

The above example for calcite mylonites demonstrates the importance of CPO on the seismic velocity of the rocks. For lower crustal rocks, crystal preferred orientation of quartz, biotite, hornblende and plagioclase can form strong seismic velocity anisotropy. Such velocity anisotropy may cause an increase or decrease in vertical and horizontal velocity, potentially causing enhancement of reflections or azimuthal variations.

6.3.3 Effects of Mineralogy and Mineral Composition on Seismic Velocity

Table 6.10 shows the calculated seismic properties of some lower crustal minerals. These results indicate a significant variation in seismic properties. In general the velocity and density of minerals increase from felsic ones toward mafics (e.g. from Qz to olivine). In ultrabasic and metabasic rocks, high contents of olivine, pyroxenes, amphibole and garnet results in higher compressional and shear velocities than rocks rich in quartz and feldspar (e.g. schist and granite, fig 6.20).

It is well documented that metamorphism and associated chemical reactions can change mineral chemistry. Such changes can be suggested as a factor affecting the seismic velocities of lower crustal rocks, in particular of rocks within shear zone in which the shearing may have been accompanied by mineralogical (modal proportion and mineral chemistry) and/or whole-rock chemical changes. Figure 6.21 shows changes in seismic velocity of single crystals of plagioclase as a function of Anorthite (An) content.

	Mu	Bi	Qz	Kf Microcline	Pl An 56%	Hb	Ens Opx	Di Cpx	Ol FO 93%
Density (gr/cm³)	2.83	2.70	2.65	2.55	2.69	3.02	3.21	3.22	3.222
Voigt									
Vp (km/s)	6.65	6.56	6.19	6.36	6.81	7.06	8.08	7.99	8.61
Vs(km/s)	3.9	3.96	4.25	3.56	3.7	3.84	4.87	4.52	5
Vp/Vs	1.71	1.66	1.46	1.79	1.84	1.84	1.66	1.77	1.72
K(GPa)	67.69	59.69	37.90	59.88	75.60	91.21	108.29	117.64	131.51
G(GPa)	43.09	42.37	47.82	32.39	36.92	44.57	76.15	65.77	80.53
E(GPa)	106.65	102.80	100.99	82.32	95.25	114.97	185.08	166.31	200.63
Reuss									
Vp(km/s)	5.5	4.62	5.9	5.7	6.42	6.82	8.04	7.62	8.46
Vs(km/s)	3.12	2.15	3.93	3.06	3.45	3.69	4.84	4.37	4.9
Vp/Vs	1.76	2.15	1.50	1.86	1.86	1.85	1.66	1.74	1.73
K(GPa)	48.68	41.16	37.41	50.93	68.17	85.74	107.28	105.14	127.24
G(GPa)	27.62	12.44	41.02	23.92	32.03	41.12	75.18	61.48	77.41
E(GPa)	69.67	33.90	90.12	62.05	83.08	106.36	182.84	154.35	193.08
Hill									
Vp(km/s)	6.07	5.59	6.04	6.03	6.62	6.94	8.06	7.8	8.53
Vs(km/s)	3.51	3.05	4.09	3.31	3.58	3.77	4.86	4.44	4.95
Vp/Vs	1.73	1.83	1.48	1.82	1.85	1.84	1.66	1.76	1.72
K(GPa)	58.18	50.42	37.65	55.41	71.89	88.48	107.79	111.39	129.38
G(GPa)	35.36	27.41	44.42	28.15	34.47	42.84	75.67	63.62	78.97
E(GPa)	88.16	68.35	95.56	72.18	89.17	110.66	183.96	160.33	196.86

Table 6.10: Calculated seismic velocity (Vp & Vs), compressibility (K), Shear modulus and Young's modulus of untextured aggregates of some important lower crustal minerals. Three different methods for averaging elastic stiffnesses of single crystals (Voigt, Reuss and Hill) were used. All values are for room pressure and temperature.

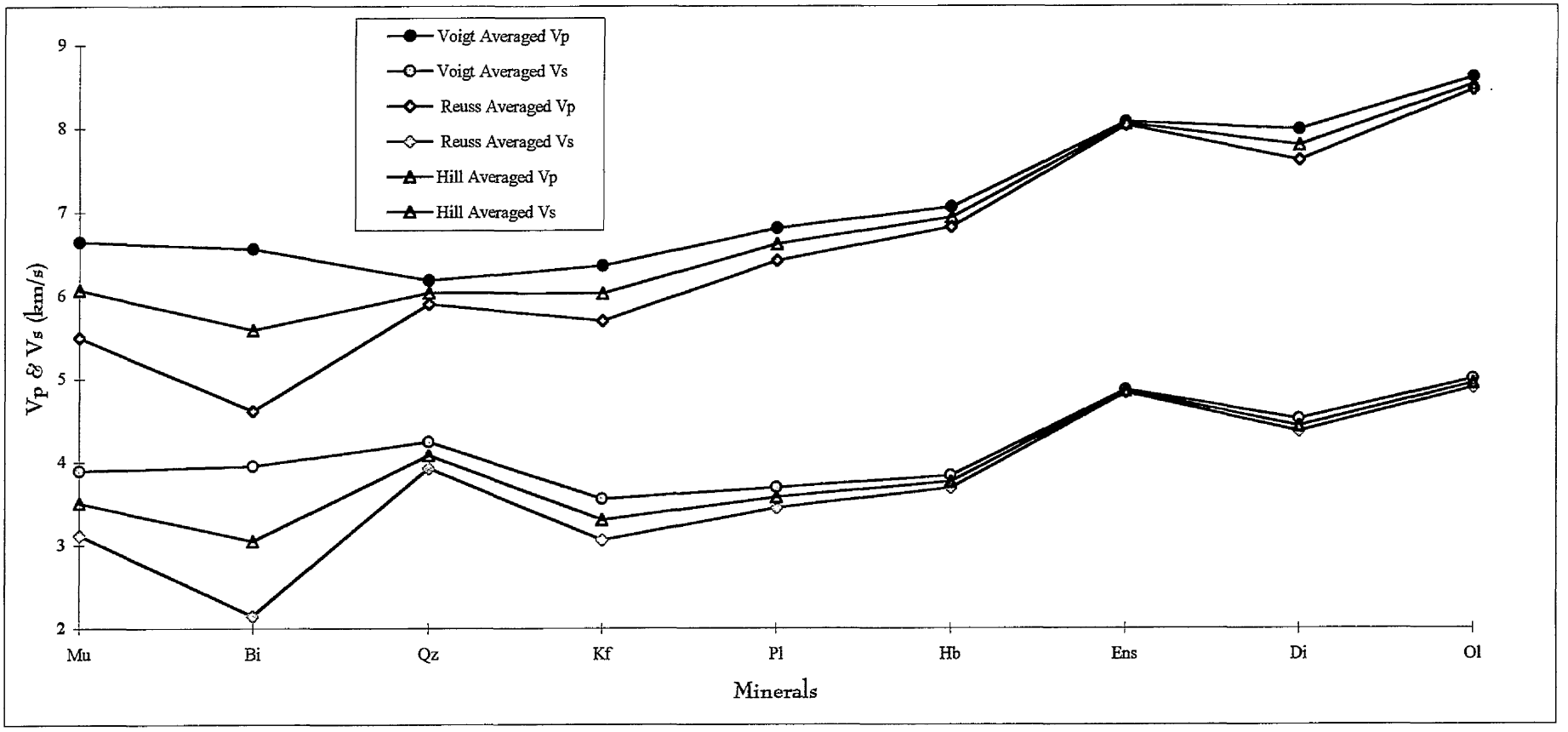

Figure 6.20: Display of calculated seismic velocities (compressional & shear waves) for some typical crustal minerals using three different averaging schemes. There is a great difference in calculated velocity for highly anisotropic minerals using different elastic moduli averaging techniques. Velocity values are calculated for room pressure and temperature conditions. Key for minerals as for table 6.10.

It is evident that both V_p and V_s increases with increase in An. A decrease of 1% in Ca ratio in plagioclase reduces the V_p by 0.17 % and V_s by 0.07 %. Chen et al (1996) measured changes in V_p along the olivine b-axis as a function of Mg fraction in olivine. He further concluded that 1% decrease in Mg/(Mg+Fe) ratio in olivine reduces the velocity about 0.21% (fig 6.22).

Above two examples support the suggestion that changes in mineral chemistry can have a significant effect on the velocity of crystalline rocks. These changes could result in lateral or vertical variation in seismic velocity of the same lithological bodies. It is difficult to say however, how much change in mineral chemistry of a polyphase aggregate is needed to cause a noticeable difference in overall velocity of the rock. This is due to two reasons: (i) in polycrystalline aggregates there is a probability that the chemistry of more than one phase is changed and (ii) any change in chemistry of a mineral may result in increase or decrease in seismic velocity of that mineral. The combination of the above two factors therefore may result in an enhancing or retarding effect on overall seismic velocity of the aggregate.

6.3.4 Characterising Lithology from Velocity &/or Density Data

The principal aim of all laboratory acoustic measurements is to establish relationships between seismic velocity, density or any combination of them with lithology. Such relationships can be used then for characterising subsurface lithology from in situ seismic measurements (reflection or refraction). Table 6.11 show the measured averaged seismic velocities (compressional and shear) and density of a number of rock types. These velocity and density values are used in following sections to derive some relationships between them.

6.3.4.1 Relationship between compressional and shear velocities

Figure 6.23 shows a plot of compressional velocity against shear velocity for all rocks in table 6.9. There is some scatter but a second order polynomial curve fit the data very well with correlation coefficient of 0.8. The following equation describes the relationship between the compressional and shear velocity:

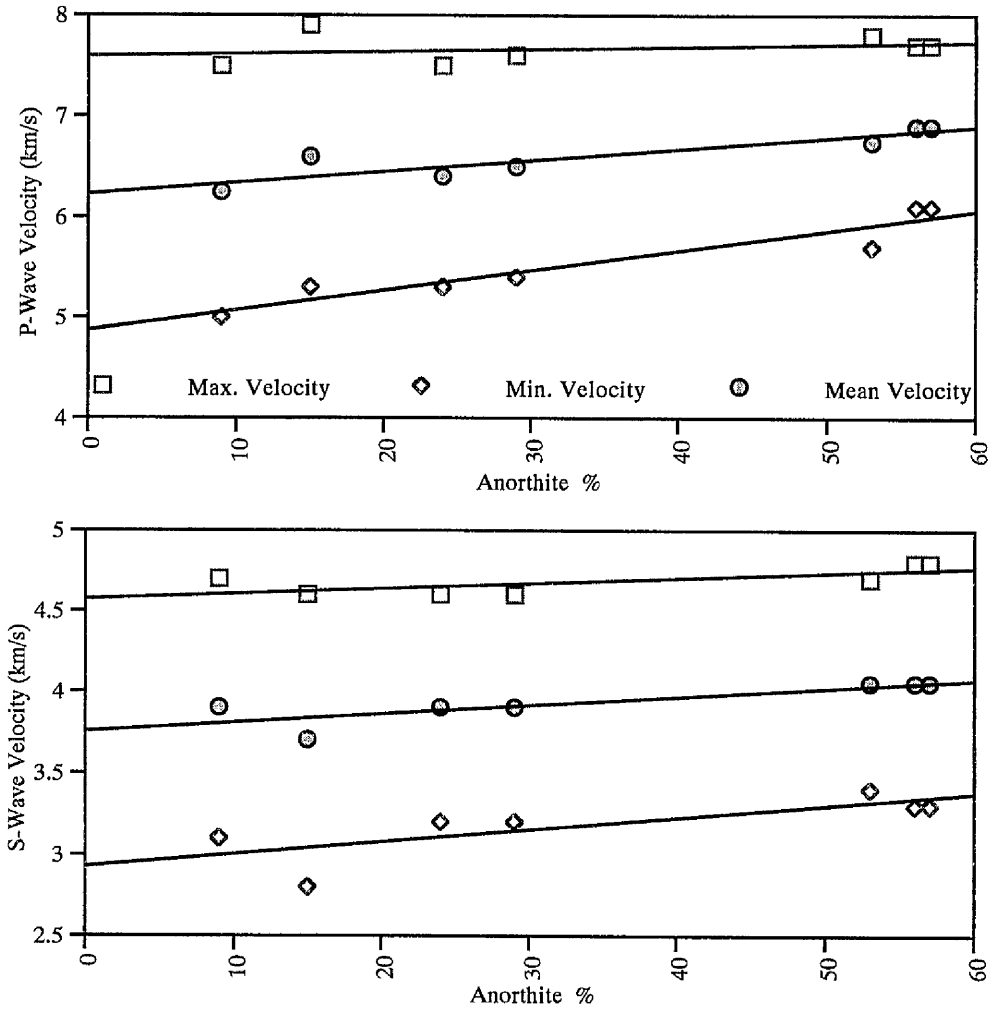

Figure 6.21: Calculated Hill averaged compressional and shear velocities as a function of Ca fraction in plagioclase.

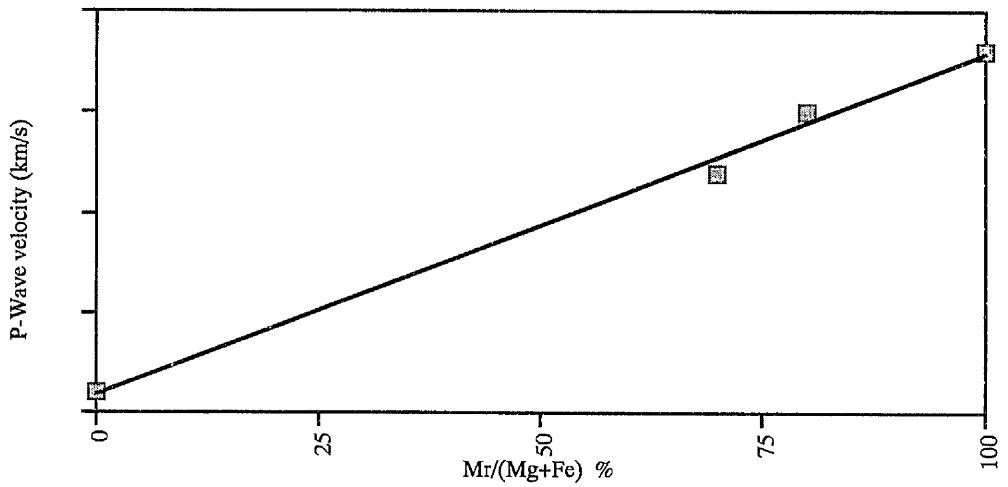

Figure 6.22: Compressional velocity along olivine b-axis as a function of Mg fraction in olivine (after Chen at al., 1996).

Sample No	Lithology	ρ	Vp	Vs	Vp/Vs	σ	K	G	E
		g/cm³	km/s	km/s			MPa	MPa	MPa
S01	Peridotite	3.291	8.102	4.634	1.748	0.257	121.80	70.67	177.65
S32	Peridotite	3.301	8.202	4.632	1.771	0.266	127.64	70.82	179.31
S60	Plog Peridotite	3.242	7.771	4.415	1.760	0.262	111.52	63.19	159.46
S24	Pyroxeite	3.223	7.444	4.400	1.692	0.232	95.40	62.40	153.69
S63	Px Granulite	3.061	6.963	4.146	1.679	0.225	78.25	52.62	128.95
S87	2Px Granulite	3.080	6.809	4.016	1.695	0.233	76.56	49.68	122.53
S70	2 Px Granulite	3.043	6.717	3.826	1.756	0.260	77.90	44.54	112.24
S28	G Granulite	3.175	7.057	3.938	1.792	0.274	92.47	49.24	125.45
S71	Meta Gabbro	2.895	6.896	4.134	1.668	0.220	71.70	49.48	120.67
B6	Meta Gabbro	3.127	7.061	4.129	1.710	0.240	84.82	53.31	132.23
B1	Sheared M Gabbro	3.089	6.824	3.970	1.719	0.244	78.93	48.69	121.15
S35	Amphibolite	3.047	6.710	3.726	1.801	0.277	80.79	42.30	108.05
S50	Amphibolite	2.972	6.684	3.932	1.700	0.235	71.51	45.95	113.53
B17	G-amphibolite	2.988	6.734	4.225	1.594	0.175	64.38	53.34	125.39
S41	Diorite	2.871	6.348	3.267	1.943	0.320	74.84	30.64	80.89
S75	Diorite	2.927	6.832	3.800	1.798	0.276	80.27	42.27	107.86
S04	Px Stronalite	2.997	6.551	3.854	1.700	0.235	69.26	44.52	109.98
S19	Stronalite	2.902	6.773	3.997	1.695	0.233	71.31	46.36	114.31
S73	Stronalite	2.785	6.188	3.721	1.663	0.217	55.23	38.56	93.84
S43	Kinzigite	2.765	6.446	3.661	1.761	0.262	65.48	37.06	93.53
S74	Metasediments	3.034	6.613	4.255	1.554	0.147	59.44	54.93	125.98
S52	Marble	2.691	6.465	3.430	1.885	0.304	70.26	31.66	82.58
LCF	Sheared Marble	2.819	6.589	3.300	1.997	0.333	81.45	30.70	81.82
S129	Felsic Charnecite	2.725	6.264	3.888	1.611	0.187	52.00	41.19	97.76
S126	Mafic Charnecite	2.940	6.876	3.876	1.774	0.267	80.11	44.17	111.93
S131	Felsic Migmatite	2.705	6.209	3.784	1.641	0.205	52.64	38.73	93.31
S135	Mafic Migmatite	2.937	6.738	3.776	1.784	0.271	77.51	41.88	106.46
S59	Geniss	2.708	5.828	3.500	1.665	0.218	47.75	33.17	80.81
S123	Orthogneiss	2.637	6.024	3.470	1.736	0.252	53.36	31.75	79.49
S99	Schist dei Laghi	2.792	6.117	3.450	1.773	0.267	60.16	33.23	84.19
B11	Schist dei Laghi	2.820	6.100	3.190	1.912	0.312	66.67	28.70	75.29
S92&s93	White Granite	2.608	6.095	3.600	1.693	0.232	51.82	33.80	83.29
S94	Pink Granite	2.592	5.941	3.610	1.646	0.207	46.45	33.78	81.56

Table 6.11: Average seismic velocities and densities of the major rock types used to calculate some elastic modulis. 'Vp/Vs is the ratio of compressional velocity to shear velocity, ' s ' is Possion's ratio, 'K' is bulk modulus of compressibility, 'G' is shear modulus and 'E' is the Young's modulus.

$$V_p = 1.049 \times V_s^2 - 6.92V_s + 17.62 \quad (6.4)$$

Figure 6.24 shows a similar plot to figure 6.23, but ultramafic rocks are not shown. This time a linear relationship between velocities can be observed but the data show some scattering and following equation can be derived at:

$$V_p = 0.82V_s + 3.34 \quad (6.5)$$

The above two equations can be used to described the relationship between compressional and shear velocity of the lower and middle crustal rocks, one with high mafic content (equation 6.4) and one with low mafic content (equation 6.5).

6.3.4.2 Velocity as compositional indicator

It was shown in section 6.3.3 that rocks rich- in mafic minerals have higher seismic velocities then those rich-in felsic minerals and that velocity of feldspar changes systematically with measured composition. This points to the existence of a relationship between seismic velocity and lithology. Figures 6.25 and 6.26 show plots of seismic velocities as a function of rock type. Both plots indicate a high seismic velocity for ultramafic and much lower velocities for metasedimentary rocks. Apart from ultramafic rocks (peridotites and pyroxenites) which can be distinguished from others by their high seismic velocities, it is not easy to relate each rock type to an exact velocity value as there is a great deal of variation. There are rocks of different types but with same velocities.

6.3.4.3 Density as compositional indicator

Figure 6.27 shows a plot of density versus rock type. There seems to be a general increase in density of rock from more felsic-rich ones towards felsic-poor ones(mafic-rich). Ultramafic rocks have much higher density than other rocks. Their high density corresponds well with them having also higher seismic velocities (P and S waves velocities).

6.3.4.4 Velocity and density relationship

Figure 6.28 show a plot of averaged seismic velocity (V_P and V_S) as a function of density for all samples in table 6.11. In general there is an increase in seismic P and

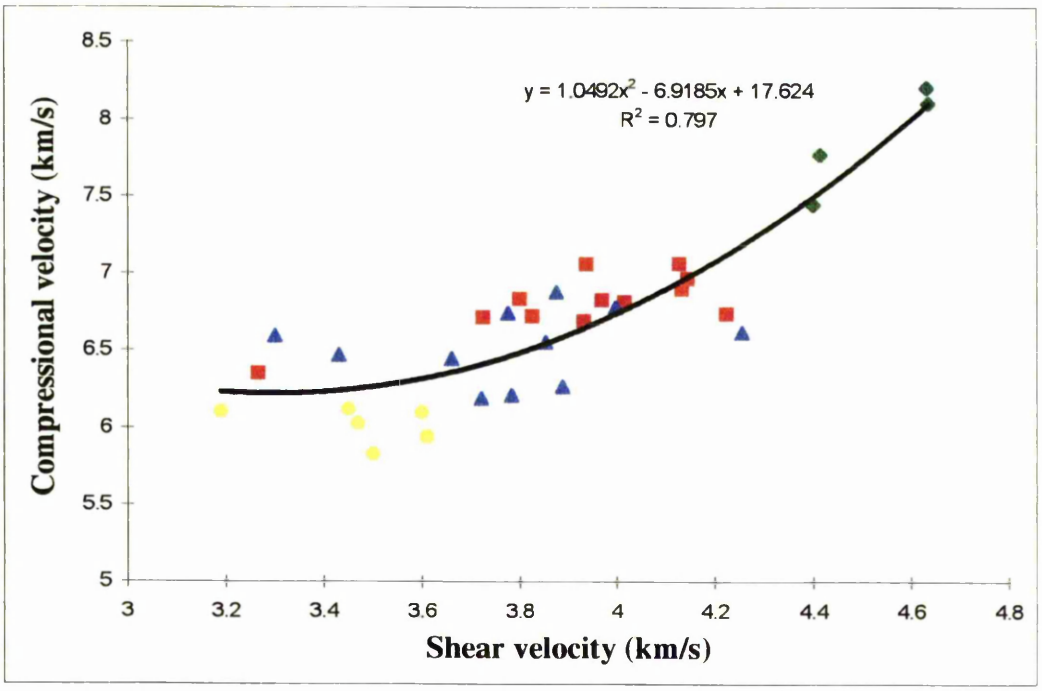

Figure 6.23: Plot of compressional velocity against shear velocity for ultramafics, metabasics, metasedimentries and rocks from SdL (Symbols are the same as fig 6.25).

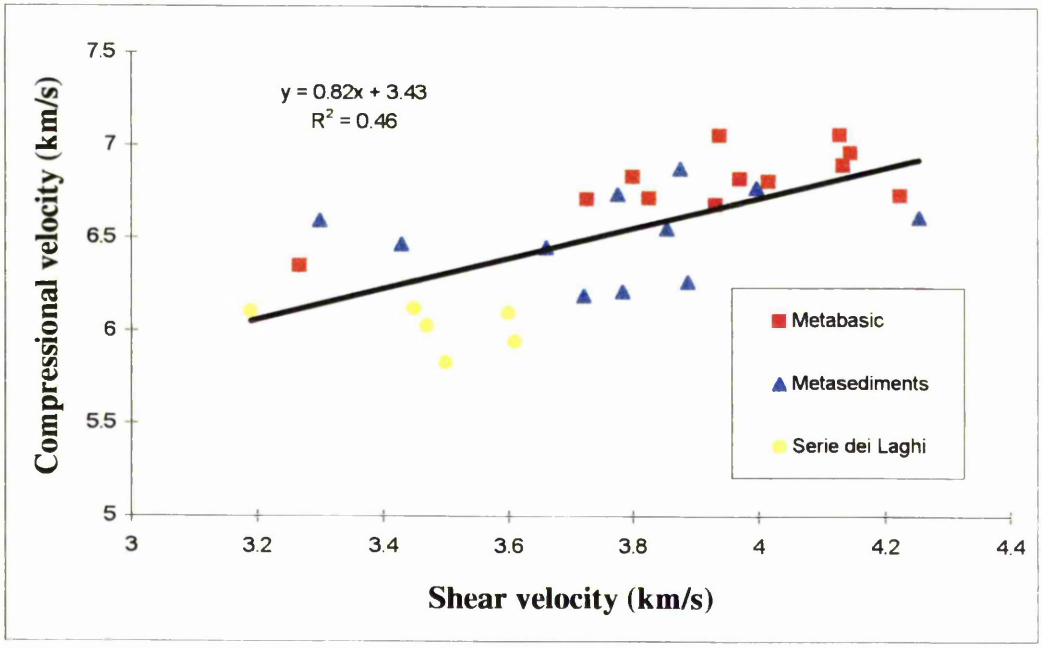

Figure 6.24: Plot of compressional velocity against shear velocity for metabasics, metasedimentries and rocks from SdL (Symbols are the same as fig 6.25).

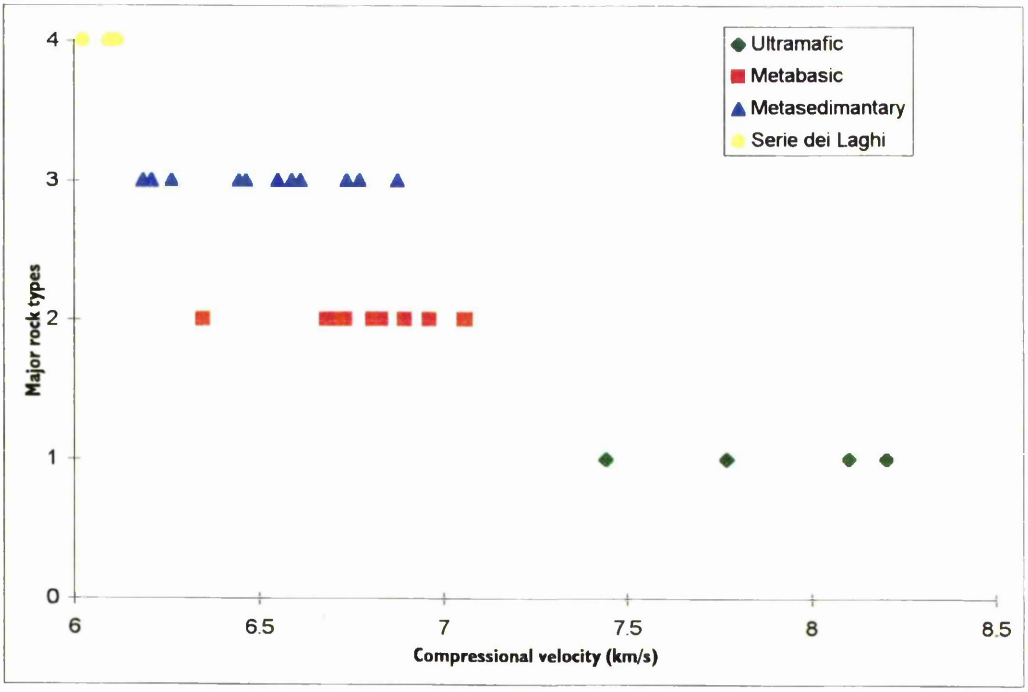

Figure 6.25: Plot of compressional velocity as a function of rock types.

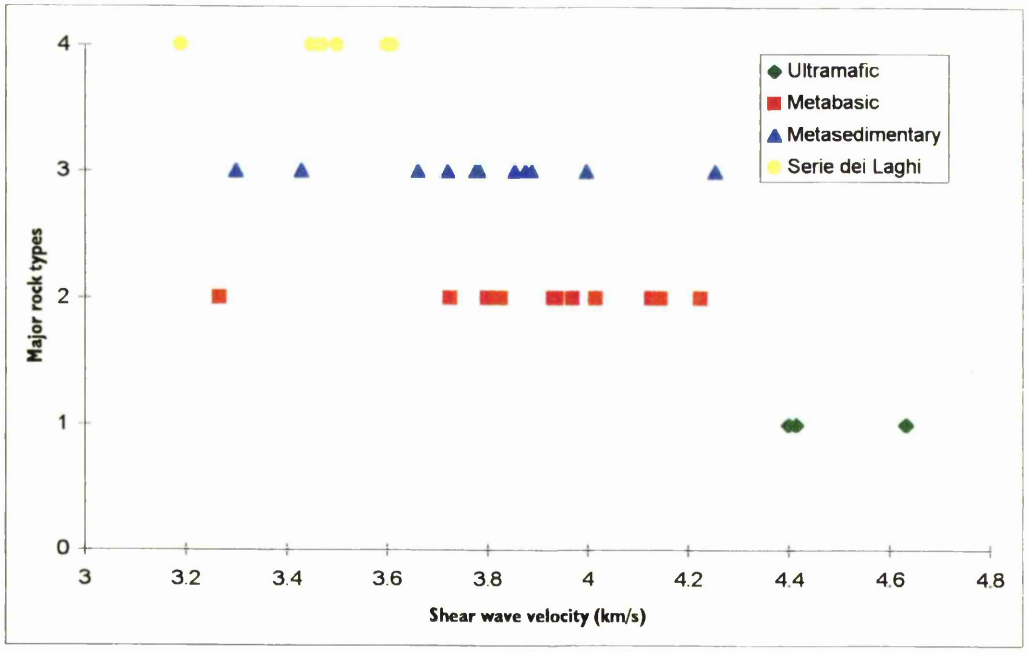

Figure 6.26: Plot of shear wave velocity as a function of major rock types.

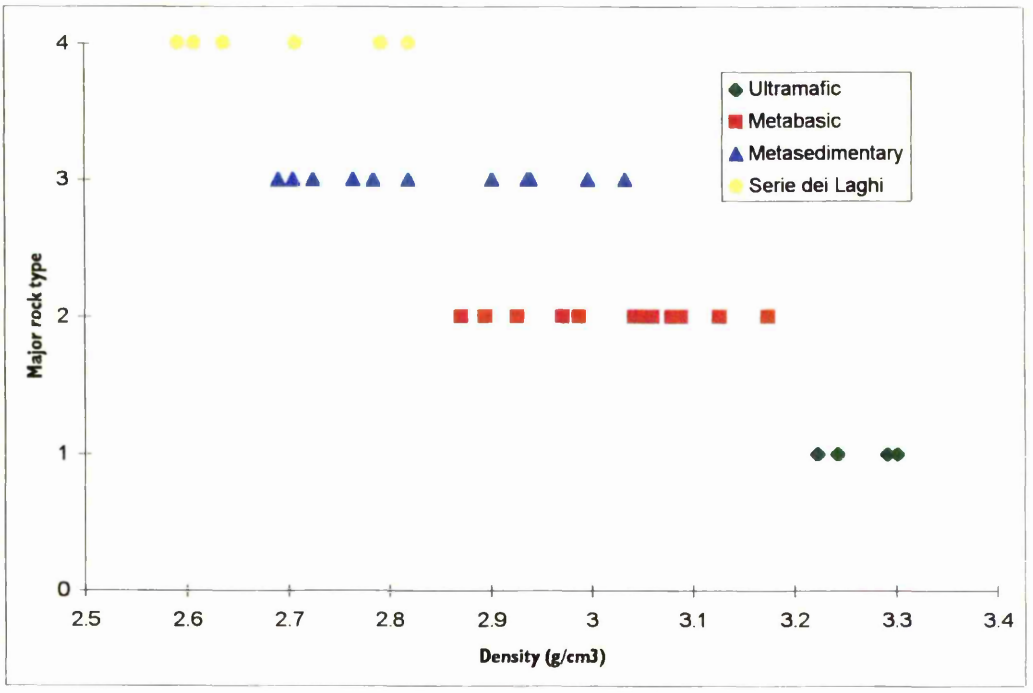

Figure 6.27: Plot of density as a function of major rock groups.

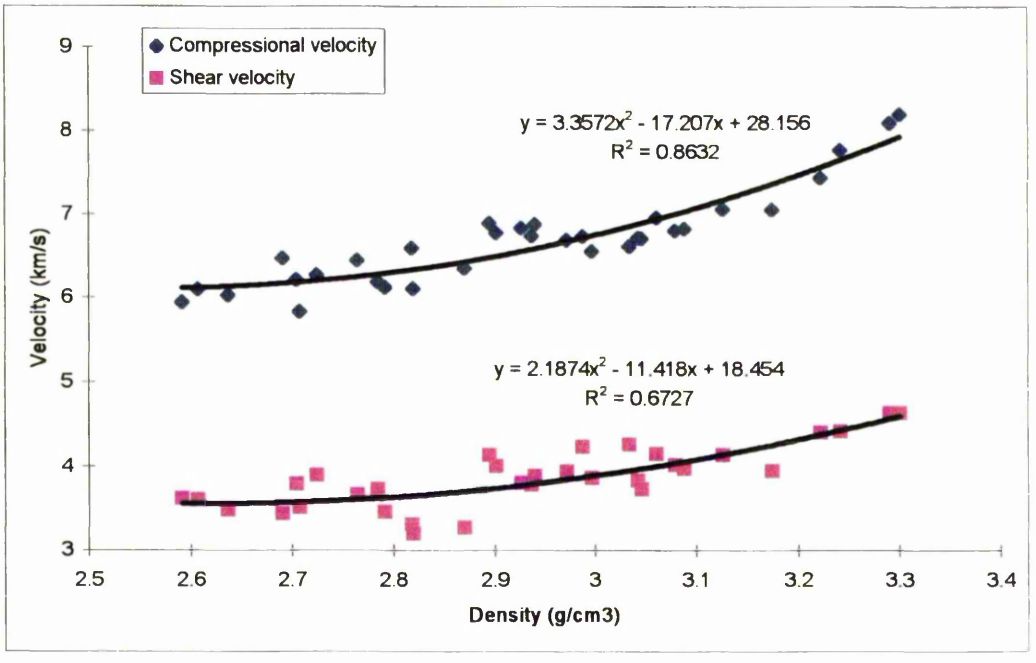

Figure 6.28: Plot of compressional and shear wave velocities as a function of density.

S-wave velocities with density. A quadratic relationship between velocities (km/s) and density (g/cm^3) can be observed. The following equations described the above relationship:

$$V_p = 3.357\rho^2 - 28.15\rho + 28.16 \quad (6.6)$$

$$V_S = 2.18\rho^2 - 11.42\rho + 18.45 \quad (6.7)$$

where V_p is compressional velocity in km/s, V_S is shear velocity and ρ is density of rock in g/cm^3. The above equations describe the relationship between seismic velocity and density of rocks at room temperature and pressure with zero crack density or porosity.

6.5. Some Concluding Remarks

High pressure velocity measurements, together with density and mineralogical composition for over 30 rock samples are described. It is clear that these lower and middle crustal rocks show wide velocity and density ranges. It was demonstrated that seismic velocity and density are higher for ultramafic rocks and lower for metasedimentary rocks. Seismic anisotropy seems mainly due to crack alignments at low confining pressure (≥300 MPa) and CPO at higher confining pressure (≤300 MPa). Rocks with strong CPO (e.g. peridotites) and those with strongly elongate minerals (e.g. amphibolites & schists) show seismic anisotropy greater than 4%.

It was demonstrated that due to the effect of microstructures on propagated seismic waves in polymineralic rocks, ultrasonic velocity measurements can differ noticeably from calculated ones. Furthermore, relationships between seismic velocities and density of rocks were obtained and some correlation was made between velocity and lithology.

Chapter 7
High Temperature Velocity Experiments

7.1 Introduction

This chapter presents the results of combined high pressure and high temperature compressional velocity measurements of 12 representative rock samples from the IV zone and 2 from the SdL. The modified Paterson deformation rig described in chapter 4 was used for these measurements. This chapter starts by discussing two important preliminary findings indicating (a) the critical importance of confining pressure on the results of high temperature velocity measurements, (b) time dependence of high temperature velocity measurements. Later, the results of high temperature measurements are presented. Due to severe technical problems associated with these measurements coupled with time constraints only the compressional velocity for cores normal to the foliation direction was measured.

7.2 Velocity-temperature Relations at less than 300 MPa Confining Pressure

In the previous chapter it was demonstrated that at room temperature, a confining pressure of around 250 to 300 MPa is needed to close all the microcracks and pores associated with the lower crustal rock samples. Thus rocks reach their intrinsic seismic properties at confining pressure above 250 to 300 MPa.

In order to investigate the temperature dependence of seismic velocity, the samples have to be heated. This causes the creation of new microcracks due to the difference in thermal expansion of the minerals constituting the sample. However thermal cracking can be suppressed by first increasing confining pressure.

Figure 7.1 illustrates the results of high temperature measurements on a peridotite sample (S60A) at a various temperatures and pressures. A linear relationship exists between velocity and confining pressure for measurements above 300 MPa and over a limited temperature range (from 300°C to 490°C). However at higher temperatures (above 490°C), the velocity/pressure relationship shows a deviation from the

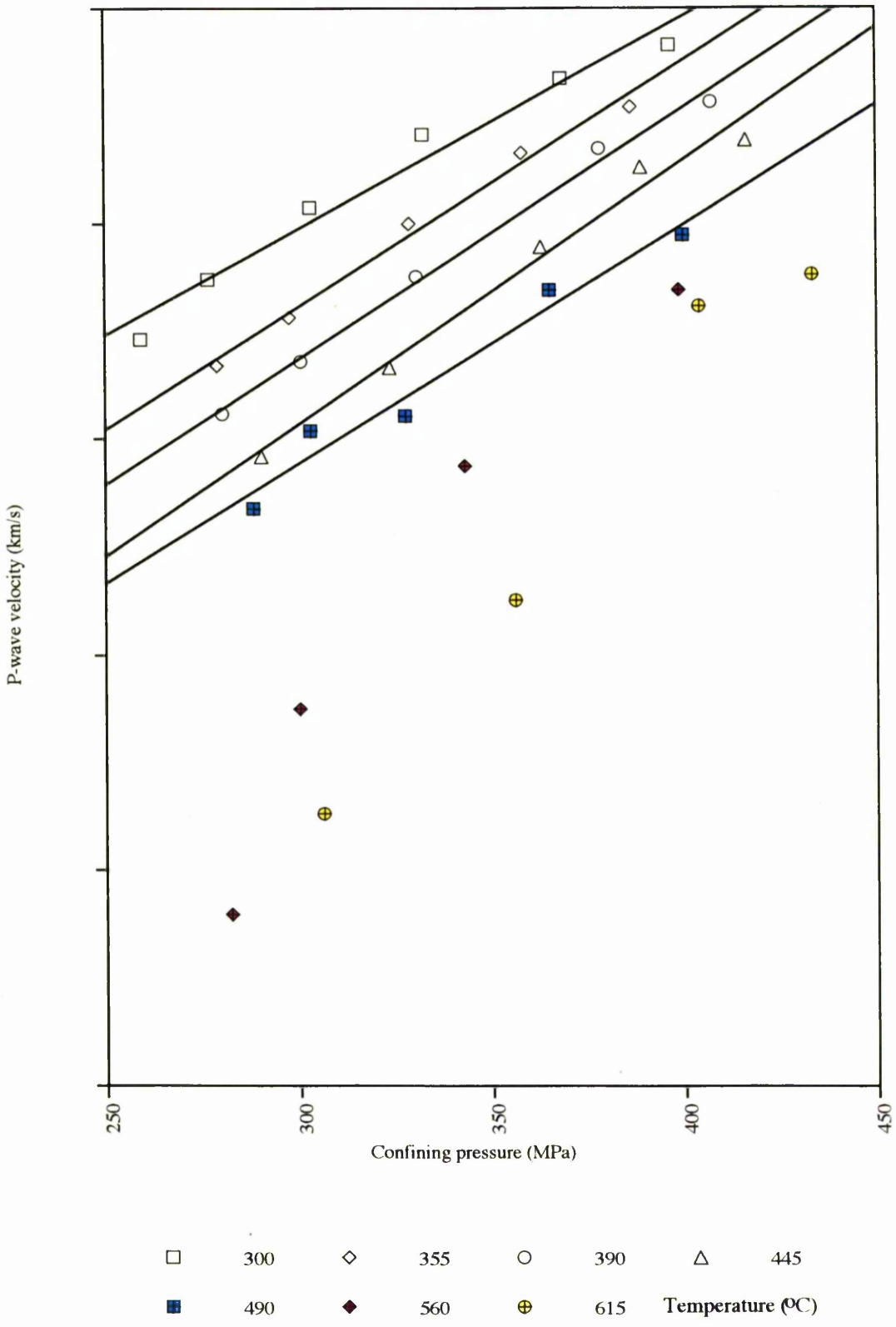

Figure 7.1: Plot of compressional velocity as a function of confining pressure and at various temperatures. There is a non-linear decrease in velocity at temperatures above 490°C.

extrapolated trend. This indicates that a homogeneous stress distribution through out the sample has not been obtained, therefore the sample has not reached to its intrinsic property.

Figure 7.2 is a 3D Cartesian mesh plot for the same data as fig 7.1. Three distinctive areas can be seen on this plot. Area A shows a range of velocity data at very low temperature (up 100 °C) and over a pressure range from 250 to 400 MPa. It is clear that velocity increases with pressure sharply at constant temperature. However in area B, a more uniform variation of velocity with pressure and temperature is observed. At temperatures above 450 °C (area C), there is an irregular decrease in velocity with temperature which seems to be more marked at lower pressure values than higher ones. This decrease of velocity is believed to be due to the opening of grain boundaries and microcracks. Clearly, higher pressures than 400 MPa are required to suppress the newly opened and/or created microcracks. This represents an important limitation associated with high temperature velocity measurements. That is, measuring the temperature dependence of velocity above 450 °C requires higher confining pressure in order to suppress the existing microcracks and prevent any thermally-induced opening of new ones. All the subsequent high temperature measurements were therefore carried out at confining pressures above 400 MPa where it was considered that the velocity values are the intrinsic ones.

7.3 Time Dependence of Velocity

In order to investigate the reproducibility of high temperature velocity measurements, the velocity of a marble sample (S52A) was measured at 450 MPa confining pressure during four temperature cycles. Temperature was varied from 25°C to 600°C (fig7.3).

In the first cycle, measurements were made with increasing temperature stepwise over a period of 6 hours. The temperature later was decreased stepwise over 14 hours (cycle no 2). The first cycle shows clearly a set of lower velocities than the second and subsequent cycles. Repeating the above two cycles (cycles 3 and 4) over additional 10 and 18 hours period shows similar velocities to second cycle within the experimental

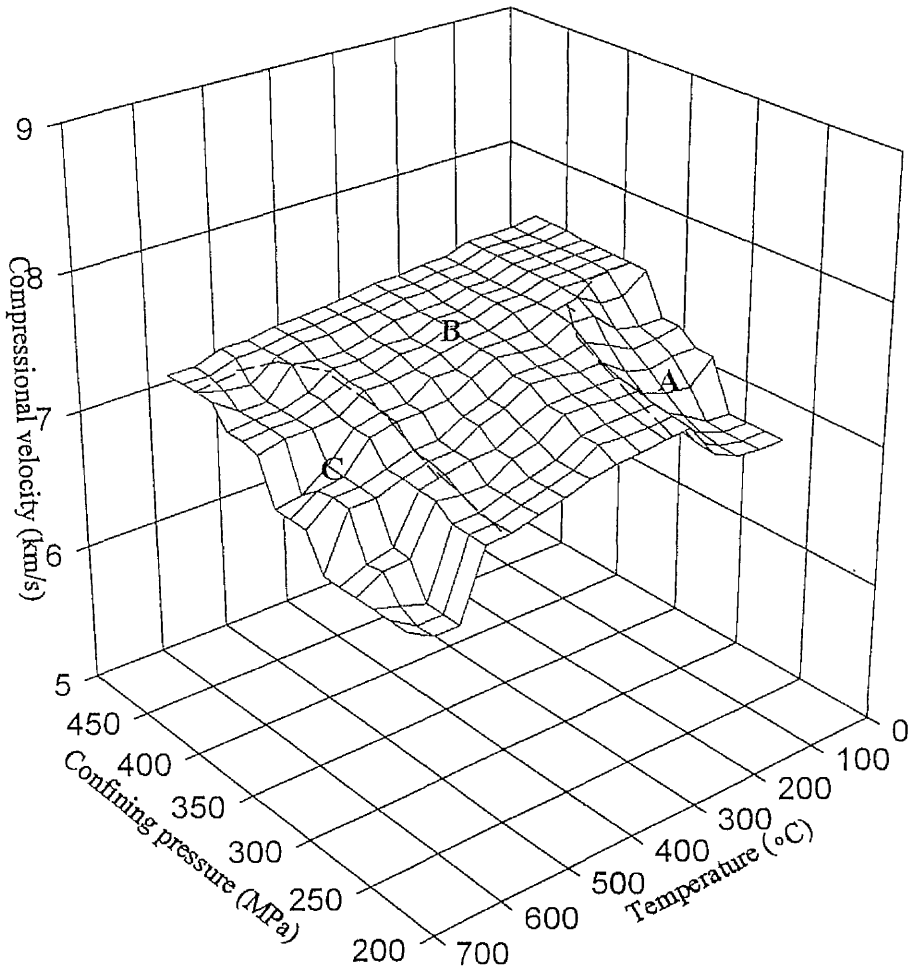

Figure 7.2: 3D diagram illustrating the effect of temperature and pressure on seismic velocity for a peridotite. The initial temperature cycle induce fresh crack damage (area A) even at high pressure. These improves with temperature and time as thermal annealing occurs (area B). At high temperature differential thermal expansion produces new cracks (area C).

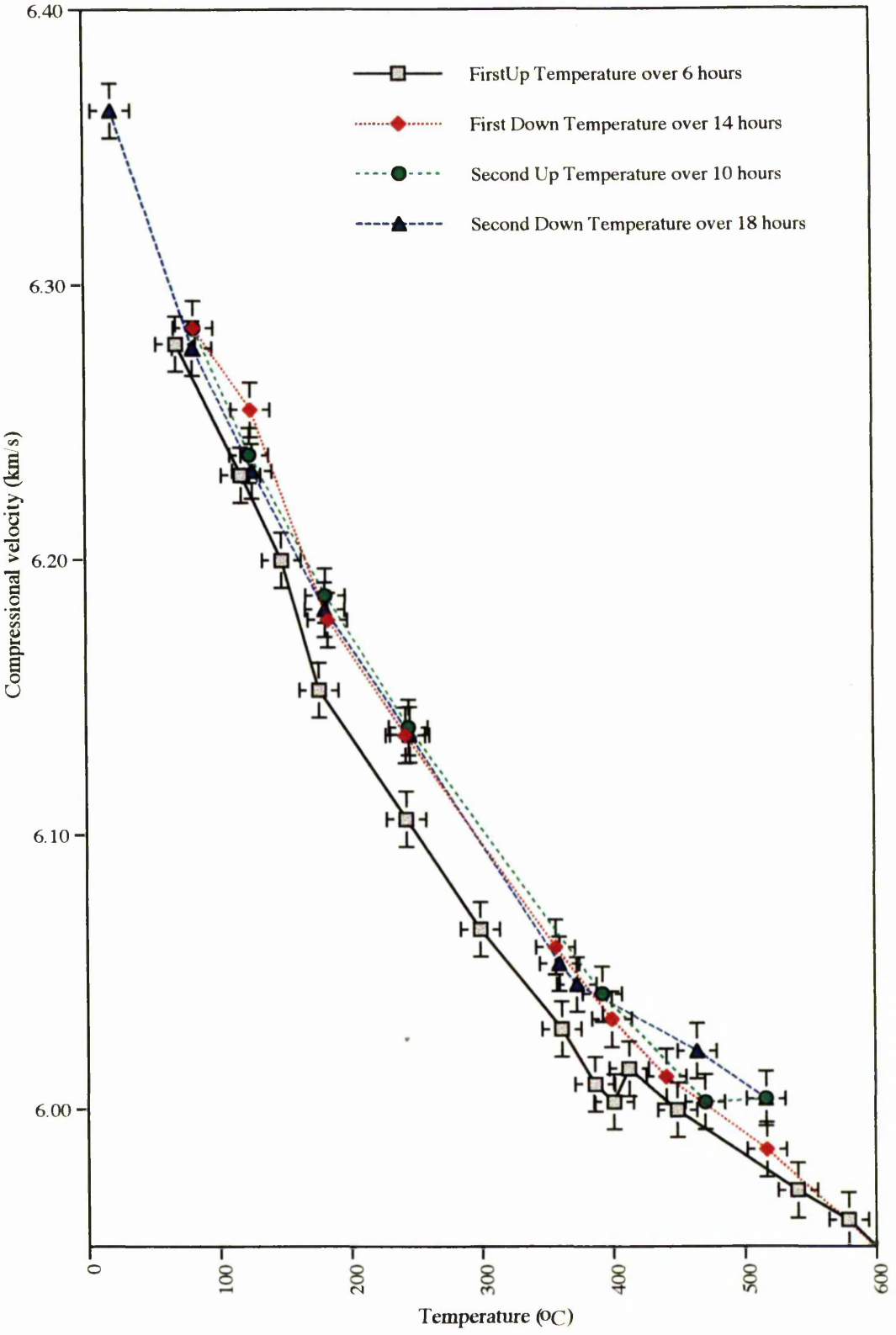

Figure 7.3: Plot of compressional velocity as a function of temperature at 400 MPa confining pressure for a marble sample (S52A). A reproduceable curve was obtained after 20 hours.

error and indicating a very good reversible velocity curve. It is believed that rapid increase of temperature during the first cycle prevented relaxation of internal stress induced by anisotropic thermal expansion of the calcite crystals. This problem however, was overcome subsequently by allowing more time at temperature for stress relaxation. Higher seismic velocity was achieved for cycles 2, 3 and 4 than the first cycle, resulting in an apparent time dependence of velocity.

In order to avoid these problems it was decided first to increase the temperature to the maximum (600 °C) at 400 MPa confining pressure and leave the sample at that temperature for at least 4 to 5 hours for thermal damage to heal. The velocity measurements were then carried out by decreasing temperature stepwise and ensuring that sufficient time (at least 2 hours) was allowed between each temperature step.

7.4 Seismic Velocity at Elevated Temperature and Confining Pressures above 400 MPa

Compressional seismic velocity as a function of temperature, at confining pressures above 400 MPa were measured for cores drilled in the direction normal to the foliation, for 14 rock types. It was assumed that 400 MPa confining pressure would be sufficient to close all the microcracks and prevent the opening of new ones, so that the intrinsic properties could be measured. The temperature-velocity curves of all measured samples are of two types. Some show a linear relationship between velocity and temperature from room temperature to 600 °C and others show a non-linear temperature velocity curve. Almost all the data show a decrease in seismic velocity as the temperature increases from room temperature to about 600 °C. Below, the compressional velocities measured at elevated pressure and over a range of temperature are discussed in more detail for each rock type. It was also attempted to compare the data with similar published ones. However, published high temperature velocity data are extremely few.

7.5 Results

All high temperature velocity experiments were carried out at a constant confining pressure of 450 MPa. Wherever the error bars have not been shown, the uncertainty in velocity is less than the size of the symbol marking the velocity point. The maximum uncertainty in velocity data at 600 °C and 450 MPa confining pressure has never been greater than ±0.034 km/s. Linear and second order polynomial regression was used to find the best fit lines for the velocity/ temperature plots. The equations of the best fit lines are also displayed.

7.5.1 Peridotites

Fig 7.4 shows the V_P-temperature curves for a phlogopite rich peridotite (S60A) and Premosella peridotite (S32a). Both curves are almost linear and show temperature derivatives of Vp -5.09×10^{-4} km/s/°C and -2.35×10^{-4} km/s/°C both at 450 MPa respectively. Kern (1982) obtained a value of -4.94×10^{-4} km/s/°C for a peridotite (more than 80 % Ol at 600 MPa). However Barrulo (1993) measured a temperature coefficient of Vp about -6×10^{-4} km/s/°C at 600 MPa in a Lherzolite rock.

7.5.2 Pyroxene-rich Granulite

Sample S88A is a pyroxene-rich granulite showing a linear relationship between velocity and temperature at 450 MPa (fig 7.5). A temperature coefficient of -2.37×10^{-4} km/s/°C was obtained for this sample. Barruol (1993) obtained a temperature coefficient of -2.34×10^{-4} km/s/°C for a similar sample at the same pressure.

7.5.3 Amphibolite

Fig 7.6 shows the V_P-temperature plot for an amphibolite (S35) sample from the IV zone at two different confining pressures. There is a linear decrease of velocity with temperature up to 650°C at both 350 and 450 MPa confining pressure and temperature coefficients of -3.833×10^{-5} km/s/°C and -3.517×10^{-5} km/s/°C respectively. Kern (1982) obtained -7.2×10^{-5} km/s/°C for an amphibolite (43% Pl, 45% Hbl , 2% Mi) and Barruol (1993) obtained a value of -1.92×10^{-4} km/s/°C (36% Pl, 55% Hbl, 10% Px) both at 600 MPa.

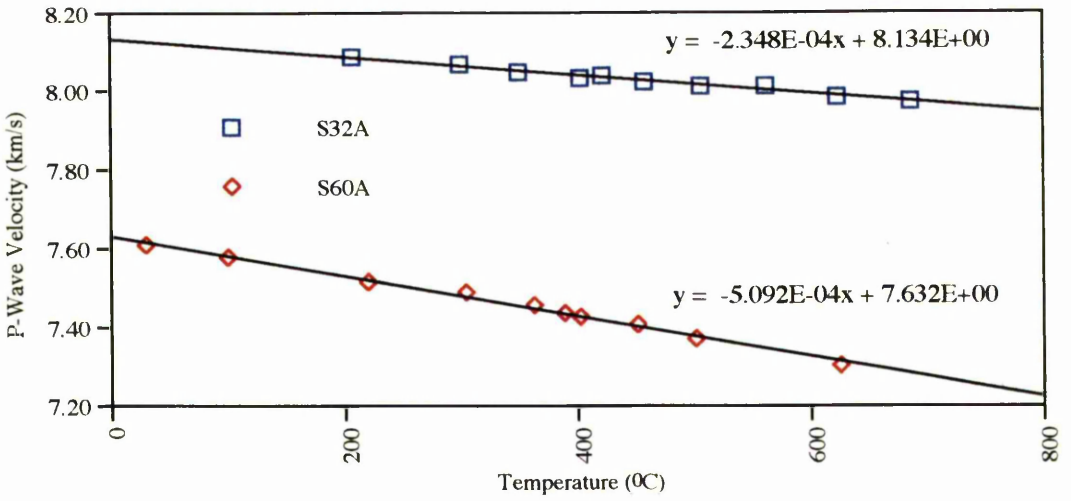

Figure 7.4: Plot of compressional velocity as a function of temperature for two peridotites. The measurements were carried out both at 400 MPa confining pressure. The specimen numbers are identified in appendix 1.

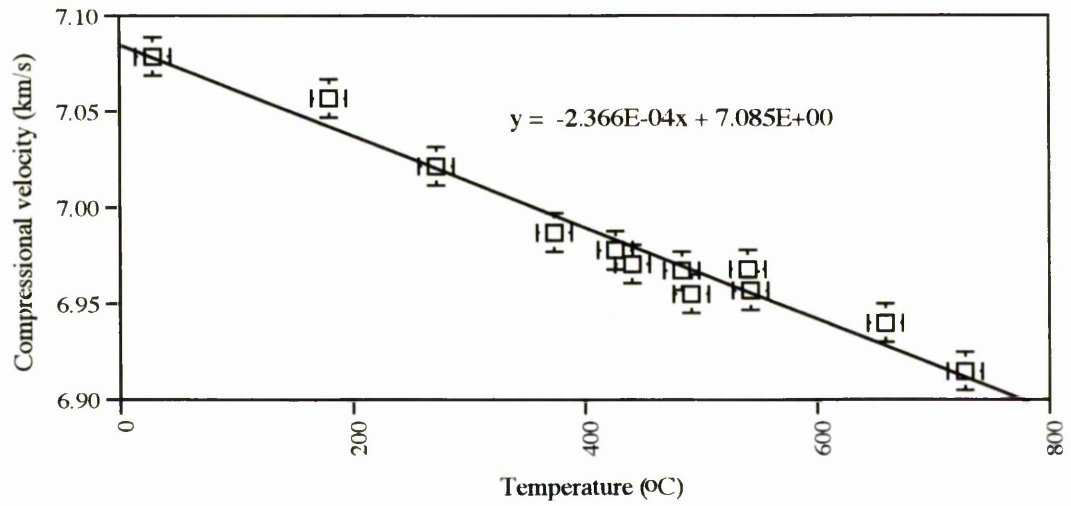

Figure 7.5: Plot of compressional velocity as a function of temperature for granulite sample (S88A). The measurements were carried out at 450 MPa confining pressure.

There is a fluctuation in velocity with temperature for both sets of measurements. This unsettling of velocity is possibly due to unstable thermal convection of gas around the sample causing a variable temperature distribution along the sample with respect to the thermocouple position. The changes are within the expected uncertainty.

Figure 7.7 shows the plot of compressional velocity as a function of temperature at three different confining pressures for an amphibolite sample (B17A) from the SdL. The graphs indicate a pressure and temperature dependence of velocity. There is a non-linear decrease of velocity at 350 MPa confining pressure over a temperature range from 25 °C to 500 °C. However, when at 500 °C the confining pressure was increased to 400 MPa, an increase in velocity was observed. Then as the temperature was dropped gradually at 400 MPa confining pressure, the velocity increased linearly. At temperature around 250 °C the confining pressure was once again increased to 450 MPa. There was an increase in velocity which was attributed to the intrinsic effect of pressure on velocity. Subsequently gradual increase of temperature of the sample at 450 MPa confining pressure resulted in a linear decrease of velocity. However, at temperatures above 550 °C a sharp decrease in velocity was observed. Although it is difficult to give a definite reason for the observed sharp drop in velocity, the microcrack opening seems to be irrelevent as such a drop was not observed at lower pressure (350 & 400 MPa) and around the same temperature. Other possibilities are discussed in section 7.6.1.2.

7.5.4 Metagabbro

The compressional velocity of a metagabbro (B6A) and its associated mylonite (B1A) were measured at 450 MPa and a range of temperatures up to 700 °C (fig 7.8). Both samples show a linear velocity/temperature relationship and temperature coefficients of -4.63×10^{-4} km/s/°C and -1.98×10^{-4} km/s/°C were obtained for sample B6 and B1. The higher temperature coefficient of metabasic mylonite (B1) in comparison to its protolith implies a higher velocity contrast between the two rocks at high temperatures than at room temperature. This indicates an important effect of temperature on velocity contrast in the lower crust.

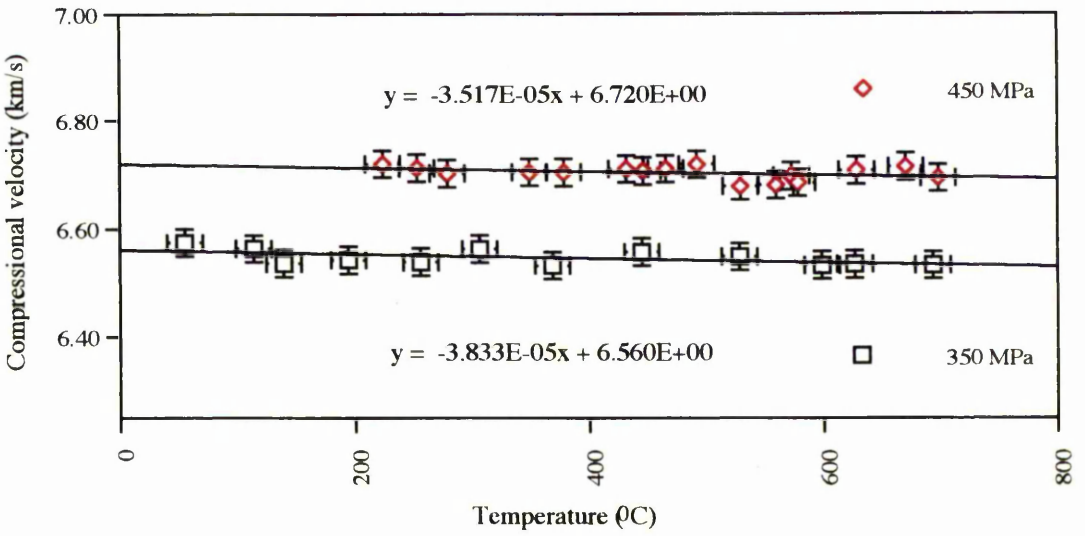

Figure 7.6: Plot of compressional velocity as a function of temperature for amphibolite sample (S35A) at two different confining pressures. The best fit lines through two sets of data have similar slope indicating a linear effect of pressure on seismic velocity. There is no sharp reduction in velocity at temperatures above 600°C, which can imply opening of microcracks.

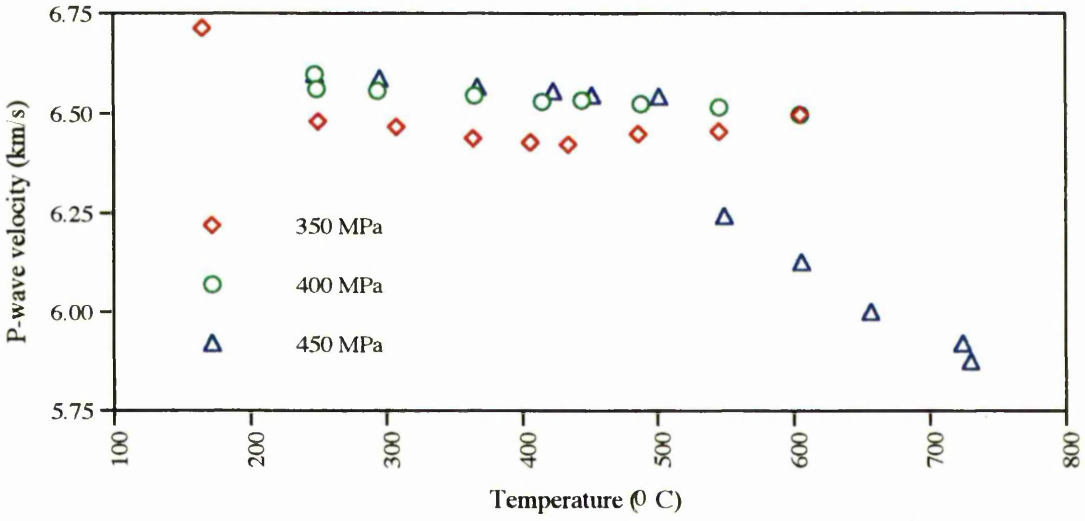

Figure 7.7: Plot of compressional velocity as a function of temperature for an amphibolite sample (B17A) from Serie dei Laghi. The velocity measured at three different confining pressure over a range of temperatures.

7.5.5 Diorite

The temperature coefficient of a diorite sample (S42A) at 450 MPa was measured over a temperature range up to maximum of 600 °C (fig 7.9). A least squares linear fit, described the data very well. A temperature coefficient of -6.13×10^{-4} km/s/°C was obtained for this sample.

7.5.6 Stronalite

A stronalite (S73A) was used for high temperature measurements. The velocity data show a linear relation with temperature (fig 7.10). A temperature coefficient of -6.38×10^{-4} °C was obtained for this sample. Barruol (1993) obtained a temperature coefficient of (-5.54×10^{-4} °C) for a stronalite of similar composition at 600 MPa.

7.5.7 Mica Schist

Fig 7.11 is a plot of V_p versus temperature for a sample of Schisti dei Laghi at 450 MPa confining pressure. A linear relationship between velocity and temperature was observed over the measured temperature range. At 450 MPa a temperature coefficient of -7.61×10^{-4} km/s/°C was obtained.

7.5.8 Marble

The compressional velocities of a marble (S52) and a calcite mylonite (LCF) were measured at 450 MPa confining pressure and a range of temperatures. Figure 7.12 & 7.13 show the velocity/temperature plots for the two samples. For temperatures in the range 25 to 400 °C a linear relationship between velocity and temperature can be inferred. However, considering additionally the velocity points above 400 °C, then a clearly non-linear relationship between velocity and temperature can be observed. A second degree polynomial regression fits the velocity/temperature data for both samples better than a least squares linear fit over the full temperature range. This decrease of velocity can not be due to microcracks opening as it has been shown that a confining pressure above 400 MPa is sufficient to suppress all microcracks over the experimental

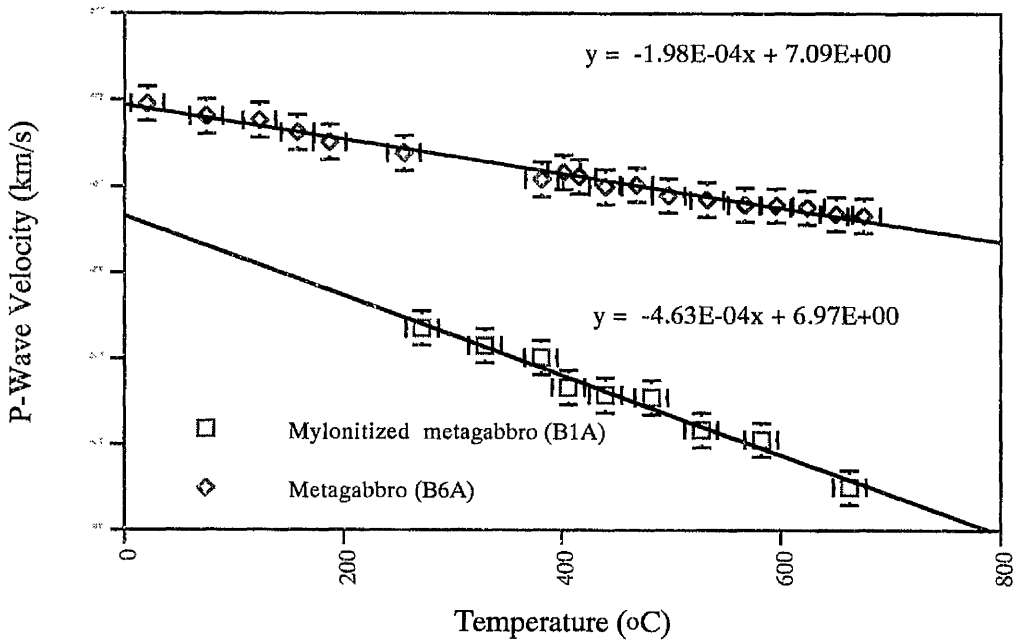

Figure 7.8: Plot of compressional velocity as a function of temperature for a metagabbro (B6A) and its mylonite (B1A). There is a greater velocity difference between the mylonite and its protolith at higher temperatures than room at temperature.

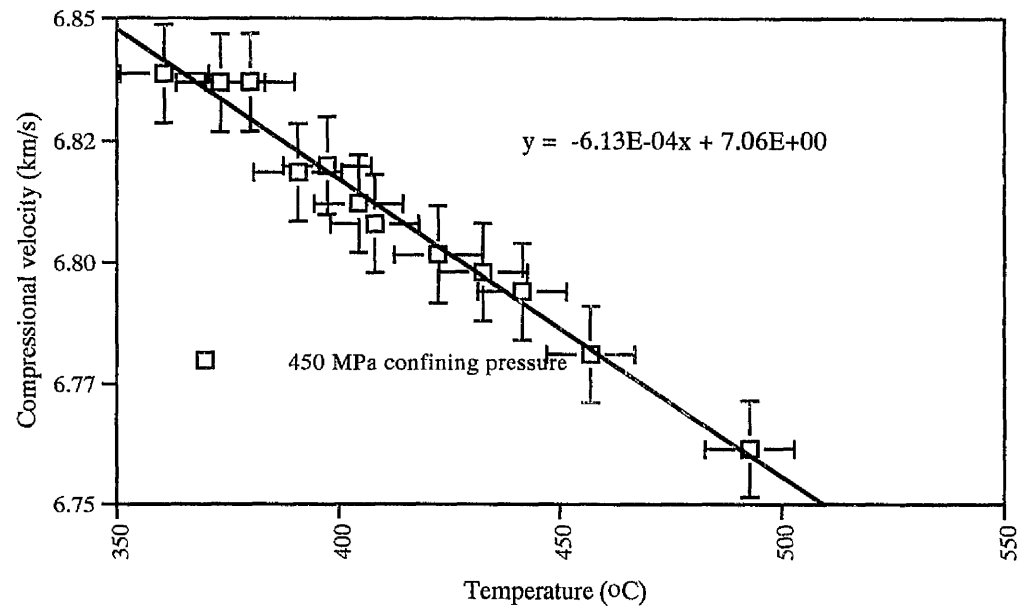

Figure 7.9: Plot of compressional velocity as a function of temperature for a diorite sample (S42A). The measurements were conducted at 450 MPa confining pressure.

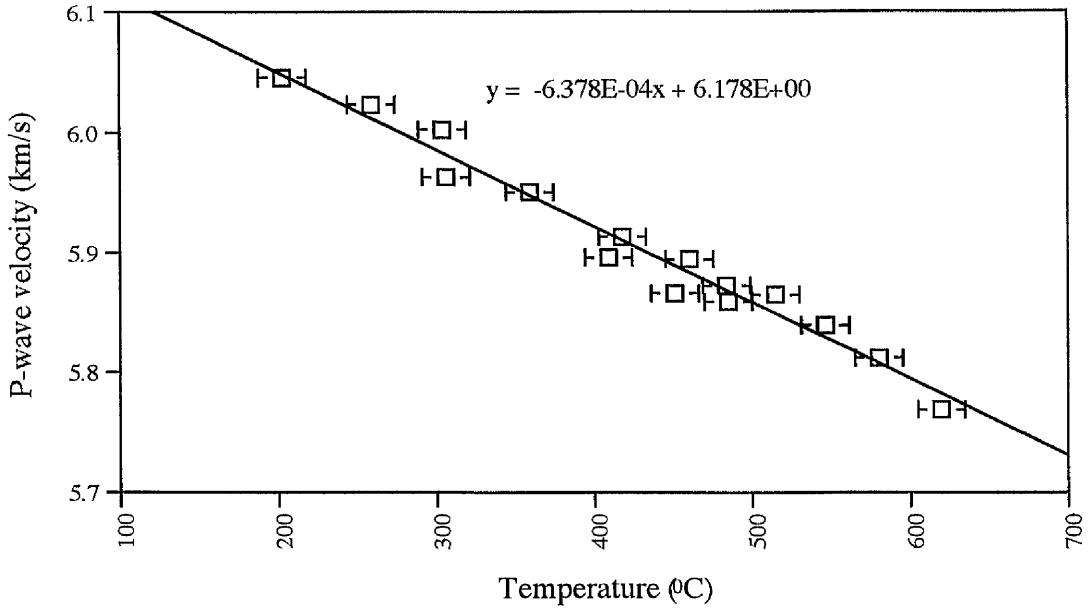

Figure 7.10: Plot of compressional velocity as a function of temperature at 450 MPa confining pressure for a stronalite sample (S73A).

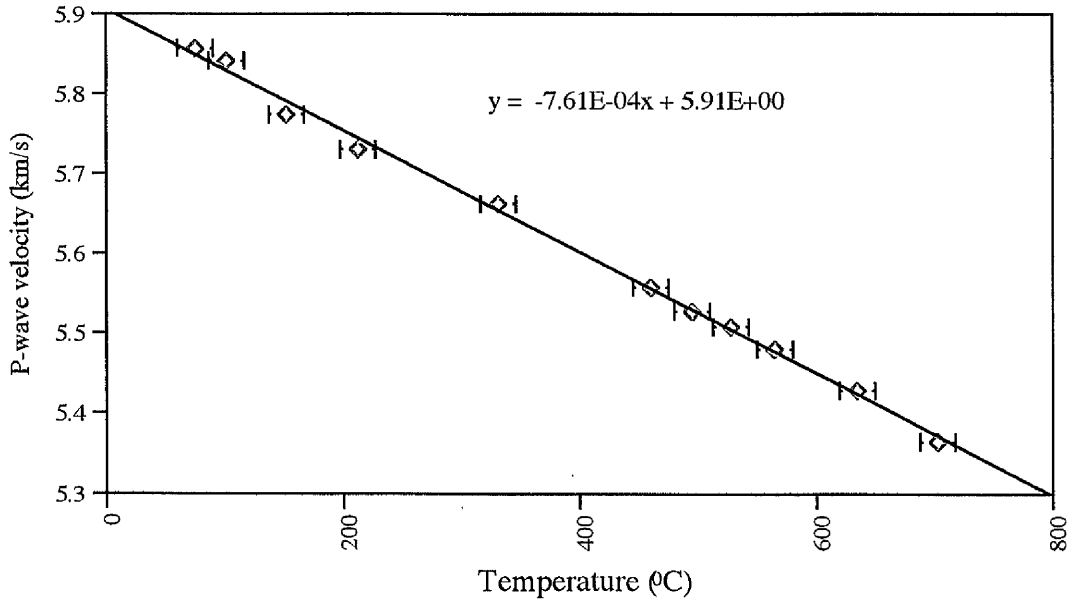

Figure 7.11: Plot of compressional velocity as a function of temperature, measured at 450 MPa confining pressure for a sample of Schisti dei Laghi (B11A).

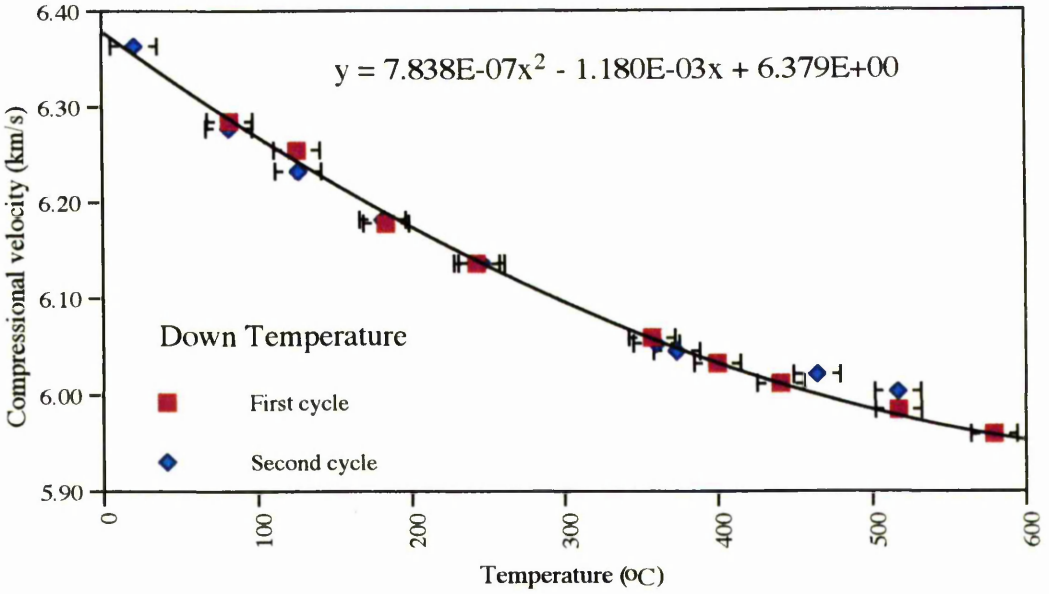

Figure 7.12: Plot of compressional velocity as a function of temperature at 450 MPa confining pressure for a marble sample (S52A). Velocity was measured at various temperatures by reducing the temperature stepwise. This was repeated for the second time to assess the reproducibility of the measurements.

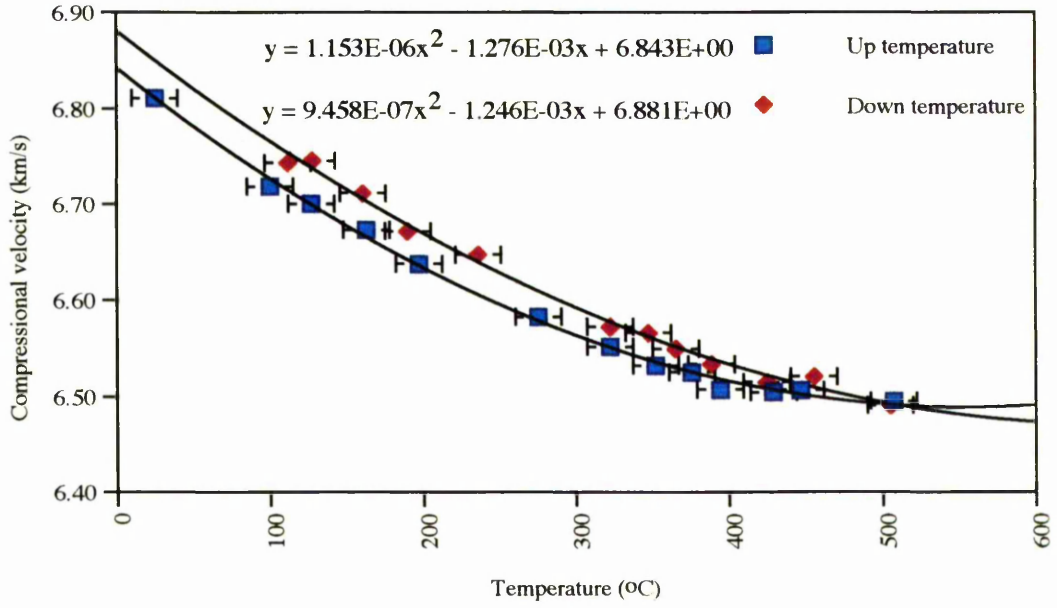

Figure 7.13: Plot of compressional velocity as a function of temperature for a calcite mylonite (LCFA). A non-linear relationship between velocity and temperature was again observed.

range of temperature. The observed non-linear decrease in velocity was discussed further in section 7.6.2.1.

7.6 Discussion

Changes in seismic properties of rocks during combined high pressure and temperature experiments can occur for two reasons; (a) changes associated with experimental procedure, (b) changes related to intrinsic properties of the rocks. Therefore it is important to be aware of the influence of each of these on the result of high temperature/pressure velocity measurements.

7.6.1 Changes in Seismic Properties Associated with Experimental Procedures

The results of combined high temperature and pressure velocity measurements highlights the importance of a number of factors affecting such measurements.

i) crack formation, suppression and healing

ii) possible chemical reactions

iii) possible phase transformations.

Any changes in cracks status, activation of chemical reactions or phase transformations due to particular pressure and temperature combinations would affect the velocity measurements.

7.6.1.1 Effects of cracks on seismic velocity

It is well known that cracks and pores generally reduce seismic velocities (Atkinson, 1989 & Crampin, 1984). In all the samples measured above the significant effect of microcracks lowering the seismic velocity is evident. At temperatures greater than 500 °C, a higher confining pressure than 400 MPa is needed to suppress cracks and prevent their opening. Another way of suppressing the crack effect is by healing them at higher temperature. At higher temperature, there is a tendency for matter to diffuse to the crack-tip interface from surrounding regions of high stress or for dislocation motion to allow crack closure, perhaps only anelastically. Such an effect

possibly was observed during the velocity measurements on a marble sample (S52, see fig 7.3 & and section 7.6.2.1). An increase of the compressional velocity with time was observed for this sample. Such an increase can be attributed to cracks healing as the sample was kept at high temperature (above 300 °C) for several hours. However as explained before such an increase in velocity can also be attributed in part to initial lack of temperature equilibration during the first few hours of heating the sample.

Due to the differences in thermal expansion coefficient between different minerals a rock would tend to develop cracks as soon as it starts it cooling cycle. However, high confining pressure will inhibit this. Depending on the thermal and effective pressure gradients with depth, the influence of cracks on seismic velocity will eliminated below a certain depth in the continental crust. Assuming an average pressure of around 450 MPa is required to suppress all cracks over the temperature range of 0 to 500 °C for a temperature gradient of 20 °C/km and pressure gradient of 30 MPa/km cracks will be closed at the depths greater than 20 km, or at deeper depths at higher thermal gradients. In fact, these depths represent an upper bound.

For over a larger time scale than that for laboratory experiments, thermally activated creep will tend to close cracks at lower pressure. Set against that, elevation of pore pressure will reduce the effective pressure and favour crack opening. However, the preservation of high grade metamorphic terrains suggests that pore pressure in such metamorphic rocks in the post-orogenic (extensional) stage may be low. In the cooler middle and upper crust which could be wetter, the effects of cracks on seismic velocity is likely to be a much more important consideration.

7.6.1.2 Seismic velocity and chemical reaction

Apart from the danger of cracking the sample at high temperature there is always a risk of activating some chemical reactions, most commonly dehydration reactions associated with rocks bearing hydrous minerals such as amphiboles and phyllosilicates. Sample B17 (amphibolite) shows a sudden and sharp decrease in velocity at 450 MPa and over a temperature ranges up to 600 °C (see fig 7.7 & fig 7.14). This sudden drop of velocity was initially thought to be due to either sudden opening of a set of

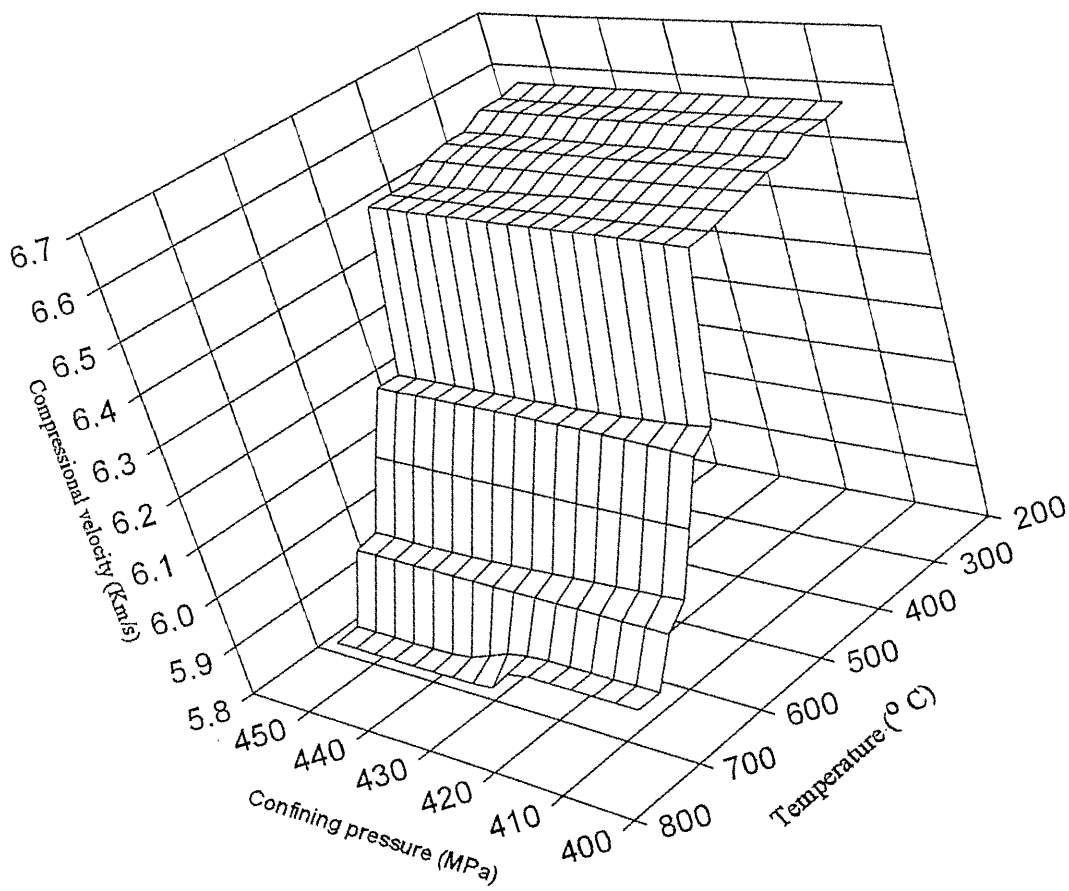

Figure 7.14: 3D diagram illustrating the effect of temperature and pressure on seismic velocity for an amphibolite. Sudden drop of compressional velocity at 450 MPa and 450 °C is attributed to opening of a new sets of microcrack.

microcracks or a chemical reaction (possibly some dehydration reaction associated with hornblende). Such drop of velocity, when previously observed by a number of authors (e.g. Popp & Kern, 1993 & Kazuhiko, 1989) was attributed to dehydration reactions. The hydrous phase in rocks can break down to a combination of less hydrous phases either at high temperature or under conditions where the activity of H_2O has been lowered by drainage or by an increase of activity of another component in the fluid such as CO_2 (Touret, 1974). The following reaction is one that might involve breakdown of hornblende ;

hornblende + quartz = orthopyroxene + augite + plagioclase + H_2O

Release of water might then be responsible for the lowering of velocity, possibly due to generation of pore fluid pressure.

In the above example the breakdown of amphibole involve reaction with another solid phase. Such reactions generally proceed at lower temperature and over much longer time scales than required for the breakdown of single phase hornblende. Hornblende is the only hydrous phase in sample B17. However, thermogravimetric analysis showed no loss of weight over a temperature range up to 1000°C on a time scale typical of velocity experiments. This indicates that no dehydration reaction could have possibly taken place over the time and temperature range of the velocity experiment, although it should be emphasised that the thermogravimetric analysis was carried out at room pressure and the effect of high confining pressure was not considered. However, even considering this it seems highly unlikely that amphiboles can dehydrate at temperatures around 550 °C and over such short time (about 2 hours).

Therefore the only explanation in this case is an un-even temperature distribution across the sample due to a malfunction of the furnace at temperatures above 450 °C. A large thermal gradient possibly formed along the sample and caused the sharp drop in velocity.

7.6.1.3 Velocity and mineral phase transformations

It is well known that certain minerals may change their structure, or their structure and composition at a certain combination of pressure and temperature. There are a

number of mechanisms involved in transformation and most of them are thermally activated (Mainprice et al., 1990). Table 7.1 summarises some of the important lower crustal minerals which could be involved in a phase transition. Any change in the structure and composition of a mineral will affect directly its physical properties including its seismic velocities.

Phase Transition		Vp before transformation (km/s)	VP after transformation (km/s)
Olivine	Ɣ-spinel	8.8	9.7
Enstatite	Clinoenstatite	7.8	7.6
a-Quartz	ß-Quartz	6.2	7.2
Calcite	Aragonite	6.7	6.3

Table 7.1: Some important lower crustal minerals that display solid state phase transformation. There is a clear change in compressional velocity. The velocity values are averaged and calculated at room pressure and temperature except for ß quartz, which is at 800°C and room pressure (Mainprice et al., 1990).

Over the pressure and temperature ranges of the experimental velocity measurements hardly any phase transformations were expected. Moreover no change in velocity which could have been attributed to phase transition was detected. But this does not mean that phase transformation can not be responsible for some regional changes in velocity of subsurface. Mainprice et al., (1990) examined the importance of velocity changes associated with some phase transformations. They further concluded that a reflection coefficient of around -0.08 could be generated purely due to transformation of a quartz to b quartz at 750 °C and 600 MPa which can correspond to region of the lower crust.

7.6.2 Change in Seismic Properties Associated with Intrinsic Properties of Rocks

It should be clear by now that elevated temperature generally reduces seismic velocity of rocks. The temperature effect on seismic velocity is opposite to the effect of pressure (see chapter 6). This implies that, depending on the pressure and temperature coefficients of velocity, the overall seismic velocity of a rock may increase or decrease at a given combination of pressure and temperature relative to its velocity at ambient

conditions. This can directly increase or decrease the velocity contrast between two rock types in the lower crust. In the next chapter, the results of high temperature and pressure velocity measurements are combined to visualise the overall velocity and the reflectivity of the lower crustal rocks. However, we will first examine a number of individual cases where the effect of temperature possibly influences the velocity of the samples more than pressure.

7.6.2.1 Non-linear temperature coefficient of velocity

Although most of the measured samples show a close to linear temperature coefficient of velocity, a non-linear temperature coefficient was measured for two marble samples. So we may ask 'why do some rocks particularly marbles, show a strongly non-linear relation between velocity and temperature ?'. To seek an answer to this question, it is important to emphasis the point that the change of velocity with temperature reflects mainly the changes in effective elastic properties of the sample. The effective elastic properties depend on three parameters

i) elastic properties of constituent minerals

ii) volume fractions of these minerals

iii) orientation of these minerals, either crystallographic preferred orientation (CPO), or microstructural (e.g. shape fabric).

In the case of marble samples, due to their monomineralic nature the whole rock should reflect the average elastic properties of the calcite grains. However, the two marble samples have strong crystallographic preferred orientations. This may have an effect strong enough to dictate the slope of the velocity/temperature plot. To investigate this, the seismic velocity of another marble with no CPO was measured at the same pressure and temperature conditions. The Carrara marble was chosen because of its lack of CPO and very weak shape fabric. Figure 7.15 shows the result of high temperature velocity measurements of Carrara marble at 450 MPa and over a wide temperature range. There is a pronounced non-linear relationship observed between velocity and temperature similar to the other marble samples. This indicates that the observed non-linearity is not due to CPO or shape fabric but is mainly due to the non-linear changes of effective

elastic properties of the calcite grains with temperature. Figure 7.16 shows the volumetric thermal expansion of a calcite single crystal over a range of temperature and at two given pressures. The non-linear increase in volume with temperature appears to explain the observed decrease of velocity with temperature for all marble samples.

In the case of polyphase aggregates, the effective elastic properties depend on the net effect of the three mentioned parameters. Therefore the higher is the number of phases, the more complex the variation in effective elastic properties of the aggregate. Each phase may have different thermal expansion, compressibility, thermal expansion anisotropy and compressibility anisotropy. The combination of changes on each of these parameters could therefore cause a linear or non-linear change of seismic velocity with temperature.

Although no comprehensive study into the influence of individual phases on the overall effective velocity of aggregate has been carried out, we may further conclude that some other lower crustal rocks may have a pronounced non-linear temperature coefficients of velocity, similar to the marbles. This would result in a more complex velocity variation in the lower part the crust.

7.6.2.2 High temperature shear zones

There is convincing evidence from the results of deep seismic reflection profiling, on the reflectivity of low angle shear zones (e.g. COCORP data from Wind River Thrust or BIRPS data from DRUM line). A number of theories have been presented to explain the necessary velocity and/or density contrast across such shear zones. Some of these those are:

1) the juxtaposition of different lithologies,
2) change in mineralogy between the mylonite and the protolith,
3) difference in seismic anisotropy between the mylonite and its protolith,
4) presence of pore water,
5) change in crack intensity.

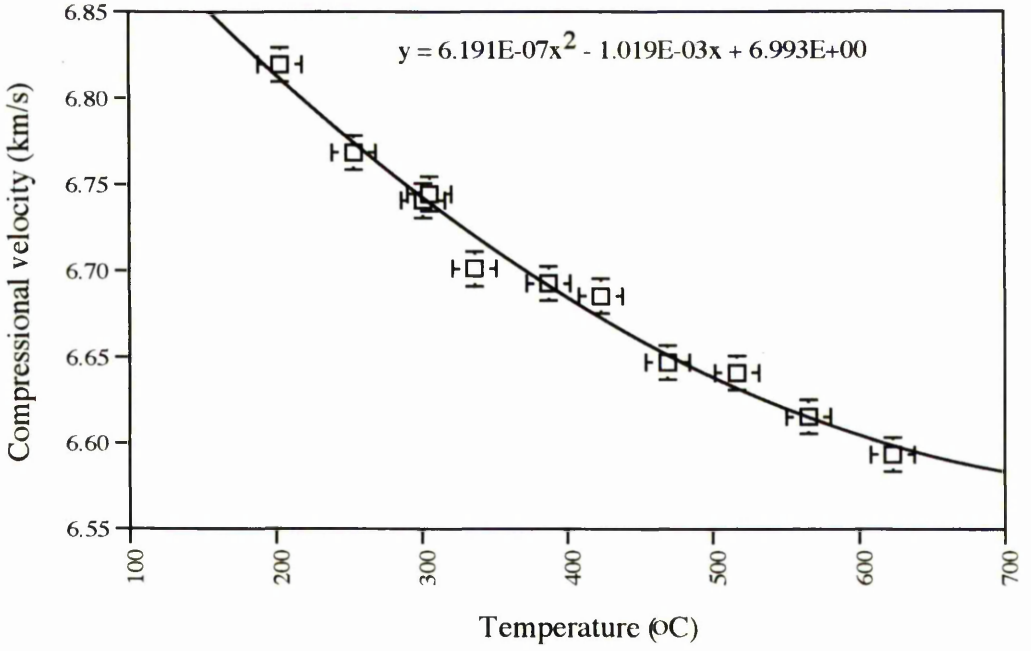

Figure 7.15: Plot of compressional velocity as a function of temperature for a Carrara marble sample. A non-linear relation between velocity and temperature is observed. The velocity/ temperature relation is similar to the one for sample LCF.

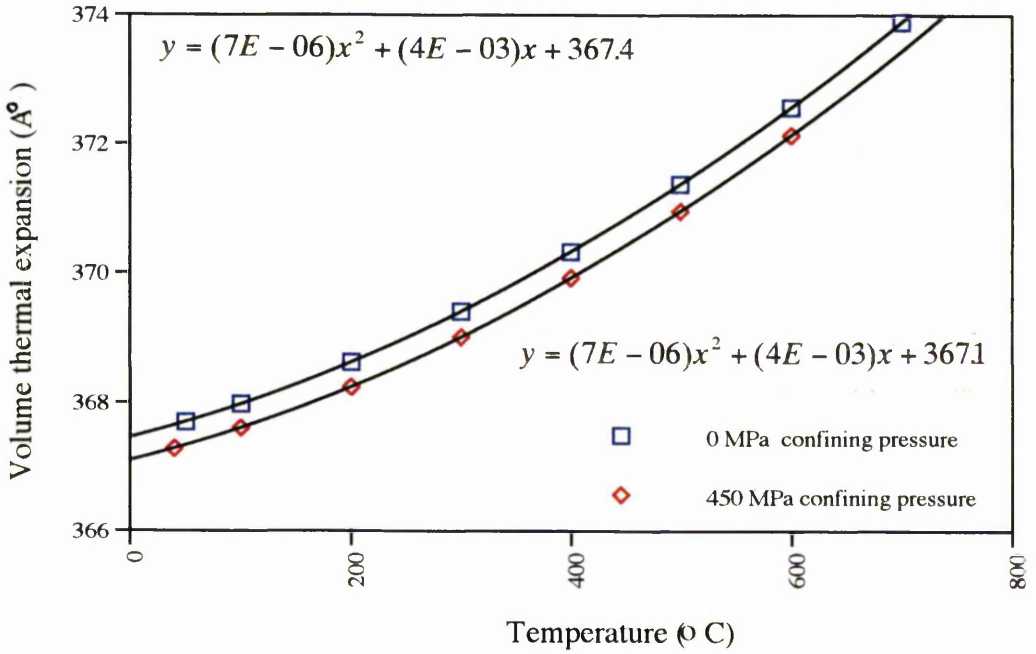

Figure 7.16: Volumetric thermal expansion data at 0 Mpa confining pressure and 450 Mpa confining pressure for calcite single crystal (after Wu et al., 1995)

The aim here is not to discuss the validity of the above theories but to show the importance effect of temperature on the relative velocity changes of rocks in the context of high temperature shear zones.

The results of high temperature, high pressure velocity measurements on a metabasic mylonite (Anzola mylonite; sample B1) and its protolith in section 7.4.4 showed that there is a greater velocity difference between two samples at higher temperature (figure 7.8). At a temperature around 600 °C and 450 MPa confining pressure the velocity difference between the two sample is nearly twice (0.45 km/s) the difference at room temperature (0.28 km/s).

Both samples mainly consist of plagioclase, hornblende and pyroxenes. The results of chemical analysies on the same shear zone by Brodie (1981) indicates that both the mylonite and the protolith have the same bulk chemical composition. However the result of modal analysis (chapter 4) shows a higher plagioclase content (around 10 % more) for the mylonite than the protolith. It is believed that during extension, a drop in pressure and a possible rise in temperature may have triggered an isochemical reaction which resulted in an increase in amount of plagioclase in the shear zone.

Such increase in plagioclase content in the shear zones has been observed in another case in the IV zone (in Rio del Ponte shear zone). Knowing that plagioclase has lower compressional velocity than the hornblende (see table 6.10), the lower velocity of the mylonite with respect to the protolith (sample B6) can be attributed to its higher plagioclase content. Furthermore, the greater temperature coefficient of velocity for the mylonite can be explained by larger effect of temperature on the plagioclase's bulk modulus than hornblende's bulk modulus (fig 7.17).

Finally, the *combination* of higher plagioclase content (by about 10 %) of the mylonite and the greater effect of temperature on the plagioclase than hornblende has resulted in a large velocity contrast between the mylonite and its protolith. Therefore the combined effect of pressure and temperature, and change in plagioclase content can result in an enhanced velocity contrast across a shear zone. More generally relative contrast due to variation in plagioclase content will be enhanced at higher temperature.

Such a velocity contrast becomes larger at greater depth, leading to enhanced reflection coefficients which are more likely to be detected on deep seismic reflection profiles.

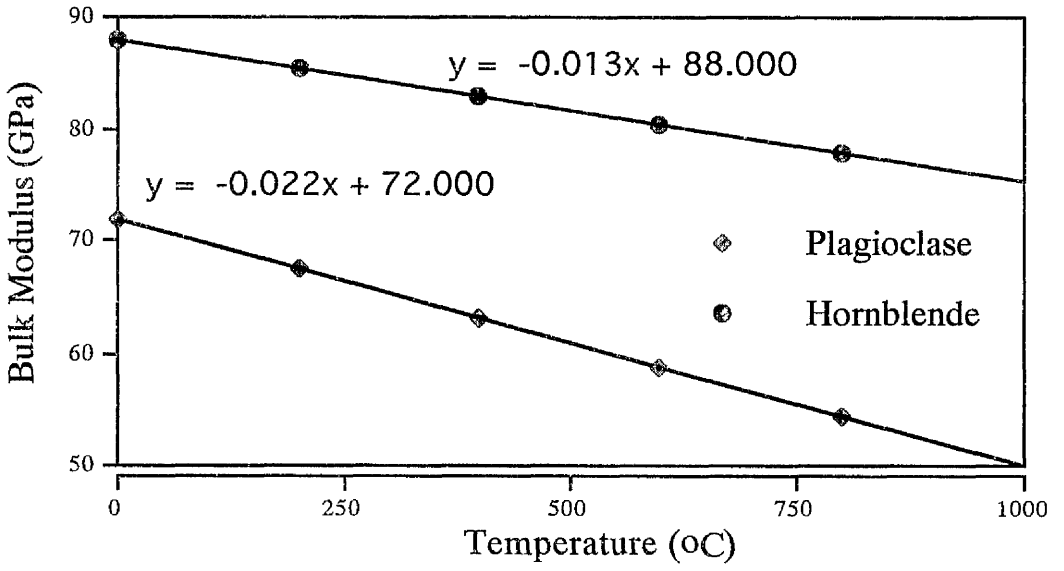

Figure 7.17: Plot of calculated isotropic polycrystal bulk modulus as a function of temperature for single crystals of hornblende and plagioclase. The points were calculated assuming a linear relationship between the thermal expansion and bulk modulus.

7.7 Concluding Remarks

The combined high temperature and pressure experiments results showed the following;

1. At a given confining pressure, temperature has a large retarding effect on compressional velocity.

2. Grain boundary opening and microcracks can be suppressed with confining pressure, but this becomes more difficult (at least over short times) at higher temperatures, as greater confining pressure is needed to prevent opening of old cracks and generation of new ones.

3. At a confining pressure of less than 450 MPa most of the samples show a sharp reduction in seismic velocity or irregular changes of it at temperatures above 550 °C to 600 °C. This was attributed to the opening of grain boundaries and/or microcracks.

4. For most of the samples except the monomineralic marbles, a near to linear relation between velocity and temperature was obtained.

5. No dehydration reactions, or phase transformations were recognised for any experiments over the experimental range of pressure (max. 450 MPa) and temperature (25 to 700 °C).

6. The combined effect of pressure and temperature on seismic velocity could result in increase or decrease of seismic velocity with depth, and can be expected to affect the velocity contrast between rock types at depth.

Chapter 8
Modelling the Velocity Structure of the IV & SdL Zones Under Lower/mid Crustal Conditions

8.1 Introduction

The long term goal of the present study has been to produce a number of velocity, density and reflection coefficient distribution sections for the IV zone and the associated SdL and ultimately a synthetic seismic reflection profile. Such models would give us a broad picture of change of velocity and density with depth (pressure) and temperature. They also would aid in the inference of lithology from seismic velocity and/or density. Furthermore, the potential reflectors and the nature of their reflectivity can be assessed.

The high pressure and temperature velocities and densities of the samples (chapter 6 & 7) were used in conjunction with a reconstructed geological cross section of the IV zone & SdL for modelling purposes. The geological cross section was constructed from all available lithological and structural information. The section then was digitised and the velocity, density and acoustic impedance were computed for each grid point after correction for the effect of hydrostatic pressure and temperature. Furthermore, the reflection coefficient was computed between all pairs of vertically separated points.

8.2 Geological Cross Section

A geological cross section along the major part of the IV zone and the SdL was drawn by E.H.Rutter (Pers. Comm – 1996) using existing structural and lithological information (fig 8.1). The section was balanced and normalised and the effects of low temperature deformation (Alpine deformation causing low temperature faulting and greenschist facies) were removed. It was assumed that the reconstructed cross section would represent a similar geometry and lithology to the post-Hercynian lower crustal section prior to tilting, uplift and emplacement into its present position during the Alpine orogeny.

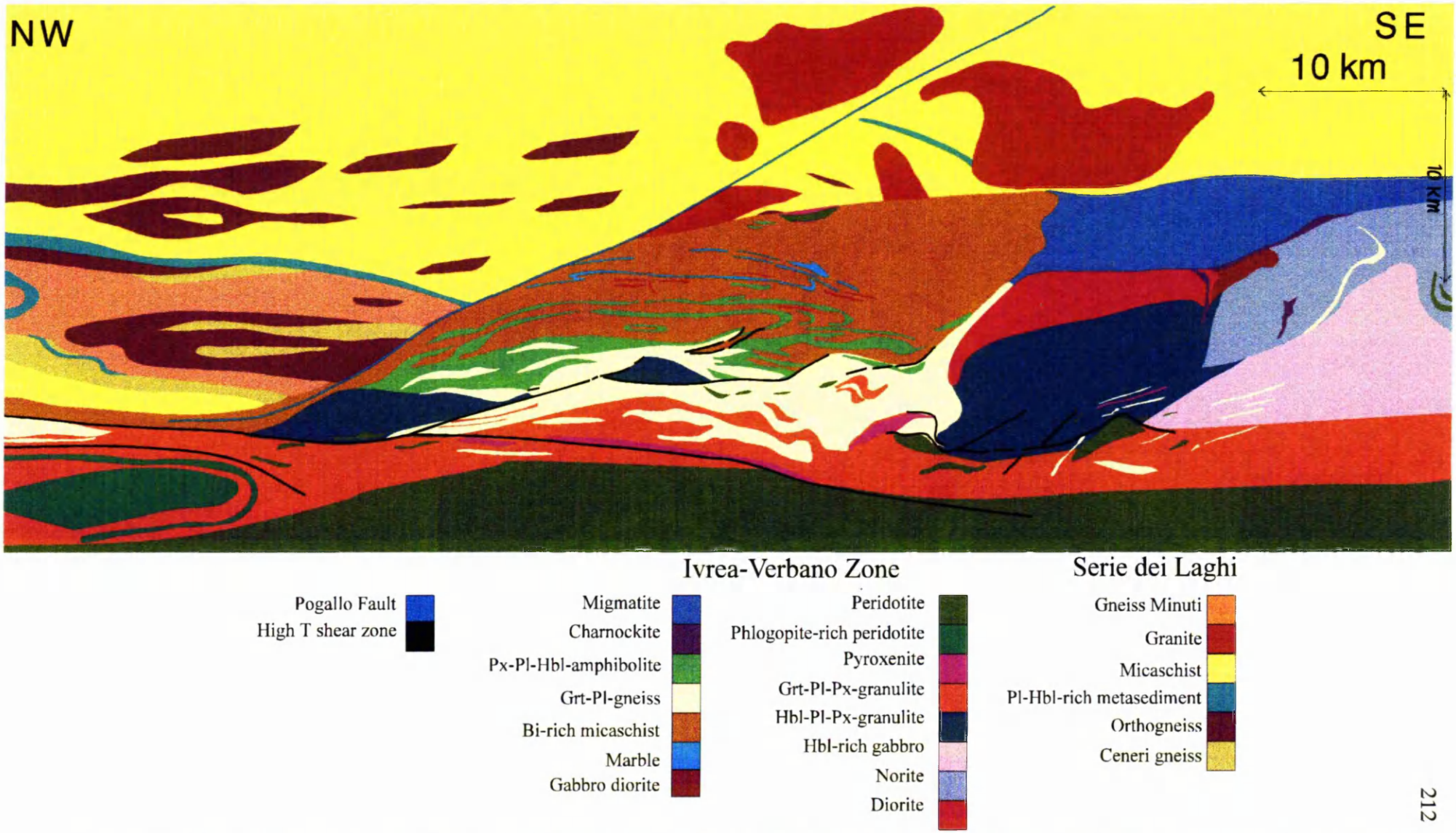

Figure 8.1: Geological cross-section of the Ivrea-Verbano Zone and Serie dei Laghi, after removing the effects of low-temperature alpine faulting.

8.3 Digitising the Cross Section

The cross section had to be digitised for seismic modelling to proceed. The section is approximately 74 km long by 26 km thick. It was decided to use a grid of 50 m vertically by 200 m horizontally. This would still be better than the vertical and horizontal resolution of typical seismic reflection sections (see chapter 2). It was clear from the start that digitising the section by hand, with such a fine grid (50m×200m) would be a formidable task, if not impossible. Therefore it was decided to digitise the section with the aid of computer. The program GRAINS, produced in this laboratory for the analysis of rock thin section images, was modified to carry out the digitising.

8.3.1 Image Digitising Program

The program GRAINS provides the basic function of reading the position and colour of each pixel on the screen, or pixels defined by points on a grid. These attributes can then be written to a data file. The user can define any grid size as long as it is not beyond the resolution of computer screen (e.g. 512 pixel by 640 pixel). Therefore the digitising of the geological cross section was carried out according to the following steps:

i) Each lithology was given a different colour on the geological cross section (23 colours).

ii) The coloured geological cross section was saved as a BITMAP on the computer.

iii) The program records the X and Y co-ordinates and the colour code of each pixel at each given grid point on the BITMAP image.

iv) Once the geological section was digitised then the next stage was to assign a velocity and density to each grid point. This was done by creating a data file containing all the velocity and density data for each lithology (colour). Then the computer program was ask to look up the data file and pick out the appropriate velocity and density according to the colour of the pixel. These were corrected for the effect of pressure and temperature according to the specified thermal (20 °C/km) and hydrostatic pressure (30 MPa/km) gradients. The program also calculated the reflection coefficient between each pair of vertically associated grid points.

v) The co-ordinates of each grid point and the corrected velocity, density and reflection coefficient were saved into an ASCII data file. The output data file consists of 7 columns and 196788 rows. The columns from left to right contain the following information: 1) row number, 2) X co-ordinates, 3) Y co-ordinates, 4) colour code, 5) density, 6) velocity and 7) reflection coefficient for each grid point.

8.4 Correcting Seismic Velocity and Density data for the effects of Pressure and Temperature

It was demonstrated in chapter 6 and 7 that seismic velocity and density are affected by pressure and temperature. The pressure and temperature increase with depth according to the regional baric and thermal gradients. Hence it is essential to make the necessary pressure and temperature corrections to velocity and density of rocks at different depth.

8.4.1 Velocity Correction

The compressional velocity of the samples were measured at elevated pressure and high temperature (chapters 6 & 7) and the pressure and temperature coefficients of velocity were obtained. These data were used to calculate the velocity of each rock type at appropriate combinations of pressure and temperature along the constructed geological cross section. The equation 8.1 was used for calculating the velocity at various pressure and temperature condition. A linear change of velocity with pressure and temperature was assumed for all rocks.

$$(V)_{P,T} = V_O + P\left(\frac{\partial V}{\partial P}\right) + T\left(\frac{\partial V}{\partial T}\right) \qquad (8.1)$$

where V is the velocity of rock at a given temperature (T) and pressure (P), V_o is the seismic velocity of rock at room temperature and pressure and $\left(\frac{\partial V}{\partial P}\right)$ and $\left(\frac{\partial V}{\partial T}\right)$ are the pressure and temperature coefficients of velocity.

In order to assess the importance of seismic anisotropy of the lower crustal rocks, two different velocity models were constructed. The first one displays the *average* compressional velocity of the rocks and the second one displays the compressional

velocity distribution for measurements made at the direction *normal* to the foliation. It was assumed that the foliation is approximately horizontal throughout the section.

8.4.2 Density correction

Density is affected by both pressure and temperature. According to the compressibility and thermal expansion coefficient of the sample, the density can increase or decrease. As no independent measurements of thermal expansion or compressibility was carried out on the samples during the course of this study it was decided to use published values in order to estimate the necessary density correction.

(a) Thermal expansion coefficients vary considerably with temperature. An average of the following thermal expansion coefficients (table 8.1) of some minerals was used to correct the effect of temperature on the density of the rocks assuming a 25 °C/km gradients.

	Thermal expansion (10-6/°C)		
Mineral	**20°C**	**400°C**	**800°C**
Quartz	34	69	-3
Feldspar	12	19	24
Olivine	26	32	34
Pyroxene	24	28	32
Garnet	19	26	30
Spinal	16.2	28	29
Average thermal expansion		**33**	

Table 8.1: Thermal expansion of selected lower crustal minerals at various temperatures. The average value of thermal expansion at 400°C was used for correcting the temperature effect on density of rocks (after Jeanloz & Knittle (1986)).

(b) In chapter 6, the compressibilities of the samples measured were calculated from their V_P and V_S and density. The average of those (0.00002 Pa^{-1}) were used to correct for the change in density due to increase in hydrostatic pressure. No change in compressibility with pressure was assumed for this correction.

The following equation was used to apply the necessary density correction:

$$\rho = \rho_o \times (1 + (0.00002 \times P) - (0.000033 \times T)) \quad (8.2)$$

where ρ is the density at a given T and P and ρ_o is the density at room pressure and temperature.

8.4.3. Calculating reflection coefficient

The reflection coefficient is a measure of reflectivity of a boundary for seismic waves. A reflection coefficient of 1 or -1 indicates that 100% of seismic waves reflects back whereas a reflection coefficient of 0 indicates zero return of seismic waves from a boundary. The following equation was used to calculate the reflection coefficient for a normal incidence wave between two vertical points on the geological section.

$$R = \frac{Z_2 - Z_1}{Z_2 + Z_1} \quad (8.3)$$

where R is the reflection coefficient of the boundary where there is a change in acoustic impedance and the $Z1$ and $Z2$ are acoustic impedance of rocks above and below the boundary.

8.5 Making the two Dimensional Models

Once the seismic velocity and density values were corrected for the effect of temperature and pressure then their two dimensional distribution over the geological cross section could be displayed. Due to the extremely large number of data points for each plot (196788), a powerful plotting program called MATLAB was used. This program is capable of handling more than 100,000 data points and takes ASCII input data in an array format. It became clear that a colour filled contouring plot is a more effective way of showing gradual changes than simple contoured plot. Therefore all the velocity and density distribution models are presented in the form of colour filled contouring plots. Only the reflection coefficient variations over the cross section are presented as a contoured plot.

8.6 Results

8.6.1 Two Dimensional Velocity Distribution

Figure 8.2 shows the average compressional velocity distribution through the IV zone and SdL zone. The velocity varies from a minimum of 5.87 km/s for the Schist dei Laghi at the top of the section to maximum of 8.24 km/s for the peridotites at the base of the section. Although in general there is an increase in seismic velocity with depth, the bottom half of the section shows repetitive layers of high and low velocity. No gradual increase in velocity can be observed from one rock unit to another. This implies that observed seismic variations on the section are mainly due to the composition changes that occur at each lithological boundary. Pressure and temperature effects are of second order and they do not change the velocity with depth in a way that provides a continues and smooth increase of velocity with depth. This point can be better emphasised by comparing the seismic velocity section with the lithology cross section. A good correlation between lithological boundaries and the major velocity changes can be seen.

The middle part of the section, which is dominated by metabasic and metasedimentary rocks shows very wide velocity variations. The SE side of the section is mainly dominated by the Mafic Formation, forming a few thick and homogeneous velocity layers. The NW side of the section mainly shows a series of thick bands of ultrabasic, metabasic and metasedimentary rocks which displaying different velocities. The base of the velocity section is assumed to be mainly peridotites with average velocity of about 8.24 km/s. In most part of the section, there is a sharp and large increase in velocity (about 1 km/s) from the metabasic to the peridotites.

There is no clear and sharp velocity change between the Serie dei Laghi (the top one third of the section) and the IV zone. Moreover there is less velocity variation between different rock types in the SdL (with exception of the amphibolite bands which show high seismic velocity) than in the IV zone. The large granite bodies show the same velocity as surrounding schist and there is little velocity variation across the Pogallo fault.

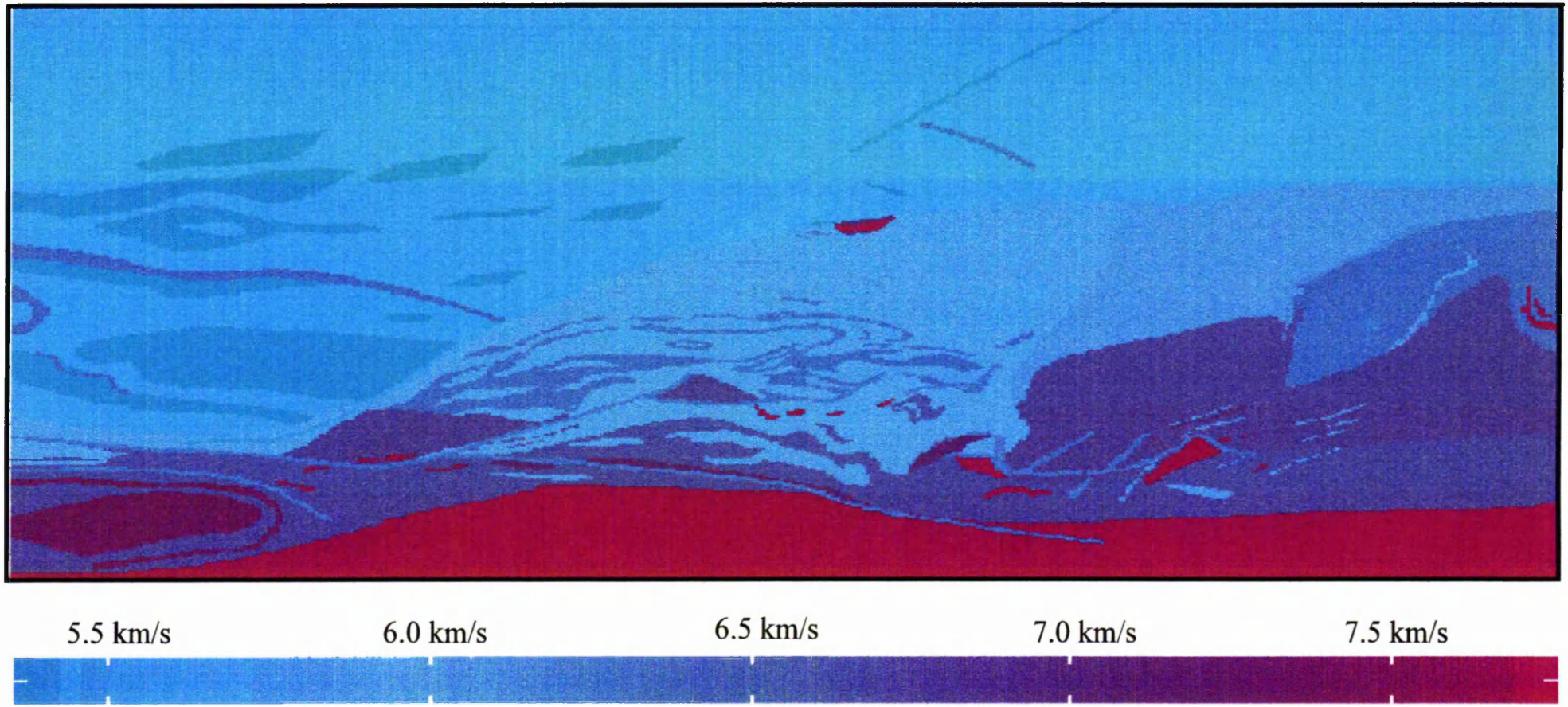

Figure 8.2: The contoured average seismic velocity distribution for the IV & SdL zones. (the scale is the same as geological cross-section).

Figure 8.3 shows a similar velocity section to figure 8.2 but all the velocity values are for the direction normal to the foliation, assuming a horizontal foliation throughout the section.

There are a number of important differences between this velocity section and the previous one. Some of these differences are summarised as follow:

i) A greater velocity contrast between the SdL and the IV zone is seen.

ii) Granites have higher velocity contrast with the host schists and orthogneisses a lower one.

iii) The Pogallo Fault appears as a narrow and continuous band having a similar velocity to granites.

iv) Kinzigite and stronalite show similar velocities and smaller velocity contrasts with the amphibolite bands.

The differences between the two seismic velocity sections (fig 8.2 & fig 8.3) are an indication of the importance of seismic velocity anisotropy on the overall velocity structure of lower and middle crustal rocks.

8.6.2 Two Dimensional Density Distribution

Figure 8.4 shows a density distribution section across the Serie dei Laghi and the IV zones after correction for the pressure and temperature effects. Ultrabasic and some metabasic rocks are well defined by their high densities at the base of the section. There is also a sharp density contrast between mantle peridotite and the metabasic rocks of the base of the crust. Stronalite shows higher density than kinzigite and they are quit distinguishable on the section. Amphibolites and marbles also showing different density. In the SdL, granites, gneisses and orthogneisses show lower density than schist. There is a small density contrast between the SdL and the IV zone. This difference is close to zero on the right side of the section.

8.6.3 Two Dimensional Acoustic Impedance Distribution

Acoustic impedance is the product of velocity and density. Figure 8.5 shows the acoustic impedance distribution for the geological cross section assuming horizontal

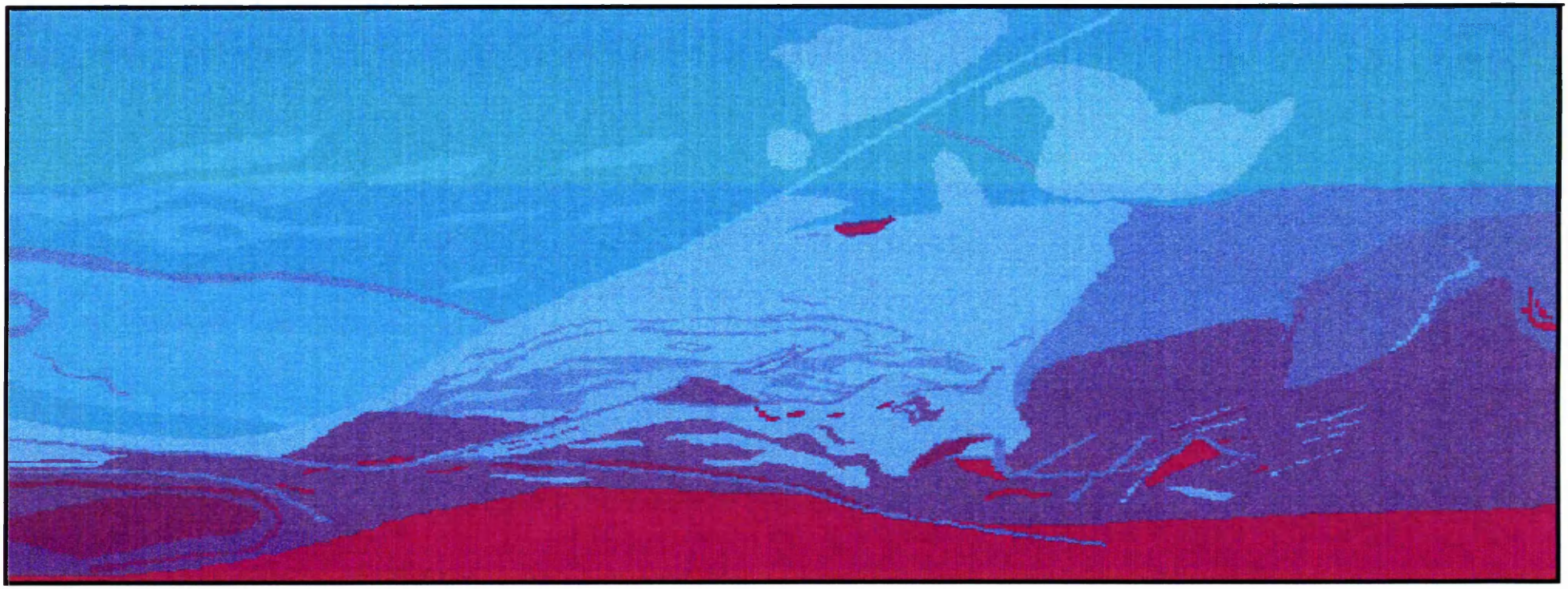

Figure 8.3: The normal to the foliation velocity distribution for the IV zone and SdL zone.
(the scale is the same as geological cross-section, the velocity key is the same as figure 8.2)

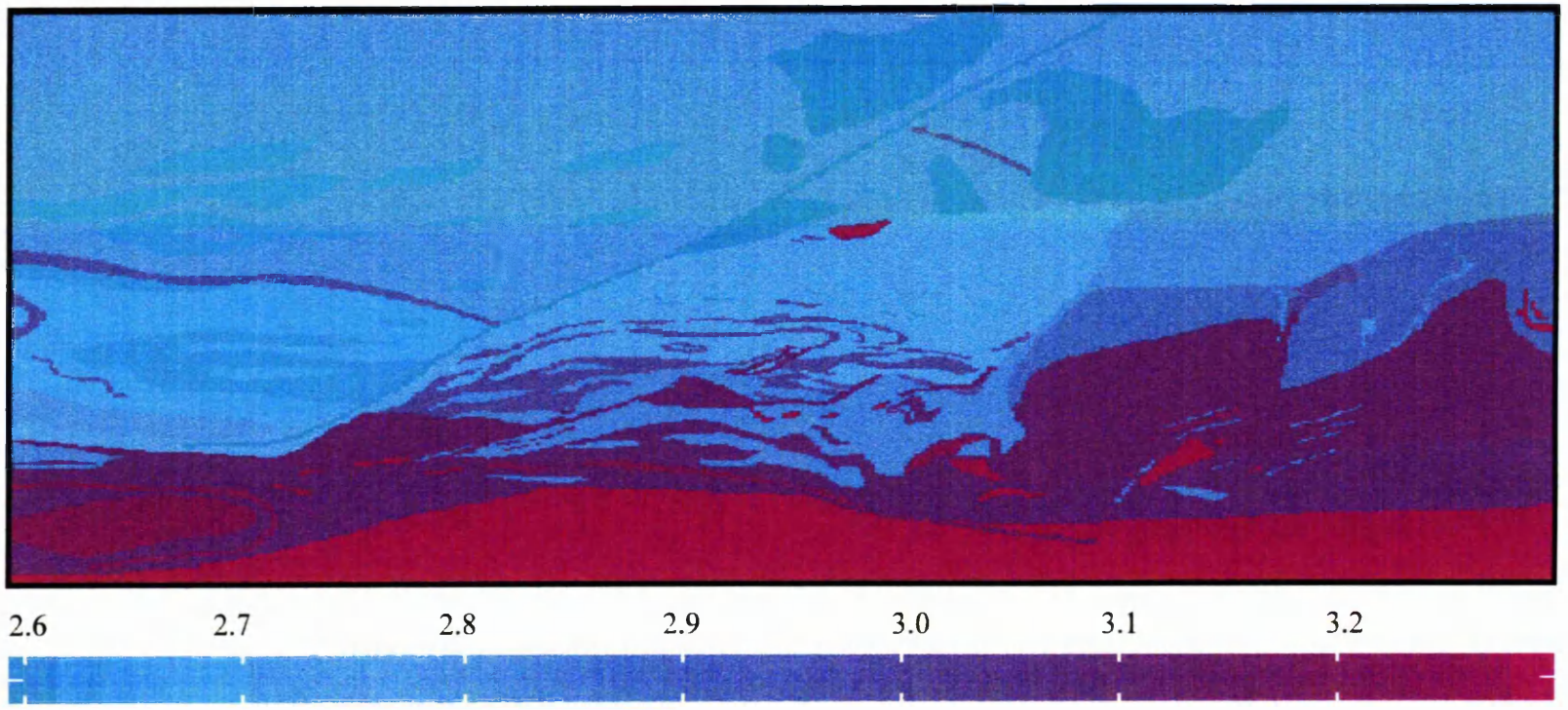

Figure 8.4: Plot of density variation with depth (pressure & temperature) for the IV and SdL zones.
(the density values are in g/cm3 and the scale of the section is the same as the geological cross-section).

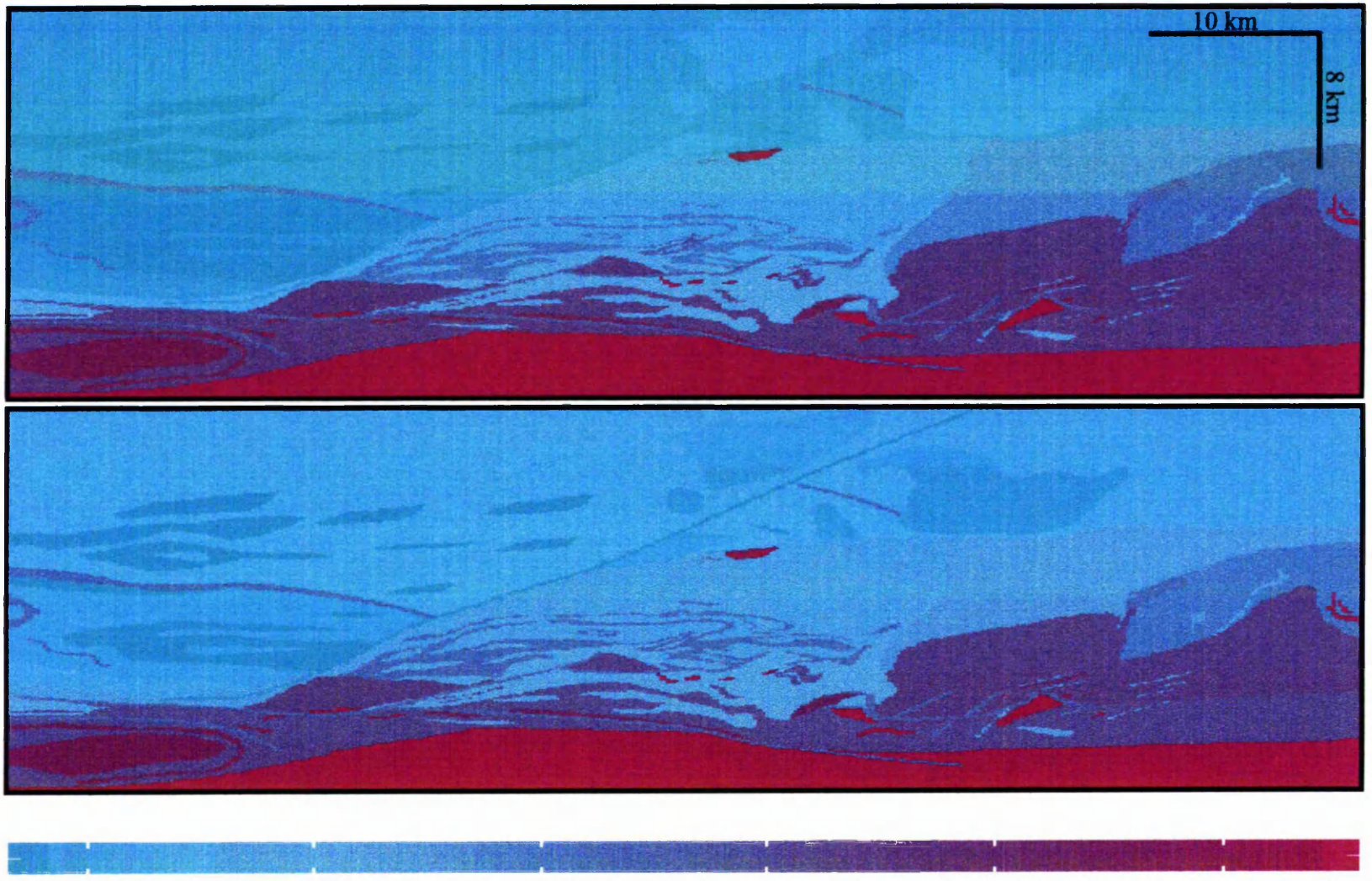

Figure 8.5: Acoustic impedance distribution with depth. (top) using velocity for the direction normal to the foliation (bottom) using average velocity. The vertical and horizontal scales are not the same.

foliation and no foliation respectively. Certainly both sections highlight more detailed information. For example, granite bodies and orthogneisses are visible on both sections and there seems to be a wider variation in the acoustic impedance between the rocks than between their individual velocities or densities.

8.6.4 Two Dimensional Reflection Coefficient Distribution

For any changes in acoustic impedance the reflection coefficient was calculated. A maximum reflection coefficient of 0.15 has been obtained which is for the boundary between peridotite and kinzigite. On average, most boundaries in the IV zone show a reflection coefficient between -0.1 and 0.1. Figure 8.6 shows the reflection coefficient distribution for the geological cross section assuming a horizontal foliation. Such a section is a way of displaying all the potentially reflective boundaries which could give rise to reflected seismic waves.

Not many reflectors can be seen in the SdL. It shows that none of the granite bodies are reflective and only a few reflections from the orthogneisses can be seen. The boundary between the SdL and the IV zones is not a strong reflector. There are few reflectors at the top of the IV zone either. Most reflectors are at the bottom half of the section.

In terms of potential reflectors the IV zone can be divided in to three regions. The central, the SE and NW parts. The SE part of the IV zone is dominated by the Mafic Formation and there are only a few reflectors associated with it. The metasedimentary and metabasic rocks in the central part of the IV zone are seems to be reflective and abundant. The horizontal reflectors and their large number make this part of the IV zone a potential area for producing series of random velocity layers and for causing constructive or destructive interference of seismic waves. This area would be likely to produce a laminated pattern on a seismic reflection section.

If we assume no foliation and use averaged velocity of the samples to calculate the reflection coefficient then a number of changes can be observed on the reflection coefficient distribution section (fig 8.7). This time the Pogallo fault appears strongly reflective and number of orthogneisses are also appearing. However the continuous and

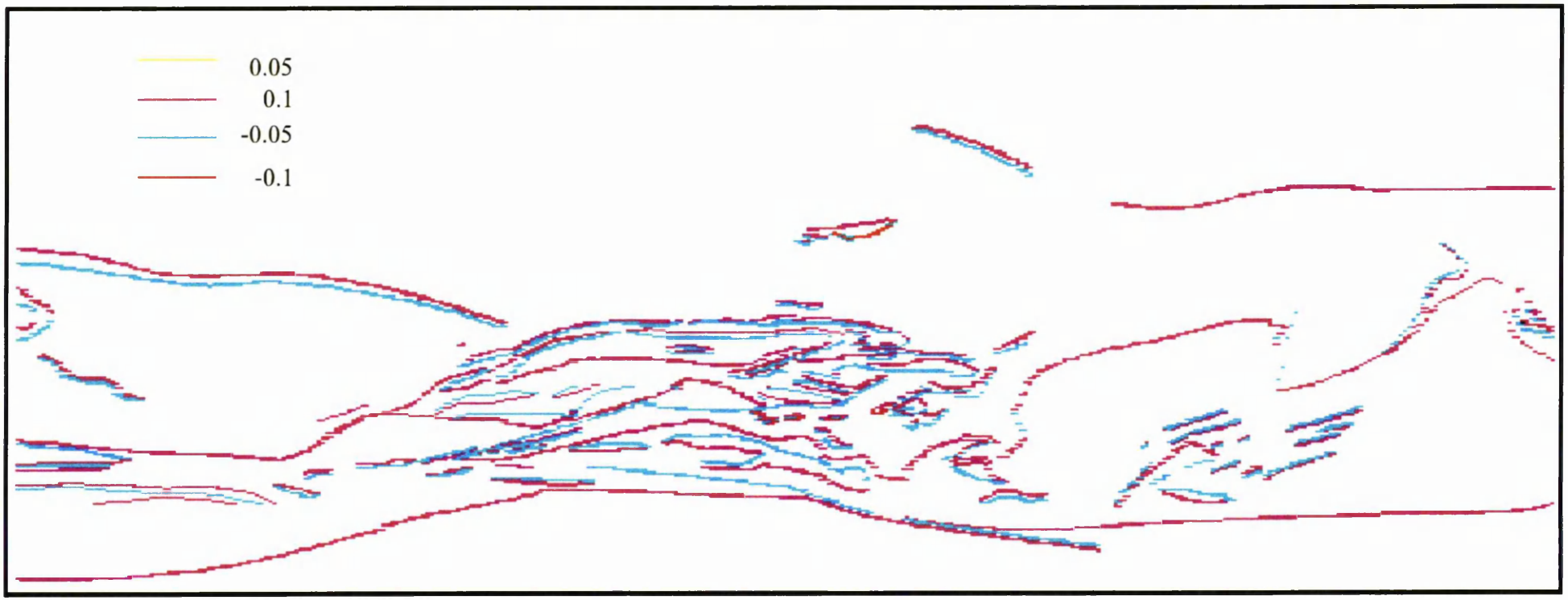

Figure 8.6: Section showing reflection coefficient distribution for the IV zone and SdL zone. Velocity values for the direction normal to the foliation was used to calculate the reflection coefficient. (The scale of the section is the same as the geological cross-section.

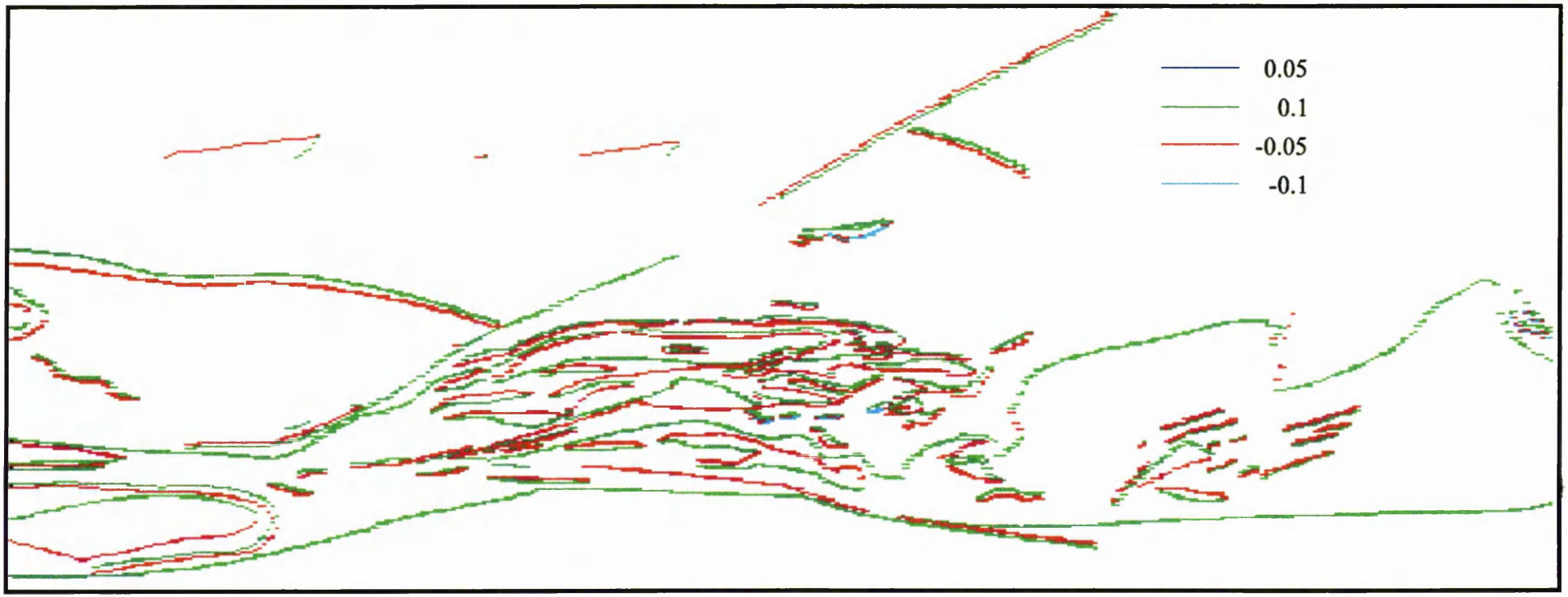

Figure 8.7: Section showing reflection coefficient distribution for the IV zone and SdL zone. Averaged velocity was used to calculate the reflection coefficient. (The scale of the section is the same as the geological cross-section.

horizontal reflector above the Mafic Formation which was presented in the other section would disappear completely. The SdL would generally appear quite transparent for seismic energy and there would be only a few scattered reflectors in this zone. However, the IV zone would appear strongly reflective. Only the Mafic Formation would appear less reflective and more homogeneous. The Moho seems to be a sharp boundary at the sides of the sections and more like a transition zone similar to the lower crust above it in the middle.

8.7 Discussion

The velocity, density and reflection coefficient distribution sections of the SdL and the IV zone described in the previous sections document the diversity in the lower crustal reflectivity patterns. These diversities directly reflect the major lithological changes and include (a) the effects of pressure and temperature on the velocity and density of rocks and (b) seismic anisotropy. Here, we attempt to find explanations if not definite answers to the following questions in the context of calculated pattern of reflection coefficients of the IV and SdL zones.

i) What is the nature of seismic reflections from the CLC ?

ii) What gives the CLC its laminated pattern ?

iii) What is the nature of the reflection Moho?

8.7.1 Origin of lower crustal reflectivity

An examination of the geological cross section (fig 8.1) and comparing it with the reflection coefficient distribution sections (fig 8.8 & Fig 8.9) suggest that four factors could be responsible for the lower crustal reflectivity of the IV zone and similar lower crustal sections. These in terms of importance are:

(i) compositional layering,

(ii) mafic intrusions and melt fractionation,

(iii) lenses of ultramafic mantle-derived rocks,

(iv) low angle shear zones and associated deformation.

Compositional layering by far seems to be the most likely cause of lower crustal reflectivity. The central part of the IV section indicates that horizontal layers of metasedimentary and metabasic rocks with their alternating high and low velocities form a number of strong reflectors. The importance of compositional layering has also been emphasised by Hale and Thompson (1982), Fountain et al., (1984); McDonough and Fountain (1988) and Christensen (1989).

The SE part of the IV geological cross section is dominated by rocks of the Mafic Complex. The basic melt fractionation and mixing with melt derived from crustal rocks as a result of the intrusion of this massive mafic body resulted in a number of thick igneous layers of different compositions. It seems that little seismic wave reflection would occur from the boundaries between these layers due to similarities in their seismic velocities and densities. However, the boundary between this complex mafic body and the surrounding rock has large velocity and density contrasts which would give rise to seismic reflections.

There are a number of ultramafic lenses which possibly originated from the mantle as a result of tectonic imbrication during compressional Hercynian or earlier tectonics (Quick et al., 1994). These high velocity rocks are surrounded by much lower velocity rocks and are anomalous bodies which would give rise to strong seismic reflections. Extreme reflection coefficients (about 0.15) at the boundary of some of these lenses would provide an answer to the origin of some bright spots observed on some deep seismic reflection profiles.

Finally, it seems likely that some high temperature shear zones would appear reflective on the seismic sections. Their reflectivity is either due to a combined velocity and density contrast between the mylonite and the protolith or due to juxtaposition of different wall rocks resulting in velocity or/and density contrast. The formation of velocity and/or density contrast between mylonite and its protolith has been discussed in chapter 7. The shear zones seem to be responsible to some extent for displacing diffrent lithological units. This has resulted in a greater velocity and density distribution in the IV zone. The low angle of these shear zones has possibly helped to enhance the

stratification of the lower crust. This point was discussed by Wever et al., (1990) and seems to be apply to some extent in the IV and SdL zones.

8.7.2 The laminated pattern of the CLC

The laminated pattern observed on some deep seismic reflection profiles is believed to be due to alternating thin, high and low velocity layers. Together with the constructive and destructive effect of interfering seismic waves, these could be responsible for the laminated patterns. The central part of IV section, as explained before, is an ideal candidate for producing such a pattern. Compositional layering (original sedimentary or metamorphic layering), strong horizontal foliation and igneous intrusions and number of high temperature shear zones together have resulted in a sequence of layers of various thicknesses and velocities. Such layering is not observed in the SE part of the section where the Mafic Formation is dominant. This would indicate that laminated patterns on some contemporary deep seismic reflection sections are indicative of not only thin layering but also that the nature of the layers involves alternations of sedimentary and metabasic rocks rather than igneous rocks. It seems that igneous bodies are very unlikely to form thin and laminated reflectors.

8.7.3 The Moho

Despite the significant velocity and density jump from the CLC to the Mantle (the peridotites at the base of the section), the Moho reflections are seems to be of two types.

(a) The first type is the transition Moho which can be seen at the middle of reflection coefficient section (figures 8.6 & 8.7). This Moho does not seems to be the strongest event. This is because the reflectors within the CLC produce similar reflection coefficients. In this part the Moho would be more like a wide transition zone than a sharp boundary.

(b) The second type is a sharp boundary Moho. This can be seen at SE and NW sides of the reflection coefficient section. In these areas the reflection from the Moho seems to be the strongest event and indicates sharp velocity and/or density changes.

8.8 How the IV zone Compares with the 'Average' Lower Crust from Contemporary Seismic Measurements.

Results of many seismic investigation (both *in-situ* and laboratory studies) indicates an average velocity of around 6.7 km/s to 6.8 km/s for the continental lower crust (e.g. Mooney and Brocher, 1987; Christensen and Fountatin, 1975). Such a high velocity for the CLC may be equated with mafic and metabasic rocks such as gabbros and mafic granulites (e.g. Christensen and Fountain, 1975).

Table 8.3 shows some statistical velocity values for the IV zone and the SdL. If we assume a horizontal foliation and consider the related mean velocity, then IV zone has similar average velocity to the CLC elsewhere. This also supports the suggestion that the average CLC has a dominantly mafic composition. However, if we consider the mean of the 'averaged' velocity of the rocks of the IV zone to be representative of the CLC a more strongly mafic CLC would be implied.

	Normal to the foliation velocity			Averaged velocity		
	IV	**SdL**	**both**	**IV**	**SdL**	**both**
Minimum velocity	6.11	5.58	5.58	6.15	5.87	5.87
Maximum velocity	8.03	6.50	8.03	8.24	6.80	8.24
Mean velocity	**6.63**	**5.66**	**6.39**	**7.04**	**6.15**	**6.65**

Table 8.2: Some statistical velocity values for the Ivrea-Verbano lower crustal section and Serie dei Laghi middle crustal section at appropriate pressure and temperature. (all the velocity values are in km/s).

These uncertainties in the determination of the average velocities of the IV zone section are mainly due to strong seismic anisotropy associated with the lower crustal rocks and should be appreciated when an in-situ or laboratory velocity data are compared. This point has also been raised by Christensen (1989). He suggests that the refraction data possibly overestimate the averaged velocity of the CLC and the lower crust may have a higher SiO_2 content than has been previously estimated. This would give the CLC a dioritic composition. Although Christensen's point could be valid for a

number of CLC sections, it clearly does not apply to the IV zone and possibly to similar lower crustal sections elsewhere..

8.9 Conclusions

The extensive number of high pressure and temperature laboratory velocity measurements of the samples from IV zone and SdL were incorporated with a detailed geological cross section of the above two zones to produce series of velocity and density sections and to study the reflection coefficient distribution for them. Some important conclusions on seismic properties and reflectivity of the deep crustal sections, based on extensive velocity and density measurements are as follows:

i) There is a general increase in velocity and density with depth.

ii) There is a variation in velocity and density in the IV zone and the SdL. The velocity and density variations are more significant and frequent in the IV zone than in the SdL.

iii) The IV zone seems to be more reflective than SdL.

iv) The granites, orthogneisses and schist of the SdL seem to have similar acoustic impedance, making them non-reflective on a seismic section.

v) The middle part of the IV zone seems to be extremely reflective. This part is associated with horizontal and sub-horizontal layers of metabasic and metasedimentary rocks. These rocks show alternating velocity and density variation. The layering are either compositional or associated with metamorphism.

vi) Mafic intrusion and high temperature shear zones have increased the velocity variations within the IV zone.

vii) Seismic anisotropy seems to most important in metabasic and metasedimentary rocks of both the IV zone and SdL.

viii) The majority of the lower crustal reflections are associated with lithological boundary indicating the importance of compositional layering.

ix) Effect of environmental factors (pressure and temperature) on seismic velocity seems to be of second order and less important than original compositional variation.

x) In both cases of (a) no seismic anisotropy (no foliation) and (b) seismic anisotropy (normal to the foliation direction) the high mean velocities correspond to a highly mafic composition.

Chapter 9

Conclusions & Scope for Future Work

9.1 Introduction

The main aim of the present study has been to produce a detailed study of the seismic properties and densities of the rocks of the IV zone and adjacent SdL. The results can be used to help clarify the interpretation of contemporary deep seismic reflection and refraction data. The above aim was completely achieved by tackling and resolving number of problems and tasks of which the following are the major ones.

i) sample collection from the IV/SdL lower crustal exposure in NW Italy,

ii) design and construction of apparatuses for measurements of seismic velocities at both elevated pressure and temperature,

iii) extensive laboratory study of the samples collected and measurements of their compressional and shear velocity measurements,

iv) finally, production of velocity, density and reflection coefficient models of this exposed lower/middle crustal section (IV zone and Serie dei Laghi).

9.2 Summary of major achievements to date

The major conclusions concerning individual aspects of the present study have been presented at the end of relevant chapters. However, highlights of these are summarised below.

During two field seasons the most representative geological units from the IV zone and SdL were sampled systematically as well as extensively. Well over 500 oriented cores of various diameters (15 mm & 20 mm) and lengths (max. 10 cm) in three orthogonal directions were obtained. These provided fresh, oriented and representative samples for a large number of laboratory seismic measurements as well as petrological and mineralogical studies.

Two high pressure apparatuses were adapted for laboratory velocity measurements at both elevated pressure and temperature. Necessary parts and a number of transducer/sample assemblies were designed and constructed which allowed the

velocity measurements of rocks to be carried out at pressures up to 550 MPa confining pressure and maximum temperature of 600 °C. All the necessary calibrations of the high temperature and pressure instruments as well as the seismic system were carried out carefully to ensure accurate and reliable velocity measurements.

The pulse transmission method was used for velocity measurements of samples. The compressional velocity of at least 146 samples and shear velocity of 74 samples were measured at room temperature and elevated pressure up to 550 MPa. Further, the compressional velocity of 14 samples were measured at both high pressure and temperature.

The large number of velocity measurements not only provided the necessary pressure and temperature coefficients of velocity for later modelling proposes but also allowed us to study the velocity and seismic anisotropy of a large number of lower crustal rock and to find relationships between lithology and seismic velocity and density. All the velocity measurements at room temperature and elevated pressure show a sharp increase in velocity at pressure range of 0 to 250 MPa. This non-linear increase in velocity was attributed to microcrack and pore closure. At pressures above 250 MPa a linear increase in velocity with pressure was observed for all samples. This linear increase is attributed to the intrinsic effect of pressure on the elastic stiffness of the samples.

The high pressure and room temperature velocity data indicate that ultramafic rocks have the highest compressional velocities (ranging from 7.36 to 8.37 km/s) and shear velocities (ranging from 4.29 to 4.68 km/s) and the metasedimentary rocks have the lowest compressional velocities (ranging from 5.54 to 6.98 km/s) and shear velocities (ranging from 3.14 to 4.07 km/s). Seismic anisotropy seems to be extremely high in rocks with elongate minerals or with crystallographic preferred orientation, such as schist (maximum compressional An= 16.9% and maximum shear An= 8.7%) and virtually non existent in mafic and igneous rocks such as granite. Most rocks with noticeable seismic anisotropy have their smallest velocity in the direction normal to the foliation or compositional banding and the largest velocity is in a direction parallel to the foliation or compositional banding.

The result of combined high temperature and pressure velocity measurements not only provided the temperature coefficient of velocity for a number of samples but also other interesting results were observed. Generally, as temperature increases, velocity decreases. Both linear and non-linear rates of decrease of velocity with temperature were observed. It also became apparent that higher confining pressure were needed to suppress the reopening of microcracks as temperature increased. The high temperature results also indicated that *relative* change of velocity with temperature for different rocks can result in larger velocity differences at higher temperatures. This can result in a greater velocity contrast, for example, between a mylonite and its protolith. The limited number of high temperature velocity measurements obtained also highlighted the extreme technical problems associated with such measurements.

The temperature and pressure coefficients of velocity for a selection of rock types (23 rock types) were used in conjunction with a reconstructed geological cross section of the IV zone and the associated the SdL. A series of velocity, density and reflection coefficient sections were produced for these zones. The results of modelling indicate a series of important points associated with the overall reflectivity of the deep continental crust:

(i) In general it was recognised that the SdL is less reflective than the IV zone. This is mainly due to similarities in acoustic impedance of the granites, the orthogneisses and the metasedimentary schists. A maximum compressional velocity of 6.83 km/s and a minimum of 5.58 km/s were obtained for the SdL.

(ii) The IV zone seems to be extremely reflective in the central part of the section. This is associated with presence of a series of horizontal to sub-horizontal layers of different lithology. These layers show alternating high and low velocity and density. Most of these layers are either compositional or associated with metamorphism. The reflection coefficient associated with these reflectors varies from 0.15 to -0.1. The Mafic Formation, which forms a complex of mafic and ultramafic rocks in the SW part of the section, seems to be homogeneous and non reflective. A maximum velocity of 8.24 km/s and minimum velocity of 6.11 km/s were obtained for the IV zone as a whole.

The Moho seems to have two different natures, one shows a sharp jump in velocity and the other one seems to produce reflections as strong as in the associated lower crustal rocks. The latter Moho seems to be more like a transition zone than a sharp discontinuity.

(iii) In general the environmental effects (pressure and temperature) seem to be of lesser important than the original compositional variations and strong seismic anisotropy in producing velocity or/and density contrasts. Four factors were suggested as the reason for velocity or density contrasts between different rocks in the IV zone. These are in order of decreasing importance are (1) compositional layering, (2) mafic intrusions and subsequent melting and melt fractionation, (3) seismic anisotropy associated with ductile deformation and mineral alignments and finally (4) juxtaposition of different lithological units associated with shear zones.

9.3 Scope for Future work

The velocity and density models can now be used in order to construct a 2D synthetic seismic reflection section of the IV zone and adjacent Serie dei Laghi. Such section would be of great help in assisting and clarifying the interpretation of contemporary deep seismic sections. This work has already been started with the help of D. Blundell at Royal Holloway College in London, but will not be completed in time for inclusion in this thesis.

Although any further high pressure velocity measurements of lower crustal rocks will be of great importance in terms of increasing the existing size of the petrophysical data base for lower crust rocks, more attention should be paid to high temperature velocity measurements. It has already mentioned that such measurements, generally are associated with substantial technical problems. Some of these problems were over come to some extent by the unique design of high temperature/pressure apparatus used in this study. However, there remains great scope for improving the design. Some such improvements would be, (a) a better furnace which can produce higher temperature, (b) better thermal insulation to minimise heat loss due to thermal convection, and finally (c) an improved design may be needed to bring the electrical connection from the bottom

transducer out (in the present design, the bottom connections were open or short circuited sometimes at high pressure).

The seismic modelling and the reconstructed geological cross sections will be subjected to continual refinement as more geological information and velocity data becomes available. This task will be followed up by Mr T. James.

9.4 General comments on the experimental velocity measurements

The majority of laboratory velocity measurements of rocks are carried out, using high frequency waves (generally in the other of 0.8 to 2 MHz). However the in-situ seismic measurements (reflection or refraction) are made using much lower frequencies (in the order of 50-100 Hz). Therefore, attention to the problem of down scaling the laboratory data to seismic frequencies may be quite important and the difference in velocity values could be substantial, especially in the case of two phase aggregates.

In section 6.2.1 it was mentioned that in a polyphase aggregate, the textural relationship between different phases can be important in terms of ultrasonic velocity measurements. For example in a two-phase aggregate with a constant mineralogy and volume fraction, differences in contiguity and continuity of the phases may result in different velocity values. This hypothesis needs to be further explored. If it is correct then the laboratory velocity measurements should be always coupled with a detailed grain size, grain shape and grain continuity and contiguity analysis, in a theoretical framework that will realistically allow extrapolation from laboratory to field conditions.

References

Ahrens, T. J. (1995). Global Earth Physics, A hand book of physical constants, AGU Publication, Reference shelf 1

Allocca, J.A. & Stuarrt, A. (1984). Transducers, Theory & Applications, Reston publishing company Inc.

Anderson, D.L. (1989). Theory of the Earth. Blackwell Scientific Publications

Atkinson, B.K. (1989). Fracture Mechanics of Rock. Academic Press, Geology series

Banthia, B.S., King, M.S. & Fatt, I. (1965).Ultrasonic shear-wave velocities in rocks subjected to simulated overburden pressure and internal pore pressure. *Geophysics*, **30**, No.1, 117-121

Barruol, G. (1993). Petrophysique della Croute inferieure. PhD thesis, University of Montpellier. France.

Barruol, G. & Mainprice, D. (1993). A quantitative evaluation of the contribution of crustal rocks to the shear-wave splitting of teleseismic SKS waves. *Physics of the Earth & Planetary Interiors*, **78**, 281-300

Barruol, G., Mainprice, D., Kern, H., Blanquat, M. & Compte, P. (1993). 3D seismic study of a ductile shear zone from laboratory and petrofabric data (Saint Barthelemy Massif, Northern pyrenees, France). *Terra Nova*, **4**, 63-76

Behrendt, J.C., Hutchinson, D.R., Lee, M., Thornber, C.R. & Trehu, A. (1990). GLIMPCE, seismic reflection evidence of deep-crustal and upper-mantle intrusions and magmatic underplating associated with the Mid-continent Rift System of North America. In: J. Hlevent, D.M. Finlayson, C. Wright, J.C. Dooley and B.L.N. Kennett (Editors), Seismic Probing of Continents and Their Margins. *Tectonophysics*, **173**, 595-615

Berthe, D. & Choukroune, P. & Jegouzo, P. (1979). Orthogneiss, mylonite and non coaxial deformation of granites: the example of the South American Shear Zone. *J.Struct.Geol.*, **1**, No.1, 31-42

Bertolani, M. (1968). La petrografic della Valle Strona (Alpi Occidentali Italiane). Schweiz. Mineral. Petrogr. Mitt., 48, 695-732.

Biot, M. A. (1956).Theory of propagation of elastic wave in a fluid-saturated solid, 1, Low frequency range, *J. Acoust. Soc. Amer.*, **28**, 162

Birch, F. (1960).The velocity of compressional waves in rocks to 10 kilobars. *Geophys. Res. Let.* **65**, No. 4, 1083-1101

Boriani, A., Bigiggero, B. & Giobbi Mancini, E. (1977). Metamorphism, tectonic evolution and tentative stratigraphy of the "Serie dei Laghi". Geological map of the Verbania area, (northern Italy). *Mem. Soc. geol. It*, **32**, 26 pp

Boriani, A., Burlini, L. & Sacchi, R. (1990). The Cossato-Mergozzo-Brissago line (southern Alps, Italy) and their relationships with late Hercynian magmatic and metamorphic events. *Tectonophysics.*, **182**, 91-102

Brace, W.F. (1971). Resistivity of saturated crustal rocks to 40 km based on laboratory measurements. In: J.G. Heacock (Editor), Structure and physical properties of the Earth's crust. AGU. *Geophys. Monogr. Ser*, **14**, 206-210

Brandet, H. (1955). A study if the speed of sound in porous granular materials, *J. Appl. Mech.* **22**, 479

Brodie, K.H. (1980). Variations in mineral chemistry across a phlogopite peridotite shear zone. *J. Struct. Geol.*, **2**, 265-272

Broduie, K.H. (1981). Variation in amphibolite and plagioclase composition with deformation. In: The relationships between metamorphism and deformation; Editor Jones, M.E., *J. Struct. Geol*, **3**, 335

Brodie, K.H. & Rutter, E.H. (1987). Deep crustal extensional faulting in the Ivrea zone of northern Italy. *Tectonophysics*, **140**, 193-212

Brodie, K. H., Rutter, E.H. & Evans, P. (1992). On the structure of the Ivrea-Verbano Zone (northern Italy) and its implications for present day lower continental crust geometry. *Terra Nova*, **4**, 34-40

Burlini, L (1990). Variazioni delle propriet sismiche delle metapeliti di medio-alto grado in relazione alle caratteristiche petrologiche e microstrutturali. L'esepio dell'Ivrea-Verbano e Serie dei Laghi (N-Italia), Tesi di Laghi (N.Italy), Tesi di Dottorato, Universit' di Milano, 83 pp

Burlini, L & Fountain, D.M (1993). Seismic anisotropy of metapelites form the Ivrea-Verbano zone and Serie dei Laghi (N.Italy). *Phys Earth Planet. Inter*, **78**: 301-317

Cannon, W.F., Lee, M.W., Hinze, W.J., Schulz, K.J & Green, A.G. (1991). Deep crustal structure of the Precambrian basement beneath northern Lake Michigan, mid-continent North America. *Geology*, **19**, 207-210

Cao, S., Kennett, B.N. & Goleby, B.R. (1990). 3D isochronal modelling of reflection from the deep crust: application to reflection profiling in central Astralia. *Tectonophysics*, **173**, 119-128

Chamberlain, C.P, Zeitler, P.K, & Jan, M.Q. (1989). The dynamics of the suture between the Kohistan island arc and the Indian plate in the Himalaya of Pakistan. *J. Metamorphic. Geol*, **7**, 135-149

Chen, G; Spetzler,H; Getting, I. C; Yoneda, A. (1996). Selected elastic moduli & their temperature derivatives for olivine & garnet with different Mg(Mg+Fe) contents: Results from GHz ultrasonic interferometry. *Geophys,Res. Lett*, **23**.1, 5-8

Choukroune, P. Roure, F. Pinet, B. & ECORS Pyrenees team. (1990). Main results of the ECORS Pyrenees profile. *Tectonophysics*, **173**, 411-423

Christensen, N.I. (1965). Compressional wave velocity in metamorphic rocks at pressures to 10 K bar, *J. Geophys. Res.*, **70**, 6147-6164

Christensen, N.I.(1984). Pore pressure and oceanic crustal seismic structure. *Geophys.J.R.Astr.Soc.*, **79**, 411-423

Christensen,N.I.(1984). Pore pressure and ocianic crustal seismic structure . *Geophys. J.R. Astron. Soc*, **79**: 411-423

Christensen, N.I. (1986). The influence of pore pressure on oceanic crustal seismic velocities. *J.Geodynamics.*, **5**,45-48

Christensen, N.I. & Wang, H.F. (1985). The influence of pore pressure and confining pressure on dynamic elastic properties of Bera sandstone. *Geophysics.*, **50**, No. 2,

Christensen, N.I. (1989). Reflectivity and seismic properties of the deep continental crust. *J. Geophys. Res.*, **94**, 17,793-17,804

Christensen, N.I. & Fountain, D.M. (1975). Constituton of the lower continental crust. based on experimental studies of seimic velocities in granulite. *Geol. Soc. Am. Bull*, **86**, 227-236

Chroston, P.N. & Max,M.D.(1988). Seismic anisotropy in the mylonites: an example from the Mannin Thrust zone, southwest Connemara, Ireland, *Tectonophysics.*,**148**, 29-39

Clowes, R.M., Kanasewich, E.R. & Cumming, G.L. (1968). Deep crustal seismic reflections at near vertical incidence. *Geophysics.*, **33**, 441-451

Cowthorne, R. G (1973). Experimental and petrological studies on amphibolites in ultra-basic rocks: Unpub. Ph.D. thesis, Edinburgh, 69 p

Crampin, S. (1984).Effective elastic constants for wave propagation through cracked solids, *Geophysical Journal.*, **76**, 135-145

Dandekar,D. (1968).Variation in elastic constants of calcite with pressure. *American Geophysical Union*, **49**; 1, page 323

Duba,A., Huenges,E., Nover, G., will,G. & Jodicke,H. (1988), Impedance of black shale from Munsterland 1 borehole: an anomalous good conductor? *Geophys.J.*, **94**: 413-419

Elliott, S.E. & Wiley, B.F. (1975).Compressional velocity of partially saturated, unconsolidated sands. *Geophysics.*, **40**, No.6, 949-954

England, P. & Houseman, G. (1989). Extension during continental convergence with applications to the Tibetan Plateau. *J.Geophys. Res.* **94**,15,561-15,575

Ernst, W. G (1978).Petrochemical study of lherzolitic rocks from the western alps. *J. Petrol.*, **19**, 341-392

Evens, P.(1995) Structural geometry of parts of the Ivrea-Verbano zone Northern Italy. PhD thesis, Manchester University

Farmer, G.L. (1992). Magmas as travers of lower crustal composition: an isotopic approach. In: Continental Lower Crust, Fountain, D.M., Arculus, R., Kay, R.W., (Editors). Developments in Geotectonics. 23

Finlayson, S.M., Leven, J.H & Wake-Dyster, K.D. (1989). Large-scale lenticles in the lower crust under an intra-continental basin in eastern Australia. In: R.F. Mereu, S. Mereu & D.M. fountain (Editors), Propertiesand Processes of Earth's Lower Crust. *Am. Geophys. Union, Geophys. Monogr.*, **51**, 3-16

Fountain, D.M. (1976).The Ivrea-Verbano and Strona-Ceneri zones, Northern Italy: a cross-section of the continental crust-new evidence from seismic velocities of rock samples. *Tectonophysics.*, **33**, 145-165

Fountain, D.M. & Salisbury, M.H. (1981). Exposed cross-section, through the continental crust: implications for crustal, petrology & evolution. *Earth & Planetary Science letters.*, **5**, 263-277

Fountain, D. M, Percival, J. & salisbury, M. H. (1990). Exposed cross sections of the continental crust-synopsis. In: M. H. Salisbury and D. M. Fountain (Editors), Exposed

cross-Sections of the Continental Crust. Kluwer Academic Publ., Dordrecht, pp. 653-662

Fountain, D. M, & Hurich, C. A, & Smithson, S. B. (1984). Seismic reflectivity of mylonite zone in the crust, *Geology.*, **12**, 195-198

Frost, B.R., Frost, C. and Touret, J.L.R., (1989). Magmas as asource of heat and fluids in granulite metamorphism. In: D. Bridgwater (Editor), Fluid Movements-Element Transport and the Composition of the Deep Crust. Kluwer, Dordecht, 1-18

Furlong, K.P & Fountain, D.M (1986).Continental crustal underplating: Thermal considerations and seismic petrologic consequences. *J. Geophys. Res.*, **91**, 8285-8294

Fyfe,W., Price,R & Thompson,A., (1978). Fluids in the Earth's Crust. Elsevier, Amsterdam, 383 pp

Glover, P. W & Vine, F. J. (1994). Electrical conductivity of the continental crust. *Geophysical Research Letters.* **21**; 22, 2357-2360

Goleby, B.R., Kennett, B.L., Wright, C., Shaw, R.D. & Lambeck, K. (1990). Seismic reflection profiling in the Proterozoic arunta Block, central Australia: processing for testing models of tectonics evolution. In: J. HLeven, D.M. Finlayson, C. Wright, J.C. Dooley and B.L.N. Kennett (Editors), seismic Probing of Continents and Their Margines. *Tectonophysics*, **173**, 257-268.

Goodwin, E.B. & McCarthy, J.C. (1990). Composition of the lower crust in west central arizona from three-component seismic data. *J. Geophys. Res.*, **95**: 20,097-20,109

Green, A., Mikereit, B., Percival, J., Davidson, A., Parrish, R., Cook, F., Geis, W., Cannon, W., Hutchinson, D., west, G. and Clowes, R. (1990). Origin of deep crustal reflections: seismic profiling across high-grad metamorphic terranes in Canada. In: J.H. Leven, D.M. Finlayson, C. Wright, J.C. Continents and their Margines. *Tectonophysics.*, **173**, 627-638

Griffin, W.L. & O'Reilly, S.Y.(1986).The lower crust in eastern Australia: xenolith evidence. In: J.B. Dawson, D.A. Carswell, J. Hall, and k.H. wedepohl (Editors), The nature of the lower continental crust. *Geol. Soc. Spec. Publ.*, **24**: 363-374

Hall, L.D., & Thompson, G.A, (1982). The seismic reflection character of the continental Mohorovicic discontinuity. *J. Geophys. Res.*, **87**, 4625-4635

Hall, J. (1986). Physical properties of layered rocks in deep continental crust, In: J. B. Dawson, D. A. Carswell, J. Hall and K. H. Wedepohl (Editors), Nature of the lower continental crust. *Geol. soc. London, Spec. Publ.*, **21**, 51-62

Handy, M.R (1986). The structure and rheological evolution of the Pogallo Fault Zone; Deep crustal dislocation in the southern Alps of northwestern Italy (Prov. Novara). Unpubl. Diss., Univ. Basel, 327 pp.

Holbrook, W.S., Mooney,W.D & Christensen,N.I. (1992). The seismic velocity structure of the deep continental crust, In: Fountain.D.M, Arculus,R & Kay,R,W (Editors), Continental lower crust, *Developments in geotechnics.*, **23**, 1-34

Hunziker, J.C. & Zingg, A. (1980). Lower Paleozoic amphibolite to granulite facies metamorphism in the Ivrea zone (Southern Alps, N. Italy). Schweiz. *Mineral. Petrogr. Mitt.*, 60, 181-213.

Hurich, C.A. & Smithson, S.B.(1987). Compressional variation and the origin of deep crustal reflection. *Earth.Plan.Science.let.*, **85**, 416-426

Hyndman, R.D. and Hyndman, D.W., 1968. Water saturation and high electrical conductivity in the lower crus. *Earth Planet.Sci.Lett.*, **4**, 427-432

Jeanloz, R & Knittle, E. (1986). Reduction of mantle and core properties to a standard state of adiabatic decompression. in: *Chemistry and Physics of Terrestrial Planets* (S.K. Saxena, ed.), 275-305, Springer-Verlag, Berlin.

Johnson, P.A. & Hopson, T.M. & Shankland,T.J. (1992).Frequency-domain travel time (FDTT) measurements of ultrasonic waves by use of linear and nonlinear sources. *J.Acoust.Soc.Am.*, **92**, No. 52

Johnson,P.A. & Migliori, A. & Shankland,T.J. (1990).Continuous wave phase detection for probing nonlinear elastic wave interactions in rocks. *J.Acoust.Soc.Am.* **89**, No. 2

Johnson, D.H & Toksoz, M.N. (1980), Ultrasonic P and S wave attenuations in dry and saturated rocks under pressure. *J.Geophys.Res*, **85**, No. B2, 925-936

Jones, A.G. (1987). MT and reflection: an essential combination. *Geophys.J.R.Astron. Soc*, **89**, 7-18

Jones, A.G. (1992). Electrical conductivity of the continental lower crust. In: Continental Lower Crust, Fountain, D.M., Arculus, R., Kay, R.W., (Editors). Developments in Geotectonics. **23**

Jones, A.G & Craven, J.A. (1990). The North American Central Plains conductivity anomaly and its correlation with gravity, magnetic, seismic and heat flow data in the Province of Saskatchewan. *Phys. Earth Planet. Inter.*, **60**, 169-194

Jones, A,G and Garland,G.D., 1984. A magnetotelluric investigationunder the Williston Basin"by J.M.Maidens and K.V.Paulson. *Can.J.Earth Sci.*, **25**, 1132-1139

Jones, A,G & Hutton, V.R.R. (1979). Amuli-station magnetotelluric study in sothern scotland, II. Monte Carlo inversion of the data and its geophysicaland tectonic implications. *Geophys. J.R.Astr.Sco.*, **56**,351-368

Juhlin, C. (1990). Interpretation of the reflections in the Siljan Ring area based on results frim the Gravberg-1 borehole. In: J.H. Leven, D.M. Finlayson, C. Wright, J.C. Continents and their Margines. *Tectonophysics,* **173**, 345-360.

Kanasewich, E.R. & Cummings, G.L. (1965). Near vertical-incidence seismic reflections from the "conrad" discontinuity. *J. Geophys. Res.*, **70**:3441-3446.

Kazuhiko, Ito. (1990). Effect of H_2O on elastic wave velocities in ultrabasic rocks at 900°C under 1 GPa. *Phys. earth.Plan.Inter.*, **61**,260-268

Kern, H. & Richter.A, (1981), Temperature deratives of compressional and shear wave velocities in crustal and mantle rocks at 6 kbar confining pressure, *J. Geophys.* **49**, 47-56.

Kern, H. (1982). P and S wave velocities in crustal and mantle rocks under the simultaneous action of high confining pressure and high temperature and the effect of the rock microstructure, in High Pressure Research in Geoscience, edited by W. Schreyer, pp. 15-45, Schwizerbar'sche Verlagsbuchandlung, Stuttgart.

Kern, H. & Schenk, V. (1988). A model of velocity structure beneath Calabria southern Italy, based on laboratory data. *Earth. Plan. Sci. let.*, **87**, 325-337

Kern, H, & Tubia,J.M. (1993). Pressure and temperature dependence of P- and S-wave velocities, seismic anisotropy and density of sheared rocks from the sierra Alpujata massif (Ronda peridotites, Southern spain). *Earth.plan.Sci.let.*, **119**, 191-205

Kern, H. & Wenk,H.R. (1990). Fabric-related velocity anisotropy and shear wave splitting in rocks from the Santa Rosa Mylonite zone, California. *J.Geophys.Res.*, **95**, No.B7, 11213-11223

King,M.S. & Fatt,I. (1962). Ultrasonic shear-wave velocity in rocks subjected to simulated overburden pressure. *Geophysics.*, **27**, No, 5. 520-598

Kozlovsky, Y.A, 1984, The world deepest well, *Sci.Am..*, **251**, 106-112

Kolsky, H. (1963).Stress waves in solids, p. 200. Dover, New York

Krutikhovskaya, Z.A. & Pashkevich, I.K. (1977).Magnetic model for the Earth's crust under the Ukrainian shield. *Can.J.Earth Sci .*, **14**, 2718-2728

Krutikhovskaya, Z.A. & Pashkevich, I.K. (1979).Long-wavelength magnetic anomalies as a source of information about deep crustal structurs. *J.Geophysics.*, **46**, 301-317

Kusznir, N.J. & Park, R. G. (1986) Continental lithoshpere strength: the critical role of lower crustal deformation. In: J. B. Dawson, D. A. Carswell, J. Hall and K. H. Wedepohl (Editors). The nature of the lower Continental crust. *Geol. Soc., Spec. Publ.*, **24**, 79-93

Le Gall, B. (1990). Evidence of an imbricate crustal thrust belt in the southern British Variscides: Contributions of Southwestern Approaches Traverse (SWAT).deep seismic reflection profiling recorded through the English Channel and the Celtic Sea. *Tectonics.*, **9**: 283-302

Lensch, G & Rost, F. (1972).Kelyphitperidotite in der mittleren Ivrea zone zwischen Val d'Ossola und Val Strona. Ein Beitrag zur herkunftstiefe der Ultramafitite der Ivrea zone. *Schweiz. Mineral .Petrogr. Mitt.*, **52**, 237-250

Lueschen, E., and fourtheen others, (1987). Near-vertical and wide-angle seismic survey in the Black Forest, SW Germany. *J. Geophys.*, **62**, 1-30

McCarthy,J. & Thompson,G.A., (1988). Seismic imaging of extended crust with emphasis on the western United States. *Geol.Soc. Am. Bull.*, **100**,1361-1374

McDonough, D.T & Fountain, D. M. (1988). Reflection characteristics of a mylonite zone based on compressional wave velocities of rock samples. *Geophys. J. R. Astron. Soc*, **93**, 547-558

Mainprice, D. (1990). A Fortran program to calculate seismic anisotropy from the Lattice prefrred orientation of minerals, *Computer & Geosciences*, **16**, 385-393

Mainprice, D. & Silver, P.G. (1992). Interpretation of SKS-waves using samples from the subcontinental lithosphere. *Physics of the Earth and Planetary Interior.*, **78**, 257-280

Mainprice,D.& Casey,M. & Schmid,S. (1990). The seismic properties of Alpin calcite and qurtz mylonites determined from the orientation distribution function. *Mem. Soc. Geol. France*, **156**, *85-95*

Mainprice,D. & Humbert,M & Wagner, F. (1990).Phase transformations and inherited lattice preferred orientations; implications for seismic properties.*Tectonophysics*, **180**, 213-228

Matthews, D. H. (1986).Seismic reflections from the lower crust around Britain. In: J.B Dawson, D.A. Carswell, J.Hall & K.H.Wedepohl (Editors), Nature of the Lower Continental Crust, *Geol.Soc.London, Spec.Publ.*, **24**, Blackwall, Oxford, pp.11-22

Meissner, R. (1986).The continental crust, a Geophysical Approch. Academic Press, London, 426 pp.

Meissner, R . & Sadowiak, P. (1990).Comparative investigations of continental reflectivity, *Tectonophysics*, **173**, 199-206

Mooney, W. D. & Brocher, T.N. (1987). Coincident seimic reflection and refraction measurements of the continental lithosphere; a global review. *Rev. Geophys.*, **25**, 723-742

Moss, F.J. (1962). Amadeus Basin (southern margin).seismic survey, Northern territory and Queensland, 1965. *Bur. Mineral. Res. Aust.*, Record 1966/28

Newton,R.C. & Perkins, D. (1982). Thermodynamic caliberation of geobarometers based on the assemblage garnet-plagioclase-orthopyroxene (clinopyroxene)-quartz. *Am. Mineral.*, **67**. 203-222

Olhoeft, G.R. (1981).Electrical properties of granit with implications for the lower crust. *J. Geophys. Res.*, **86**, 931-936

Perls, T.A. (1952). Electrical noise from instroment cables subjected to shouk and vibration. *J.Appl.Physics.*, **23**, No 6, 674-680

Percival, J.A. Parrish,R.R. Krogh, T.E. & Peterman, Z.E. (1988). When did the Kapuskasing zone come up? *KSZ Lithoprobe workshop, Univ, Toronto*, 43-47

Percival, J.A. (1989). Granulite terranes and the lower crust of the northwestern margin of the superior province: Implications for its tectonic evolution. *J.Geol.*, **94**, 381-394.

Percival,J.A. (1992).Exposed crustal cross sections as windows on the lower crust. In: Fountain.D.M, Arculus,R & Kay,R,W (Editors), Continental lower crust, *Developments in geotechnics*, **23**, 317-350

Percival, J. A., Fountain, D.M. & Salisbury, M.H. (1992). Exposed crustal cross sections as windows on the lower crust. In: Continental Lower Crust, Fountain, D.M., Arculus, R., Kay, R.W., (Editors). Developments in Geotectonics. 23

Pfiffner, O.A., Frei. W., Finckh, and Valasek, P. (1988).Deep seismic reflection profiling in the Swiss Alps: Explosion seismology results for line NFP 20-East, *Geology*, **16**, 987-990

Pinet, B. Colletta, B. (1990). Probing into extensional sedimentary basins: comparison of recent dat and derivation of tentative models. *Tectonophysics*, **173**, 185-197

Popp, T & Kern, H. (1993). Thermal dehydration reactions characterised by combined measurements of electrical conductivity and elastic wave velocities. *Earth.Plan.Sci. let.*, **120**, 43-57

Quick, J.E., Sinigoi, S. & Mayer, A. (1994). Emplacement dynamics of a large mafic intrusion in the lower crust, Ivrea-Verbano zone, northern Italy. *J.Geophys. Res.*, **99**, No 21,599-21,573

Quick, J.E., Sinigoi, S. & Mayer, A. (1995). Emplacement of mantle peridotite in the lower continental crust, Ivrea-Verbano zone, northwest Italy, *Geology.*, **23**, No 8, 739-742

Reston, T.J. (1987). Spatial interference, reflection character and the structure of the lower crust under extension-Results from 2-D seismic modelling. *Ann. Geophys.*, **5B**, 339-348

Reston, T.J. (1988). Shear in the lower crust during extension: not so pure and simple. *Geophysics.*, **173**, 175-183

Rey, P.F. & Fountain,D.M. & Clement,W.P. (11994). P wave velocity across a noncoaxial ductile shear zone and its associated strain gradient: Consequences for upper crustal reflectivity. *J.Geophys.Res.*, **99**, No. B3, 4533-4548

Ritz, M. (1983). Use of the magnetotelluric method for a better undrestanding of the West African Shield., *J.Geophys.Res.*, **88**, No 10, 625-633

Rivalenti, G. (1979). Guide to the excursion in the Balmuccia zone, Sesia Valley, Ivrea-Verbano Complex. *Mem. Sci.Geol.*, **33**, 3-9

Rivalenti, G., Garuti, G., Rossi, A., Siena, F. & Sinigoi, S. (1981). Existance of different peridotite types and of a layered ignious complex in the Ivrea zone of the western Alps. J. Petrol., 22, 127-153.

Roermund, H.V. & Lister, G.S. & Williams,P.F.(1979).Progresive development of quartz fabric in a shear zone from Monte Mucrone, Sesia-Lanzo Zone, Italian Alps. *J.Stract.Geol.*, **1**, No.1, 43-52

Rudnick, R.L. (1996). Making continental crust., *Nature.* Vol. **378**, 7. 571-578.

Rudnick, R.L. & Fountain, D.M. (1995). Rev.Geophys., **33**, 267-309.

Rutter,E.H, & Brodie,K.H. (1989).Some geophysical implication of the deformation and metamorphism of the Ivrea Zone, northern Italy. *Tectonophysics.* **182**, 147-160

Rutter, E.H. & Brodie, K.H. (1992). Rheology of the lower crust. In : Continental Lower Crust, Fountain, D.M., Arculus, R., Kay, R.W., (Editors). Developments in Geotectonics. 23.

Rutter, E.H & Brodie, K.H. & Evens, P.J. (1993). Structural geometry, lower crustal magmatic underplating and lithospheric streching in the Ivrea-Verbano zone, northen Italy. *J. struct. Geol.*, **15**, 647-662

Schmid, R. & Wood, B. J. (1976). Phase relationships in granulite metapelites from the Ivrea-Verbano zone (N. Italy). *Contrib. Mineral. Petrol.*, **54**, 255-279.

Schmid, R. (1967). Zur petrographic und strukur der zone Ivrea-Verbano zwischen Valle d'Ossola und Valle Grande. *Schweiz. Mineral. Petrogr. Mitt*, **47**, 935-1117.

Schmid, S.M., Zingg. A. & Handy, M. R. (1987). The kinematics of movements along the Insubric Line and the emplacement of the Ivrea zone. *J. Struc. Geol.*, **135**, 47-66

Silk, M.G & Maurice, G. (1984).Ultrasonic transducer for non-distructyive testing

Shankland, T.J. & Johnson,P.A. & Hopson,R.M. (1993).Elastic wave attenuation and velocity of Berea sandstone measured in the frequency domain. *Geophys. Res. Let..*, **20**, No. 5, 391-394

Shaw, D.M., Cramer, J.J., Higgins, M. D. & Truscott, M. G. (1986). In: Dawson, J.B., Carswell, D.A, Hall, J. & Wedepohl, K.H. (Editors). The nature of the lower Continental crust, *Geol. Soc. London.* 257-282.

Shervais, J.W. (1979). Thermal emplacement model for the Alpine lherzolite massif at Balmuccia, Italy. *J. Petrol.*, **20**, 795-820.

Shive, P.N; Blakely,R.J; Frost, B. R & Fountain, D.M. (1992). Magnetic properties of the lower continental crust. In: Fountain.D.M, Arculus,R & Kay,R,W (Editors), Continental lower crust, *Developments in geotechnics*, **23**, 145-170

Sill, J.D. & Tarney, J. (1984). Petrogenesis and tectonic significance of amphibolites interlayered with metasedimentary gneisses in the Ivrea zone, S.alps, N. Italy. *Tectonophys.*, **107**, 187-206.

Sinigoi, S; Antonini, P; Demarchi, G; Longinelli, A; Mazzucchelli, M; Nergrini, L. & Rivalenti, G. (1991). Interactions of the mantle and crustal magmas in the southern part of the Ivrea Zone (Italy). *Contrib. Mineral. Petrol.*, **108**, 385-395.

Sinigoi, S; Quick, J. E; Clemens-Knott, D; Mayer, A; Demarchi, G., Mazzucchelli, M., Negrini, L. & Rivalenti, G. (1994). Chemical evolution of a large mafic intrusion in the lower crust, Ivrea-Verbano Zone, northen Italy. *J. Geophys. Res.*, **99**, 21,575-21,590

Sinigoi, S; Quick, J.E; Mayer, A; Demarchi,G. (1995). Density controlled assimilation of underplated crust, Ivrea-Verbano Zone, Italy. *Earth & Planetray Science Letters.* **129**; 1-4, p 183-191

Siegesmund,S; Takeshita,T. & Kern,H. (1989).Anisotropy of Vp and Vs in an amphibolite of the deeper crust and its relationship to mineralogical, microstructural and textural characteristics of the rock. *Tectonophysics*, **157**, 25-38

Smith, J. (1995) The relationship between structure and metamorphism of the Ivrea-Verbano Zone, Northern Italy. PhD thesis , Manchester University

Smithson, S. B. (1986). A physical model of the lower crust from North America based on seismic reflection data. In: J. B. Dawson (Editor), The nature of the lower continental crust. Geol. Soc. London, *Geol. Soc. Spec. Publ*, **25**, 23-34

Spencer,J.W & Nur, A. M (1976). The effect of pressure, temperature and pore water on velocities in Westerly Granite. *J.Geophys.Res.*, **81**, No.5, 899-904

Steck, A. & Tieche, J. C (1976). Carte geologique de l'antiforme peridotitique de Finero avec des observations sur les phases de deformation et de recristallisation. *Schweiz, miner, petrogr. Mitt.*, **56**, 501-512

Tatsumi, Y; Ito, K. & Goto,A. (1994). Elastic wave velocities in isochemical granulite and amphibolite: Origin of low-velocity layer at the slab/mantle wedge interface. *Geophys. Rse. Let.*, **21**, No.1, 17-20

Taylor, S. R. & McLennan, S. M. (1985). The Continental Crust: its Composition and Evolution. Blackwell, Oxford.

Timur, A. (1968). Velocity of compressional waves in porous media at permafrost temperatures. *Geophysics*, **33**, No.4, 581-595

Todd, T. & Simmons,G. (1972).Effect of pore pressure on the velocity of compressional waves in low-porosity rocks. *J.Geopys.Res.* **77**, No.20, pp 3731-3743

Valley, J. W. (1986). Stable isotope geochemistry of metamorphic rocks. In : J. W. Valley, H.P. Taylor & J. R. O'Neil (Editors). Stable isotops at high temperature geological processes. *Mineral. Soc. Am. Rev. Mineral.*, **16**: 445-489

Valasek, P. A., Snoke, A.W., Hurich, C. A. & Smithson, S. B. (1989). Nature and origin of seismic reflection fabric, Ruby- East Humboldt metamorphic core complex, Nevada. *Tectonics*, **8**. 2, **391-415.**

Wagner, J.J., Klingele, E. & Mage, R. (1984): Regional geomagnetic study of the southern border of the western Alps- the Ivrea body. Mater. Geol. Suisse. *Geophys.*, **21**, 21-29

Wagner, J.J. & Mueller, S. (1984). Geophysical studies of the Ivrea Zone - a review. *Mater. Geol. Swisse Geophys*, **21**: 13-19.

Warner, M. R. (1990a). Seismic reflections from the lower continental crust: free fluids. *J. Geophys. Res.*, **94**, 2850-2855

Warner, M. R. (1990b). Basalts, water, or shear zone in southern California. *J.Geophys. Res.*, **94**, 2989-3005

Warner, M. R. (1990c). Absolute reflection coefficient from deep seismic reflections. *Tectonophysics.*, **173**, 15-23.

Weaver, E.B & Tarney, J. (1984).Major and trace element composition of the continental lithosphere. In: H.N. Bollack and V. R. Murthy (Editors), *Phys. Chem. Earth*, **17**, 39-68

Wenzel, F., Sandmeier,K.J., & Walde,W. (1987). Properties of the lower crust from modeling refraction and reflection data, *J.Geophys. Res.*, **92**, 11,575-11,583

Wood, B.J. (1987).Thermodynamics of multicomponent systems containing several solutions. In: I.S.E. Carmichael and H.P. Eugster (Editors), Thermodynamic Modelling of Geological Materials: Mineral, Fluieds and Metals. *Mineral. Soc. Am*, 71-95

Wu,T. C. (1995).Anisotropic thermal expantion of calcite at high pressure; an in situ x-ray diffrection study in a hydrothermal diamond-anvil cell. *American Mineralogist.* **80**; 9-10, 941-946

Zappone, A. (1992). Relazioni tra la petrologia della rosta profonda e le velocita'sismiche: applicazioni alle alpi occidentali. Tesi di Dottorato, Universit' di Milano

Zingg. A. (1983). The Ivrea & Strona-Ceneri zones (southern Alps, Ticino & N, Italy)- a review. *Schweiz. Mineral. Petrogr. Mitt.*, **63**, 361-392.

Zingg, A. (1980). Regional metamorphism of the Ivrea zone (S. Alps, N. Italy): field and microscopic investigations. *Schweiz. Mineral. Petrogr. Mitt.*, **60**, 153-179.

Zingg, A. (1990). The Ivrea crustal cross-section (Northern Italy and Southern Switzerland). In: Salisbury, M, H, & Fountain, D.M. (eds), Exposed Cross-sections of the Continental Crust. NATO ASI Series C: *Mathematical and Physical Sciences*, **317**,1-19.

Zingg, A., Handy, M.R., Hunziker, J.C. & Schmid, S.M. (1990).Tectonometamorphic history of the Ivrea-Verbano Zone and its relationship to the crustal evolution of the Southern Alps. *Tectonophys.*, **182**, 169-192

APPENDICES

Appendix 1 :

* **List of samples**
* **Sample location**
* **Location map**

Sample No	Lithology / Location
	Peridotite / Balmuccia
S01A	
S01B	
S02C	
S02A	
S3A	
	Px Stronalite / Isola
S4A	
S4B	
S4C	
S5A	
S6A	
S7A	
	Kinzigite / Strona
S8A	
S9A	
S9B	
S9C	
S10A	
S10B	
	Gneiss Minuti / Nivetta/
S11A	
S11B	
S11C	
S12A	
S13B	
S14B	
	Amphibolite / Falmetta /
S15A	
S15B	
S15C	
S16A	
S16B	
S16C	
S16C`	
S17A	
S17B	
S18A	
S18B	
S18C	
	Stronolite / Val Dossola /
S19A	
S19B	
S19C	
S20A	
S21A	
	Stronolite Mylonite / Val Dossola /
S22A	
S23A	
	Pyroxenite / Reo del ponte
S24A	
S24B	
S24C	
S24A`	
	Meta Gabbro / Reo del ponte
S26A	
S26B	
S26C	
S27A	
S27C	
S27A`	

Sample No	Lithology / Location
S27A``	
S28B	
S28C	
S28A`	
	Mylonite Metabasic / Reo del ponte
S29A	
S29B	
S29C	
S29C`	
	Px Granulite / Reo del ponte
S30A	
S30B	
S30C	
S30A`	
	Garnet Granulite / River Cort
S31A	
S31B	
S31C	
S31C`	
S31A`	
	Peridotite / Permosella
S32A	
S32B	
S32C	
S32A`	
S32B`	
S32C`	
	Amphibolite / Nibbio
S35A	
S35B	
S35C	
S35C`	
S35C``	
S36A	
S36A`	
S36A``	
S36A```	
S37A	
S37A`	
	Granulite / Sesia
S38A	
S38A``	
S38B	
S38C	
S38A```	
S39A	
S39B	
S39C	
S39D	
S40A	
S40B	
S40C	
S40A`	
S40A``	
S40C	
S40A`	
S40A``	
	Diorite / Sesia
S41A	
S41B	

Sample No	Lithology / Location
S41C	
S42A	
S42B	
S42C	
	Xenolith / sesia
S43A	
S43A`	
S43A``	
S43B	
S43A```	
S44A	
S45A	
S46A	
S47A	
S48A	
	Amphibolite / Teglia
S50A	
S50B	
S50A`	
S50C	
S51A	
S51B	
S51C	
S51A`	
	Marble Teglia
S52A	
S52A`	
S52A``	
S52B	
S52C	
S52C`	
S52B`	
S52B``	
Granit	
S53A	
S53A`	
S53B	
S53C	
S54A	
S54B	
S54B`	
S54C	
S55B	
S56A	
S56A`	
S56B	
S56C	
S56C`	
S56A``	
	Schist / Cannobino
S57A	
S57A`	
S57B	
S57B`	
	Amphibolite / Cannobino
S58A	
S58A`	
S58C	
S58A``	
S58A```	
	Ceneri Gniess / Val Grande

Sample No	Lithology / Location
S59A	
S59A`	
S59B	
S59C	
S59A``	
S59C`	
PERIDOTITE (FINERO)	
S60A	
S60B	
S60C	
S60A`	
S60A``	
PERIDOTITE MYLONITE (FINERO)	
S61A	
S61A`	
S61B	
S61C	
S61A``	
S61B`	
S61B``	
S61B```	
GABBRO (MASTOLLONE RIVER; MAIN GABBRO)	
S62A	
S62A`	
S62A``	
S62B	
S62C	
S62A```	
2 PX GRANULITE (MASTOLLONE ; GARNET POOR)	
S63A	
S63B	
S63A`	
S63A``	
S63C	
GARNET GRANULITE (MASTOLLONE; PX LAYER)	
S64A	
S64B	
S65A	
S65B	
S65B`	
S65A`	
S65C	
S65C`	
S65A``	
S65A```	
PROTOMYLONITE (GULA MYLONITE)	
S66A	
S66B	
S66B`	
S66C	
S66A`	
(GULA VILLAGE)	
S67A	
S67B	
S67C	
S67B`	
S67C`	
S67C``	
S67A`	
S67A``	
S67B``	
S67B```	

Sample No	Lithology / Location
S67A```	
GARNET GRANULITE (VALL MASTELLONA)	
S68A	
S68A`	
S68A``	
2 PX GRANULITE UNDEFORMED (GULA VILLAG	
S69A	
S69B	
S69A`	
S69B`	
S69C	
S69C`	
S70A	
S70A`	
S70B	
S70B`	
S70B``	
META GABBRO (MASTELLONE)	
S71A	
S71B	
S71B`	
S71A`	
S71B``	
S71C	
S71A``	
STRONOLITE (VAL SABBIA)	
S72A	
S72A`	
S72A``	
S72B	
S72B`	
S72C	
S72A```	
S72A````	
S72B``	
S73A	
S73A`	
S73B	
S73C	
S73A``	
S73C`	
S73C``	
S73A```	
S73B`	
S73B``	
S73B```	
META SEDIMENTS (ISOLA)	
S74A	
S74B	
S74C	
S74C`	
S74A`	
S74C``	
S74B`	
S74A``	
S74A```	
DIORITE (VAL MASTELLONA)	
S75A	
S75B	
S75C	
S75A`	

Sample No	Lithology / Location
GABBRO DIORITE	
S`75A	
S`75B	
S`75B`	
S`75A`	
S`75A``	
S`75A```	
S`75C	
S`75C`	
S`75C``	
S`75C```	
S76A	
S76A`	
S76A``	
S76A```	
STROLITE MYLONE	(PERMOSELA)
S77A	
S77A`	
S77A``	
S77A```	
S77C	
S77C`	
S77C``	
S78B	
S78B`	
S79A	
S79A`	
S79A``	
S79B	
S79B`	
S79C	
S79C`	
S79C``	
S80A	
S80A`	
S81A	
S81A`	
S82A	
S82A`	
S83A	
META BASIC	(POINT 363)
S84A	
S84A`	
S84A``	
S84A```	
S84B	
S84B`	
S84B``	
S84C	
S84C`	
S85A	
S85A`	
2 PX GRANULITE (ANZOLA)	
S87A	
S87A`	
S87B	
S87B`	
S87C	
S87C`	
S87C``	

Sample No	Lithology / Location
	META BASIC (FINERO- CANNOBINO)
S88A	
S88A`	
S88A``	
S88B	
S88B`	
S88B``	
S88C	
S88C`	
	HORNBLEND PERIDOTITE
S89A	
S89A`	
S89B	
S89B`	
S89B``	
S89C	
S89C`	
S90A	
S90A`	
S90A``	
S90C	
S90C`	
S91C	
S91C`	
S91C``	
S91A	
S91A`	
	GRANITE (GRAVELLONA)
	AT TWO ORTHGONAL DIRECTIONS
S92	
S93	
S94	
S95	
S96	
S97	
S98	
	SCHIST DE LUGI (UNCHIO)
S99A	
S99A`	
S99A``	
S99B	
S99B`	
S99C	
S99C`	
S100C	
S100C`	
S101A	
S102A`	
	ORTHOGNEISS
S103B	
S103B`	
S103A	
S103A`	
S104A	
S105A	
S106A	
S107A	
S107A`	
S107A``	
	META BASIC (FINERO)
S108A	
S108A`	

Sample No	Lithology / Location
S109A	
S109A`	
S110B	
S111A	
S111A`	
S111B	
S112D	
S113A	
S114A	
S114A`	
S114A``	
S114B	
S114B`	
S114C	
S114C`	
S115A	
S115C	
S115C`	
S116A	
S116A`	
S116B	
S117B	
S117B`	
S118A	
S118C	
S118C`	
S119A	
S119B	
S119C	
S120A	
S120A`	
S120B	
S120B`	
S120B``	
S121B	
S121B`	
	ORTHOGNEISS (PIZZO DELL`OHO)
S122B	
S122B`	
S122B``	
S123A	
S123B	
S123C	
S123C`	
S123A`	
S123A``	
S123A```	
S123B`	
S123B``	
S123B```	
S123A`````	
	ORTHOGNEISS HIGHLY DEFORMED (VAL POGALLO)
S124A	
S124B	
S124C	
S124A`	
S124A``	
S124A```	
S124C`	
S124B`	
S124B``	

Sample No	Lithology / Location
	GNEISS MINNOTI (VAL POGALLO)
S125B	
S125B`	
S125B``	
S125C	
S125C`	
S125C``	
S125A	
S125A`	
S125A``	
S125A```	
S125A````	
	IN THE CHARNACAITE (VAL SESSERA)
S126A	
S126A`	
S126A``	
S126B	
S126B`	
S126C	
S126C`	
S126C``	
S126A```	
S127A	
S127A`	
S127B	
S127B`	
S127C	
S127C`	
S128A	
S128A`	
S128A``	
S128A````	
S128B	
S128B`	
S128C	
S128C`	
S128C``	
S129A	
S129A`	
S129B	
S129B`	
S129C	
S129C`	
	MIGMATITE
S131A	
S131A`	
S131A``	
S131A```	
S131B	
S133A	
S133B	
S133B`	
S133B``	
S133A`	
S133A``	
S134B	
S134A	
S134A`	
S135A	
S135A`	
S135B	
S135B`	
S135B``	
S135A``	
S135B```	
S135A```	
	KINZIGITE (STRONA VAL) INTO THE MICA RICH
S136A	
S136A`	
S136A``	
S136A```	
S136A````	
S136A`````	
S136B	
S136B`	
S136B``	
S136B```	
S136B````	
	INTO THE QUARTZ RICH
S137A	
S137A`	
S137B	
S137B`	
S137B``	
	PROTOLITH (GULA MYLONIETE)
S138A	
S138A`	
S138B	
S138B`	
S138B``	
S138B```	
S138C	
S138C`	
S138C``	
S138C```	
	METABASIC
S139A	
S139A`	
S140A	
S140A`	
S140B	
S141A	
S141A`	
S142A	
S143A	
S143A`	
S145A	
S146A	
S147A	
S147A`	
S147A``	
S147A```	
S148A	
S148A`	
S148A``	
	POGALLO
S149A	MYLONITE
S149A`	
S149B	
S149B`	
S149C	

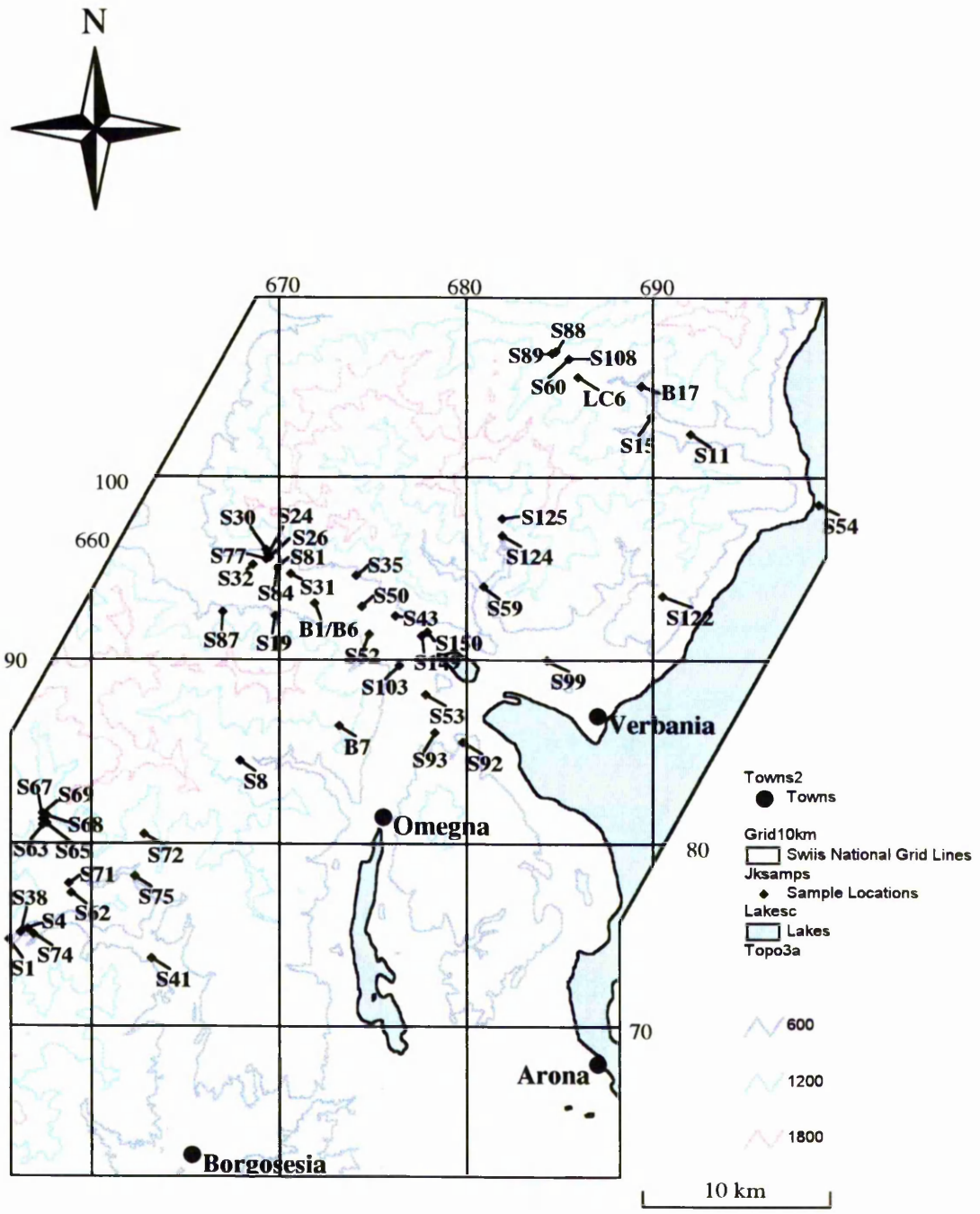

Sample location map

Appendix 2:

Listing of the computer program used for data logging and processing of seismic waveforms.

```
 10 REM*****"SEISMIC PROGRAM ***** LAST MODEFIED 20 JULY 1994 ***************

 20 REM******IEEE CONNECTION FOR DOWN LOADING DATA FROM LeCroy 9310*******

 30 REM***SERIAL PORT FOR COMUNICATION WITH FUNCTION GENERATOR**********
 40 REM****"SERIAL PORT FOR PRESSURE INDICATOR CONNECTOR*****************
 50 REM*********"********B.B.C BASIC PROGRAM***********"*********************

 60 REM*****************BY JALAL. KHAZANEHDARI*******************************
 70 MODE 20:GOTO 8200
 80 :
 90 DEF PROCdata
100 FOR n=1 TO nn2%
110 datag(n)=0:dataf(n)=0
120 NEXT n
130 dt=1:k%=1
140 fn=50:K=0
150 PROCwipe(0,5):PRINT TAB(0,2)"GENERATE SIN WAVES"
160 PRINT TAB(0,3)"TYPE THE FIRST FREQUENCY";:INPUT f
170 REMPRINT TAB(0,5)"TYPE THE SECAND FREQUENCY";:INPUT f2
180 f=f/(fn*2)
190 REMf2=f2/(fn*2)
200 FOR n%=1 TO nn2%
210 datag(n%)=0
220 NEXT n%
230 REMPRINT"THERE ARE NN2 REAL AND IMAGENERY NUMBERS IN ARRAY , HOW
MANY DO YOU WANT TO FILL A TO b"
240 REMNPUT NY,NX
250 FOR n%=1 TO nn2% STEP 2
260 datag(n%)=100*SIN(2*pi*f*n%*dt)
270 REMdatag(n%)=datag(n%)+30*SIN(2*pi*(0.3*f2)*k%*dt)
280 k%=k%+1:PRINT k%,datag(n%)
290 NEXT n%
300 ENDPROC
310 REM*****************************************FAST FOURIER
TRANSFORM************************
320 DEF PROCacfft
330 PROCattension:PRINT TAB(65,10)"WAIT PLEASE"
340 :
350 n%=2*nn%
360 j%=1
370 FOR ii%=1 TO nn%
380 i%=2*ii%-1
390 IF j%>i% THEN GOTO 400 ELSE GOTO 470
400 tempr=datag(j%)
410 tempi=datag(j%+1)
420 datag(j%)=datag(i%)
430 :
440 datag(j%+1)=datag(i%+1)
450 datag(i%)=tempr
460 datag(i%+1)=tempi
470 :
480 m%=n% DIV 2
490 WHILE (m%>=2) AND (j%>m%)
500 j%=j%-m%
```

```
510 m%=m% DIV 2
520 ENDWHILE
530 j%=j%+m%
540 NEXT ii%
550 mmax%=2
560 WHILE (n%>mmax%)
570 istep%=2*mmax%
580 theta=6.28318530717959/(ising*mmax%)
590 wpr=-2.0*(SIN(0.5*theta)*SIN(0.5*theta))
600 wpi=SIN(theta)
610 wr=1.0
620 wi=0.0
630 FOR ii%=1 TO(mmax% DIV 2)
640 m%=2*ii%-1
650 FOR jj%=0 TO ((n%-m%)DIVistep%)
660 i%=m%+jj%*istep%
670 j%=i%+mmax%
680 tempr=(wr)*datag(j%)-(wi)*datag(j%+1)
690 tempi=(wr)*datag(j%+1)+(wi)*datag(j%)
700 datag(j%)=datag(i%)-tempr
710 datag(j%+1)=datag(i%+1)-tempi
720 datag(i%)=datag(i%)+tempr
730 datag(i%+1)=datag(i%+1)+tempi
740 NEXT jj%
750 wtemp=wr
760 wr=wr*wpr-wi*wpi+wr
770 wi=wi*wpr+wtemp*wpi+wi
780 NEXT ii%
790 mmax%=istep%
800 ENDWHILE
820 FOR N%=1 TO nn2%:datag(N%)=datag(N%)/SQRnn%:PRINT datag(N%):NEXT N%
830 REMIF CO$="Y" GOTO 832 ELSE ENDPROC
832 IF NM=1 ENDPROC
834 FOR N%=1 TO nn2%:datag2(N%)=datag(N%):PRINT datag2(N%),   datag(N%):NEXT N%:NM=1
840 ENDPROC
850 :
860 DEF PROCfft
870 PROCwipe(0,5)
880 PRINTTAB(0,2)"CHOOSE fft(1) OR ifft(-1)";:INPUT ising
890 :
900 :
910 PROCacfft
920 COLOUR 132
930 ENDPROC
940 :
950 DEF PROCgetdata
960 PROCwipe(0,5):C=0:
961 PRINT TAB(0,1)"CORRELATION(Y/N)":INPUT CO$:XX1%=0:XX2%=0
962 PRINT TAB(0,2)"TYPE 1 FOR CURRENT DATA AND";
970 PRINT TAB(0,4)"TYPE 2 TO LOAD FROM DATA FILE";:INPUT C:
980 PROCwipe(0,5):PRINT TAB(0,1)"BIGINING OF THE DATA POINTS":INPUT XX1%
990 PRINT TAB(0,5)"END OF THE DATA POINTS":INPUT XX2%
1000 FOR n=1 TO nn2%:datap(n)=0:datag(n)=0:NEXT n
1010 k%=1
1020 :
1030 IF C=1 GOTO 1050
1040 FOR n%=XX1% TO XX2%:datap(k%)=DAT1(n%,1):k%=k%+1:NEXT n%:GOTO 1060
1050 FOR n%=XX1% TO XX2%:datap(k%)=DAT(n%,1):k%=k%+1:NEXT n%
1060 k%=1
1070 FOR n%=1 TO nn2% STEP 2:datag(n%)=datap(k%):k%=k%+1:NEXT n%
1080 COLOUR 132
1090 ENDPROC
1100 :
1110 DEFPROCshow
```

```
1120 PROCwipe(0,5):PRINTTAB(0,2)"TYPE (1) FOR data AND (0.5) FOR fft";
1130 INPUT m
1140 COLOUR 132:M%=0:N%=0
1150 Z=nn2%*m
1160 IF m=1 GOTO 1310 ELSE GOTO 1170
1170 FOR N=1 TO nn2%
1180 dataf(N)=datag(N)
1190 NEXT N
1200 PROCmodri
1210 CLS
1220 MODE20:MOVE 0,200:VDU19,0,4,0,0,0
1230 K=0:FR%=1
1240 FOR n%=1 TO nn% STEP 2
1250 GCOL0,1:PLOT &05,(K)*1000/nn%,dataf(n%)*0.5+200
1260 K=K+2
1270 NEXT n%
1280 MOVE0,200:GCOL0,2:DRAW 0,800:PRINT TAB(0,15)"AMPLITUDE"
1290 MOVE0,200:GCOL0,2:DRAW 1000,200:PRINT
TAB(60,50)"FREQUENCY(MHz)":GCOL0,7:ENDPROC
1300 :
1310 CLS:MODE20:MOVE 0,500:VDU19,0,4,0,0,0
1320 k=0:FR%=0:IF ising=1 GOTO 1330 ELSE GOTO1340
1330 MM=2:DD=1:FOR n%=1 TO nn2%/2 STEP 2: GOTO 1350
1340 MM=1:DD=0.5:FOR n%=1 TO nn2% STEP 2
1350 GCOL0,1:PLOT
&05,(k)*1000/2000,datag(n%)*MM+500:M%=(datag(n%)+500):N%=((k)*(1000/2000)):GCOL0,1:IF
M%>500 LINE N%,500,N%,M%
1360 k=k+DD
1370 NEXT n%
1380 GCOL0,7:ENDPROC
1390 :
1400 DEF PROCcorectsin
1410 FOR n=1 TO nn2
1420 dataf(n)=-SIN(2*pi*n/nn)-dataf(n)
1430/ 1430 NEXT n
1440 ENDPROC
1450 :
1460 DEF PROCfilter
1470 PROCwipe(0,5)
1480 FOR n=1 TO nn2%:dataf(n)=0:NEXT n
1490 PRINTTAB(0,2)"what kind of filter LP(1),HP(2),BP(3)";
1500 INPUT m
1510 IF m=1 PROClp:GOTO 1550
1520 IF m=2 PROChp:GOTO 1550
1530 IF m=3 PROCbp:GOTO 1550
1540 IF m=4 PROCb:PROCinvert:GOTO 1550
1550 FOR n=1 TO nn2%
1560 datag(n)=datag(n)*dataf(n)
1570 NEXT n
1580 ENDPROC
1590 :
1600 DEF PROChp
1610 PROCwipe(0,4):PRINT TAB(0,2) "WHAT FREQUENCY SHOULD BE THE LOW-
CUT";:INPUT hp
1620 :
1630 n=nn%-1:hp=hp/(fn):hp=hp*nn%
1640 WHILE n>hp:dataf(n)=1:n=n-2:ENDWHILE
1650 FOR n=1 TO nn%-1:dataf(n+nn%)=dataf(nn%-n):NEXT n
1660 REMFOR N=1 TO nn2% :PRINT dataf(N):NEXT N
1670 ENDPROC
1680 :
1690 DEFPROCbp
1700 n=nn%-1
1710 PRINTTAB(0,3)"WHAT SHOULD BE THE VALUE OF LOW-CUT  ";
```

```
1720 INPUT lc
1730 lc=lc/(fn):lc=lc*nn%
1740 WHILE n>lc
1750 dataf(n)=1:dataf(n+1)=1:n=n-2:ENDWHILE
1760 PRINTTAB(0,4)"WHAT SHOULD BE THE VALUE OF HIGH-CUT ";
1770 INPUT hc
1780 hc=hc/(fn):hc=hc*nn%:n=hc+1
1790 WHILE n>=hc AND n<nn%
1800 dataf(n)=0:dataf(n+1)=0:n=n+2
1810 ENDWHILE
1820 FOR n=1 TO nn%-1
1830 dataf(n+nn%)=dataf(nn%-n)
1840 NEXT n
1850 ENDPROC
1860 :
1870 DEF PROCinvert
1880 FOR n=1 TO nn2%
1890 IF dataf(n)=1 THEN dataf(n)=0 ELSE dataf(n)=1
1900 NEXT
1910 ENDPROC
1920 :
1930 DEFPROClp
1940 PROCwipe(0,4):PRINT TAB(0,2);"WHAT FREQUENCY SHOULD BE THE HIGH
CUT";:INPUT lp
1950 n=1
1960 lp=lp/fn
1970 lp=lp*nn%
1980 WHILE n<lp
1990 dataf(n)=1
2000 dataf(n+1)=1
2010 n=n+2
2020 ENDWHILE
2030 FOR n=1 TO nn%-1:dataf(n+nn%)=dataf(nn%-n):NEXT n
2040 REMFOR n=1 TO nn2%:PRINT dataf(n):NEXT n
2050 ENDPROC
2060 :
2070 DEFPROCmodri
2080 FOR n%=1 TO nn2%/2 STEP 2
2090 dataf(n%)=SQR((dataf(n%)*dataf(n%))+(dataf(n%+1)*dataf(n%+1)))
2100 NEXT n%:F=1
2110 ENDPROC
2120 :
2130 DEFPROCsmooth
2140 REMPRINT "smooth over n points(even)"
2150 REMdavr=0:m=0
2160 REMFOR n=1 TO nn2-2000
2170 REMdavr=davr+datag(n+m)
2180 REMdavi=davi+datag(n+m+1)
2190 REmm=m+1
2200 REMdatag(n)=davr /2000
2210 REmdatag(n+1)=davi/2000
2220 K=0
2230 FOR n=1 TO nn2%
2240 K=K+1
2250 PRINT K,  datag(n),  datatf(n),
2260 NEXT n
2270 ENDPROC
2280 :
2290 DEFPROCcorrelation
2300 no2%=nn% DIV 2
2310 FOR i%=1 TO no2%+1
2320 ii%=2*i%
2330 dum=datag(ii%-1)
2340 datag(ii%-1)=(datag2(ii%-1)*datag(ii%-1)+datag2(ii%)*datag(ii%))/no2%
```

```
2350 datag(ii%)=(datag2(ii%)*dum-datag2(ii%-1)*datag(ii%))/no2%
2360 NEXT i%
2370 datag(2)=datag(nn%+1)
2380 FOR N%=1 TO nn2%:datag2(N%)=0:NEXT N%
2382 ENDPROC
2390 REM**********SIGNAL***************
2400 DEF PROCdraw:?&73=1:?&74=1:O%=1:?&77=O%
2410 MOVE 50,O%*256:PLOT 1,-50,0:PLOT 1,0,500:PLOT 1,50,0
2420 MOVE 0,O%*256:PLOT 1,984,0
2430 MOVE 984,O%*256:PLOT 1,17,0:PLOT 1,0,500:PLOT 1,-50,0
2440 REMPRINT TAB(66,25)"GAIN=";G%
2450 REMPRINT TAB(66,26)"AMPL=";P
2460 REMPRINT TAB(66,27)"FREQ=";E
2470 REMVDU 5:@%=&20105:MOVE 1000,O%*256+256:MV=255*20/GAIN:IF MV>99.99 THEN
PRINT MV/1000;"V" ELSE IF MV<0.1 THEN PRINT MV*1000;" ";CHR$240;"V" ELSE PRINT
MV;"MV"  400@%=10:VDU 4
2480 U%=U% EOR 1 :PROCscale:ENDPROC
2490 DEF PROCscale:REM CHANGE SCALES
2500 :
2510 GOTO 2550:REMIF U%=0 THEN GOTO 3170
2520 VDU 5:MOVE 250,225:DRAW 250,175:DRAW750,175:DRAW 750,225
2530 MOVE 150,150:PRINT125*S%;" MS":VDU4
2540 U%=0:ENDPROC
2550 VDU 5:MOVE0,200:DRAW 1000,200
2560 FOR X=0 TO NRM STEP 500
2570 MOVE X,200:DRAW X,100:PRINTSTR$(B%+X*S%DIV4)
2580 NEXT X
2590 VDU 4:ENDPROC
2600 :
2610 REM **********FUNCTION KEYS***************
2620 G=INKEY(0)
2630 :
2640 :
2650 :
2660 :
2670 G=INKEY(25):IF G<>-1 THEN 2420
2680 :
2690 DEF PROCsetup:REM SET GAIN AND TIME
2700 PROCwipe(0,5):P=0:XRM=0:S%=0:B%=0
2710 :
2720 GAIN=1
2730 PRINTTAB(0,1)"ENTER ANY PRE-AMPLIFICATION = ";:INPUT P
2740 GAIN=GAIN*P:REM G=GAIN FACTOR
2750 PRINTTAB(0,3)"NUMBER OF SAMPLES";:INPUT XRM
2760 NOM=XRM
2770 XRM=XRM+22
2780 PRINTTAB(0,5)"WHICH TRACE,C1,TC,etc";:INPUT CMD$
2790 PROCwipe(0,5):PRINTTAB(1,2)"ORIGIN =  ";:INPUT B%
2800 PRINTTAB(20,2)"SCALE = ";:INPUT S%:
2810 PROCwipe(0,5)
2820 ENDPROC
2830 :
2840 DEF PROCwipe(FL,LL)
2850 :
2860 FOR L=FL TO LL
2870 PRINT TAB(0,L) SPC(39);
2880 REMCOLOUR 128
2890 NEXT
2900 :
2910 ENDPROC
2920 :
2930 DEF PROCattension
2940 GCOL0,13
```

```
2950 LINE1028,842,1224,842:LINE1028,872,1224,872:LINE 1028,842,1028,872:LINE
1224,842,1224,872
2960 GCOL0,7
2970 ENDPROC
2980 :
2990 DEF PROCavrage
3000 PRINT TAB(2,1); "  AVERAGING  "
3010 PROCwipe(0,5):PRINT TAB(1,2);"ENTER NUMBER OF AVRAGING";:INPUT nav;
3020 FOR n=1 TO XRM
3030 BAT(n,1)=0
3040 NEXT n
3050 FOR I=1 TO nav
3060 FOR n=1 TO XRM
3070 BAT(n,1)=BAT(n,1)+DAT(n,1)
3080 BAT(n,1)=BAT(n,1)*(nav-1)/nav
3090 NEXT n
3100 :
3110 FOR m=1 TO XRM
3120 DAT(m,1)=BAT(m,1)
3130 DAT(m,1)=0
3140 NEXT m
3150 PROCtransform
3160 NEXT I
3170 FOR n=1 TO XRM
3180 DAT(n,1)=0
3190 DAT(n,1)=BAT(n,1)
3200 NEXT n
3210 PROCsig:PROCdraw
3220 ENDPROC
3230 :
3240 DEF PROCerror(T1,T2)
3250 PRINTTAB(T1,T2)"ERROR";
3260 G=GET
3270 PRINT TAB(T1,T2),SPC(6)
3280 ENDPROC
3290 :
3300 DEF PROCpage
3310 CLS:VDU19,0,4,0,0,0:COLOUR 2:VOL=0:DEN=0
3320 PRINT TAB(14,1)"EXPERIMENTAL ROCK DEFORMATION"
3330 PRINT TAB(3,3)"SEISMIC VELOCITY MEASURMENTS OF ROCK SAMPLES UNDER
CONFINING "
3340 PRINT TAB(14,5) "PRESSURE AND TEMPERATURE"
3350 PRINT TAB(1,7)
"************************************************************"
3360 PRINT TAB(1,10) "Sample NO:";:INPUT AS$
3370 PRINT TAB(1,14) "Specimen Description:";:INPUT BS$
3380 PRINT TAB(1,20) "Source Location/Storage Details:";:INPUT CS$
3390 PRINT TAB(1,26)"Core Height(mm):";:INPUT DS$
3400 PRINT TAB(1,32)"Core Weight(gr):";:INPUT ES$
3410 PRINT TAB(1,36)"Core Diameter(mm):";:INPUT
FS$:REMVOL=(pi*(FS/2)*(FS/2)*DS):GS=ES/VOL*1000
3420 PRINT TAB(1,40)"Core Density(gr/cm3):";:INPUT GS$:REM@%=131850:PRINT TAB(23,40)
GS
3430 REMPRINT TAB(1,44)":";:INPUT PS$
3440 PRINT TAB(15,50)"PRESS SPACE BAR TO CONTINUE"
3450 PROCpresskey:GCOL0,7
3460 ENDPROC
3470 :
3480 DEF PROCpresskey
3490 REPEAT
3500 UNTIL GET = 32
3510 ENDPROC
3520 REM******************
3530 DEF PROCwfile
```

```
3540 PROCwipe(0,5):WA=0
3550 PRINT TAB(0,2);"ENTER FILE NAME ";:INPUT fname$
3560 Tfile=OPENOUT(fname$)
3570 PRINT TAB(0,3);"TYPE(1)WAVEFORM-(2)FREQUENCY SPECTRUM";:INPUT WA
3580 BPUT#Tfile,CHR$(13)+AS$+CHR$(10)+CHR$(13);:REMAA$:REM+CHR$(10)+CHR$(13);
3590 BPUT#Tfile,BS$+CHR$(10)+CHR$(13);
3600 BPUT#Tfile,CS$+CHR$(10)+CHR$(13);
3610 BPUT#Tfile,DS$+CHR$(10)+CHR$(13);
3620 BPUT#Tfile,ES$+CHR$(10)+CHR$(13);
3630 BPUT#Tfile,FS$+CHR$(10)+CHR$(13);
3640 BPUT#Tfile,GS$+CHR$(10);
3650 IF WA<>1 GOTO 3680
3660 FOR n=1 TO NRM
3670 AA$=STR$(DAT(n,1)):BPUT#Tfile,AA$:NEXT n:PROCwipe(0,5):ENDPROC
3680 k=1
3690 FOR n=1 TO nn%*2 STEP 2
3700 DAT1(k,1)=dataf(n)
3710 AA$=STR$(DAT1(k,1))
3720 BPUT#Tfile,AA$
3730 k=k+1
3740 NEXT n:PROCwipe(0,5)
3750 ENDPROC
3760 :
3770 REM******************
3780 DEF PROCcfile
3790 PROCwipe(0,5)
3800 PRINT TAB(0,2);"THE FILE HAS BEEN CLOSED"
3810 CLOSE#Tfile:PROCwipe(0,5)
3820 ENDPROC
3830 :
3840 REM********************
3850 DEF PROCrfile :PROCwipe(0,10):M=0:CONT=0:m=0:N=0:TX=0:FR%=0
3860 PRINT TAB(2,1); "WAFORM (1) or SPECTRUM (2)";:INPUT spec
3870 PRINT TAB(2,3); "WOULD YOU LIKE TO SEE THE TEXT(1)";:INPUT TX
3880 PRINT TAB(2,5); "NUMBER OF TRACES TO BE DISPLAYED";:INPUT
ND:PROCwipe(0,10)
3890 PRINT TAB(2,1); "TYPE THE FIRST  FILE NAME ";:INPUT rfname1$:Tfile1=OPENIN
(rfname1$):CONT=CONT+1: IF CONT=ND GOTO 3940
3900 PRINT TAB(2,3); "TYPE THE SECAND FILE NAME ";:INPUT rfname2$:Tfile2=OPENIN
(rfname2$):CONT=CONT+1: IF CONT=ND GOTO 3940
3910 PRINT TAB(2,5); "TYPE THE THIRD  FILE NAME ";:INPUT rfname3$:Tfile3=OPENIN
(rfname3$):CONT=CONT+1: IF CONT=ND GOTO 3940
3920 PRINT TAB(2,7); "TYPE THE FOURTH FILE NAME ";:INPUT rfname4$:Tfile4=OPENIN
(rfname4$):CONT=CONT+1: IF CONT=ND GOTO 3940
3930 PRINT TAB(2,9); "TYPE THE FIFETH FILE NAME ";:INPUT rfname5$:Tfile5=OPENIN
(rfname5$):CONT=CONT+1: IF CONT=ND GOTO 3940
3940 PROCpara
3950 :
3960 PRINT TAB(65,2);:INPUT NS%
3970 PRINT TAB(65,4);:INPUT SS%
3980 PRINT TAB(65,6);:INPUT PA
3990 IF TX=1 GOTO 4000 ELSE GOTO 4010
4000 PROCreadpage
4010 FOR n=0 TO NS%
4020 DAT1$(n,1)=GET$#Tfile1:DAT1(n,1)=VAL(DAT1$(n,1)):IF ND=1 GOTO 4070
4030 DAT1$(n,1)=GET$#Tfile2:DAT2(n,1)=VAL(DAT1$(n,1)):IF ND=2 GOTO 4070
4040 DAT1$(n,1)=GET$#Tfile3:DAT3(n,1)=VAL(DAT1$(n,1)):IF ND=3 GOTO 4070
4050 DAT1$(n,1)=GET$#Tfile4:DAT4(n,1)=VAL(DAT1$(n,1)):IF ND=4 GOTO 4070
4060 DAT1$(n,1)=GET$#Tfile5:DAT5(n,1)=VAL(DAT1$(n,1)):IF ND=5 GOTO 4070
4070 NEXT n
4080 :
4090 CLS:M=0:MODE20:VDU19,0,4,0,0,0
4100 SS1%=(SS%*100)
4110 M=NS%-SS1%:CONT=0
```

```
4111 IF spec<>1 GOTO 4256
4120 SEFR=900:k=0:CONT=CONT+1:SEFR=SEFR-(150*CONT):MOVE 0,SEFR
4150 m=1:FOR n%=SS1% TO NS%
4160 IF CONT=1 GOTO 4180 ELSE GOTO 4190
4170 :
4180 GCOL0,1:PLOT &05,k*1000/M,DAT1(n%,1)*PA+SEFR:k=k+m:NEXT
n%:PRINTTAB(8,12)rfname1$:IF ND=1 GOTO 4280 ELSE GOTO 4120
4190 IF CONT=2 GOTO 4200 ELSE GOTO 4210
4200 GCOL0,2:PLOT &05,k*1000/M,DAT2(n%,1)*PA+SEFR:k=k+m:NEXT
n%:PRINTTAB(8,22)rfname2$:IF ND=2 GOTO 4280 ELSE GOTO 4120
4210 IF CONT=3 GOTO 4220 ELSE GOTO 4230
4220 GCOL0,3:PLOT &05,k*1000/M,DAT3(n%,1)*PA+SEFR:k=k+m:NEXT
n%:PRINTTAB(8,32)rfname3$:IF ND=3 GOTO 4280 ELSE GOTO 4120
4230 IF CONT=4 GOTO 4240 ELSE GOTO 4250
4240 GCOL0,5:PLOT &05,k*1000/M,DAT4(n%,1)*PA+SEFR:k=k+m:NEXT
n%:PRINTTAB(8,42)rfname4$:IF ND=4 GOTO 4280 ELSE GOTO 4120
4250 IF CONT=5 GOTO 4252 ELSE GOTO 4280
4252 GCOL0,7:PLOT &05,k*1000/M,DAT5(n%,1)*PA+SEFR:k=k+m:NEXT
n%:PRINTTAB(8,50)rfname5$:GOTO4280
4254 :
4256 MOVE0,200:GCOL0,2:DRAW 0,800:PRINT TAB(0,15)"AMPLITUDE"
4258 MOVE0,200:GCOL0,2:DRAW 1000,200 :PRINT TAB(60,50)"FREQUENCY(MHz)":GCOL0,7
4262 m=1:M=(nn%/8):k=0:CONT=CONT+1:SEFR=200:PA=PA/2:MOVE 0,SEFR:
4263 FOR n%=SS1% TO nn%/8
4264 IF CONT=1 GOTO 4265 ELSE GOTO 4266
4265 GCOL0,1:PLOT &05,k*1000/M,DAT1(n%,1)*PA+SEFR:k=k+m:NEXT
n%:PRINTTAB(50,10)rfname1$:LINE 900,850,950,850:IF ND=1 GOTO 4280 ELSE GOTO 4262
4266 IF CONT=2 GOTO 4267 ELSE GOTO 4268
4267 GCOL0,2:PLOT &05,k*1000/M,DAT2(n%,1)*PA+SEFR:k=k+m:NEXT
n%:PRINTTAB(50,12)rfname2$:LINE 900,820,950,820:IF ND=2 GOTO 4280 ELSE GOTO 4262
4268 IF CONT=3 GOTO 4269 ELSE GOTO 4270
4269 GCOL0,3:PLOT &05,k*1000/M,DAT3(n%,1)*PA+SEFR:k=k+m:NEXT
n%:PRINTTAB(50,14)rfname3$:LINE 900,790,950,790:IF ND=3 GOTO 4280 ELSE GOTO 4262
4270 IF CONT=4 GOTO 4271 ELSE GOTO 4272
4271 GCOL0,5:PLOT &05,k*1000/M,DAT4(n%,1)*PA+SEFR:k=k+m:NEXT
n%:PRINTTAB(50,16)rfname4$:LINE 900,760,950,760:IF ND=4 GOTO 4280 ELSE GOTO 4262
4272 IF CONT=5 GOTO 4273 ELSE GOTO 4280
4273 GCOL0,7:PLOT &05,k*1000/M,DAT5(n%,1)*PA+SEFR:k=k+m:NEXT
n%:PRINTTAB(50,18)rfname5$:LINE 900,730,950,730
4274 REMIF CONT=6 GOTO 4277 ELSE GOTO 4280
4277 REMGCOL0,7:PLOT &05,k*1000/M,DAT5(n%,1)*PA+SEFR:k=k+m:NEXT
n%:PRINTTAB(50,18)rfname5$:LINE 900,700,950,700
4275
4280 CLOSE#0:MOVE0,200:PROCcopy:ENDPROC:GCOL0,2:DRAW 1000,200:GCOL0,7
4290 ENDPROC
4300 :
4310 DEF PROCpara
4320 REMLINE 1000,750,1200,750
4330 REMLINE 1000,800,1200,800
4340 REMLINE 1000,850,1200,850:LINE 1000,900,1200,900:LINE 1000,950,1200,950
4350 REMLINE 1100,750,1100,1000:LINE 1200,750,1200,1000
4360 PRINT TAB(46,2);"NUMBER OF POINTS"
4370 PRINT TAB(46,4);"STARTING TIME"
4380 PRINT TAB(46,6);"PRE-AMPLIFICATION"
4390 REMPRINT TAB(69,2.5);"MAX/MIN"
4400 ENDPROC
4410 REM**********************************************************
4420 DEFPROCreadpage
4430 :
4440 FOR n=1 TO 7:AS$=GET$#Tfile1:PRINT GET$#Tfile1:NEXT n:IF ND=1 ENDPROC
4450 FOR n=1 TO 7:AS$=GET$#Tfile2:PRINT GET$#Tfile2:NEXT n:IF ND=2 ENDPROC
4460 FOR n=1 TO 7:AS$=GET$#Tfile3:PRINT GET$#Tfile3:NEXT n:IF ND=3 ENDPROC
4470 FOR n=1 TO 7:AS$=GET$#Tfile4:PRINT GET$#Tfile4:NEXT n:IF ND=4 ENDPROC
4480 FOR n=1 TO 7:AS$=GET$#Tfile5:PRINT GET$#Tfile5:NEXT n:IF ND=5 ENDPROC
```

```
4490 :
4500 DEFPROCleast
4510 N=0:AX=0:AY=0:BX=0:BY=0:A=0:B=0
4520 PROCPoint
4530 TX1=X*2:PY1=Y*4
4540 N=N+1
4550 AX=AX+TX1:AY=AY+PY1:BX=BX+(TX1*TX1):BY=BY+(TX1*PY1)
4560 IF N=5 GOTO 4580 ELSE GOTO 4570
4570 TX1=0:PY1=0:GOTO 4520
4580 A=((AX*BY)-(BX*AY))/((AX*AX)-(N*BX))
4590 B=(AY-(A*N))/AX
4600 FOR n=0 TO 1000
4610 JA=A+(B*n)
4620 BAT(n,1)=JA
4630 NEXT n
4640 :
4650 VDU19,0,4,0,0,0
4660 FOR I=1 TO 10 STEP2
4670 GCOL0,3:PLOT &05,I,BAT(I,1)
4680 :
4690 NEXT I:PROCtransform:ENDPROC
4700 REM********DOWN LOAD*********
4710 REM ** PROCEDURES LIBRARY INSTPROCS **
4720DEFPROCinitialise_IEEE
4730REM PROCeos_in_1chr(10)
4740PROCeos_out_1chr(10)
4750REM PROCtimeout_on
4760PROCinit
4770IF seismic<>1 PROCselected_device_clear(15)
4780IF seismic=1PROCselected_device_clear(5)
4790convert=(100/(2^30))
4800ENDPROC
4810REM INTELLIGENT INTERFACES LTD IEEE488 PROCEDURES AND FUNCTIONS
LIBRARY V1.02
4820REM abort on error
4830REM Copyright Intelligent Interfaces Ltd
4840REM 18 January 1988
4850
4860DEF PROCeos_out_1chr(eos1%)
4870SYS &40340,&00,&03,&01,eos1%
4880ENDPROC
4890
4900DEF PROCeos_out_2chr(eos1%,eos2%)
4910SYS &40340,&00,&03,&02,eos1%,eos2%
4920ENDPROC
4930
4940DEF PROCeos_in_1chr(eos1%)
4950SYS &40340,&00,&04,&01,eos1%
4960ENDPROC
4970
4980DEF PROCeos_in_2chr(eos1%,eos2%)
4990SYS &40340,&00,&04,&02,eos1%,eos2%
5000ENDPROC
5010
5020DEF PROCtimeout_period(period)
5030 SYS &40340,&00,&05,INT(&00200000*(period/8))
5040ENDPROC
5050DEF PROCtimeout_on
5060 SYS &40340,&00,&06
5070 ENDPROC
5080DEF PROCtimeout_off
5090SYS &40340,&00,&07
5100ENDPROC
5110DEF PROCoutput(mode%,data$)
```

```
5120SYS &40340,&00,&08,mode%
5130SYS &40340,&00,&36,&00,&00,&00,data$,LEN(data$)
5140ENDPROC
5150DEF PROCadrandoutput(mode%,lad%,data$)
5160SYS &40340,&00,&08,mode%
5170SYS &40340,&00,&3C,&00,lad%,&00,data$,LEN(data$)
5180ENDPROC
5190DEF PROCinit
5200LOCAL d0%,d1%,ma%
5210SYS &40340,&00,&02 TO d0%,d1%,ma%
5220IF (ma% AND &80) THEN SYS &40340,&00,&11,ma% ELSE SYS &40340,&00,&10,ma%
5230ENDPROC
5240DEF PROCadrandoutput(mode%,lad%,data$)
5250SYS &40340,&00,&08,mode%
5260SYS &40340,&00,&3C,&00,lad%,&00,data$,LEN(data$)
5270ENDPROC
5280
5290DEF PROCadrextandoutput(mode%,lad%,sad%,data$)
5300SYS &40340,&00,&08,mode%
5310SYS &40340,&00,&3E,&00,lad%,sad%,data$,LEN(data$)
5320ENDPROC
5330
5340DEF PROCoutputmem(mode%,memadr%,bytecnt%)
5350SYS &40340,&00,&08,mode%
5360SYS &40340,&00,&36,&00,&00,&00,memadr%,bytecnt%
5370ENDPROC
5380
5390DEF PROCadrandoutputmem(mode%,lad%,memadr%,bytecnt%)
5400SYS &40340,&00,&08,mode%
5410SYS &40340,&00,&3C,&00,lad%,&00,memadr%,bytecnt%
5420ENDPROC
5430DEF FNadrandinput(mode%,tad%,bytecnt%)
5440LOCALd0%,d1%,d2%,d3%,d4%,databuf$,d6%,xcnt%
5450IFbytecnt%>254THEN bytecnt% = 254
5460databuf$ = STRING$(bytecnt%," ")
5470SYS &40340,&00,&09,mode%
5480SYS &40340,&00,&3D,&00,tad%,&00,databuf$,bytecnt% TO
d0%,d1%,d2%,d3%,d4%,databuf$,d6%,xcnt%
5490=LEFT$(databuf$,xcnt%)
5500DEF PROCgo_to_local(lad%)
5510SYS &40340,&00,&20,&00,&00,&00,CHR$(lad%),&01
5520ENDPROC
5530
5540DEF PROCdevice_clear
5550SYS &40340,&00,&24
5560ENDPROC
5570DEF PROCinputmem(mode%,memadr%,bytecnt%)
5580SYS &40340,&00,&09,mode%
5590SYS &40340,&00,&37,&00,&00,&00,memadr%,bytecnt%
5600ENDPROC
5610
5620DEF PROCadrandinputmem(mode%,tad%,memadr%,bytecnt%)
5630SYS &40340,&00,&09,mode%
5640SYS &40340,&00,&3D,&00,tad%,&00,memadr%,bytecnt%
5650ENDPROC
5660
5670DEF PROCadrextandinputmem(mode%,tad%,sad%,memadr%,bytecnt%)
5680SYS &40340,&00,&09,mode%
5690SYS &40340,&00,&3F,&00,tad%,sad%,memadr%,bytecnt%
5700ENDPROC
5710
5720DEF PROCifc
5730SYS &40340,&00,&0D
5740ENDPROC
```

```
5750
5760DEF PROCren_true
5770SYS &40340,&00,&0E
5780ENDPROC
5790
5800DEF PROCren_false
5810SYS &40340,&00,&0F
5820ENDPROC
5830
5840DEF PROCdevice(archadr%)
5850SYS &40340,&00,&10,archadr%
5860ENDPROC
5870
5880DEF PROCcontroller(archadr%)
5890SYS &40340,&00,&11,archadr%
5900ENDPROC
5910
5920DEF PROCatn_true
5930SYS &40340,&00,&12
5940ENDPROC
5950
5960DEF PROCatn_true_sync
5970SYS &40340,&00,&13
5980ENDPROC
5990
6000DEF PROCcmd(cmd%)
6010SYS &40340,&00,&14,&00,&00,&00,CHR$(cmd%),&01
6020ENDPROC
6030
6040DEF PROClisten(lad%)
6050SYS &40340,&00,&15,&00,lad%
6060ENDPROC
6070
6080DEF PROClistenext(lad%,sad%)
6090SYS &40340,&00,&16,&00,lad%,sad%
6100ENDPROC
6110
6120DEF PROCtalk(tad%)
6130SYS &40340,&00,&17,&00,tad%
6140ENDPROC
6150
6160DEF PROCtalkext(tad%,sad%)
6170SYS &40340,&00,&18,&00,tad%,sad%
6180ENDPROC
6190
6200DEF PROCsecondary(sad%)
6210SYS &40340,&00,&19,&00,&00,sad%
6220ENDPROC
6230
6240DEF PROCunlisten
6250SYS &40340,&00,&1A
6260ENDPROC
6270
6280DEF PROCuntalk
6290SYS &40340,&00,&1B
6300ENDPROC
6310
6320DEF PROCadr_to_listen(lad%)
6330SYS &40340,&00,&1C,&00,lad%
6340ENDPROC
6350
6360DEF PROCadr_to_listenext(lad%,sad%)
6370SYS &40340,&00,&1D,&00,lad%,sad%
6380ENDPROC
```

```
6390
6400DEF PROCadr_to_talk(tad%)
6410SYS &40340,&00,&1E,&00,tad%
6420ENDPROC
6430
6440DEF PROCadr_to_talkext(tad%,sad%)
6450SYS &40340,&00,&1F,&00,tad%,sad%
6460ENDPROC
6470
6480
6490
6500DEF PROCselected_device_clear(lad%)
6510SYS &40340,&00,&21,&00,&00,&00,CHR$(lad%),&01
6520ENDPROC
6530
6540DEF PROCgroup_execute_trigger(lad%)
6550SYS &40340,&00,&22,&00,&00,&00,CHR$(lad%),&01
6560ENDPROC
6570
6580DEF PROClocal_lockout
6590SYS &40340,&00,&23
6600ENDPROC
6610
6620
6630
6640DEF PROCparallel_poll_unconfigure
6650SYS &40340,&00,&25
6660ENDPROC
6670
6680DEF PROCatn_false
6690SYS &40340,&00,&26
6700ENDPROC
6710
6720DEF PROCrequest_service(stb%)
6730SYS &40340,&00,&29,stb%
6740ENDPROC
6750
6760DEF FNserial_poll(tad%)
6770LOCAL d0%,d1%,stb%
6780SYS &40340,&00,&2B,&00,tad% TO d0%,d1%,stb%
6790=stb%
6800
6810DEF PROCparallel_poll_enable(lad%,sp3p2p1%)
6820SYS &40340,&00,&2E,sp3p2p1%,lad%
6830ENDPROC
6840
6850DEF PROCparallel_poll_disable(lad%)
6860SYS &40340,&00,&2F,&00,lad%
6870ENDPROC
6880
6890DEF FNparallel_poll
6900LOCAL d0%,d1%,ppr%
6910SYS &40340,&00,&30 TO d0%,d1%,ppr%
6920=ppr%
6930
6940DEF PROCpasscontrol(tad%)
6950SYS &40340,&00,&31,&00,tad%
6960ENDPROC
6970
6980
6990DEF PROCadrextandoutputmem(mode%,lad%,sad%,memadr%,bytecnt%)
7000SYS &40340,&00,&08,mode%
7010SYS &40340,&00,&3E,&00,lad%,sad%,memadr%,bytecnt%
7020ENDPROC
```

```
 7030
 7040DEF FNinput(mode%,bytecnt%)
 7050LOCALd0%,d1%,d2%,d3%,d4%,databuf$,d6%,xcnt%
 7060IFbytecnt%>254THEN bytecnt% = 254
 7070databuf$ = STRING$(bytecnt%," ")
 7080SYS &40340,&00,&09,mode%
 7090SYS &40340,&00,&37,&00,&00,&00,databuf$,bytecnt% TO
d0%,d1%,d2%,d3%,d4%,databuf$,d6%,xcnt%
 7100=LEFT$(databuf$,xcnt%)
 7110
 7120
 7130DEF FNadrextandinput(mode%,tad%,sad%,bytecnt%)
 7140LOCALd0%,d1%,d2%,d3%,d4%,databuf$,d6%,xcnt%
 7150IFbytecnt%>254THEN bytecnt% = 254
 7160databuf$ = STRING$(bytecnt%," ")
 7170SYS &40340,&00,&09,mode%
 7180SYS &40340,&00,&3F,&00,tad%,sad%,databuf$,bytecnt% TO
d0%,d1%,d2%,d3%,d4%,databuf$,d6%,xcnt%
 7190=LEFT$(databuf$,xcnt%)
 7200
 7210
 7220
 7230DEF PROCadrextandinputmem(mode%,tad%,sad%,memadr%,bytecnt%)
 7240SYS &40340,&00,&09,mode%
 7250SYS &40340,&00,&3F,&00,tad%,sad%,memadr%,bytecnt%
 7260ENDPROC
 7270
 7280:REM****************************** MENU
************************************
 7290 DEFPROCtran
 7300 REMDAT=0:nr%=0:display%=0:dt%=0:ofset%=0
 7310 REMDIM DAT(10000,1)
 7320 PROCdevice_clear
 7330 PROCgo_to_local(5)
 7340 REMDIM nr% 4
 7350 REMDIM display% 330000
 7360 ENDPROC
 7370 :
 7380 DEFPROCtransform
 7390 seismic=1:PROCinitialise_IEEE
 7400 PROCtimeout_period(20.0):PROCtimeout_on
 7410 PROCadrandoutput(1,5,"COMM_FORMAT?"):rpt$=FNadrandinput(1,5,255):REMPRINT rpt$
 7420 PROCadrandoutput(1,5,"C1:INSPECT?
'VERTICAL_GAIN'"):rpt$=FNadrandinput(1,5,255):REMPRINT rpt$
 7430 VGAIN =VAL(rpt$):REMPRINT"VGAIN";VGAIN
 7440 PROCadrandoutput(1,5,"COMM_FORMAT DEF9,WORD,BIN")
 7450 REMINPUT"NUMBER OF SAMPLES";XRM
 7460 REMINPUT"which trace, C1, TA etc ";CMD$
 7470 PROCseisdata:ENDPROC
 7480 :
 7490 DEFPROCseisdata
 7500 PROCdevice_clear
 7510 PROCgo_to_local(5)
 7520 PROCadrandoutput(1,5,CMD$+":WF? DAT1")
 7530 PROCadrandinputmem(1,5,display%,300000)
 7540 PROCdevice_clear:PROCgo_to_local(5)
 7550 offset=0
 7560 REM convert buffer, first the waveform descriptor
 7570 g%=?(display%+4)
 7580 ?(nr%)=g%:?(nr%+1)=0:?(nr%+2)=0:?(nr%+3)=0
 7590 gain%=!nr%
 7600 REMPRINT gain%
 7610 vg%=?(display%+5)
 7620 ?(nr%)=vg%
```

```
7630 vgain%=!nr%
7640 REMPRINT vgain%
7650 ofst1%=?(display%+8):ofst2%=?(display%+9)
7660 ?(nr%)=ofst2%:?(nr%+1)=ofst1%
7670 ofst%=!nr%
7680 REMPRINT ofst%
7690 REM decode data
7700 ?(nr%)=0:?(nr%+1)=0:?(nr%+2)=0:?(nr%+3)=0
7710 FOR index%=1 TO XRM
7720 d1%=?(display%+index%)
7730 d2%=?(display%+index%+1)
7740 ?(nr%)=d1%
7750 ?(nr%+1)=d2%
7760 dt%=!(nr%)
7770 IF dt% > 32767 THEN dt%=dt%-65535
7780 REMconvert to signed voltage
7790 volt=dt%:REM=gain%:REM*(((dt%-128)/32)-((ofst%-200)/25))*(200/(vgain%+80))
7800 REMPRINTindex%;"     ";dt%;"        ";volt
7810 DAT(index%,1)=volt
7820 offset=offset+1
7830 NEXT index%
7840 :
7850 PROCdevice_clear
7860 PROCgo_to_local(5)
7870 ENDPROC
7880 XRM=XRM
7890 DEFPROCsig:REM (to get rid of the first 21 points)
7900 K=1:FOR n=1 TO XRM:HAT(n,1)=0
7910 NEXT n
7920 FOR N=21 TO XRM
7930 HAT(K,1)=DAT(N,1)
7940 K=K+1
7950 NEXT N
7960 :
7970 FOR n=1 TO XRM
7980 DAT(n,1)=0
7990 NEXT n
8000 NRM=XRM-20
8010 FOR n=1 TO NRM
8020 DAT(n,1)=HAT(n,1)
8030 NEXT n
8040 :
8050 CLS
8060 MODE20:M%=0:N%=0:G%=0
8070 MOVE 0,500:VDU19,0,4,0,0,0
8080 b%=(B%*100)+1
8090 RM=NRM-(B%*100)
8100 k=0
8110 FOR n%=b% TO NRM
8120 DAT(n%,1)=DAT(n%,1)*(P/100)
8130 GCOL0,1:PLOT &05,k*1000/RM,DAT(n%,1)+(500-(100*S%))
8140 G%=(500-(100*S%)):M%=(DAT(n%,1)+G%):N%=(k*1000/RM):GCOL0,1
8150 REMIF M%>G% LINE N%,G%,N%,M%
8160 k=k+1
8170 NEXT n%
8180 GCOL0,7:ENDPROC
8181 :
8182 DEFPROCreplot:CLS:MOVE 0,500:k=0:PRINT TAB(65,10)X3:PRINT
TAB(65,15)X4:RM2=X4-X3:D6%=-1:BI=X3/100
8183 FOR n%=X3 TO X4
8184 DAT1(n%,1)=DAT(n%,1)
8185 GCOL0,1:PLOT &05,k*1000/RM2,DAT1(n%,1)+(500-(100*S%))
8186 G%=(500-(100*S%)):M%=(DAT1(n%,1)+G%):N%=(k*1000/RM2):GCOL0,1
8187 IF M%>G% LINE N%,G%,N%,M%
```

```
 8188 k=k+1
 8189 NEXT n%
 8190 GCOL0,7:ENDPROC
 8191 :
 8200
TX1=0:TX2=0:PY1=0:PY2=0:AA=0:TT=0:N=0:FR%=0:BI=0:DI=0:spec=0:NS%=0:SS%=0:SS1%=0
 8210 :
 8220 DIM
AX(10),AY(10),TI(10),AM(10),dataf(30000),datag(30000),datap(30000),DAT(10000,1),DAT$(10000,1),
wpi(30000),theta(30000),double(10000),nr% 4,display% 300000,tempr(30000),tempi(30000)
 8230 DIM
DAT1(10000,1),DAT2(10000,1),DAT3(10000,1),DAT4(10000,1),DAT5(10000,1),DAT1$(10000,1),H
AT(10000,1),BAT(10000,1),TAT(10000,1),wtemp(10000),wr(10000),wpr(10000),datag2(10000)
 8240
pi=3.14159265358979:nn%=4096:nn2%=nn%*2:fn=50:rdt=0.01:sta=0:ising=0:RM2=0:D6%=0:NM=0
 8250 X=0:Y=0:quit=0:F=0:W%=0:C4%=0
 8260 CC%=0
 8270 VDU23,240,254,192,160,144,136,132,130,129
 8280 ONERRORPROCmenu
 8290 PROCpage:CLS
 8300 PROCmenu
 8310 END
 8320 KNT%=0
 8330 :
 8340 A=0:B=0:X=0:Y=0
 8350 PROCPoint
 8360 END
 8370 :
 8380 REMVDU23,240,128,128,128,128,128,128,128
 8390 DEF PROCPoint
 8400 REPEAT
 8410 C% = INKEY(-10):IF C% = -1 GOTO 8410
 8420 VDU5:MOVE X*2,Y*4:VDU240:VDU4
 8430 A%=128:X%=7:A= USR(&FFF4)
 8440 A%=128:X%=8:B= USR(&FFF4)
 8450 X=INT((A-128)/511.8):Y=INT((B-128)/1023)
 8460 @%=&00004: PRINT TAB(60,60);"AX=",X*2," AY=",Y*4
 8470 :
 8480 @%=&00004: PRINT TAB(1,60);"QUIT CLEAR SETUP SIG  COPY C.T.M W-FI  C-FI  R-FI
"
 8490 @%=&00004: PRINT TAB(70,22);"F-F-T":@%=&00004: PRINT
TAB(70,28);"SMOOTH":@%=&00004:PRINT TAB(70,34);"FILTER"
 8500 @%=&00004: PRINT TAB(70,41);"GET-DATA":@%=&00004: PRINT TAB(70,47);"SHOW
":@%=&00004: PRINT TAB(70,53);"S-Trace"
 8510 VDU5:MOVE BY -15,0:GCOL4,0:VDU240:GCOL4,0:VDU4
 8520 C%=INKEY(-10):D5%=INKEY(-12):E%=INKEY(-11)
 8530 UNTIL C% = -1 OR E%=-1 OR D5%=-1
 8540 :
 8550 ENDPROC
 8560 :
 8570 DEFPROCfaxis:W=0:V%=0
 8572 IF D6%=-1 GOTO 8574 ELSE GOTO 8580
 8574 D1%=RM2:DI=100000:PRINT TAB(65,8)"TIME(mic-sec)":D6%=0:GOTO 8640
 8580 IF FR%=1 GOTO 8590 ELSE GOTO 8600
 8590 DI=80:D1%=1:BI=0:PRINT TAB(65,8)"FREQUENCY (MHz)":GOTO 8640
 8600 IF spec=0 GOTO 8610 ELSE GOTO 8620
 8610 D1%=NOM-(B%*100):BI=B%:DI=0:DI=100000:PRINT TAB(65,8)"TIME (mic-sec)":GOTO
8640
 8620 IF spec=1 GOTO 8630 ELSE GOTO 8590
 8630 D1%=NS%-(SS%*100):BI=SS%:DI=100000:PRINT TAB(65,8)"TIME(mic-sec)":GOTO 8640
 8640 PROCwipe(0,4):REMPRINTTAB(0,1)"Frequency(1) or Time measurments(2)"
 8650 :
 8660 PROCwipe(0,4):PRINT TAB(0,1)"USE ARROW KEYS TO MOVE THE LINE"
 8670 PRINT TAB(0,2)"TO EXIT PRESS SPACE BAR"
```

```
8680 REPEAT
8690 C5%=INKEY(-99)
8700 IF C5%=-1 ENDPROC
8710 YV%=750+V%:VY%=250+V%
8720 TT=(BI+((W*D1%)/DI))
8730 @%=131850:PRINT TAB(65,10),TT
8740 VDU5:MOVE W,500
8750 LINE W,VY%,W,YV%
8760 GCOL4,0:PROCdelay(2):LINE W,VY%,W,YV%:GCOL4,0:VDU4
8770 C1%=INKEY(-122)
8780 C2%=INKEY(-26)
8790 C3%=INKEY(-58)
8800 C4%=INKEY(-42)
8810 UNTIL C1% = -1 OR C2%=-1 OR C3%=-1 OR C4%=-1
8820 IF C1%=-1 W=W+0.25
8830 IF C2%=-1 W=W-0.25
8840 IF C3%=-1 V%=V%+1
8850 IF C4%=-1 V%=V%-1
8860 GOTO 8680
8870 :
8880 DEF PROCdelay(n)
8890 TIME=0:REPEAT UNTIL TIME>=n:ENDPROC
8900 :
8910 DEFPROCpick:AVV=B%*100:D2%=NRM/1000
8920 E%=INKEY(-11):IF sta=0 GOTO 8930 ELSE GOTO 8980
8930 X1=X*2:Y1=Y*4
8940 REPEAT
8950 VDU5
8960 sta=sta+1
8970 PROCPoint
8980 X2=X*2:Y2=Y*4:PROCbox:GCOL4,0:PROCdelay(3)
8981 X4=(X2*D2%):X3=(X1*D2%)
8982 @%=131850:PRINT TAB(65,10);X3:REMPROCwipe(X2,10)
8983 @%=131850:PRINT TAB(65,16);X4:REMPROCwipe(X1,Y1)
8984 PROCbox:GCOL4,0:VDU4
8990 UNTIL E%<>-1
9000 ENDPROC
9002 :
9004 DEFPROCcopy
9006 *FX6
9008 *HARDCOPY
9012 SS$=GET$
9014 IF SS$="H" THEN *HARDCOPYFX
9016 ENDPROC
9018 :
9020 DEFPROCbox:
9030 LINE X1,Y1,X2,Y1:LINE X1,Y2,X2,Y2:LINE X1,Y1,X1,Y2:LINE X2,Y1,X2,Y2
9040 ENDPROC
9050 :
9060 DEFPROCmenu
9070 VDU3
9080 VDU19,0,4,0,0,0
9090 COLOUR1
9100 COLOUR1
9110 COLOUR2
9120 LINE 10,10,80,10
9130 LINE 10,40,80,40
9140 LINE 10,10,10,40
9150 LINE 80,10,80,40
9160 LINE 100,10,170,10
9170 LINE 100,40,170,40
9180 LINE 100,10,100,40
9190 LINE 170,10,170,40
9200 LINE 190,10,260,10
```

```
9210 LINE 190,40,260,40
9220 LINE 190,10,190,40
9230 LINE 260,10,260,40
9240 LINE 280,10,350,10:LINE 280,40,350,40:LINE 280,10,280,40:LINE 350,10,350,40
9250 LINE 370,10,440,10:LINE 370,40,440,40:LINE 370,10,370,40:LINE 440,10,440,40
9260 LINE 450,10,520,10:LINE 450,40,520,40:LINE 450,10,450,40:LINE 520,10,520,40
9270 LINE 550,10,600,10:LINE 550,40,600,40:LINE 550,10,550,40:LINE 600,10,600,40
9280 LINE 650,10,700,10:LINE 650,40,700,40:LINE 650,10,650,40:LINE 700,10,700,40
9290 LINE 750,10,800,10:LINE 750,40,800,40:LINE 750,10,750,40:LINE 800,10,800,40
9300 LINE 1200,100,1250,100:LINE 1200,150,1250,150:LINE 1200,100,1200,150:LINE
1250,100,1250,150
9310 LINE 1200,200,1250,200:LINE 1200,250,1250,250:LINE 1200,200,1200,250:LINE
1250,200,1250,250
9320 LINE 1200,300,1250,300:LINE 1200,350,1250,350:LINE 1200,300,1200,350:LINE
1250,300,1250,350
9330 LINE 1200,400,1250,400:LINE 1200,450,1250,450:LINE 1200,400,1200,450:LINE
1250,400,1250,450
9340 LINE 1200,500,1250,500:LINE 1200,550,1250,550:LINE 1200,500,1200,550:LINE
1250,500,1250,550
9350 LINE 1200,600,1250,600:LINE 1200,650,1250,650:LINE 1200,600,1200,650:LINE
1250,600,1250,650
9360 REMLINE 1200,700,1250,700:LINE 1200,750,1250,750:LINE 1200,700,1200,750:LINE
1250,700,1250,750
9370 :
9380 PROCPoint
9390 IF E%=-1 GOTO 9400 ELSE GOTO 9405
9400 PROCpick:X1=0:Y1=0:sta=0:GOTO 9070
9405 IF D5%=-1 PROCreplot:PROCdraw:GOTO 9070
9410 IF Y*4>40 AND X*2<1001 THEN GOTO 9420 ELSE GOTO 9570
9420 LINE (X*2)-10,Y*4,(X*2)+10,Y*4:LINE X*2,(Y*4)-10,X*2,(Y*4)+10:SOUND1,-
15,255,10:@%=131850:REMPRINT TAB(65,10)X1
9430 IF N=0 TX1=X*2:PY1=Y*4:N=1:GOTO 9380
9440 TX2=X*2:PY2=Y*4:GOTO 9510
9450 :
9460 IF TX2=TX1 AND PY2=PY1 THEN GOTO 9470 ELSE GOTO 9510
9470 GCOL 3,6:LINE (X*2)-10,Y*4,(X*2)+10,Y*4:GCOL 7,6:LINE X*2,(Y*4)-
10,X*2,(Y*4)+10:GCOL4,0
9480 TX1=0:TX2=0:PY1=0:PY2=0:AA%=0:TT%=0:N=0:GOTO9380
9490 TX1=0:TX2=0:PY1=0:PY2=0:AA=0:TT=0:N=0:GOTO9380
9500 :
9510 AA%=ABS(PY1-PY2):REMIF PY2>PY1 THEN AA%=PY2-PY1 ELSE AA%=PY1-PY2
9520 TT%=ABS(TX1-TX2):REMIF TX2>TX1 THEN TT%=TX2-TX1 ELSE TT%=TX1-TX2
9530 :
9540 :
9550 :
9560 TX1=0:TX2=0:PY1=0:PY2=0:AA%=0:TT%=0:N=0:GOTO9380
9570 IF Y*4<40 GOTO 9580 ELSE GOTO 9800
9580 IF X*2>100 AND X*2<170 THEN GOTO 9590 ELSE GOTO9610
9590 FILL X*2,Y*4:SOUND1,-15,40,10:SOUND1,-15,50,10:CLS:COLOUR 132:GOTO9070
9600 :
9610 IF X*2>190 AND X*2<260 THEN GOTO 9620 ELSE GOTO 9640
9620 FILL X*2,Y*4:SOUND1,-15,40,10:SOUND1,-15,50,10:PROCsetup:GOTO 9070
9630 :
9640 IF X*2>280 AND X*2<350 THEN GOTO 9650 ELSE GOTO 9670
9650 FILL X*2,Y*4:SOUND1,-15,40,10:SOUND1,-15,50,10:COLOUR
132:PROCtran:PROCtransform:PROCsig:PROCdraw:GOTO 9070
9660 :
9670 IF X*2>370 AND X*2<440 THEN GOTO 9680 ELSE GOTO 9700
9680 FILL X*2,Y*4:SOUND1,-15,40,10:SOUND1,-15,50,10:PROCfgen:GOTO 9070
9690 :
9700 IF X*2>450AND X*2<520THEN GOTO 9710ELSE GOTO 9730
9710 FILL X*2,Y*4:SOUND1,-15,40,10:SOUND1,-
15,50,10:fr=0:PROCattension:GCOL4,0:PROCfaxis:PROCwipe(0,8):PROCwipe(65,10):GOTO 9070
9720 :
```

```
9730 IF X*2>550 AND X*2<600THEN GOTO 9740ELSE GOTO 9750
9740 FILL X*2,Y*4:SOUND1,-15,40,10:SOUND1,-15,50,10:PROCwfile:GOTO 9070
9750 IF X*2>650 AND X*2<700 THEN GOTO 9760 ELSE GOTO 9780
9760 FILL X*2,Y*4:SOUND1,-15,40,10:SOUND1,-15,50,10:PROCcfile:GOTO 9070
9770 :
9780 IF X*2>750 AND X*2<800 THEN GOTO 9790 ELSE GOTO 9800
9790 FILL X*2,Y*4:SOUND1,-15,40,10:SOUND1,-15,50,10:PROCrfile:GOTO 9070
9800 IF X*2<1200 GOTO 9930 ELSE GOTO 9810
9810 IF Y*4>600 AND Y*4<650GOTO 9820 ELSE GOTO9830
9820 FILL X*2,Y*4:SOUND1,-15,40,10:SOUND1,-15,50,10:PROCfft:GOTO 9070
9830 IF Y*4>500AND Y*4<550GOTO 9840 ELSE GOTO9850
9840 FILL X*2,Y*4:SOUND1,-15,40,10:SOUND1,-15,50,10:PROCcorrelation:GOTO 9070
9850 IF Y*4>400AND Y*4<450GOTO 9860 ELSE GOTO9870
9860 FILL X*2,Y*4:SOUND1,-15,40,10:SOUND1,-15,50,10:PROCcorrelation:GOTO 9070
9870 IF Y*4>300AND Y*4<350GOTO 9880 ELSE GOTO9890
9880 FILL X*2,Y*4:SOUND1,-15,40,10:SOUND1,-15,50,10:PROCgetdata:GOTO 9070
9890 IF Y*4>200AND Y*4<250GOTO 9900 ELSE GOTO9910
9900 FILL X*2,Y*4:SOUND1,-15,40,10:SOUND1,-15,50,10:PROCshow:GOTO 9070
9910 IF Y*4>100 AND Y*4<150GOTO 9920 ELSE GOTO9930
9920 FILL X*2,Y*4:SOUND1,-15,40,10:SOUND1,-15,50,10:PROCdata:GOTO 9070
9930 :
9940 IF Y*4>10 AND Y*4<80 AND Y*4<40 GOTO 9950 ELSE GOTO 9070
9950 FILL X*2,Y*4:SOUND1,-15,40,10:SOUND1,-15,10,10:SOUND1,-
15,50,10:PP=INKEY(25):quit=1:COLOUR 132:GOTO 10040
9960 :
9970 UNTIL quit=1
9980 ENDPROC
9990 :
10000
10010
10020
10030 :
10040 :
10050 IF quit=1 ENDPROC
10060 :
10090 DEFPROCfgen
10092 PROCwipe(0,10):
10093 PRINT TAB(0,2)"FUNCTION  GENERATOR"
10094 PRINT TAB(0,3)"  REMOTE CONTROLE"
10095 PRINT TAB(0,5)"TYPE THE INPUT AMPLITUDE":INPUT AF:PROCwipe(0,10)
10096 PRINT TAB(2,5)"TYPE Min Frequency":INPUT MI
10097 PRINT TAB(2,7)"TYPE Max Frequency":INPUT MA
10098 PRINT TAB(2,9)"TYPE Step Frequency":INPUT ST:NFS%=(MA-MI)/ST:PROCattension
10100 *FX8,7
10200 *FX5,2
10300 *FX3,5
10400 PRINT"!"
10400 PRINT"A";AF:
10500 F=MI:seismic=1:PROCinitialise_IEEE: PROCadrandoutput(1,5,"*TRG")
10510 F=0.7:M=0
10600 FOR Q=1 TO 100
10700 :
10800 @%=&20409:PRINTTAB(65,10)"F";F;"E6I"
10900 PROCdelay(80)
10902 :
10905 REMPROCdevice_clear:PROCgo_to_local(5):
10906 IF M=0 GOTO 10907 ELSE GOTO 10908
10907 F=F+0.01:M=1:NEXT Q:GOTO 10910 10908 F=F-0.01:M=0:NEXT Q 10910
PRINT"$" 11000 *FX3,0 11010 PROCwipe(0,10) 11100 ENDPROC
```

Appendix 3:

Plots of compressional and shear velocities as a function of confining pressure and at room temperature for a wide range of samples. See appendix 1 for the rock types and their locations

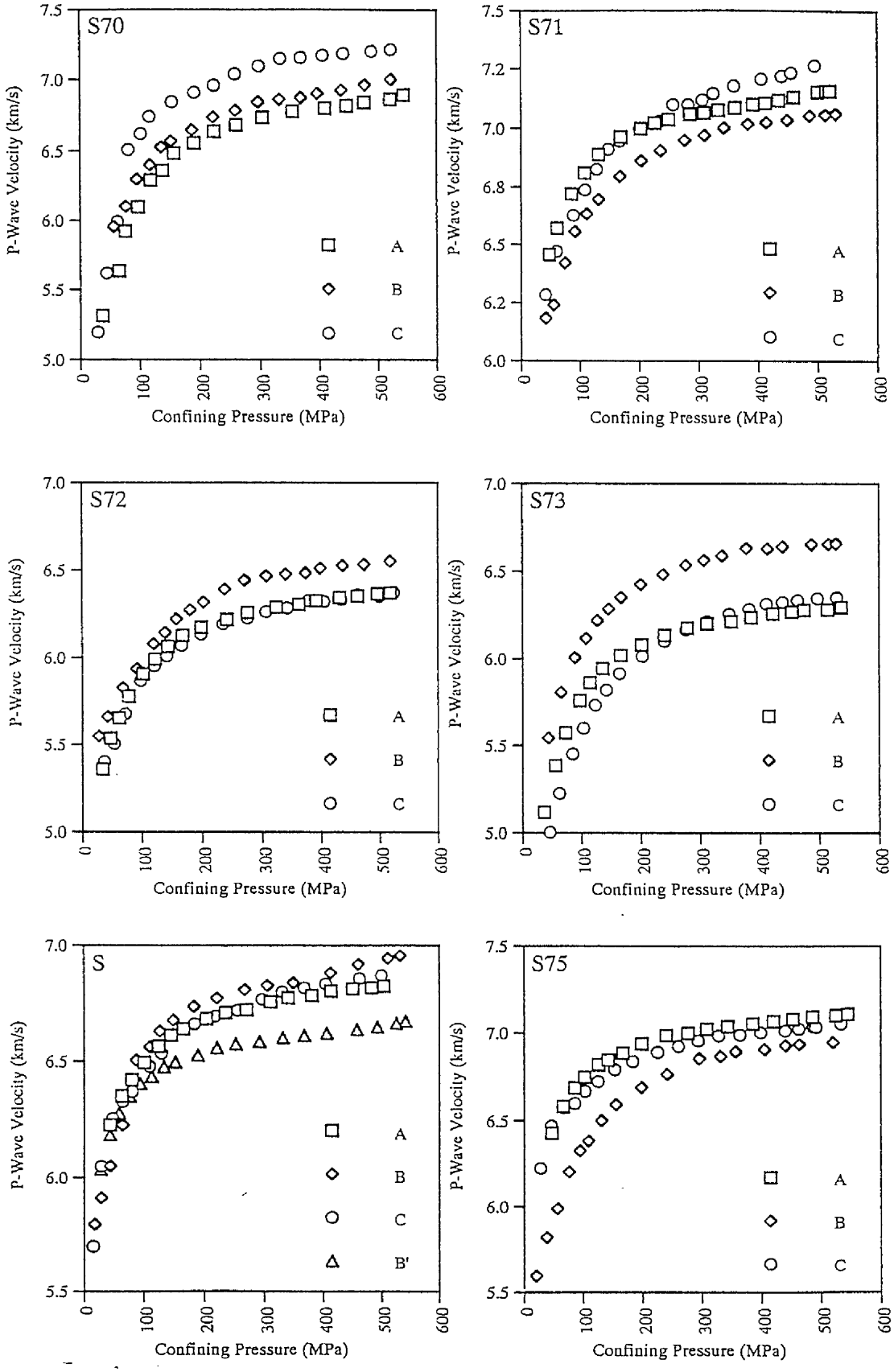
S70
S71
S72
S73
S
S75
P-Wave Velocity (km/s)
Confining Pressure (MPa)
A
B
C
B'

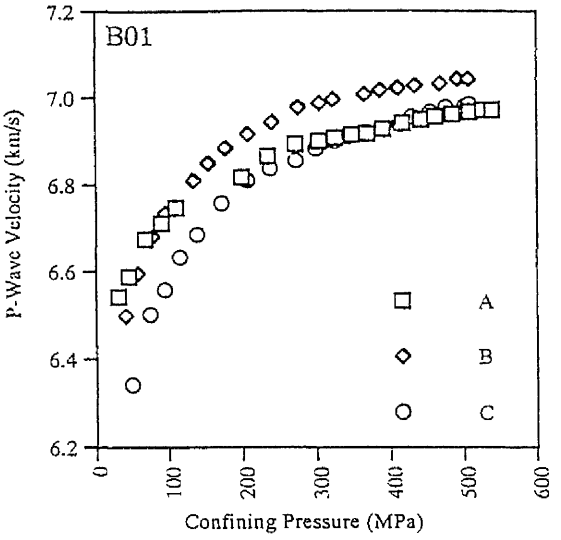
B01
P-Wave Velocity (km/s)
Confining Pressure (MPa)
A
B
C

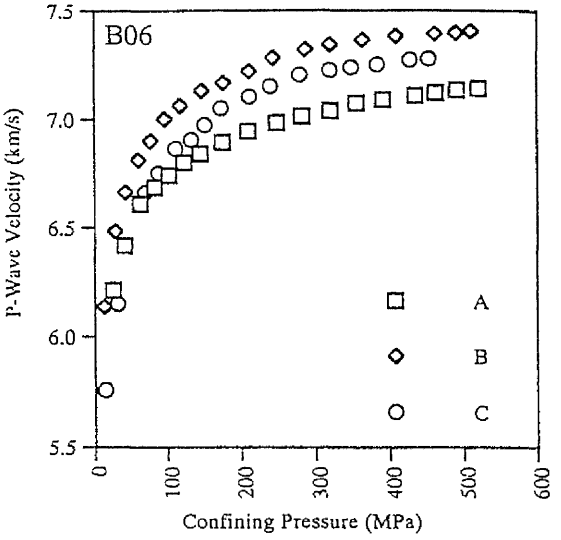
B06
P-Wave Velocity (km/s)
Confining Pressure (MPa)
A
B
C

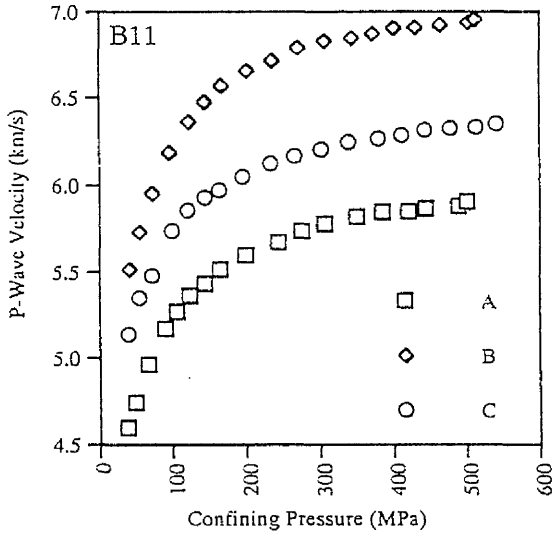
B11
P-Wave Velocity (km/s)
Confining Pressure (MPa)
A
B
C

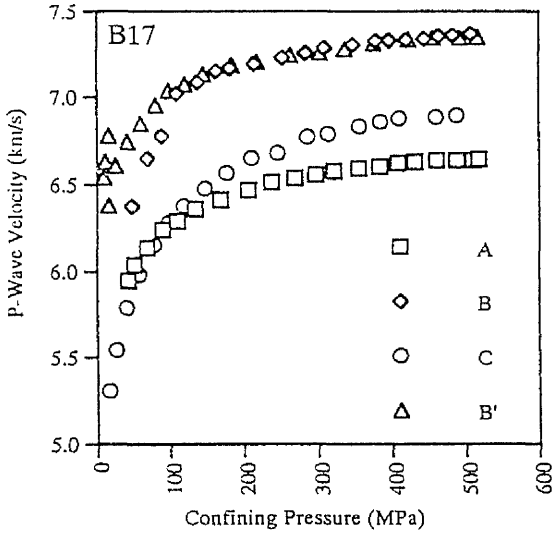
B17
P-Wave Velocity (km/s)
Confining Pressure (MPa)
A
B
C
B'

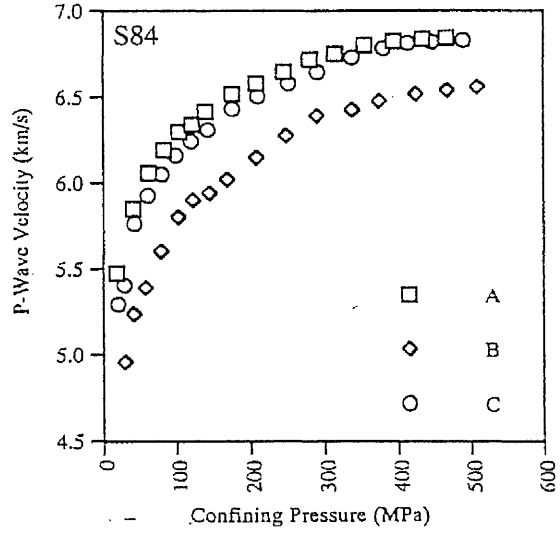
S84
P-Wave Velocity (km/s)
Confining Pressure (MPa)
A
B
C

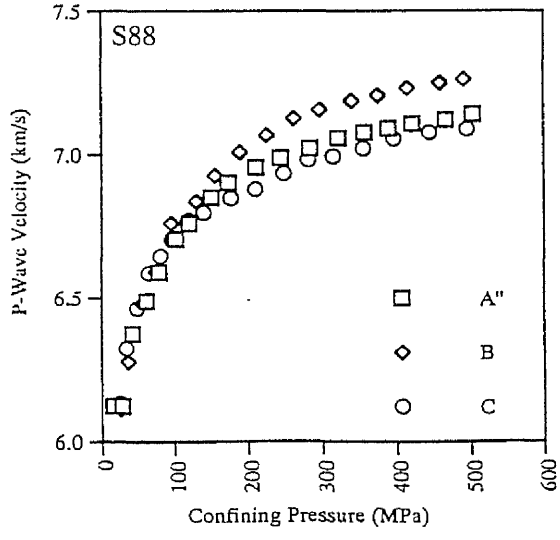
S88
P-Wave Velocity (km/s)
Confining Pressure (MPa)
A"
B
C

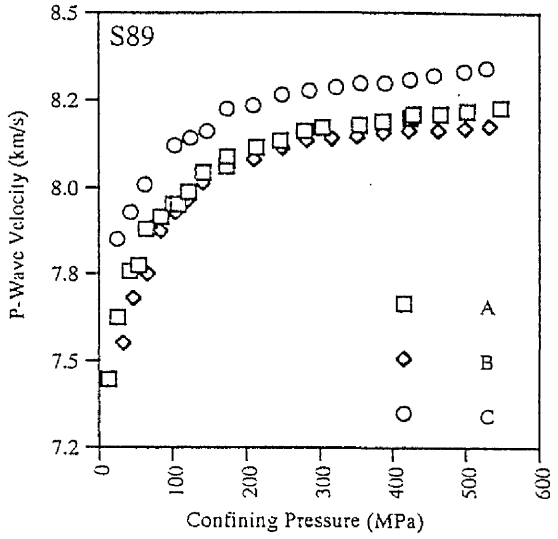
S89
P-Wave Velocity (km/s)
Confining Pressure (MPa)
A
B
C

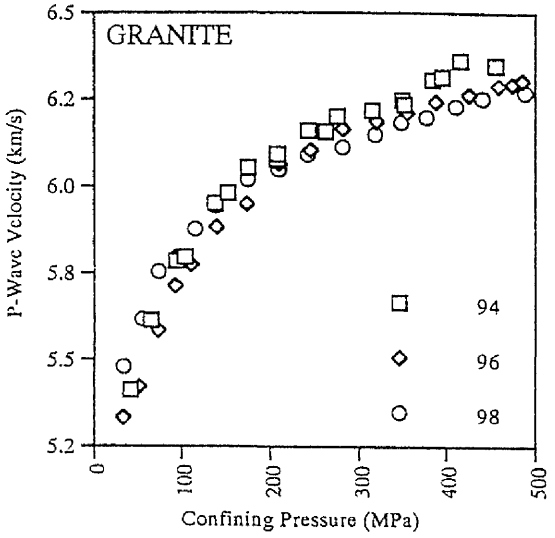
GRANITE
P-Wave Velocity (km/s)
Confining Pressure (MPa)
94
96
98

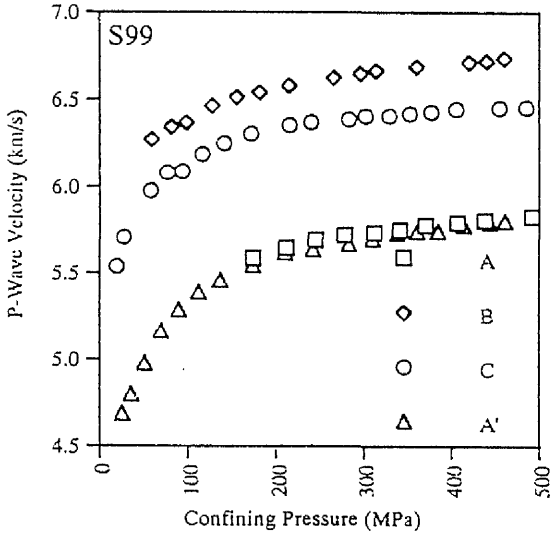
S99
P-Wave Velocity (km/s)
Confining Pressure (MPa)
A
B
C
A'

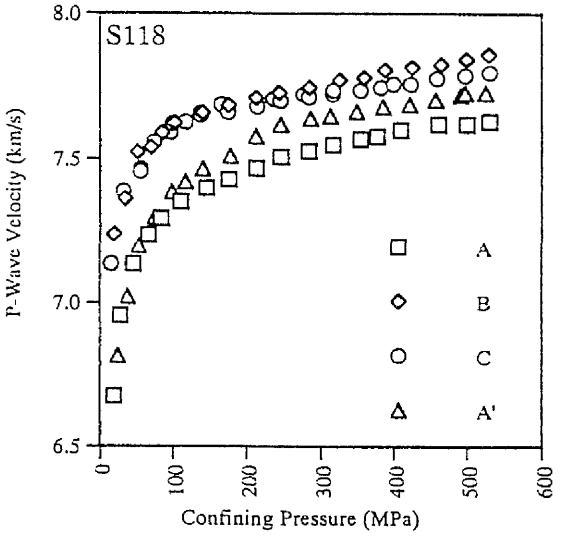
S118
P-Wave Velocity (km/s)
Confining Pressure (MPa)
A
B
C
A'

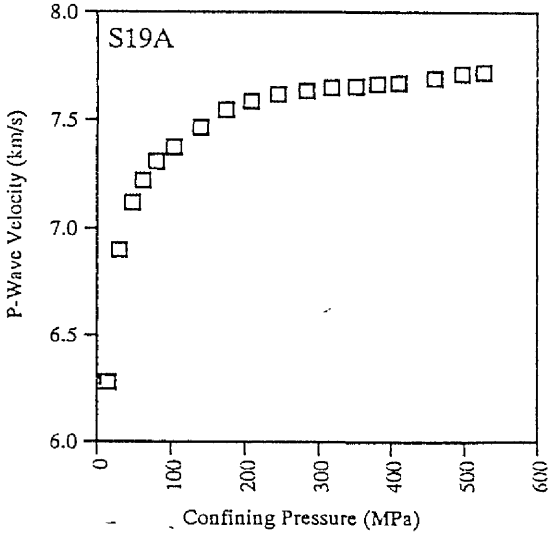
S19A
P-Wave Velocity (km/s)
Confining Pressure (MPa)

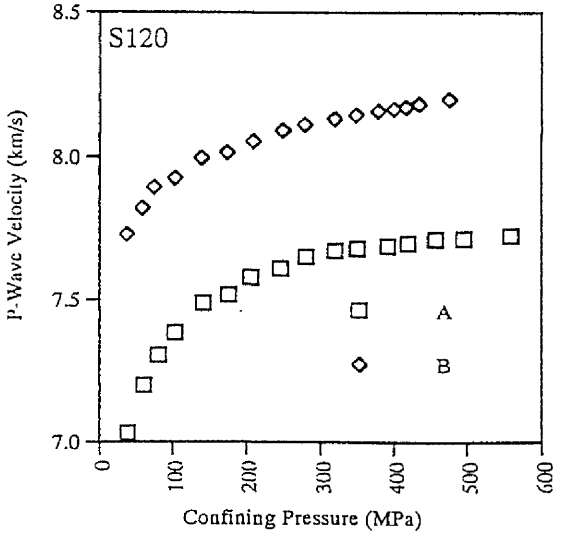
S120
P-Wave Velocity (km/s)
Confining Pressure (MPa)
A
B

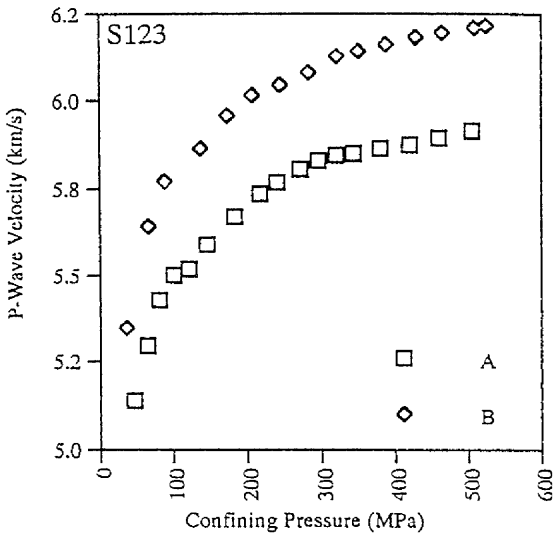
S123
P-Wave Velocity (km/s)
Confining Pressure (MPa)
A
B

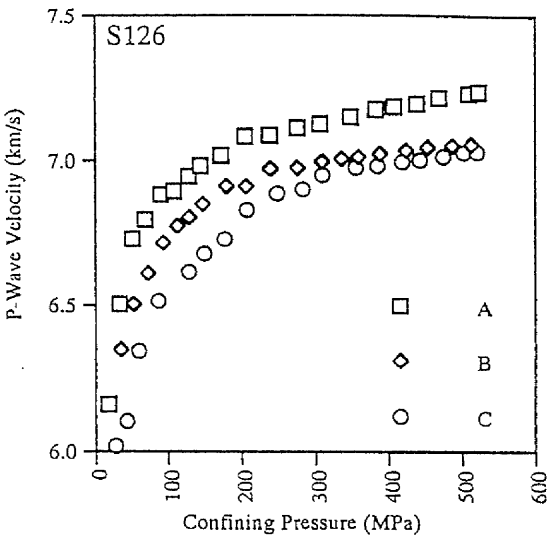
S126
P-Wave Velocity (km/s)
Confining Pressure (MPa)
A
B
C

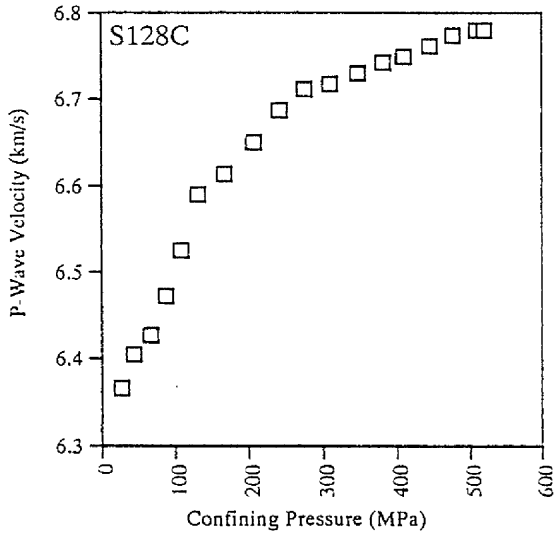
S128C
P-Wave Velocity (km/s)
Confining Pressure (MPa)

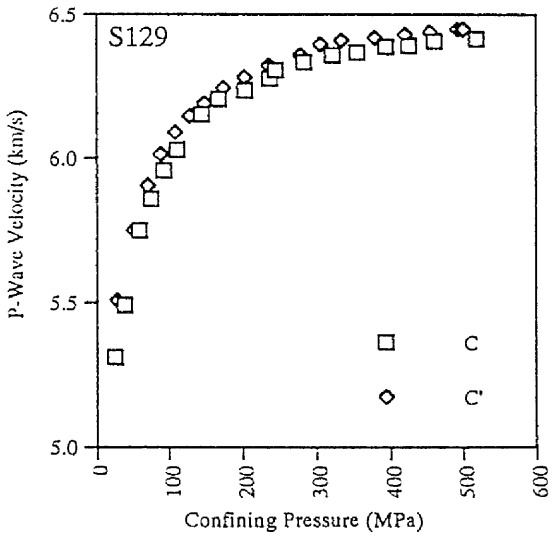
S129
P-Wave Velocity (km/s)
Confining Pressure (MPa)
C
C'

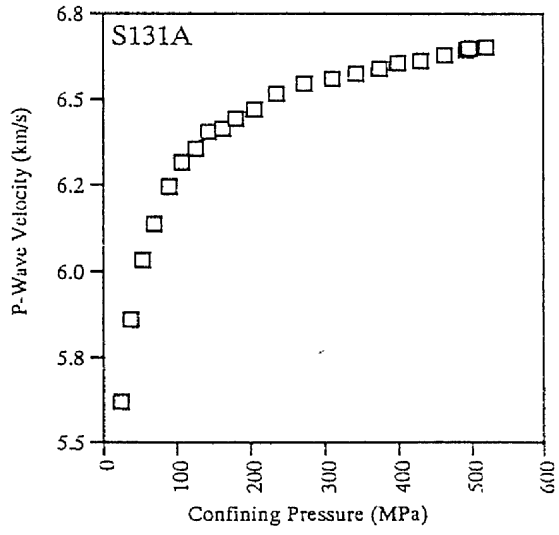
S131A
P-Wave Velocity (km/s)
Confining Pressure (MPa)

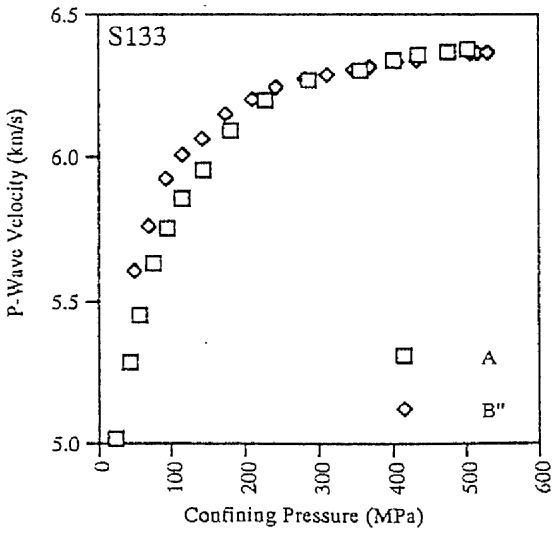
S133
P-Wave Velocity (km/s)
Confining Pressure (MPa)
A
B"

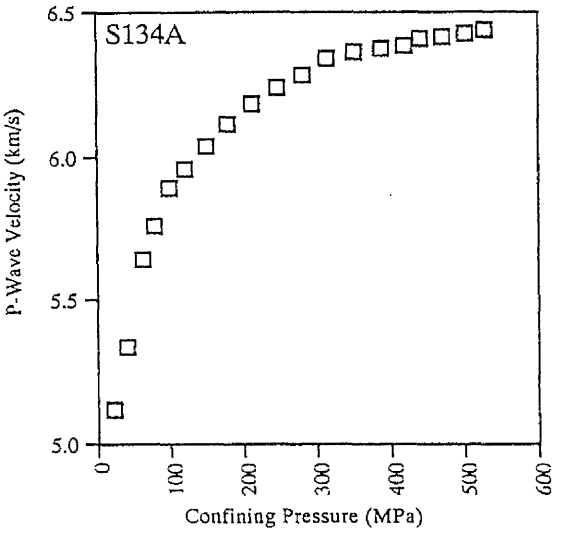
S134A
P-Wave Velocity (km/s)
6.5
6.0
5.5
5.0
0
100
200
300
400
500
600
Confining Pressure (MPa)

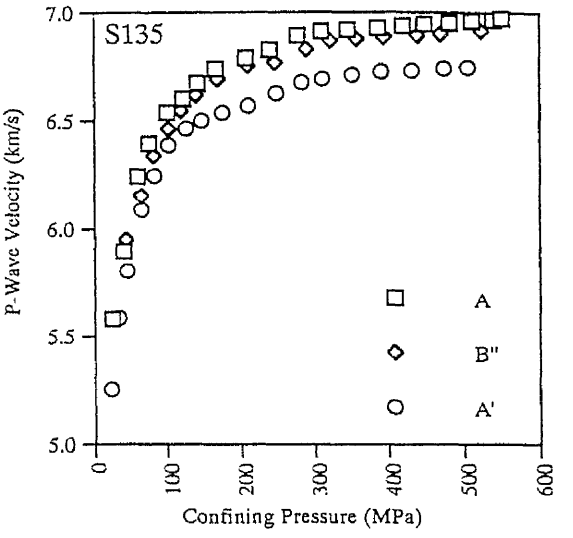
S135
P-Wave Velocity (km/s)
7.0
6.5
6.0
5.5
5.0
A
B"
A'
0
100
200
300
400
500
600
Confining Pressure (MPa)

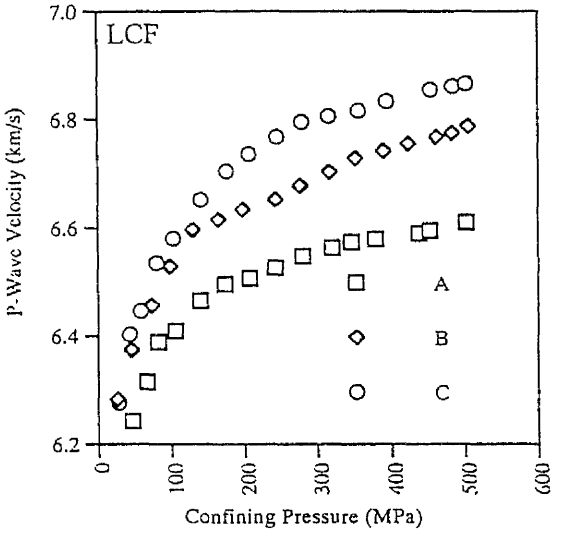
LCF
P-Wave Velocity (km/s)
7.0
6.8
6.6
6.4
6.2
A
B
C
0
100
200
300
400
500
600
Confining Pressure (MPa)

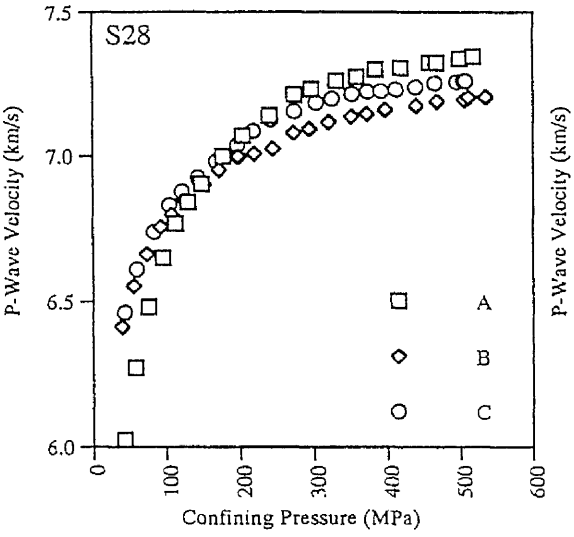
S28
P-Wave Velocity (km/s)
7.5
7.0
6.5
6.0
0
100
200
300
400
500
600
Confining Pressure (MPa)
A
B
C

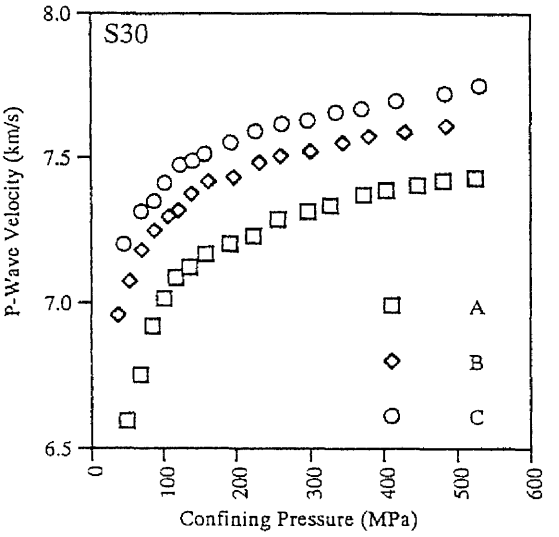
S30
P-Wave Velocity (km/s)
8.0
7.5
7.0
6.5
0
100
200
300
400
500
600
Confining Pressure (MPa)
A
B
C

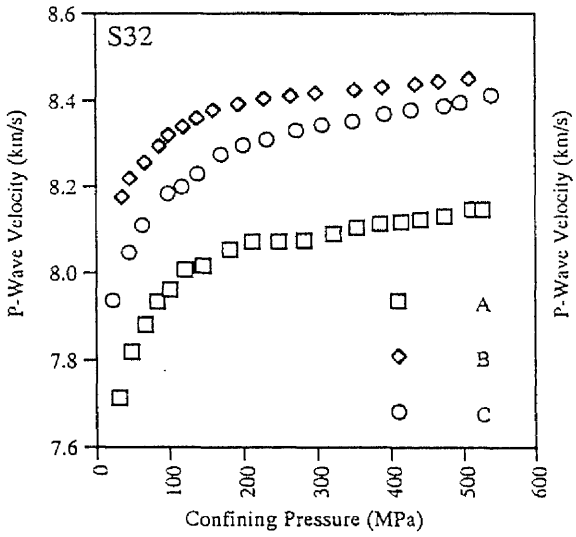
S32
P-Wave Velocity (km/s)
8.6
8.4
8.2
8.0
7.8
7.6
0
100
200
300
400
500
600
Confining Pressure (MPa)
A
B
C

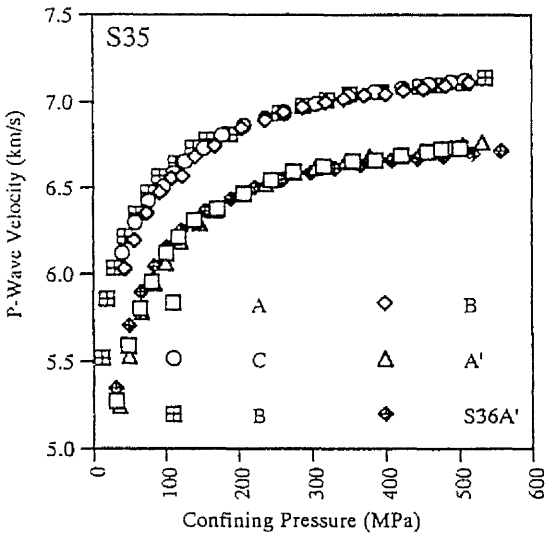
S35
P-Wave Velocity (km/s)
7.5
7.0
6.5
6.0
5.5
5.0
0
100
200
300
400
500
600
Confining Pressure (MPa)
A
B
C
A'
B
S36A'

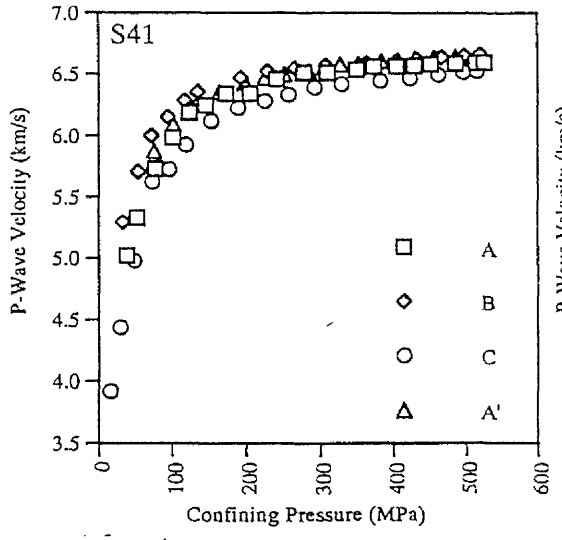
S41
P-Wave Velocity (km/s)
7.0
6.5
6.0
5.5
5.0
4.5
4.0
3.5
0
100
200
300
400
500
600
Confining Pressure (MPa)
A
B
C
A'

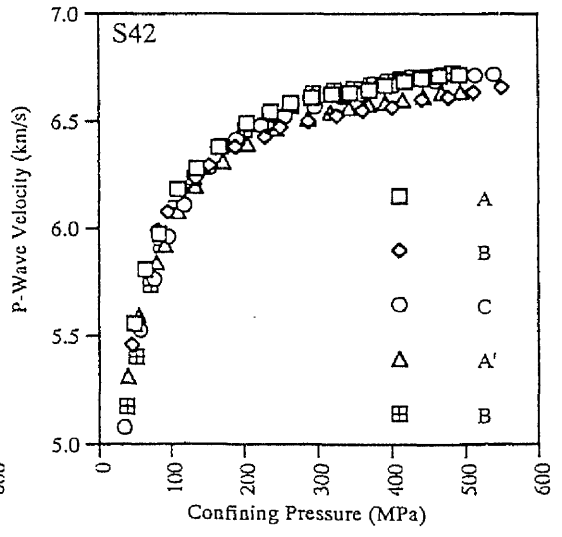
S42
P-Wave Velocity (km/s)
7.0
6.5
6.0
5.5
5.0
0
100
200
300
400
500
600
Confining Pressure (MPa)
A
B
C
A'
B

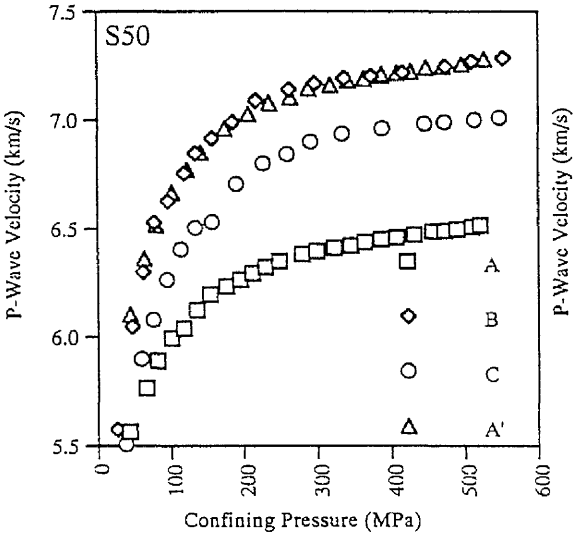
S50
P-Wave Velocity (km/s)
Confining Pressure (MPa)
A
B
C
A'

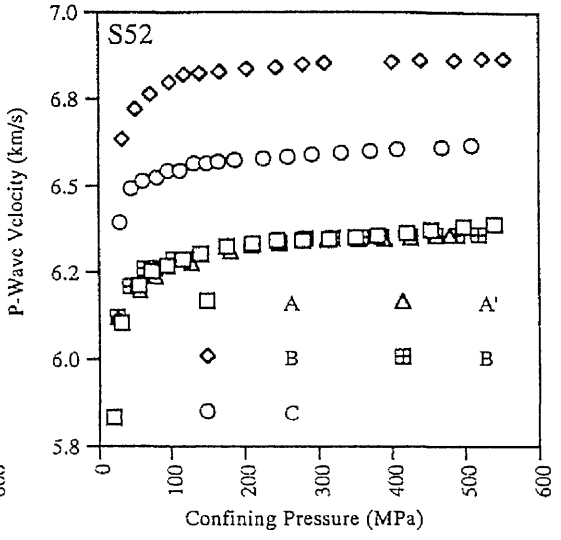
S52
P-Wave Velocity (km/s)
Confining Pressure (MPa)
A
A'
B
B
C

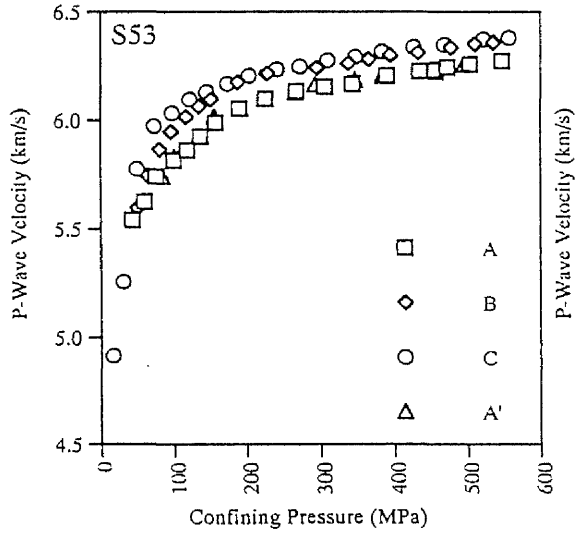
S53
P-Wave Velocity (km/s)
Confining Pressure (MPa)
A
B
C
A'

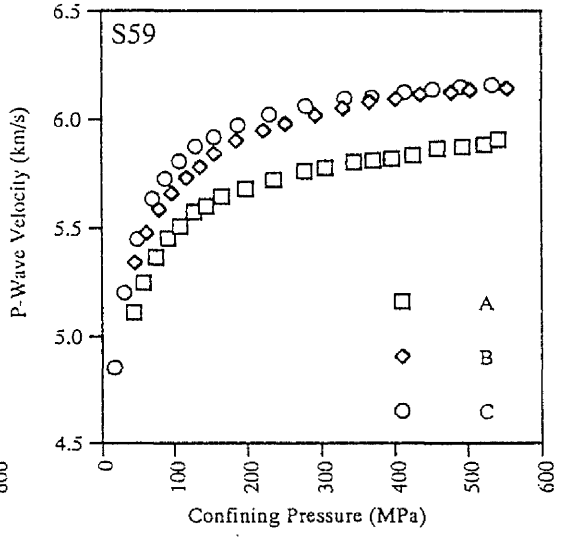
S59
P-Wave Velocity (km/s)
Confining Pressure (MPa)
A
B
C

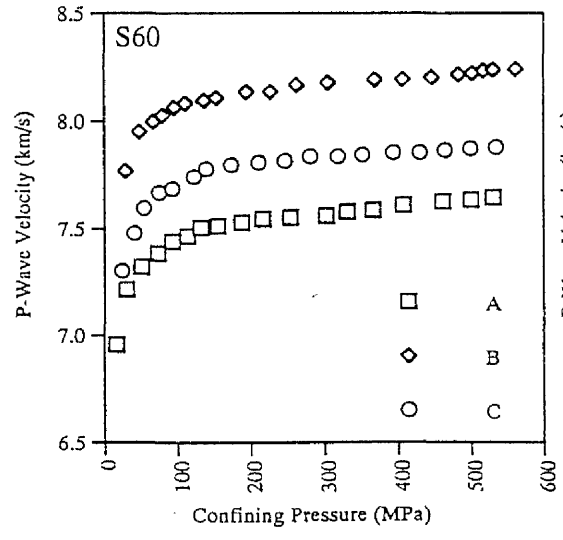
S60
P-Wave Velocity (km/s)
Confining Pressure (MPa)
A
B
C

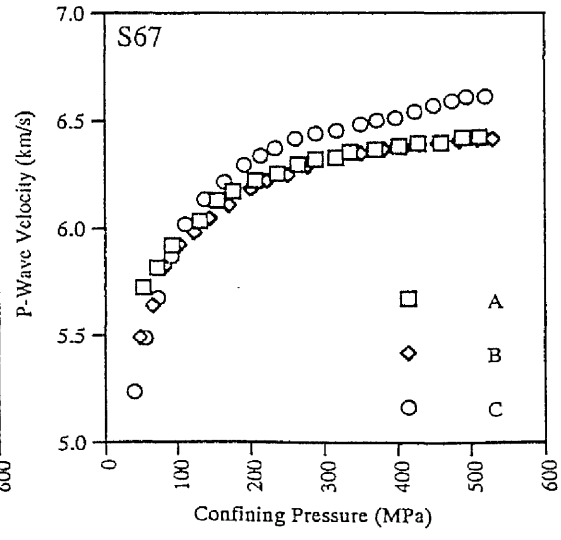
S67
P-Wave Velocity (km/s)
Confining Pressure (MPa)
A
B
C

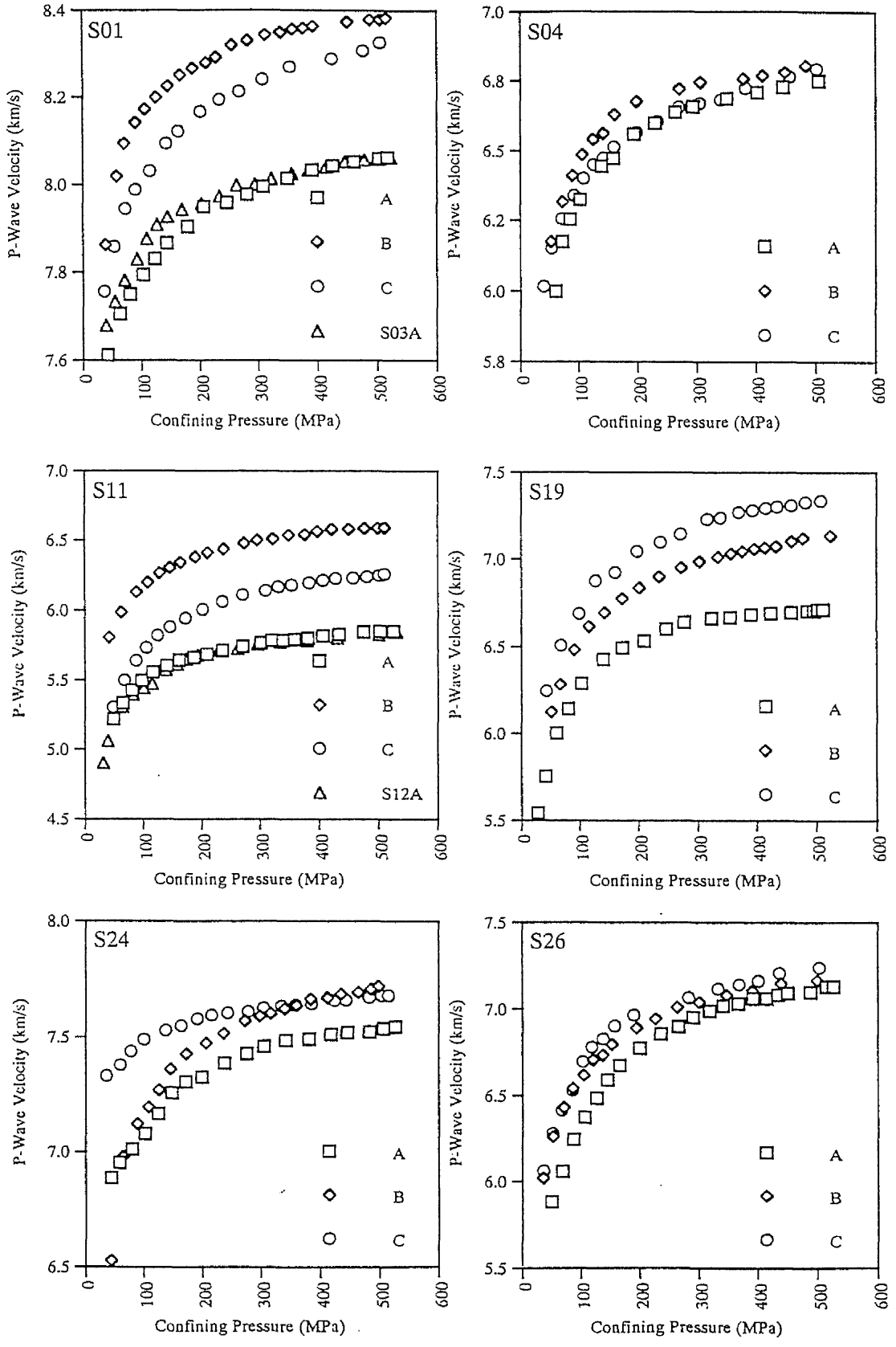
S01
P-Wave Velocity (km/s)
Confining Pressure (MPa)
A
B
C
S03A
S04
A
B
C
S11
A
B
C
S12A
S19
A
B
C
S24
A
B
C
S26
A
B
C

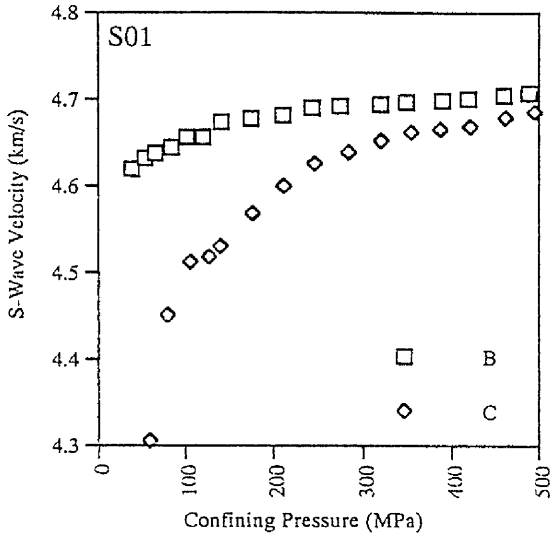
S01
S-Wave Velocity (km/s)
Confining Pressure (MPa)
B
C

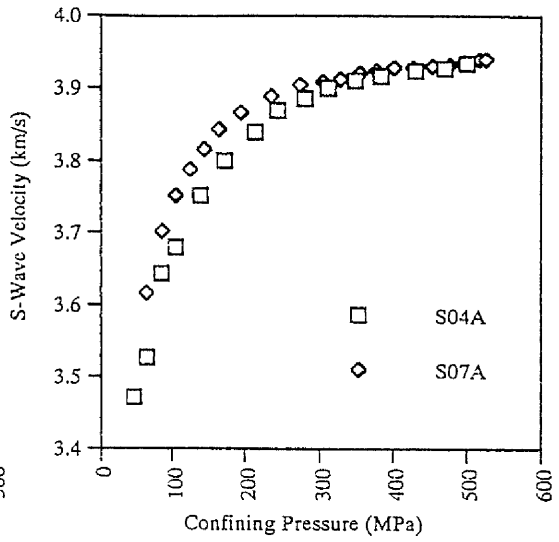
S-Wave Velocity (km/s)
Confining Pressure (MPa)
S04A
S07A

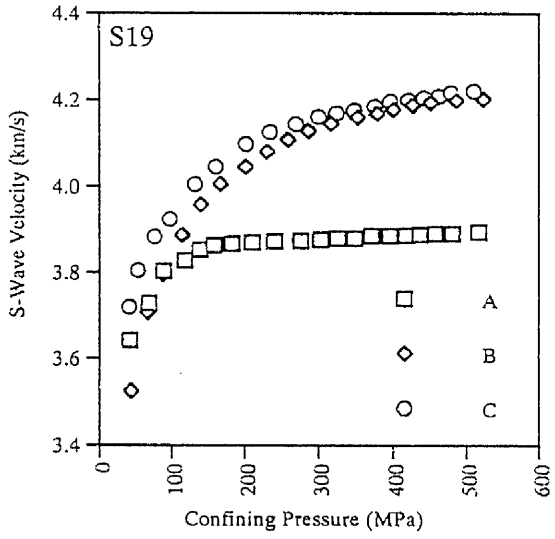
S19
S-Wave Velocity (km/s)
Confining Pressure (MPa)
A
B
C

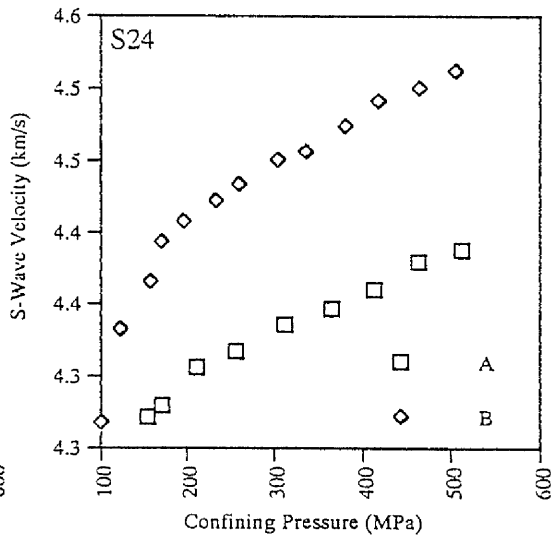
S24
S-Wave Velocity (km/s)
Confining Pressure (MPa)
A
B

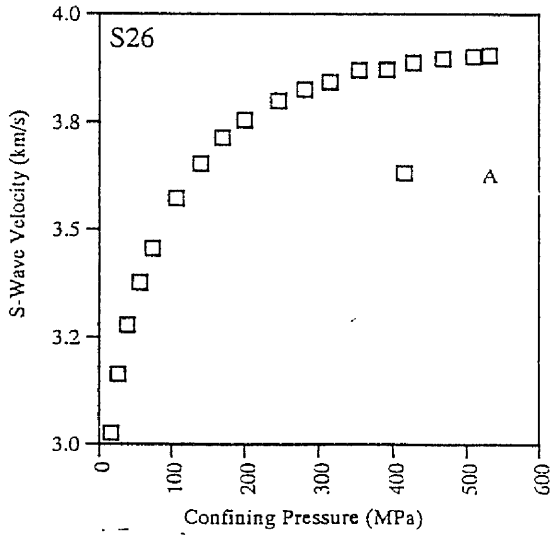
S26
S-Wave Velocity (km/s)
Confining Pressure (MPa)
A

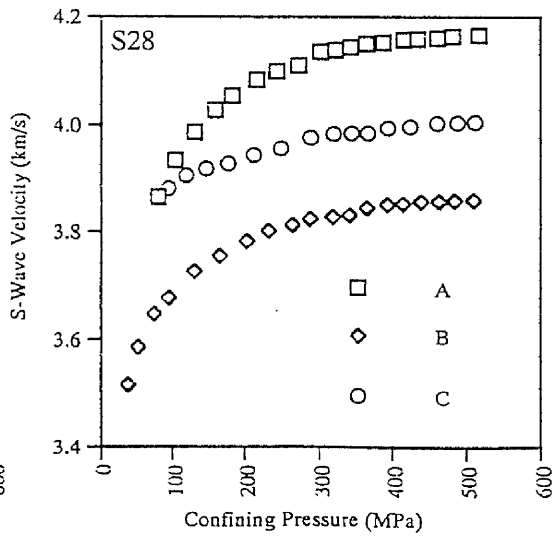
S28
S-Wave Velocity (km/s)
Confining Pressure (MPa)
A
B
C

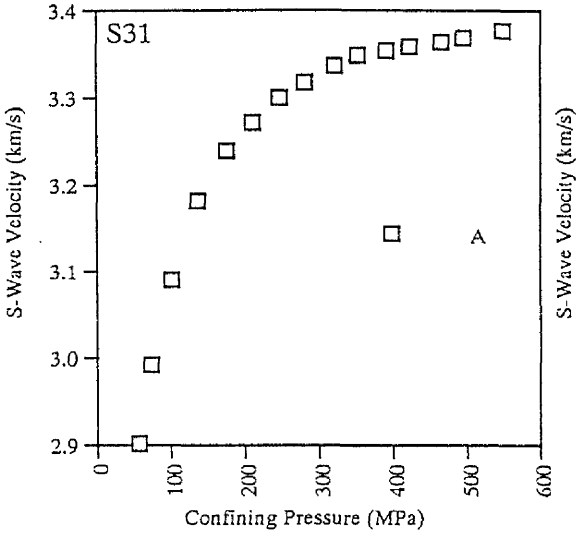
S31
S-Wave Velocity (km/s)
Confining Pressure (MPa)
A

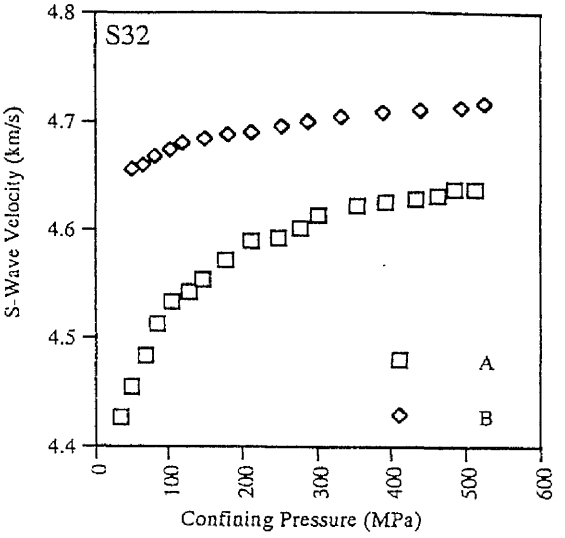
S32
S-Wave Velocity (km/s)
Confining Pressure (MPa)
A
B

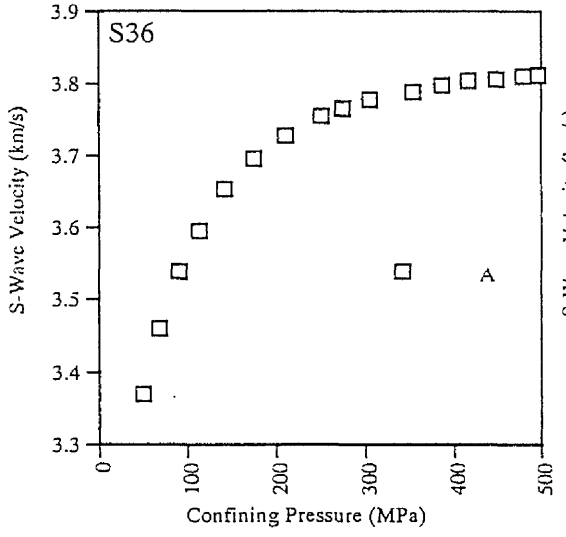
S36
S-Wave Velocity (km/s)
Confining Pressure (MPa)
A

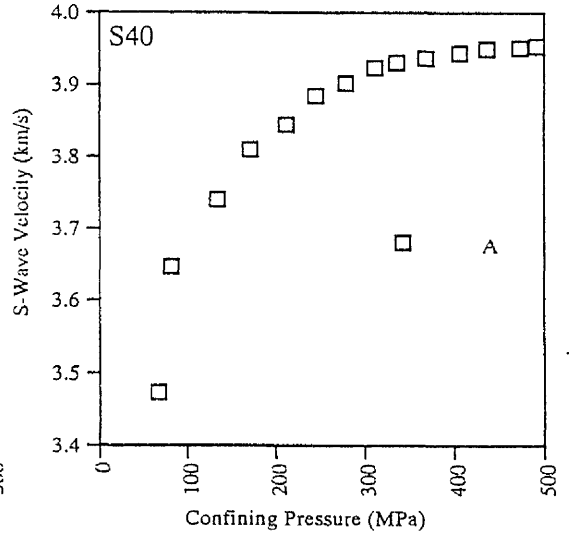
S40
S-Wave Velocity (km/s)
Confining Pressure (MPa)
A

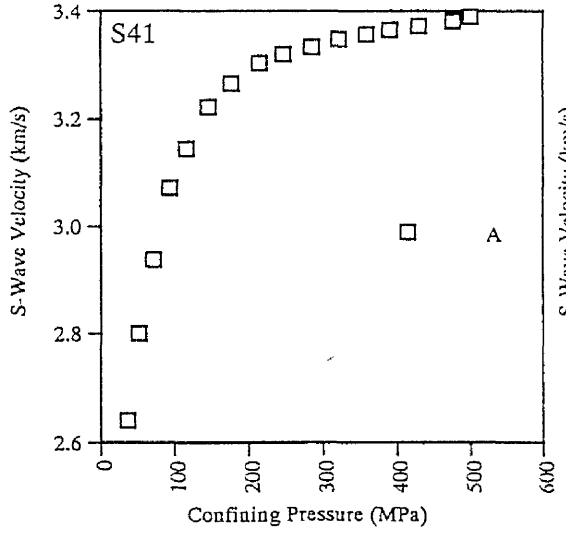
S41
S-Wave Velocity (km/s)
Confining Pressure (MPa)
A

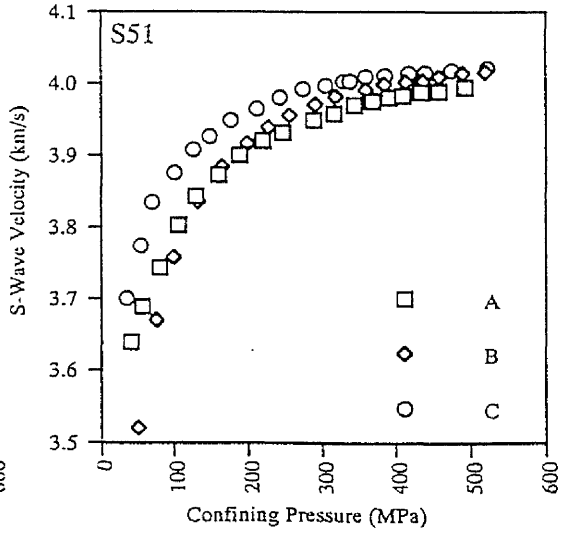
S51
S-Wave Velocity (km/s)
Confining Pressure (MPa)
A
B
C

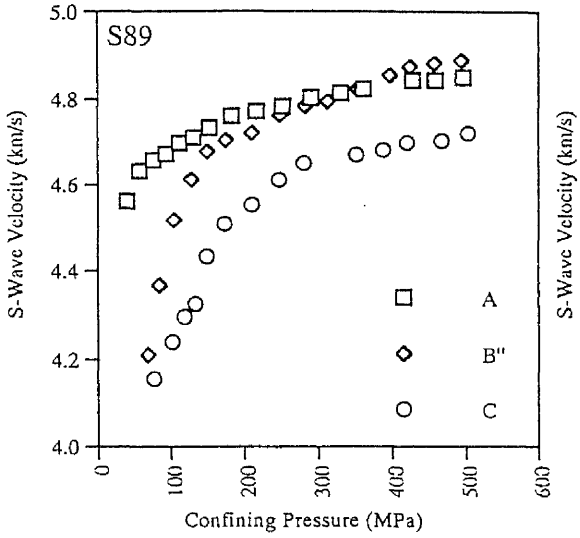
S89
S-Wave Velocity (km/s)
Confining Pressure (MPa)
A
B"
C

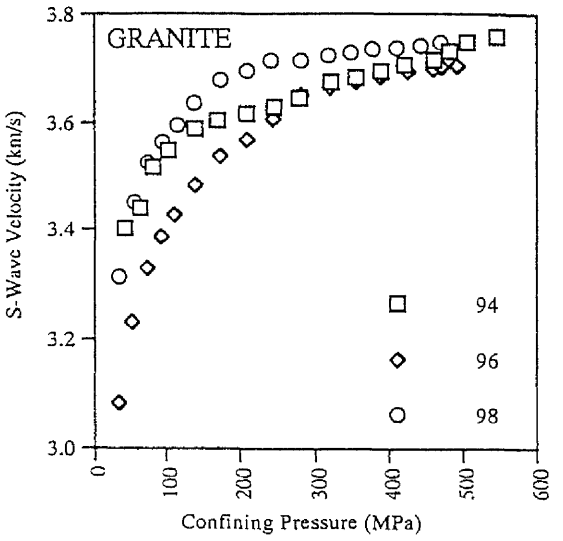
GRANITE
S-Wave Velocity (km/s)
Confining Pressure (MPa)
94
96
98

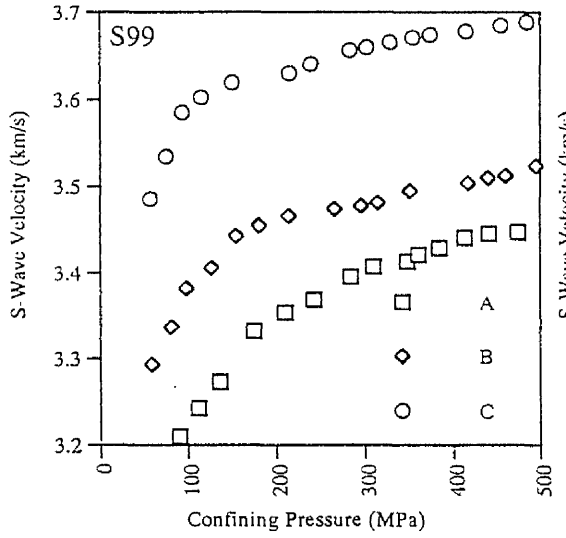
S99
S-Wave Velocity (km/s)
Confining Pressure (MPa)
A
B
C

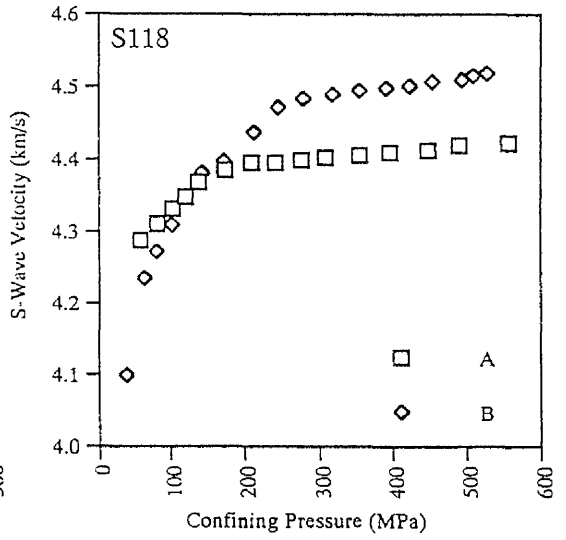
S118
S-Wave Velocity (km/s)
Confining Pressure (MPa)
A
B

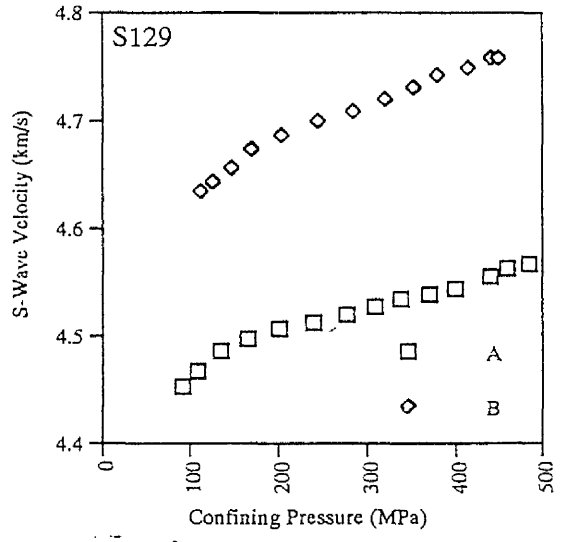
S129
S-Wave Velocity (km/s)
Confining Pressure (MPa)
A
B

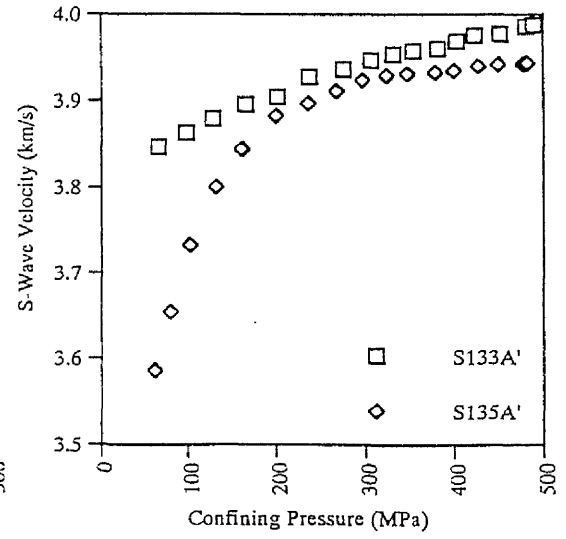
S-Wave Velocity (km/s)
Confining Pressure (MPa)
S133A'
S135A'